AD-A233 515

N89-29491

NASA Technical Memorandum 101634

AVSCOM Technical Report 89-B-003

DTIC FILE COPY

Energy-Absorption Cabability of Composite Tubes and Beams

Gary L. Farley
and
Robert M. Jones

DTIC
ELECTE
MAR 2 7 1991
S C D

September 1989

NASA

National Aeronautics and
Space Administration

Langley Research Center
Hampton, Virginia 23665-5225

US ARMY
AVIATION
SYSTEMS COMMAND
AVIATION R&T ACTIVITY

91 3 22 074

ENERGY-ABSORPTION CAPABILITY OF COMPOSITE TUBES AND BEAMS

by

Gary L. Farley

and

Robert M. Jones

ABSTRACT

In this study the objective was to develop a method of predicting the energy-absorption capability of composite subfloor beam structures. Before it is possible to develop such an analysis capability, an in-depth understanding of the crushing process of composite materials must be achieved. Many variables affect the crushing process of composite structures, such as the constituent materials' mechanical properties, specimen geometry, and crushing speed. A comprehensive experimental evaluation of tube specimens was conducted to develop insight into how composite structural elements crush and what are the controlling mechanisms.

In this study the four characteristic crushing modes, transverse shearing, brittle fracturing, lamina bending, and local buckling were identified and the mechanisms that control the crushing process defined. An in-depth understanding was developed of how material properties, affect energy-absorption capability. For example, an increase in fiber and matrix stiffness and failure strain can, depending upon the configuration of the tube, increase energy-absorption capability. An analysis to

predict the energy-absorption capability of composite tube specimens was developed and verified. Good agreement between experiment and prediction was obtained.

Sine-wave and integrally stiffened composite beams were evaluated. Composite energy-absorbing beams crush in modes similar to tubular specimens that are made from the same material and have similar geometry. Energy-absorption trends of the composite beams are similar to energy-absorption trends from composite tube specimens. Composite beams are equal or superior energy absorbers to comparable geometry metallic beams. Finally, a simple and accurate method of predicting the energy-absorption capability of composite beams was developed. This analysis is based upon the energy-absorption capability of the beams' constituent elements.

QUALITY
INSPECTED
4

ii

TABLE OF CONTENTS

iv

LIST OF FIGURES

LIST OF TABLES

xiii

NOMENCLATURE

$A_{c.e.}$	Cross-sectional area of characteristic elements
$A_{s.e.}$	Cross-sectional area of structural elements
D	Inside diameter of circular cross-section tube
EI	Bending stiffness
$E-Gl$	E-glass
F	Fabric
G, G_c	Total and critical strain energy release rates
G_I, G_{II}, G_{III}	Mode I, mode II, and mode III strain-energy release rates
H	Hybrid woven fabric composed of graphite and Kevlar
Gr	Graphite
K	Kevlar
K_f	Foundation stiffness
L	Column length
N	Crushing mode indicator
P_{cr}	Buckling load of a column
P_{sus}	Sustained crushing force
R	Tube radius
T	Tape
t	Tube wall thickness
S	Symmetric
W	Tube width of square cross-section tubes

Θ	Ply angle
Φ	Included angle
σ	Stress
ρ	Density

Chapter 1 - INTRODUCTION

1.1 Definition of Problem

Vehicle crashworthiness, as specified in Mil-Std-1290 (ref. 1), is an envelope of noninjurious crash conditions that future U.S. Army helicopters must be designed to meet. These crash conditions are related to both impact speed and vehicle attitude. The requirements set forth in Mil-Std-1290 also mandate that a protective shell be maintained around the occupants during the crash. In the case of a helicopter, the protective shell is the fuselage structure.

Although the crashed CH-47 helicopter, depicted in Fig. 1, was not designed to meet the requirements of Mil-Std-1290, its crash scenario is representative of the different crash events of a helicopter. The first crash event is usually the contact of the landing gear with the ground. The landing gear strokes to the limit of the hydraulic shock absorbers and then progressively fails at its attachment points on the fuselage. Next, the bottom of the fuselage makes contact with the ground. The subfloor beams, located between the cargo floor and bottom of the fuselage, deform. If the subfloor beams do not crush uniformly and progressively, then the helicopter floor can "heave"; that is, the floor moves upward into the occupied volume of the fuselage, forcing cargo and occupants into the sides of the fuselage, as depicted in Fig. 2.

Crash-induced loads are transferred from the subfloor beams to the fuselage frames and skin structure. These crash-induced loads transfered to the adjacent fuselage structure can be significantly higher in magnitude than those produced by

Figure 1. Crash test of CH-47 helicopter.
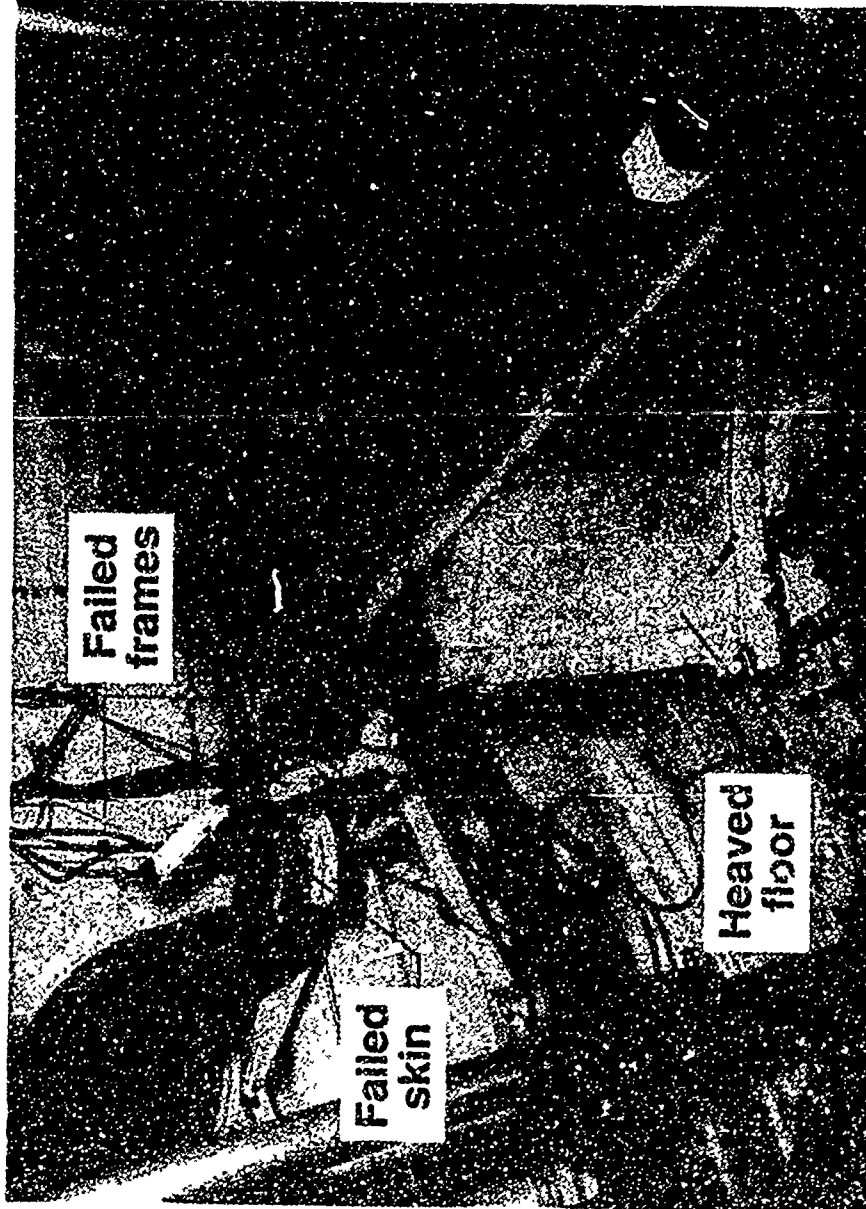
Figure 2. Interior of crashed CH-47 helicopter.
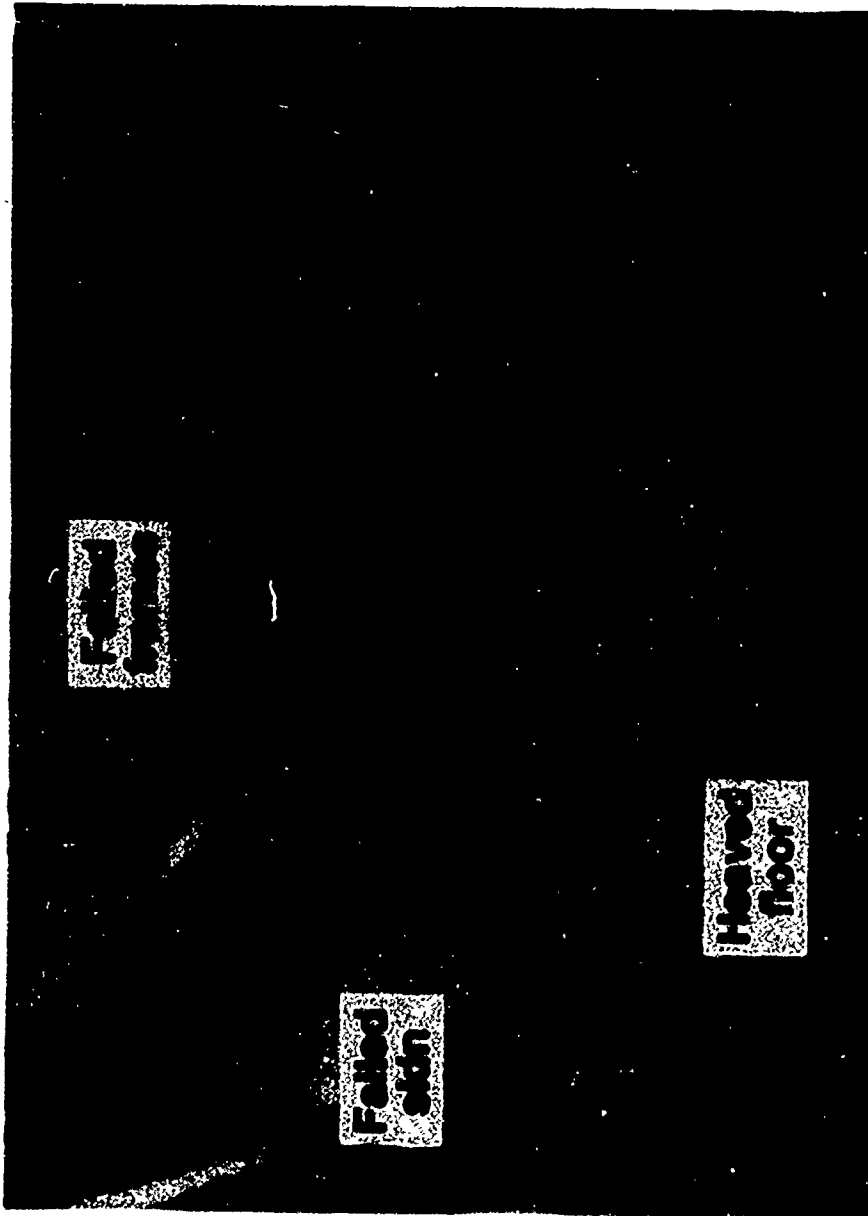
Figure 2. Interior of crashed CH-47 helicopter.

the non-crash loads. If the fuselage frames and skins are not designed to carry these crash-induced loads, then large deformation or failure of the fuselage structure is possible. The rear portion of the CH-47, depicted in Fig. 1, experienced large deformations and failure of the protective shell.

In the next generation of military helicopters, composite materials will be used extensively in all primary structure. Composite materials offer considerable advantages over metallic materials from the perspective of weight and fabrication cost. Composite materials and structures exhibit brittle failure characteristics, in contrast to the relatively benign ductile failure characteristics of most metallic structures. Therefore, prior to the design of the next generation of military helicopters, sufficient technology must be developed to design crashworthy fuselage structures utilizing composite materials.

The kinetic crash energy is primarily absorbed by the landing gear and the subfloor beam structure. A sketch of a utility helicopter showing the subfloor assembly consisting of frangible and energy-absorbing beams is depicted in Figure 3. These subfloor beams are also the principal load-carrying members that react the fuselage bending loads. Based upon current design practices for vehicles designed to meet the requirements of Mil-Std-1290, approximately 40 percent of the crash-related kinetic energy is absorbed by progressive crushing of the subfloor beam structure. However, energy-absorbing subfloor beams must be designed to perform the dual role of reacting the fuselage bending loads and progressively crush in a crash to minimize the weight of the fuselage structure. Three beam web designs that can be used to meet these requirements are the tangent-half circle (sine-wave) beam and circular and rectangular tube integrally stiffened beams, as in Fig. 4.

4

HELICOPTER FUSELAGE
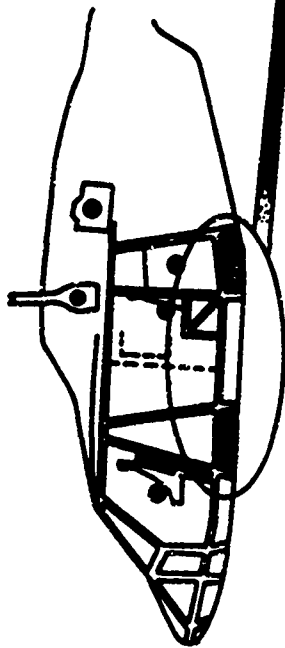
SUBFLOOR STRUCTURE

ENERGY-ABSORBING BEAM

Frangible structure

Energy-absorbing structure

Energy-absorbing beam web

Beam cap
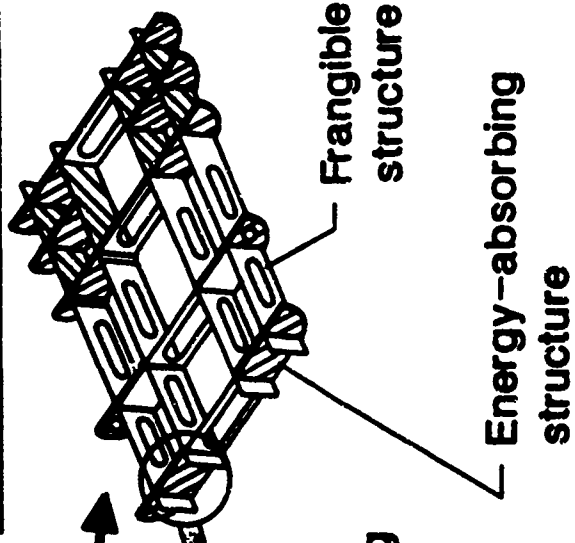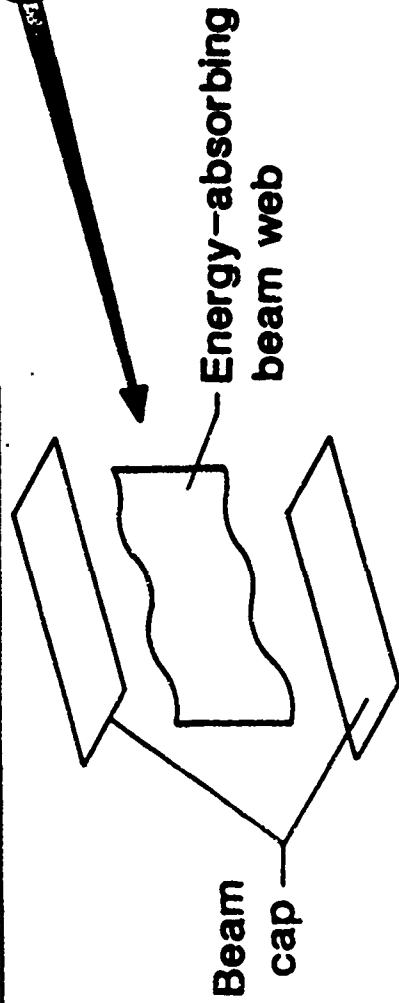
Figure 3. Energy-absorbing helicopter subfloor structure.
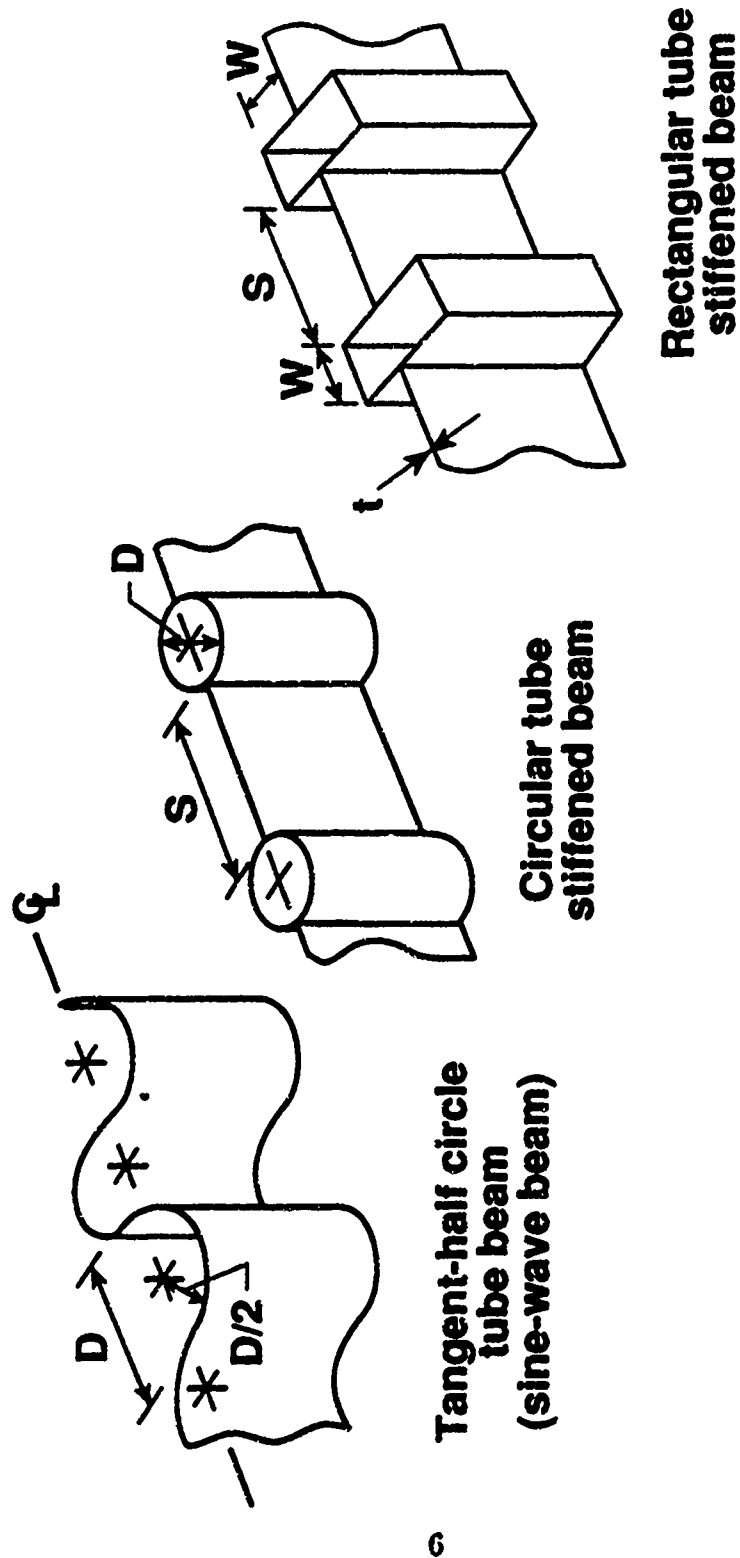
Figure 4. Energy-absorbing beam concepts (typical beam web construction).

6

Simple analytical tools and/or statistical data bases are typically utilized to design conventional composite structure. Only a small fraction of a comparable data base exists for energy-absorbing subfloor beams, and no analytical methods exist for the prediction of the energy-absorption capability of composite materials and structures. Development of sufficient data to establish a statistically valid design data base would be cost- and time-prohibitive. An alternative to the data base is the development of a method to predict the energy-absorption capability of subfloor beam structure.

An in-depth understanding of the cause and effect relationships of crash-energy absorption in composite materials and structures is necessary prior to the development of a method to predict the energy-absorption capability of subfloor beam structure. Tubular specimens with circular, near-elliptical, and square cross-sectional geometry, as depicted in Fig. 5, are crushed to evaluate the energy-absorption characteristics of composite materials. These tube-crushing tests are analogous to the material coupon tests used to characterize the mechanical properties of a material system. Once the material response is understood and analysis tools have been developed, efficient energy-absorbing structural subfloor beam concepts, such as those depicted in Fig. 4, can be designed in a manner consistent with conventional composite structure design practice.

1.2 Review of Pertinent Literature

Crash-energy absorption of composite materials and structures is a recently developed technology area. The initial research in this technology area began around 1976. Upon review of contributions by other researchers in this technology area,

Top view of near-elliptical tube

Near-elliptical cross-section tube specimen

Circular cross-section tube specimen

Square cross-section tube specimen
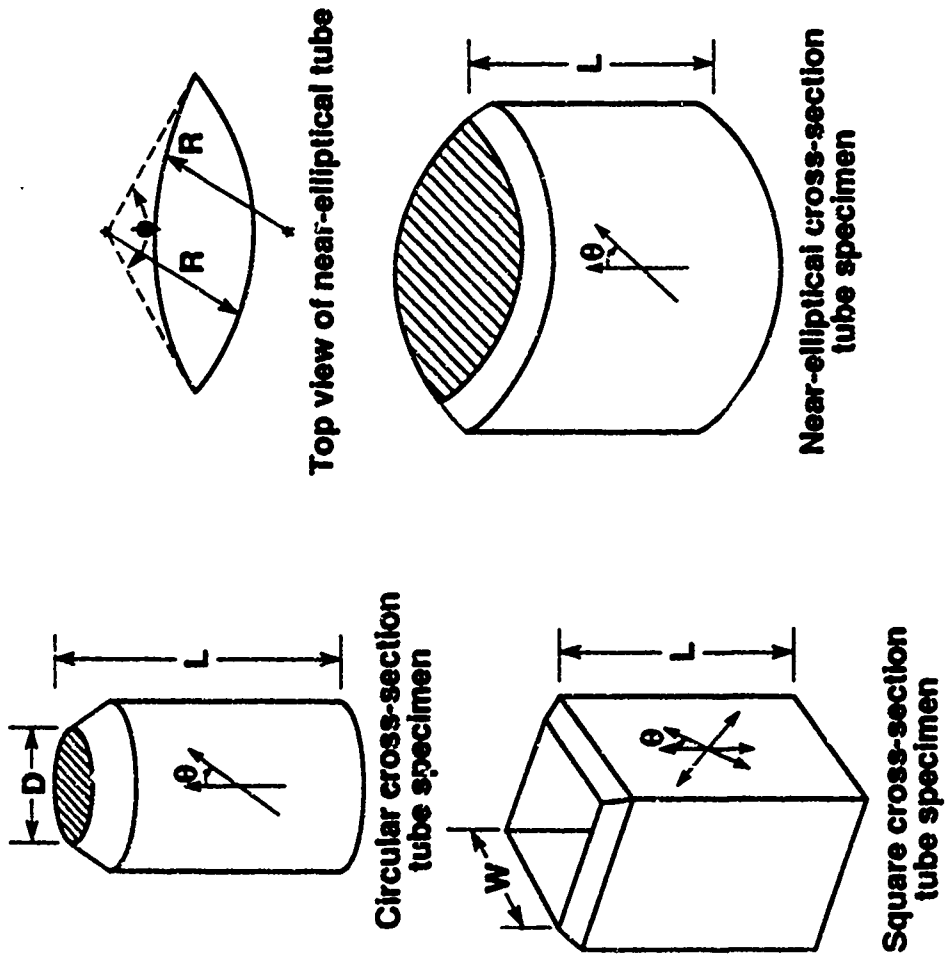
Figure 5. Typical composite tube specimens.

8

refs. 1-19, it is obvious that a very limited understanding exists of how composite materials absorb energy in a crash. As recent as 1983, D. Hull, ref. 6, stated that *"there was no scientific basis for selection of particular combinations of fibers, resin, etc.".* Hull further stated that there is, *"no physical understanding of the processes involved in the crushing although there has been a considerable amount of work all over the world on the microfracture of composite materials".* Fairfull and Hull, ref. 8, in 1987 reiterated a similar feeling in that *"there can be no universal relationship to predict the specific energy absorption of composite tubes".*

Without understanding the fundamental relationships that control the material and structural response, the designer of energy-absorbing structures must utilize a very limited data base of validated concepts which would result in less-than-optimum structures. Furthermore, to develop analytical tools to model the crushing response, an in-depth understanding of the fundamental mechanisms controlling the crushing response must be developed.

The number of individuals and/or research groups conducting research in this technical area is small. Five different research groups can be identified that have made significant contributions to the literature on energy absorption of composite material and non-sandwich subfloor concepts. These research groups and their respective leaders are: Ford Motor Co. (Thornton, refs. 2-4), University of Cambridge (formerly Liverpool University) (Hull, refs. 5-8), DFVLR (Kindervater, refs. 9-15), McDonnell Douglas Helicopter (Sen, refs. 16-19) and the U.S. Army's Aerostructures Directorate (Farley, refs. 20-27). One of the strongest proponents of crashworthiness in helicopters is J. D. Cronkhite of Bell Helicopter Textron,

9

Inc. Cronkhite has made significant contributions to the area of crashworthiness although he has contributed sparingly to the literature pertaining to the crushing response of composite material and non-sandwich subfloor beam concepts.

The review of pertinent literature will be listed by research groups. The literature review will be focused upon energy-absorption characteristics of composite materials with continuous reinforcements and the energy-absorption characteristics of non-sandwich subfloor concepts. Discontinuous fiber-reinforced composites are not applicable to primary helicopter structure because of their lower specific mechanical properties.

1.2.1 Thornton

Thornton and others, refs. 2-4, have investigated the crushing characteristics of graphite-, Kevlar-, and glass-reinforced composite materials. The application of this research is for the automotive industry. Thornton evaluated the material-crushing response of composite materials using circular, square, and rectangular cross-section tube specimens. Studies were conducted to investigate how different material and specimen structural parameters influence energy-absorption capability. These studies included the effects of specimen geometry, ply orientation, crushing trigger mechanism, crushing speed, and reinforcement fiber.

Thornton, refs. 2 and 3, showed that composite materials can be efficient energy absorbers. Energy-absorption capability was determined to not be a function of crushing speed for the specimens evaluated. However, crushing speed was found to affect energy-absorption capability of other materials and specimen

geometry by Berry and Hull, ref. 7, Kindervater, ref. 10, and Farley, ref. 21. Specimen tube geometry, specimen extensional stiffness, and ply orientation were determined to influence energy-absorption capability. However, these studies were of limited scope, and general energy-absorption trends were not readily definable. Thornton also concluded that Kevlar and Kevlar-hybrid composites exhibit unstable crushing response and are not suitable energy-absorbing materials. This conclusion was shown to be inaccurate for other hybrid configurations by Kindervater, ref. 9, Bannerman and Kindervater, refs. 11 and 12, Sen, ref. 16, and Farley, refs. 20, 23, and 26. Specimens fabricated by Thornton from unidirectional prepreg were determined to produce higher energy-absorption capability than woven material. Farley, refs. 20 and 23 found that for certain combinations of fiber and matrices, woven materials could exhibit superior energy-absorption capability to tubes fabricated from unidirectional material. Thornton described the brittle-fracturing-crushing mode that is exhibited by certain graphite-and glass-reinforced composite materials. The local buckling mode exhibited by Kevlar-reinforced composite materials was also described. Thornton attempted to develop an understanding, from a mechanistic perspective, of how composite materials absorb energy. Thornton was one of the pioneering researchers in this technology area and has made many contributions.

1.2.2 Hull

Hull and others, refs. 5-3, conducted several studies on the energy-absorption capability of glass-reinforced composite materials. Hull, attempted to discuss the crushing of composite materials based upon mechanisms. Berry and Hull in ref. 7

11

made a valuable finding in determining that composite materials energy-absorption capability can be a function of crushing speed. They experimentally determined that energy-absorption capability was a logarithmic function of crushing speed for the woven glass-reinforced composite specimens tested. The energy-absorption characteristics as a function of crushing rate are attributed to the strain-rate sensitivity of the critical Mode I strain energy-release rate (G) of the glass-reinforced composite specimens.

Fairfull and Hull, ref. 8, investigated the effects of tube diameter (D) and wall thickness (t) on the energy-absorption capability of woven glass-reinforced epoxy tubes. In their study, it was determined that, as D/t increases, energy-absorption capability decreases in a nonlinear fashion. These findings are similar to those reported by Farley, ref. 24, for graphite-epoxy and Kevlar-epoxy tubular specimens. Fairfull and Hull further identified three different crushing modes. These modes were described as Type I - a long single central interlaminar crack whose length is greater than the thickness of the wall of the tube, Type II - a central interlaminar crack whose length is less than the thickness of the tube wall, and Type III - no central interlaminar crack with the tube wall bending outward from the center of the tube. The Type I crushing mode is similar to that reported by Farley, ref. 22, as a lamina bending mode, while the Type II and III modes seem to be combination of more fundamental crushing modes and geometry-related failure modes. Finally, Fairfull and Hull, ref. 8, stated that *"friction in the crush zone and between specimen and platen accounts for a significant proportion of the overall level of energy dissipation"*.

12

1.2.3 Kindervater

Kindervater and others, refs. 9-15, conducted several studies investigating the crushing response of composite material and helicopter subfloor beam concepts. Kindervater investigated the effect of reinforcement fiber, ply orientation, crushing trigger mechanism, and crushing speed on the energy-absorption capability of composite materials. Kindervater concluded that $\pm$ 45 graphite-epoxy specimens had the highest energy-absorption capability of all specimens evaluated. Farley in refs. 20, 21, 23, and 26 has shown alternative ply orientations exhibit energy-absorption capability superior to the $\pm$ 45 ply orientations. Crushing trigger mechanism and crushing speed were also determined to influence energy-absorption capability. Kindervater did not discuss crushing mechanisms or address what properties control the crushing response.

Kindervater has evaluated several energy-absorbing subfloor-beam concepts, such as sine-wave and integrally stiffened beams. Kindervater concluded that the composite subfloor beams are good energy absorbers relative to metallic beams. Geometrically unsymmetric beam concepts exhibited predominantly column instability collapse modes. Sine-wave beams were determined to be excellent energy absorbers that exhibited progressive crushing behavior. A relatively constant crushing load was achieved as well as a progressive crushing response. The specific energy-absorption capability of the composite sine-wave beams was comparable to, and in some cases substantially better than, metallic beams.

1.2.4 Sen

Sen and others, refs. 16-19, investigated the crushing response of composite

materials and subfloor beam concepts. Tube specimens were used to evaluate material crushing response. The parameters investigated in the material tests were ply orientation, reinforcement fibers, and tube geometry. Sen concluded that Kevlar-reinforced composites were superior energy absorbers to graphite-reinforced composite materials and $\pm$ 45 ply orientations produced higher energy-absorption capability than other ply orientations. Sen showed that energy-absorption capability was a nonlinear function of diameter-to-thickness ratio for Gr-E composite tubes. The mechanisms that control the crushing process were not discussed.

Sen evaluated the energy-absorption capability of foam sandwich and monolithic subfloor beams. Sen concluded that the sandwich beam concepts are superior energy absorbers as compared to sine-wave and integrally stiffened concepts. However, Kindervater, ref. 15, and Farley, ref. 26, have presented data to show sandwich beam concepts are significantly less efficient energy absorbers than sine-wave or integrally stiffened concepts.

1.2.5 Summary

It is difficult to develop a consistent rationale for the crushing response of composite tubes and beams based upon the results of the previously mentioned studies. These studies have not gone deeply enough into the problem to uncover the vital signs of the phenomena. Interpretations based on sparse data bases have often been erroneous and misleading. The fifth researcher is the author of this dissertation. One of the objectives of the author's research is to develop a consistent understanding of the crushing response of composite materials. The

14

research that has been conducted in this technology area, refs. 20-27, is included in the dissertation along with other material.

1.3 Objective, Scope, and Approach of Research

Previous researchers have yet to determine the fundamental relationship between material and structural variables and the crushing response. Therefore, prior to the application of this technology to helicopter or automotive applications in a routine design process, considerable understanding of the basic cause-effect relationship must be developed.

The objective of this research is to develop a method of predicting the energy-absorption capability of composite subfloor beam structures. A sketch of a representative helicopter, subfloor assembly, and energy-absorbing beam is depicted in Fig. 3. However, it is first necessary to develop an in-depth understanding of how composite materials absorb energy, how material and structural variables influence energy-absorption capability, and how the material-crushing response is related to the crushing behavior of structural elements.

The scope of this research consists of material and structural characterization of tubular specimens as well as the experimental evaluation and analytical prediction of the crushing response of subfloor beam concepts. Tubular specimens were circular, square, and near-elliptical in cross-sectional geometry as in Fig. 5. The near-elliptical tubes depicted in Fig. 5 are elliptic-like cross-section tubes composed of circular-shaped halves whose centers are not coincident. The beam concepts were tangent-half circle tubes (henceforth denoted as sine-wave) and integrally

15

stiffened, as in Fig. 4. The integrally stiffened beams consisted of tubular elements connected by flat webs. The material and structural characterization of tubular specimens in this investigation consists of 1) defining the crushing characteristics of composite materials, such as the modes, processes, and efficiency, and relating these crushing characteristics to understandable mechanistic phenomena; 2) determining the cause and effect relationship of material and specimen structural variables on energy-absorption capability; 3) determining how crushing speed influences energy-absorption capability; and 4) developing an analysis capability to predict the crushing response of composite tube specimens. Specimen structural variables investigated are; fiber and matrix stiffness and failure strain, ply orientation, stacking sequence, fiber volume fraction, hybridization, and specimen geometry.

In the subfloor beam concept phase, only sine-wave and integrally stiffened beams, as depicted in Fig. 4, will be evaluated. Energy-absorption trends of beam specimens will be determined and compared with energy-absorption trends of tube specimens. The relative energy-absorption efficiency of the different subfloor beam concepts will be determined. A method for predicting the energy-absorption capability of subfloor beams will be developed. Comparison of predicted and measured energy-absorption capability will be performed for sine-wave and integrally stiffened subfloor beams.

The energy-absorption process in composite materials is a complex sequence of local failures. Ideally, analytical methods would be utilized to guide the investigation of important material property and geometry issues related to the energy-absorption process. However, prior to this investigation, accurate analytical modeling of the

16

energy-absorption process was impossible because of a lack of understanding of the fundamental mechanisms controlling the crushing response. Therefore, investigation of the crushing response of composite materials and structural elements must be initially accomplished by experiment. Once an understanding of the basic phenomena that control the crushing process has been developed, an analytical capability can be devised. Circular, near-elliptic, and square cross-section tubular specimens, as depicted in Fig. 5, are used to investigate the crushing response of composite materials. Representative subfloor beam webs, such as the sine-wave and integrally stiffened beam web concepts, as depicted in Fig. 4, are used to study the structural response and validate the prediction method.

1.4 Organization of the Dissertation

In Chapter 2, the fabrication methods used to produce the tube and beam test specimens are described along with the static and dynamic test methods and test equipment. In Chapter 3, how the material and structural variables influence crushing response is discussed. Furthermore, the effects of crushing speed are described. The finite element analysis method for modeling the crushing response of tube specimens and the analytical predictions is described in Chapter 4. The finite element discussion includes (1) how the tube specimens and the different crushing mechanisms were modeled and (2) prediction of energy-absorption capability of selected specimens. An experimental and analytical evaluation of subfloor beam concepts is given in Chapter 5. Finally, in Chapter 6, this investigation is summarized including conclusions and a discussion of future work.

17

Chapter 2 - SPECIMEN FABRICATION METHODS, TEST EQUIPMENT, AND PROCEDURES

2.1 Specimen Fabrication Methods

Making high-quality parts using composite materials still requires a considerable level of craftsmanship on the part of the fabricator. The government and industry have expended a vast amount of resources in the last two decades to make the fabrication process of composite materials governed by science rather than by the proficiency of an individual. Structural shapes as simple as tubes can pose considerable problems even for the experienced composite fabricator. Therefore, a cost-effective method of fabricating tubular test specimens was one of the first steps taken in investigating the energy-absorption capability of composite materials. The variables evaluated were extensive and included; layup method, processing procedure, and material form.

2.1.1 Composite Tube Specimen Fabrication Method

The circular cross-section tubes were fabricated using a solid metal mandrel. Mandrels were typically machined to lengths of 2 to 3 feet because multiple tube specimens were machined from a single long tube. A conventional release agent, appropriate for the composite material, was first applied to the mandrel. Composite material in the form of resin-impregnated fiber in either a unidirectional or planar woven cloth, henceforth denoted as prepreg, was wrapped around the mandrel, using a "table wrapper".

18

A table wrapper is a machine that facilitates the tight and uniform wrapping of the prepreg around the mandrel. The prepreg, prior to being wrapped on the mandrel was laid-up in sheets, denoted as step 1 in Fig. 6, of dimensions equal to the length of the tube and having a width equal to the distance of the total number of revolutions about the mandrel required to produce the appropriate number of layers. Sheets of prepreg were laid-up in this manner for each different ply orientation in the layup. The second step, depicted in Fig. 7, was to stack the prepreg sheets on top of each other in the appropriate sequence with the beginning of each sheet staggered approximately 90 to 120 degrees around the circumference of the tubes from the previous sheet. The third step consists of wrapping the stack of prepreg sheets about the mandrel using the table wrapper, as depicted in Fig. 8. Once the prepreg was tightly wrapped around the mandrel, a peel ply was overwrapped followed by a layer of teflon. A heat-sensitive shrink tube was slid over the mandrel-prepreg assembly, and a heat gun was used to initially shrink and smooth the tubing onto the mandrel-prepreg assembly. The assembly was then placed vertically in an oven for curing. As heat was applied, the tubing shrinks and applies pressure to the composite. The time versus oven temperature profile is dependent on specimen and material thickness.

The aforementioned process was used to fabricate all circular cross-section composite tubes. Initially, several other processing methods were also evaluated, such as filament winding of tow prepreg to achieve a uniform layup of material, wrapping shrink tape around the composite material instead of using shrink tubing, and autoclave curing of the composite tubes instead of the use of shrink tubing and a oven. The table-wrapping-shrink-tubing-oven process produced the best results

19
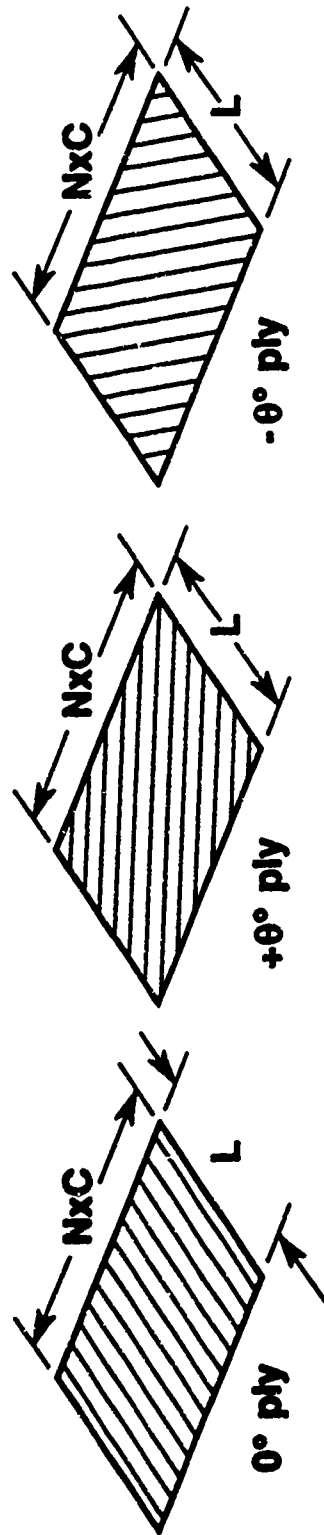
L - length of tube
C - circumference of mandrel
N - number of sets of layers

NxC

L

0° ply

NxC

L

+θ° ply

NxC

L

-θ° ply

Figure 6. Step 1 of layup sequence for $[0/\pm\Theta]_N$ composite tube.
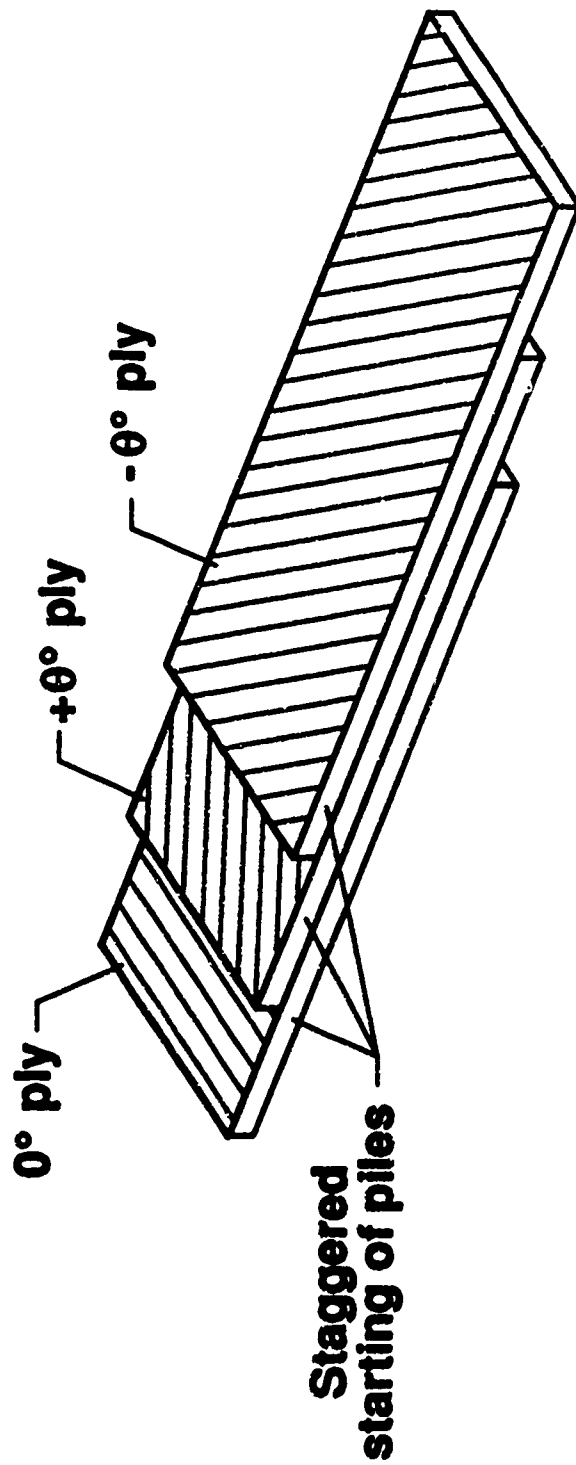
Figure 7. Step 2 of layup sequence for $[0/\pm\Theta]_N$ composite tube.

-Θ° ply

+Θ° ply

0° ply

Staggered
starting of plies
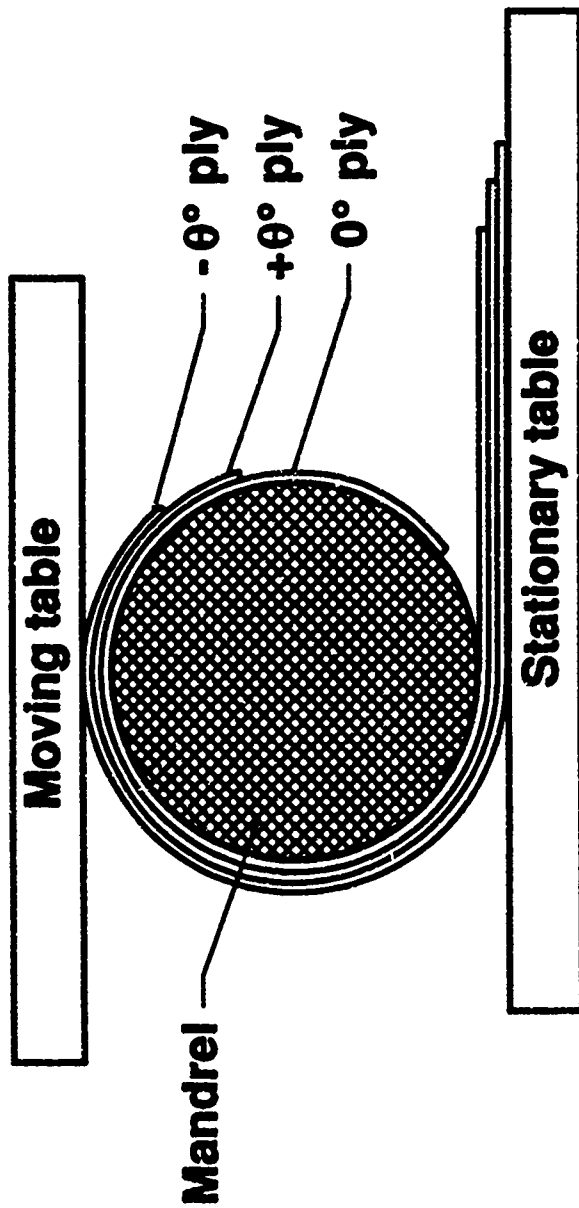
Figure 8. Step 3 of layup sequence for $[0/\pm\Theta]_N$ composite tube.

during the fabrication evaluation process in this study. However, with increased experience and more modern equipment (e.g., a filament winder) than was available at the time of the fabrication evaluation, the other techniques could be utilized to produce high-quality composite tubes.

After the tube was processed, it was removed from the oven and the mandrel extracted. Individual tube specimens were machined from the long tube. Typically, the tubes were machined to lengths of 10.16 cm and one end was chamfered at a 60 degree angle, as depicted in Fig. 9. The chamfer was incorporated for all composite specimens to limit the initial failure load and initiate the crushing process. Chamfering on the end of the tube reduces the cross-sectional area of the tube that is initially subjected to an applied load. The load required to fail the chamfered region of the tube is much less than the load that would cause catastrophic failure of the tube. Therefore, the crushing should initiate at the chamfered end of the tube.

The near-elliptical cross-section tube specimens, in Fig. 5 on p. 8, are ellipse-like cross-section tubes composed of circular-shaped halves whose centers are not coincident. These near-elliptical cross-section tubes were fabricated by a different method than the circular cross-section tubes. Prepreg sheets were laid-up in the same manner as the circular cross-section tubes. However, the prepreg stack was hand wrapped around the mandrel. After the prepreg was wrapped around the mandrel and followed by the peel ply and teflon layer, then the tube was bagged and cured in an autoclave in a conventional manner. Shrink tubing produced non-uniform compaction of the prepreg so this approach was not used. The autoclave
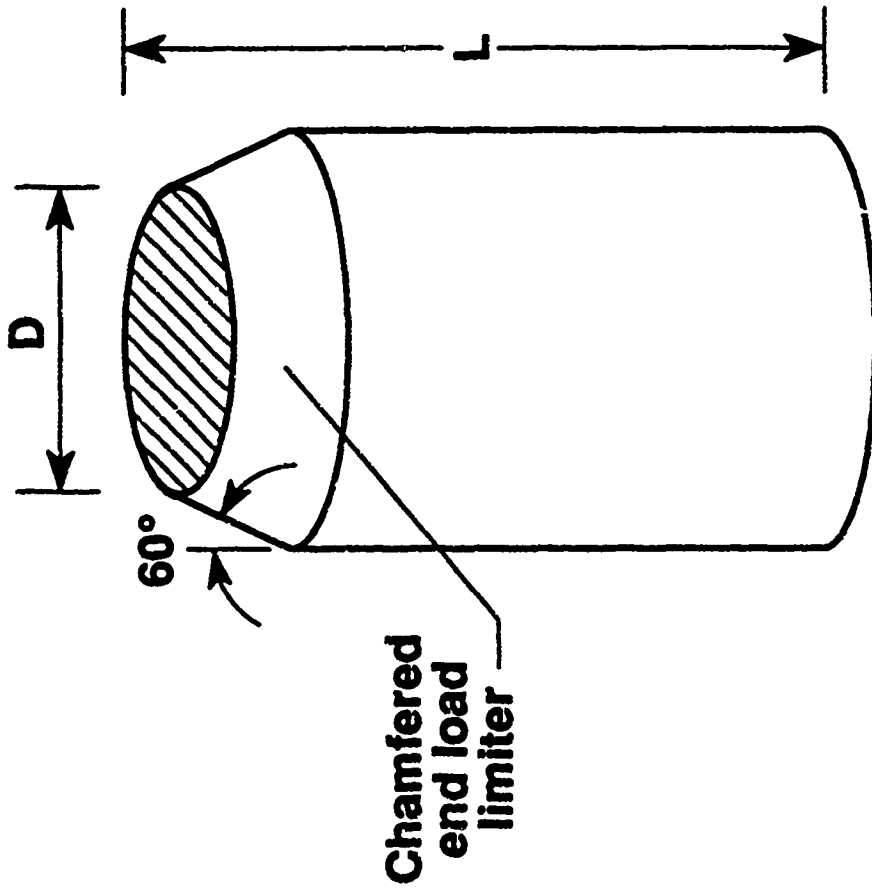
Figure 9. Typical chamfered region of tube specimen.

cure cycle was dependent on both specimen thickness and material. After the tubes were cured, the mandrel was extracted, and the tube specimens were machined from the tube as previously described for the circular cross-section tube specimens.

A "trapped rubber" mold technique was used for all square cross-section tubes to uniformly apply pressure to the composite for curing. A sketch of a typical square cross-section tube specimen is shown in Fig. 5. The prepreg was cut, stacked, and wrapped around a square cross-section metal mandrel. Flat metal plates were positioned on the outside of each surface of the tube to assist in obtaining uniform compaction of the prepreg at the corners of the tube and produce a smooth outer surface on the square cross-section tubes. The metal plates were coated with a release agent and positioned on the prepreg exterior. Shrink tubing was applied over the assembly and heated to hold the metal plates in place. This assembly was inserted in a circular cross-section silicon rubber mold. The rubber mold had a square cross-section hole which was slightly larger than the mandrel-prepreg-metal-plate assembly. The rubber mold and composite were then inserted in a circular cross-section pipe, and the ends were clamped. The pipe was then placed vertically in an oven to cure. The time versus oven temperature profile to cure the composite was dependent upon the material and thickness of the specimen. After the composite tube was processed, the mandrel was extracted, and tube specimens were machined to length and one end was chamfered.

2.1.2 Aluminum Tube Specimen Fabrication Method

The aluminum tube specimens were machined from a long section of constant-wall-thickness extruded tube stock. Ends of the tube specimens were machined flat

25

and parallel. No chamfering was machined on either end of the aluminum tubes because the tubes will not catastrophically fail as is possible with the composite tubes.

2.1.3 Composite Beam Specimen Fabrication Method

Both the sine-wave and integrally stiffened beam concepts, as depicted in Fig. 4 on p. 6, were fabricated using conventional "hard" tooling, bagging, and autoclave cure processing methods. Once cured, the sine-wave beams were machined to final dimension. The top of the beam web, similar to the tube specimens, and the non-chamfered edge was mounted in a room-temperature curing epoxy compound. More discussion of the beam geometry is provided in Chapter 5. The integrally stiffened beams were fabricated in symmetrical half sections and secondarily bonded together using a room-temperature curing adhesive (EA-934). The beams were machined to final dimensions, chamfered, and the non-chamfered end mounted in a room-temperature curing epoxy compound.

2.1.4 Aluminum Beam Specimen Fabrication Method

Integrally stiffened aluminum beams, similar to the beam concepts depicted in Fig. 4, were fabricated in symmetrical half sections using conventional metal cold-forming methods. After the beam halves were formed, they were heat treated to a T-6 condition. The beam halves were then secondarily bonded together with EA-934 adhesive, machined to final dimensions, and one end was mounted in a room-temperature curing epoxy compound. No chamfer was incorporated on the aluminum beams.

26

2.2 Test Equipment and Procedures

Static crushing tests of tubes and beams were conducted using conventional hydraulic loading frames and data acquisition equipment. High-speed crushing tests were performed using a modified closed-loop hydraulic loading frame that provided relatively constant crushing speed during the crushing process.

2.2.1 Static Test Equipment and Procedures

The test equipment used to load both tube and beam specimens consisted of universal hydraulic testing machines and automated data acquisition systems. In the static tests, only two channels of data, crushing force and crushing stroke, were recorded for each test.

The load platens of the test machine were set parallel to each other and perpendicular to the load axis. The specimen was centered on the lower test machine platen, and the upper load platen was lowered until it touched the specimen. During the initial part of the test, prior to the initial failure of the chamfered part of the specimen, the crushing rate was between 0.05 cm/min. and 0.08 cm/min. After the initial failure of the chamfered region and the crushing process initiated, the crushing rate was increased to between 0.5 cm/min. and 0.8 cm/min. Specimens were generally crushed in excess of 5.0 cm during a test with between 100 and 400 data points recorded during a test.

The crushing rate during the static tests varied slightly. Variation in crushing rate was due to operator error or inability to hold a setting in the time frame

27

available and control variability of the test machines. However, the differences in crushing rate are small relative to the Mil-Std-1290 maximum vertical impact speed of 12.8 m/sec (ref. 1).

Crushing force data were reduced to a specific sustained crushing stresses for comparative purposes. The specific sustained crushing stress is the average or sustained crushing force, as depicted in Fig. 10, divided by the product of the cross-sectional area and density of the tube. Inclusion of density in the energy-absorption capability parameter, specific sustained crushing stress, facilitates the comparison between materials of different densities. This parameter is analogous to the specific stiffness and specific strength properties used in comparing the mechanical properties of different material systems.

2.2.2 High-Speed Crushing Test Equipment and Procedures

A closed-loop hydraulically operated impact system (CLHOIS), in Fig. 11, was used to crush composite tube specimens at constant crushing speeds between 0.01 m/sec and 12 m/sec and crushing forces up to 22 kN. The CLHOIS consists of a stationary and sliding platens mounted to a movable ram, as depicted in Fig. 12. Tube specimens 19.3 cm in length were positioned between the stationary and sliding platens, as in Fig. 12. The load cell was mounted in line with the hydraulic ram. When the sliding platen impacted the impact plate, the tube specimen is crushed between the sliding and stationary platens. The tubes were crushed at a constant crushing speed for approximately 10.2 cm. Entrapped air escape holes were incorporated in the design of the sliding platen to reduce any air spring effects that could occur during the dynamic crushing of a tube specimen. After the tube
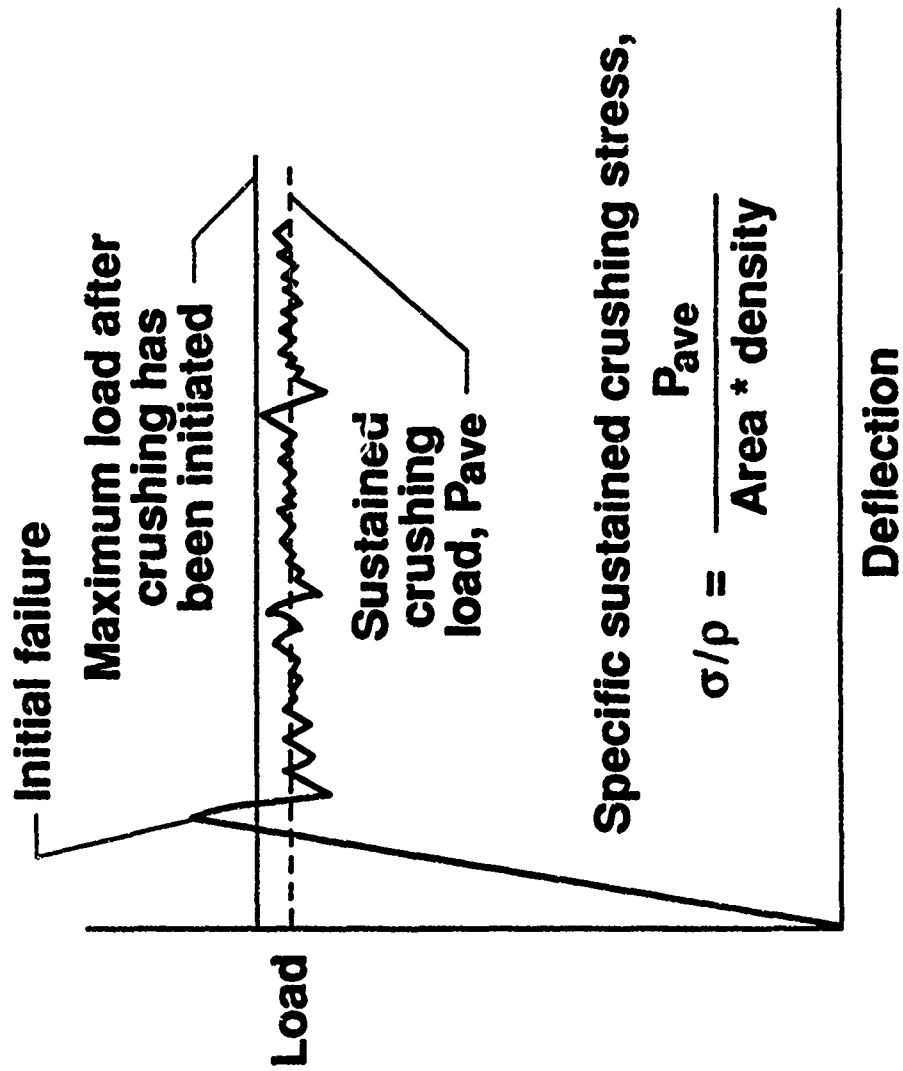
Figure 10. Schematic of load-deflection curve of composite tube specimen.

Figure 11. High speed test machine.

30

Figure 12. Close-up view of tube-crushing device.

Impact Plate

Ram

Sliding Platten

Protective Box

Stationary Platten

Crushed K/E Tube

31

Figure 12. Close-up view of tube-crushing device.

31
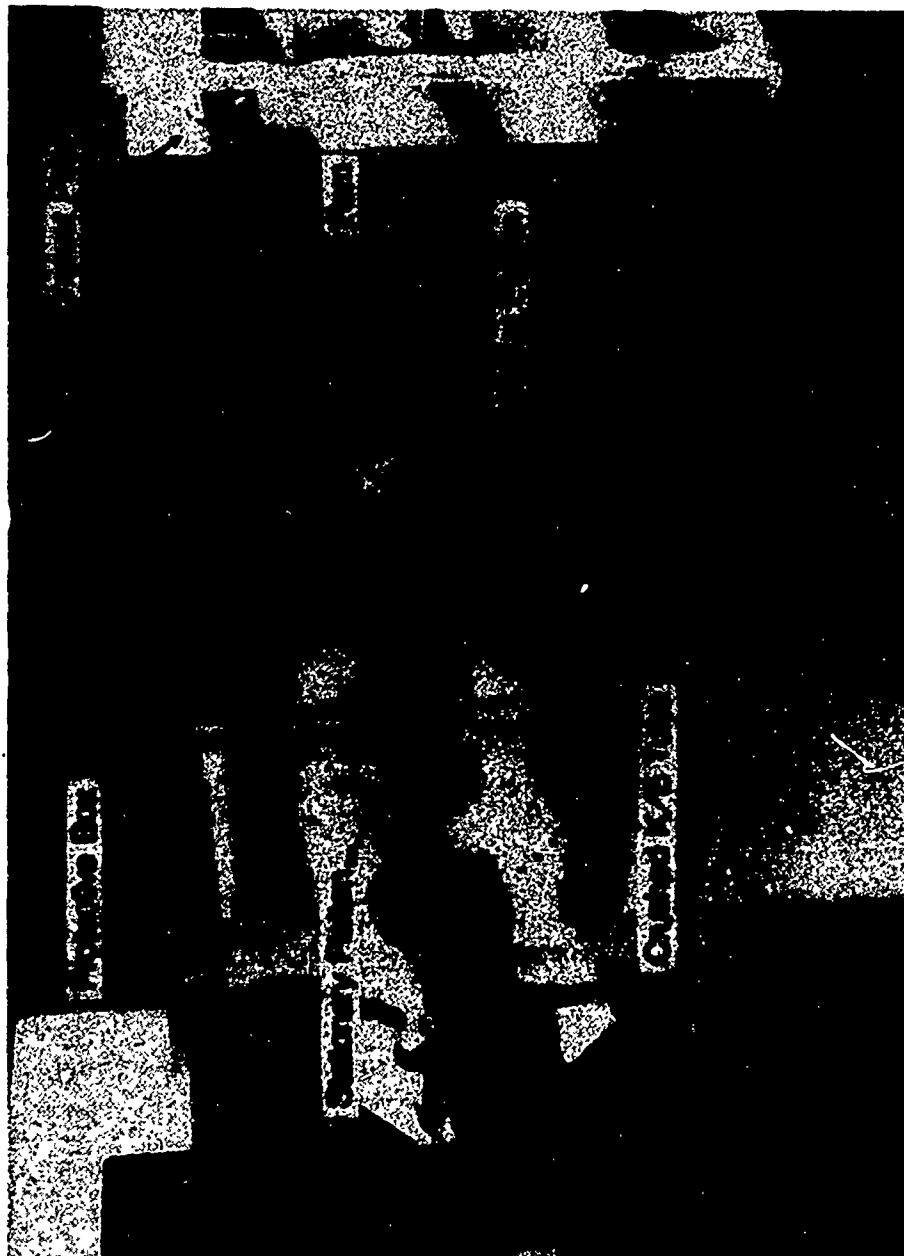
was crushed 10.2 cm, the ram was decelerated, stopped, and returned to its initial pre-firing position.

A 21 MPa hydraulic pressure supply provided the means to propel the ram and crushing apparatus at the required speed. The desired crushing speed was set prior to each test. A ram fire order was initiated, and hydraulic pressure accelerated the ram to the specified speed. The hydraulic feed-back loop was closed by a speed transducer feeding back ram speed to a signal conditioner. Actual ram speed was compared with specified values to produce any necessary changes in ram speed. The acceleration of the ram to the specified speed was achieved within 10.2 cm of ram travel. Crushing force and ram speed as a function of time were recorded on a high-speed storage oscilloscope. All force and speed data were subsequently stored on a removable mass storage device (floppy diskette) for later analysis.

A representative ram speed profile consists of an acceleration region, a constant-speed region, and a ram-deceleration region, as depicted in Fig. 13. Ram speed typically exceeds the set point speed during the acceleration of the ram. However, the ram is slowed down to the set point speed prior to the crushing of the tube. The tube is crushed during the constant-speed region. After the ram accelerated to the constant-speed region, the sliding load platen contacted the impact plate.

The first step in the procedure for dynamically crushing a tube consisted of mounting the tube in the crushing apparatus. The chamfered end was always positioned adjacent to the sliding platen. The required impact speed was set, and the storage oscilloscope was readied. An electronic trigger on the oscilloscope was
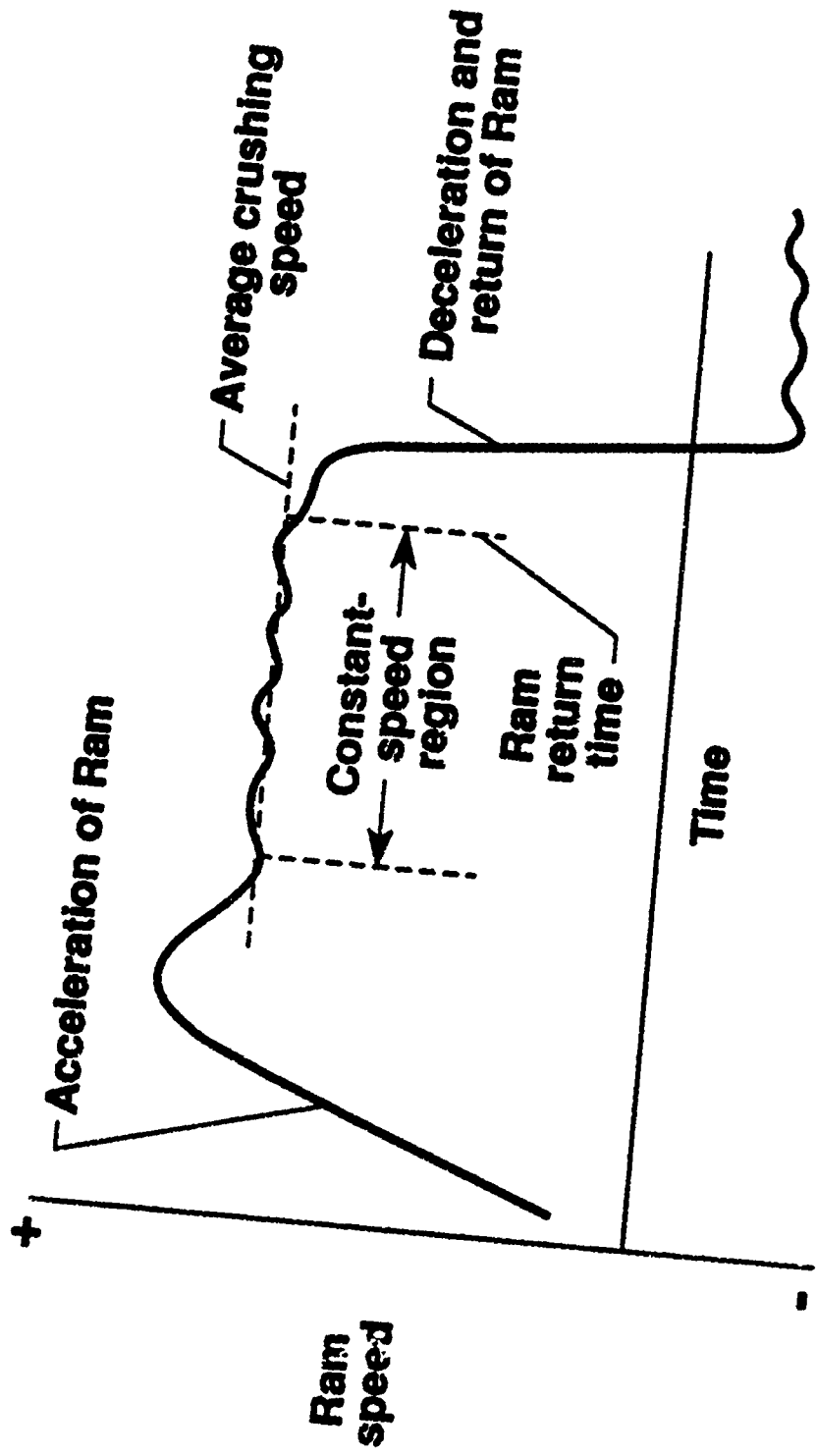
Figure 13. Typical ram speed profile.

33

set to trigger prior to the initial impact of the sliding platen on the impact plate. The CLHOIS and oscilloscope were set, and the system was fired.

The test data stored in the oscilloscope were transferred to a floppy diskette for subsequent analysis. From each test, ram speed and crushing force profiles as a function of time were developed similar to those depicted in Fig. 13. Approximately 2000 data points, evenly spaced in time, were recorded per ram speed and crushing force data channel. Within the time interval corresponding to a relatively constant velocity and uniform crushing response, the maximum, minimum, and average crushing force and ram speed were determined. Crushing force data were reduced to specific sustained crushing stresses for comparative purposes.

2.3 Summary

Several different methods were devised and evaluated for the fabrication of the three different cross-section composite tubular and composite beam specimens. The quality of the cured tubes was a strong function of the proficiency of the individual performing the different fabrication steps. The beam specimens were fabricated using conventional hard tooling, bagging, and autoclave curing procedures.

Tube specimens were tested at quasi-static and high crushing rates while the beams were tested only at quasi-static crushing rates. The quasi-static tests were conducted using conventional hydraulic loading frames while the high-rate crushing tests were conducted in a closed-loop hydraulically operated impact system.

process are presented. The crushing efficiency of composite materials is also discussed.

3.1.1 Crushing Modes

Four different crushing modes and combinations of the four modes have been identified for structural elements (tubes) made of composite materials. These four crushing modes are 1) transverse shearing, 2) brittle fracturing, 3) lamina bending, and 4) local buckling. The transverse shearing, brittle fracturing, and lamina bending crushing modes are exhibited exclusively by brittle fiber-reinforced composites, i.e., never by ductile fiber-reinforced composite materials. Both ductile and brittle fiber-reinforced composites can exhibit the local buckling crushing mode. Most specimens exhibit a combination of these crushing modes. These crushing modes are a function of the mechanical properties of the constituent materials and structure of the specimen. These four crushing modes are depicted in Fig. 14 by the crushed tubes and photo-micrographs of the cross section of the crushed tube wall. Each mode will be discussed in detail.

Transverse Shearing Crushing Mode. The transverse shearing mode is characterized by conical-shaped laminate cross section with one or multiple short interlaminar and longitudinal cracks which form partial lamina bundles. The crushing surface of the tube is scalloped, as in Fig. 15, such that load is not transfered uniformly across the surface of the tube. The principal energy-absorption mechanism is the transverse shearing of the edges of the lamina bundles as depicted in Fig. 15. The number, location, and length of the cracks are functions of specimen structure and

36
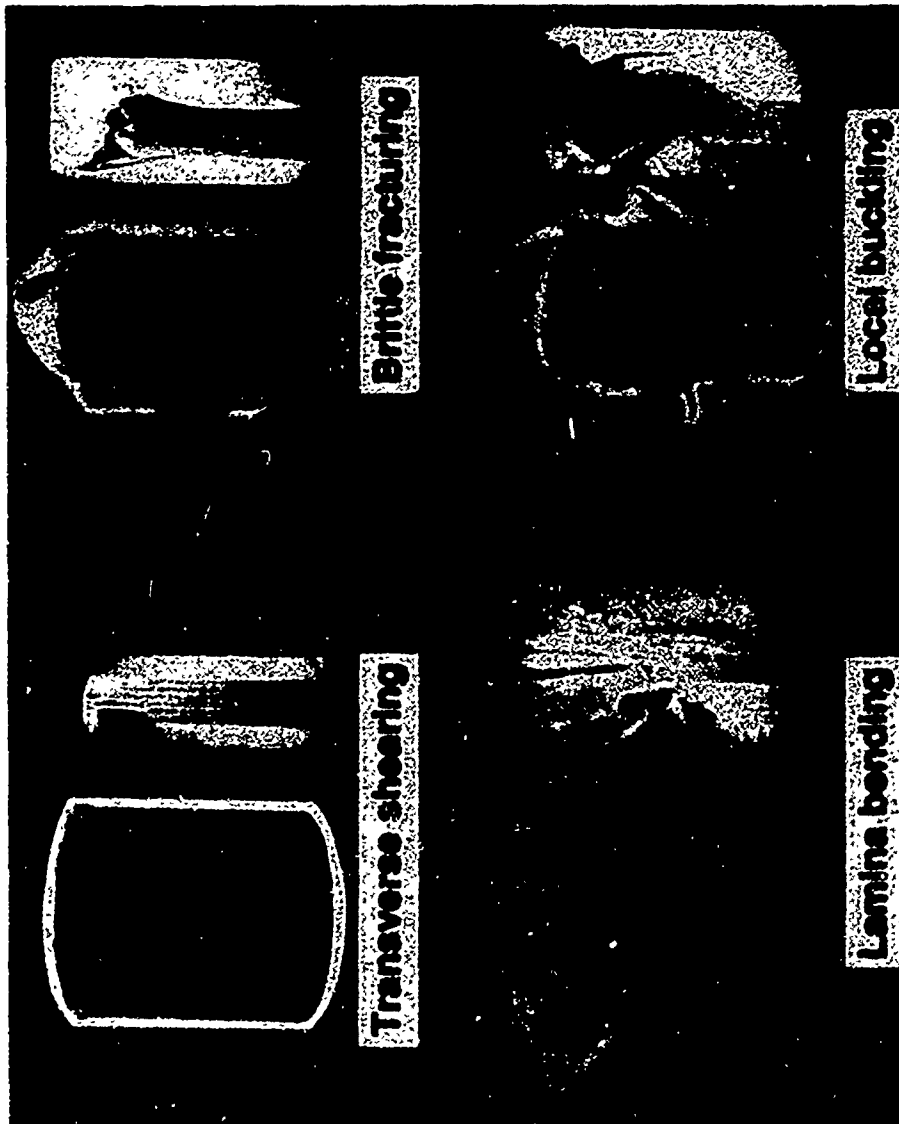
Figure 14. Four characteristic crushing modes of composite tubes.
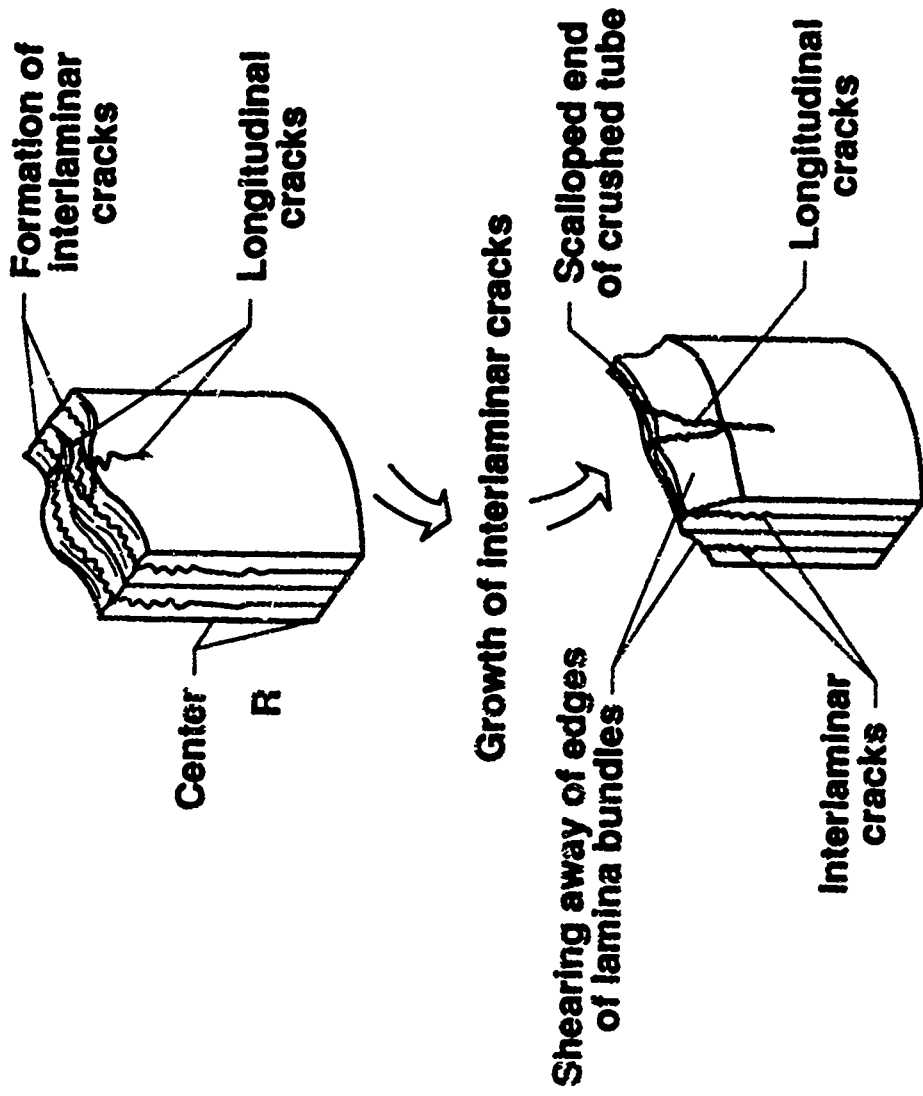
Figure 15. Crushing characteristics of transverse shearing crushing mode.
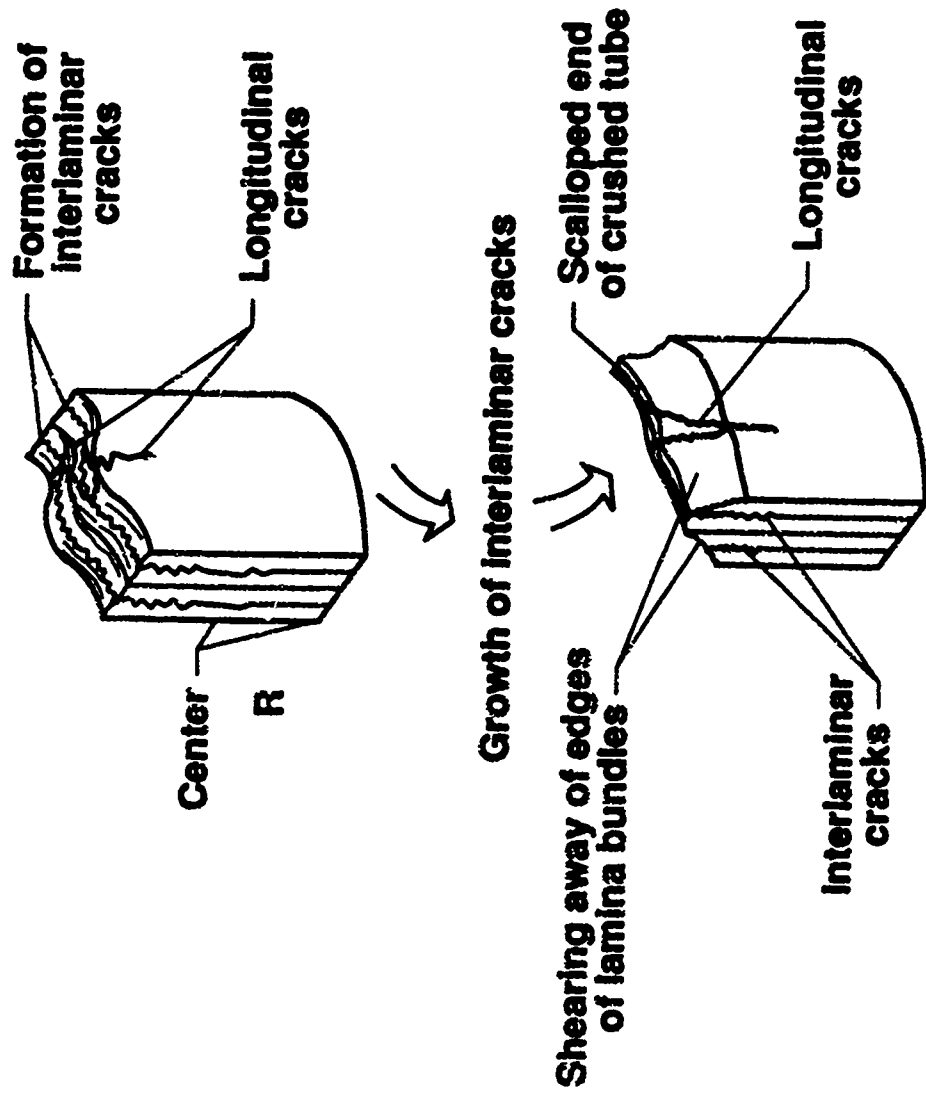
Figure 15. Crushing characteristics of transverse shearing crushing mode.

constituent material properties. The length of the interlaminar and longitudinal cracks is typically less than the thickness of the laminate. The interlaminar and longitudinal cracks form lamina bundles composed of a single lamina or multiple laminae. The lamina bundles act as columns to resist the applied load. As the load is applied, the interlaminar cracks grow until the edges of the column are sheared away forming a conical-shaped cross section as in Figs. 14 and 15. The short length of the failed material results in an efficient crushing mode.

Brittle Fracturing Crushing Mode. The brittle fracturing crushing mode exhibits similar crushing characteristics to the transverse shearing mode. The similarities between modes are (1) interlaminar and longitudinal cracks, (2) scalloped crushing surface, and (3) principal energy-absorption mechanism (failure of the lamina bundles) as depicted in Figs. 14 and 16. However, the length of the interlaminar cracks in the brittle fracturing crushing mode are between one and ten laminate thicknesses in length as compared to the only one laminate length in the transverse shearing mode. Long lamina bundles result in more material used in the fracture of each lamina bundle. The longer the fractured lamina bundle, the less efficient the crushing mode. Lamina bundles in the brittle fracturing mode exhibit some bending and usually fracture near the base. When a fracture of a lamina bundle occurs, the load is redistributed within the specimen and the cyclic process of crack growth and lamina bundle fracture is repeated.

Lamina Bending Crushing Mode. The lamina bending crushing mode is characterized by very long interlaminar, intralaminar, and parallel-to-fiber cracks, as in Figs. 14

39
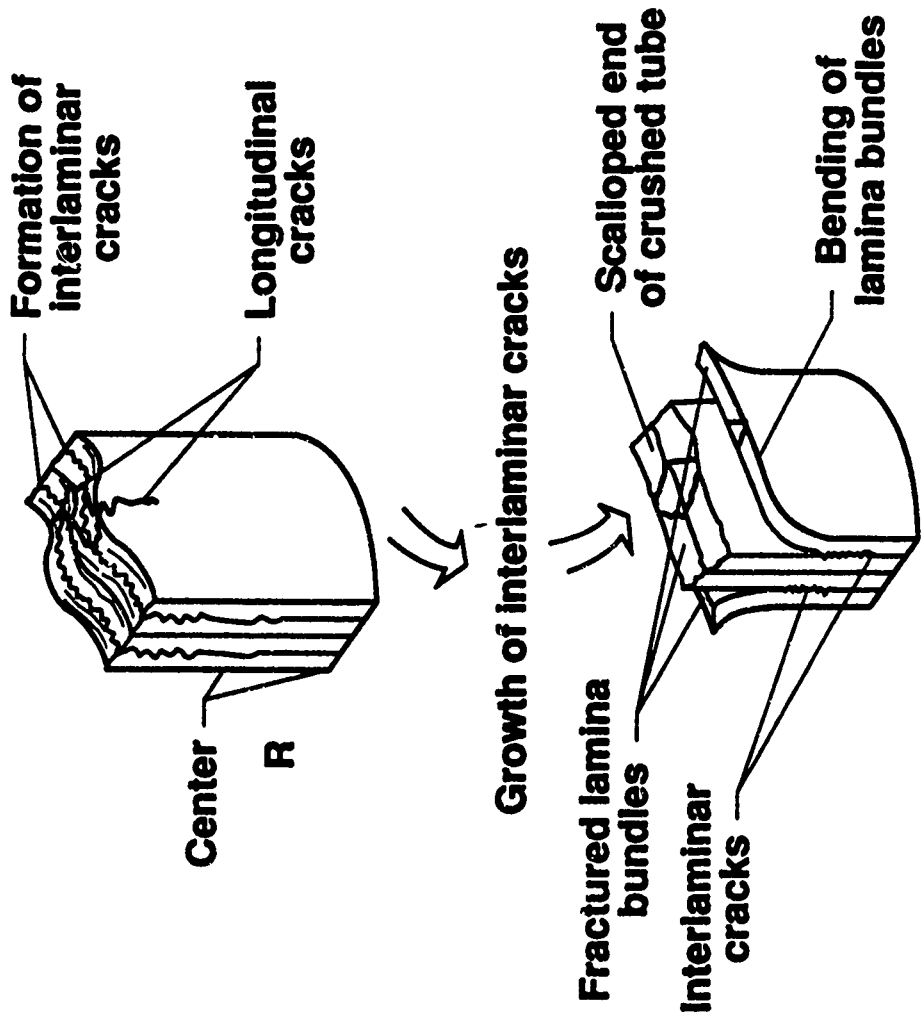
Figure 16. Crushing characteristics of brittle fracturing crushing mode.

and 17, but the lamina bundles do not fracture. The principal energy-absorption mechanism is crack growth. Whereas the interlaminar cracks form and grow at the interface of adjacent layers, the intralaminar cracks form and grow within individual layers. The parallel-to-fiber cracks propagate parallel to the fiber direction within a ply or within several adjacent laminae that have common fiber orientation. The lamina bundles exhibit significant bending deformation, but do not fracture. The length of the interlaminar, intralaminar, and parallel-to-fiber cracks are generally greater than ten times the laminate thickness. The long length of the lamina bundles and the lack of fracturing of the lamina bundles results in an inefficient crushing mode.

Local Buckling Crushing Mode. The local buckling mode exhibited by both brittle fiber-reinforced and ductile fiber-reinforced composite materials is similar to that exhibited by ductile metals. The crushing mode consists of the formation of local buckles, as depicted in Figs. 14 and 18, by means of plastic deformation of the material. Ductile fiber-reinforced composite materials (Kevlar) plastically deform at the buckle site along the compression side of the buckled fibers. The fibers can also split along the tension side of the buckled fibers and local delaminations between plies can occur. Ductile fiber-reinforced composites remain intact after being crushed and thereby demonstrate post-crushing integrity. The post-crushing integrity of ductile fiber-reinforced composites is a result of fiber and matrix plasticity (i.e., significant deformation without fracture) and fiber splitting. When the fibers are not fractured, the composite remains intact as opposed to the progressive failure of the material exhibited by the transverse shearing and brittle fracturing crushing modes.

41

Formation of Interlaminar & Intralaminar cracks

Parallel-to-fiber cracks

Center

R

θ

Growth of interlaminar & intralaminar cracks

Extensive bending of lamina bundles
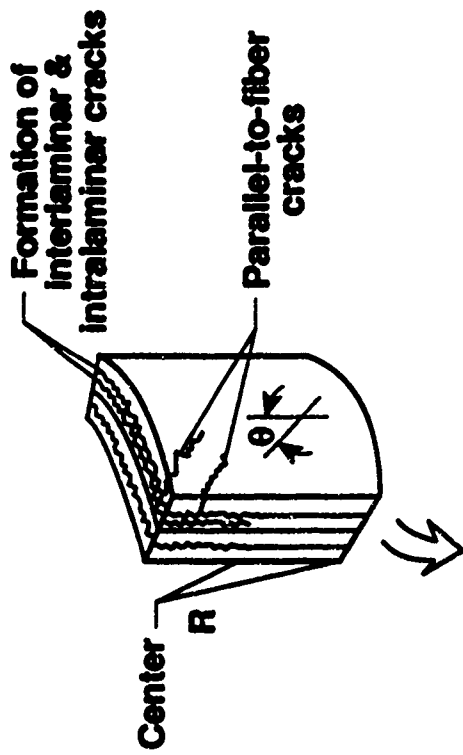
Interlaminar cracks

Intralaminar cracks
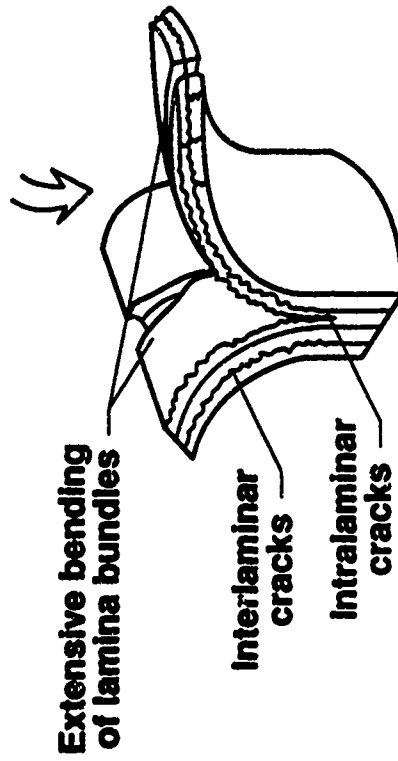
Figure 17. Crushing characteristics of lamina bending crushing mode.

42
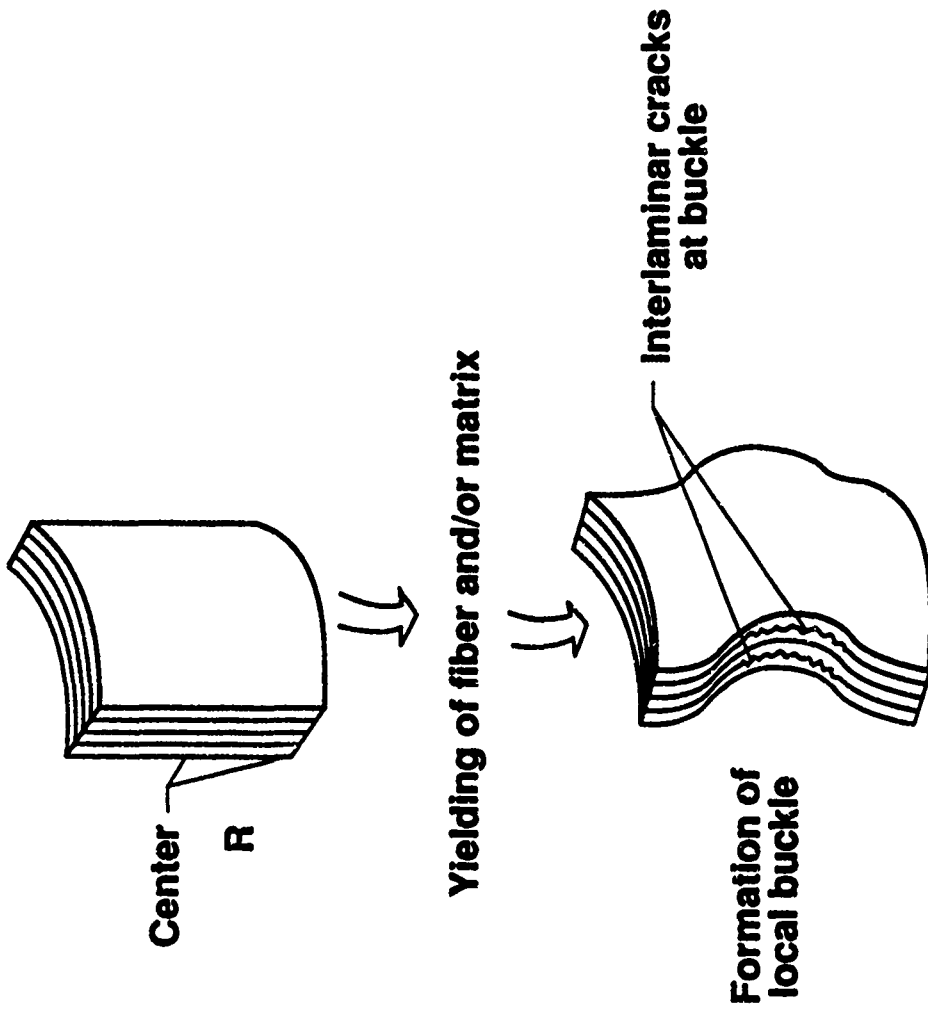
Figure 18. Crushing characteristics of local buckling crushing mode.

Center

R

Yielding of fiber and/or matrix

Interlaminar cracks
at buckle

Formation of
local buckle

43

Brittle fiber-reinforced composites exhibit the local buckling crushing mode only when (1) the interlaminar stresses are small relative to the strength of the matrix, (2) the matrix has a higher failure strain than the fiber, and (3) the matrix exhibits plastic deformation under high stress. Brittle fibers, by definition, do not have plastic stress-strain response. The high-failure-strain matrix reduces interlaminar cracks or prevent them from occurring in the crushing process. If the interlaminar cracks are eliminated, then the tube potentially can fail in a catastrophic manner. As the buckles form, interlaminar cracks can form at the buckle and propagate away from the buckle and along the tube.

The local buckling mode is generally an inefficient crushing mode for thin-walled specimens. The distance between the buckles for thin-walled tubes is large, typically in excess of ten times the laminate thickness, and only the material in the region of the buckle is plastically deformed. Therefore, the energy absorbed in thin-walled tubes by the local buckling mode is inefficient because only a small portion of the total energy-absorbing potential of the tube is used. The distance between buckles decreases as wall thickness increases resulting in an increased crushing efficiency.

Summary. Four characteristic crushing modes have been identified for tubes reinforced with continuous (not short) fibers. Except for tubes that crush in the local buckling mode, most tubes crush in a combination of the transverse shearing and brittle fracturing modes or brittle fracturing and lamina bending modes rather than any single mode. The principal crushing characteristics of the four modes are:

1. Transverse shearing - interlaminar cracks less than a laminate thickness in

44

length that form lamina bundles. The c ges of the lamina bundles progressively shear to form a conical cross section resulting in an efficient crushing mode.

2. Brittle fracturing - interlaminar cracks of a length between one and ten laminate thicknesses that form lamina bundles. The lamina bundles bend and fracture near the base of the interlaminar crack. The fracturing of the lamina bundles results in an efficient crushing mode.

3. Lamina bending - interlaminar, intralaminar, and parallel-to-fiber cracks of a length in excess of ten laminate thicknesses that form lamina bundles. The lamina bundles exhibit significant bending but do not fracture. The crack-growth, energy-absorption mechanism results in an inefficient crushing mode.

4. Local buckling - yielding of the fiber and/or matrix which produces buckles in the tube. The distance between buckles is large for thin-walled tubes. The local buckling mode is an inefficient crushing mode for thin-wall tubes. As the tube wall thickness increases, the crushing efficiency increases.

3.1.2 Crushing Process

Just as strain rate can affect the mechanical response of a material, crushing speed can affect the energy-absorption capability of structural elements fabricated from composite materials. To understand how crushing speed influences energy-absorption capability, it is necessary to determine how crushing speed affects the mechanisms that control the crushing process. The controlling mechanisms in the four crushing modes are: transverse lamina bending strength (transverse shearing crushing mode), matrix strength (brittle fracturing and lamina bending

45

crushing modes), lamina bundle tensile strength (brittle fracturing-crushing mode), and matrix nonlinear stress-strain response (local buckling-crushing mode). Each mechanism will be described in the following sub-sections.

Transverse Bending. The transverse bending strength of a lamina is primarily a function of fiber stiffness and strength. Therefore, if the fiber mechanical response is a function of strain rate, then the energy-absorption capability of specimens that crush in a transverse shearing mode should be a function of crushing speed.

Matrix Strength. Matrix strength controls the interlaminar, intralaminar, and parallel-to-fiber crack growth in both the brittle fracturing and lamina bending-crushing modes. Many polymeric matrix materials exhibit mechanical responses that are a function of strain rate. Therefore, a specimen that exhibits either the brittle fracturing mode or lamina bending mode can exhibit energy-absorption capability that is a function of crushing speed. Crushing speed will affect energy-absorption capability when the percentage of energy absorbed by the interlaminar, intralaminar, or parallel-to-fiber crack growth is a significant portion of the total energy absorbed. For that reason, specimens that crush in the lamina bending mode will have energy-absorption capabilites that are affected more by crushing speed than specimens that crush in the brittle fracturing mode.

Tensile Strength of Lamina Bundle. The tensile strength of the lamina bundle controls the fracturing of the lamina bundle in the brittle-fracturing-crushing mode. The mechanical response of the lamina bundle is primarily a function of the mechanical

46

properties of either fiber (e.g., 0 degree lamina bundle) or matrix (e.g., 90 degree lamina bundle or low fiber volume fraction material). Therefore, if the mechanical response of the dominant property (fiber or matrix) is a function of strain rate, then the energy-absorption capability of the lamina bundle can be a function of crushing speed.

Matrix Nonlinear Stress-Strain Response. The mechanism that controls the local buckling-crushing mode is the nonlinear stress-strain response of the fiber-matrix combination. Brittle fiber-reinforced composites can produce the local buckling crushing mode only if the matrix has a high failure strain. If the matrix mechanical properties are a function of strain rate, then the energy-absorption capability can be a function of crushing speed. The material property that controls the local buckling-crushing response of ductile fiber-reinforced composites can be either fiber or matrix stiffness. Therefore, if either the fiber or matrix mechanical response is a function of strain rate, then the energy-absorption capability can be a function of crushing speed.

Summary. The crushing response of composite tubes can be a function of crushing speed (strain rate). The mechanical properties of most matrix materials and of some fibers are a function of strain rate. Whether a tube's crushing response is a function of crushing speed is determined by whether the mechanical properties of the mechanism(s) that control the crushing process are a function of strain rate.

3.1.3 Crushing Efficiency

Debris size of crushed material (characteristic crushing length) is a qualitative

47

measure of energy-absorption efficiency. An estimate of the characteristic crushing length of specimens that exhibit the transverse shearing mode, the brittle fracturing mode, the lamina bending mode, and the local buckling mode are typically less than a laminate thickness, between one and ten laminate thicknesses, greater than ten laminate thicknesses, and greater than ten laminate thicknesses, respectively. The smaller the characteristic crushing length, the higher the energy-absorption efficiency.

The energy-absorption potential of a composite material is a function of the mechanical properties of the constituent materials. The crushing mode can be used as an indication of how efficiently a composite specimen is being crushed. Composite specimens fabricated from materials that have high energy-absorption potential can crush in an inefficient crushing mode (such as lamina bending) yet still have a higher energy-absorption capability than a composite specimen of the same geometry but fabricated with a material having a lower energy-absorption potential that crushes in an efficient crushing mode (such as transverse shearing).

3.1.4 Summary

The crushing response of composite materials exhibits multiple modes, and the mechanisms that control these different crushing modes are a function of the mechanical properties of the constituent materials and structure of the specimen. Crushing response of composite materials can be a function of crushing speed provided the mechanical properties of the mechanisms that control the crushing process are strain-rate sensitive. The characteristic crushing length defines the

efficiency of the crushing process. The smaller the characteristic crushing length, the higher the crushing efficiency.

3.2 Column-On-An-Elastic-Foundation Analogy

Whenever possible, it is instructive to relate a complex process, such as the crushing response of composite materials, to simpler processes that are more familiar as well as being more easily defined and predictable. These simpler processes need not necessarily incorporate all of the behavioral characteristics of the more complex process to be useful. It is sufficient in many cases for the simpler processes to provide only qualitative trends for the more complex response. For example, being able to predict, without the use of a sophisticated computer program, whether the sustained crushing force increases or decreases due to a change in material properties or structural variables would be beneficial for the designer of an energy-absorbing structure.

A simple problem that includes many of the important behavioral characteristics of the crushing response of composite material is the buckling of a column on an elastic foundation. The buckling load associated with the column on an elastic foundation exhibits changes similar to the sustained crushing force due to changes in material properties and specimen structure. That is, for a change in a material or structural parameter, both the buckling load and crushing force would either increase or decrease. The similarities in response of these problems, even though the column on an elastic foundation is an eigenvalue problem and the crushing problem is a boundary value problem, suggest that most of the important parameters that control the response of these problems are of similar form.

49

The column-on-an-elastic-foundation analogy is used only as a qualitative analogy to determine whether a change in a material or structural parameter will result in a higher or lower crushing force. This simple analogy is not being proposed as a method of predicting the crushing force or as a method to quantify the change in crushing force.

The equation for the buckling load of a column on an elastic foundation, as reported in ref. 28, is:

$$P_c = \left(\frac{N\Pi}{L}\right)^2 * EI + \left(\frac{L}{N\Pi}\right) * K_f \qquad (1)$$

where EI is the bending stiffness of the column which is the product of the extensional stiffness (modulus of elasticity, E) and the moment of inertia (I). The foundation stiffness (modulus) is K, L is the length of the column, and N is a positive integer related to the number of half waves of the buckled column.

The column-on-an-elastic-foundation analogy for the crushing of composite tubes is depicted in Fig. 19. The sustained crushing force is the summation of the crushing force on each layer. In this analogy each *"column"* would represent a layer.

In the case of the sustained crushing force (P_{sus}) of composite tubes, the coefficents of the stiffness terms in equation (1) must be modified. The change would consist of elimination of the square term on the *"column"* stiffness coefficient and moving the length (L) coefficient of the *"foundation"* stiffness to the denominator. The sustained crushing force (P_{sus}) of the tube is the summation of the sustained

50

Column on an elastic foundation

Tube

P

P_i

Cross section of tube wall

Layer	
i+1	
Layer i	
3	
2	
Layer 1	
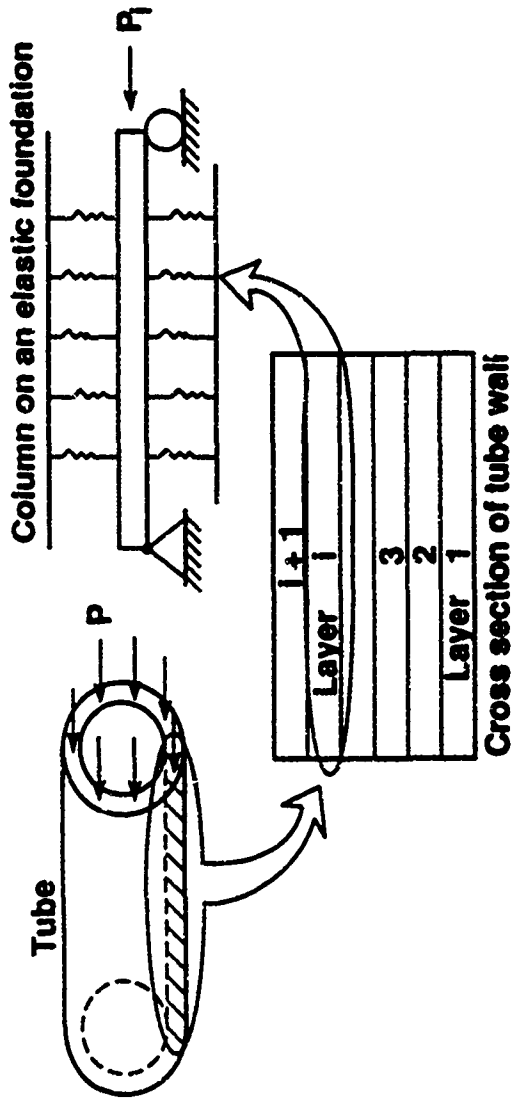
$P_{sustained} = \sum_{i=1}^{n} P_i$

$P_{sustained} = \sum_{i=1}^{n} L_i^{-1} \left[N_i \cdot (EI)_i + N_i^{-1} \cdot K_{fi} \right]$

EI - column bending stiffness
K_f - foundation stiffness
L_i - length of column
N - crushing mode indicator
$P_{sustained}$ - sustained crushing force

Figure 19. Column-on-an-elastic foundation.

crushing force for each layer as defined below:

$$P_{sus} = \sum_{i=1}^{n} \left[L_i^{-1} * \left(N_i * (EI)_i + N_i^{-1} * K_{f\,i} \right) \right] \tag{2}$$

The summation is from 1 to n, the number of layers. The modulus (E_i) of the ith "column" would be the component of the stiffness of the ith layer along the axial direction of the tube and the moment of inertia (I_i) is that of the ith layer. In determination of the bending stiffness $(EI)_i$ of the ith "column" , the relative location of each layer through the thickness is important. The "foundation" stiffness K_{fi} is the circumferential stiffness component of the ith layer. The remaining parameters L_i and N_i are the characteristic crushing length of the tube and crushing mode indicator, respectively.

When fibers are oriented in the circumferential direction of the tube, the resulting "foundation" stiffness can be much larger than the "foundation" stiffness provided solely by the matrix material. The higher the stiffness of the "foundation", the higher the potential crushing force. Increasing "foundation" stiffness produces higher crushing forces for all modes. However, tubes that crush in the lamina bending crushing mode and certain cases of the local buckling crushing mode benefit the most.

The transverse shearing, brittle fracturing, and lamina bending crushing modes all exhibit some form of crack formation and growth. In these crushing modes, the "foundation" stops at the crack tip. The function of the "foundation" becomes that of an end support of the lamina bundle. A low "foundation" stiffness would

be analogous to a pinned end of a column with a flexible torsional spring while a high *"foundation"* stiffness would be equivalent to a stiff torsional spring. A low *"foundation"* stiffness would result in a lower crushing force than a high *"foundation"* stiffness.

The crushing mode indicator N is used to indicate which term, *"column"* stiffness or *"foundation"* stiffness, is the term that will most affects the crushing force. However, this choice does not mean that the subordinate term can not significantly affect the crushing force. The coefficient that multiplies the *"column"* bending stiffness term in equation (2) has N in the numerator while the coefficient that multiplies the *"foundation"* stiffness term has N in the denominator. If N is greater than 1, then the *"column"* stiffness coefficient increases whereas the *"foundation"* stiffness decreases and hence, the *"column"* stiffness term is the dominate term. The converse of this statement is also true.

If a crushed tube exhibits a transverse shearing or brittle fracturing crushing mode, then N is greater than 1 with the magnitude of N larger for the transverse shearing crushing mode than for the brittle fracturing crushing mode. Crushed tubes exhibiting a lamina bending crushing mode would have an N value between 0 and 1. Tubes that crush in the local buckling mode can, depending upon the mechanism that is controlling the crushing mode, have an N value that is either between 0 and 1 or greater than 1.

For example, an increase in crushing force is achievable for tubes that crush in transverse shearing or brittle fracturing crushing modes by increasing the *"column"* stiffness rather than the *"foundation"* stiffness. With N greater than 1, the *"column"*

53

stiffness term becomes the dominant term. Similarly, an increase in crushing force can be obtained by a tube that exhibits a lamina bending crushing mode by increasing *"foundation"* stiffness. Increasing the *"foundation"* stiffness of a tube that crushes in the lamina bending crushing mode can result in a change of crushing mode to the brittle fracturing crushing mode. When the tube crushes in a different mode, then the dominant term can change. Many tubes crush in a combination of these modes: therefore, the crushing force might be significantly affected by the increase of either the *"column"* or *"foundation"* stiffness.

Not all material and structural parameters are contained in the column-on-an-elastic-foundation analogy. Fiber and matrix failure strain and tube geometry (i.e., inside diameter or width) are parameters with significant effect on energy absorption that are not incorporated in this analogy. Omission of these parameters does not invalidate the analogy but just limit the applicability of the analogy.

3.2.1 Transverse Shearing Crushing Mode

The characteristics of tubes that crush in the transverse shearing mode are short interlaminar cracks with shearing of the edges of the lamina bundles. The characteristic crushing length is less than a laminate thickness. No significant amount of bending of the lamina bundles occurs. For tubes that crush in this mode, there is ample *"foundation"* stiffness to resist local bending or buckling of the *"column"*. Therefore, further increase of the *"foundation"* stiffness has little effect on increasing the crushing force. The *"column"* stiffness has the most effect on increasing the crushing force. As previously mentioned, N is greater than 1 for tubes that crush in a transverse shearing mode.

3.2.2 Brittle Fracturing Crushing Mode

Tubes that crush in the brittle fracturing mode exhibit interlaminar cracks that have lengths of between one and ten laminate thicknesses. The "foundation" stiffness is sufficiently high to produce fracturing of the lamina bundles. The lamina bundles exhibit some local bending, but they fracture rather than splay as in the case of the lamina bending crushing mode. Because some local bending does occur, an increase of "foundation" stiffness would increase the crushing force. The crushing mode indicator N is greater than 1. The shorter the interlaminar cracks, the larger the value of N.

3.2.3 Lamina Bending Crushing Mode

Tubes that crush in a lamina bending crushing mode exhibit long interlaminar, intralaminar, and parallel-to-fiber cracks with splaying but no fracturing of the lamina bundles. Increasing "column" stiffness would have some effect on increasing crushing force, but increasing "foundation" stiffness generally has the most effect on increasing crushing force. The crushing mode indicator N is between 0 and 1. The longer the cracks, the smaller the value of N.

3.2.4 Local Buckling Crushing Mode

Two different mechanisms can produce the local buckling crushing mode. The first mechanism is typically associated with Kevlar-reinforced composite tubes. The Kevlar-reinforced tubes crush in the local buckling mode because of the compressive yielding characteristics of the Kevlar fiber. Increasing the stiffness of the "column" has the greatest effect on increasing the crushing force.

The second mechanism is associated with brittle fiber- (graphite or glass) reinforced composite tubes. Brittle fiber-reinforced tubes crush in the local buckling mode when the *"foundation"* stiffness is sufficient low to allow the *"column"* to buckle.

The *"foundation"* stiffness has the most effect on increasing the crushing force for tubes that are made from brittle fiber reinforcements and crush in the local buckling mode. The higher the *"foundation"* stiffness, the higher the crushing force.

3.3 Effects of Changes in Constitutive Material Mechanical Properties on Crushing Response

A series of studies was conducted to determine the effects of fiber and matrix stiffness and failure strain on the crushing response of composite materials. Ideally, only a single variable is changed to evaluate the corresponding effect. However, in experimental studies, changing the properties of a single variable without changing the properties of other variables is often difficult to accomplish.

In this study, fifteen different fiber and matrix combinations are evaluated to quantify the effects of fiber and matrix stiffness and failure strain on the crushing response. The materials and the tube ply orientations used in these investigations are listed in Table 1. In this study, six different brittle fibers (T300, AS4, AS6, P55S, and P75S graphite and E-Glass) and one ductile fiber (Kevlar-49), and five epoxy matrices (934, 974, 5245, HX205, and F185) were evaluated. In all cases, tubes having ply orientations of $[0/\pm\Theta]_4$ and $[\pm\Theta]_6$, where $\Theta=15$, 45, and 75 degrees, were evaluated to ensure any influence of ply orientation was not overlooked. The

56

Table 1. Description of tubes used in evaluating the effects
of fiber and matrix stiffness and failure strain

Composite Material	Ply Orientations*		
	$[0/\pm\Theta]_4$	$[\pm\Theta]_6$	$[0/\pm45/90]_S$
Graphite-Epoxy			
T300-934	Yes	Yes	Yes
T300-5245	Yes	Yes	No
AS4-934	Yes	Yes	No
AS4-5245	Yes	Yes	No
AS6-934	Yes	Yes	No
AS6-5245	Yes	Yes	No
AS6-HX205	Yes	Yes	No
AS6-F185	Yes	Yes	No
P55S-934	Yes	Yes	No
P75S-934	Yes	Yes	No
E-Glass-Epoxy			
E-Gl-934	Yes	Yes	Yes
E-Gl-HX205	Yes	Yes	No
E-Gl-F185	Yes	Yes	No
Kevlar-Epoxy			
K-49-934	Yes	Yes	Yes
K-49-974	Yes	Yes	No

*Θ = 15, 45, and 75 degrees

stiffness and failure strains of the fibers and matrices used in this study are listed in Table 2. All tubes were approximately 10.16 cm in length and had an inside diameter of 3.81 cm. Unless otherwise noted, three specimens of the same ply orientation and material were evaluated, and the results presented are the average of those tests.

In the subsequent sections, comparisons demonstrating the effects of different material properties on crushing response were conducted using a single set of test data. In these studies, the results are rearranged to demonstrate the appropriate cause-effect relationship.

3.3.1 Effects of Fiber Stiffness on Crushing Response of Brittle Fiber-Reinforced Composite Tube Specimens

Three studies were conducted to evaluate the effect of changes in fiber extensional stiffness (modulus of elasticity, E) on the crushing response of composite tube specimens. Composite materials with common matrices and fibers of different stiffnesses were compared. The composite materials used in the first study were T300-934, AS4-934, AS6-934, P55S-934, P75S-934, E-Gl-934. In the second study, AS6-HX205, E-Gl-HX205, AS6-F185, and E-Gl-F185 composite materials were examined. Ply orientations of the tube specimens in the first two studies were $[0/\pm\Theta]_4$ and $[\pm\Theta]_6$. The third study consisted of comparing the energy-absorption capability of $[0/\pm15]_4$ AS4-5245, T300-5245, P55S-934, and P75S-934 tubes.

Effects of Fiber Stiffness in a Low Failure Strain Matrix (934). In the first study, the energy-absorption capability as a function of fiber stiffness is presented for T300,

58

Table 2. Fiber and matrix material mechanical properties.

Material	Manufacturer	Extensional Stiffness (E), GPa	Extensional Failure Strain, cm/cm
Fiber			
T300	Union Carbide	231.0	0.012
AS4	Hercules	235.0	0.015
AS6	Hercules	235.0	0.018
P55S	Union Carbide	380.0	0.005
P75S	Union Carbide	520.0	0.004
K-49	DuPont	124.0	0.028
E-Gl	Owens Corning	74.0 *	0.030 *
Matrix			
934	Fiberite	4.00	0.010
974	Fiberite	3.90	0.020
5245	Narmco	3.80	0.020
HX205	Hexcel	3.86	0.030
F185	Hexcel	2.00	0.130

* Estimated value based upon unidirectional lamina properties.

AS4, AS6, P55S, and P75S graphite- and E-Glass-reinforced 934 epoxy composite tubes. Ply orientations of the tube specimens were $[0/\pm\Theta]_4$ and $[\pm\Theta]_6$.

The energy-absorption trends of the composite tubes are similar for all ply orientations evaluated. Energy-absorption capability increases as fiber stiffness increased ("column" stiffness increased) from 74 GPa (E-Gl) to approximately 235 GPa (T300, AS4, and AS6) as in Fig. 20. As fiber stiffness further increased to 380 GPa (P55S), a significant decrease in energy-absorption capability resulted. Energy-absorption capability generally decreased as fiber stiffness subsequently increased to 520 GPa (P75S). Furthermore, the tubes with the lowest stiffness reinforcement fiber (E-Gl) generally had higher energy-absorption capability than tubes with the highest stiffness fiber reinforcements (P55S and P75S). Besides the differences in fiber stiffness, these fibers also have a wide range of failure strain. The failure strain of E-glass fiber (the lowest stiffness fiber) is more than seven times higher than the P75S graphite fiber (the highest stiffness graphite fiber). It was not possible to change the fiber stiffness without also varying the failure strain. Thus, the column analogy cannot be perfectly utilized.

The E-Glass-reinforced tubes with a ply orientation of $[0/\pm15]_4$ and $[\pm15]_6$ crushed in a lamina bending mode whereas the T300, AS4, and AS6 tubes crushed in a combined lamina bending and brittle fracturing mode. Both the P55S and P75S tubes crushed in transverse shearing modes.

Energy-absorption capability increased up to 175 percent as fiber stiffness increased from 74 GPa (E-Gl) to 235 GPa (T300, AS4, and AS6). The only other
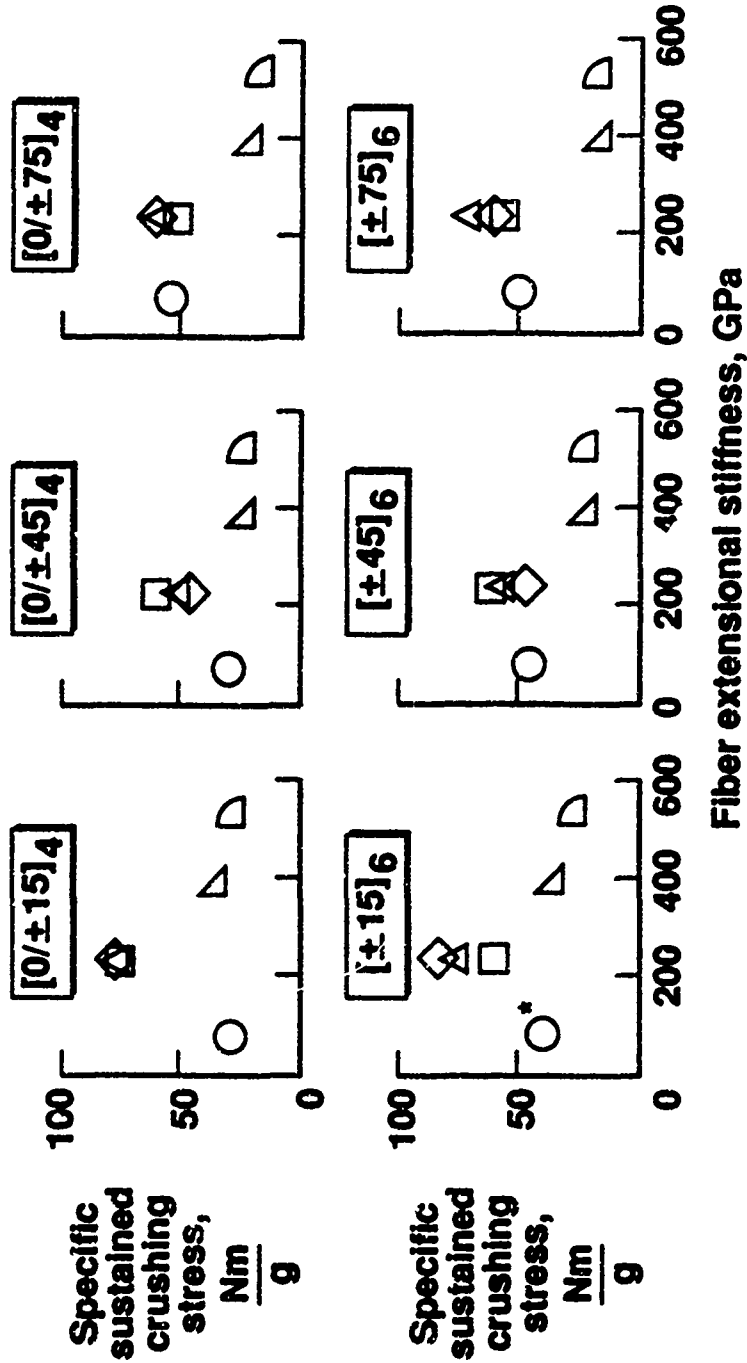
Figure 20. The effect of fiber extensional stiffness on the energy-absorption capability of graphite- and E-Gl-reinforced 934 epoxy composite tubes.

61

change in fiber mechanical properties between the E-glass and the graphite fibers is a decrease in fiber failure strain, which in itself would cause a decrease in energy-absorption capability. Therefore, this increase in energy-absorption capability was due to increased fiber stiffness. As fiber stiffness increased further from 235 GPa (T300, AS4, and AS6) to 380 GPa (P55S) and 520 GPa (P75S), energy-absorption capability decreased. The decrease in energy-absorption capability was due to a decrease in fiber failure strain. The P55S and P75S fibers have failure strains of less than half that of the T300, AS4, or the AS6 fibers.

As ply angle Θ increased to 45 and 75 degrees, the *"foundation"* stiffness of the tubes increased due to the circumferential orientation of the fibers. Also, the *"column"* stiffness decreased because fewer fibers were oriented along the axis of the tube. However, the energy-absorption trends were essentially unchanged from those described for the $\Theta=15$ degrees ply orientations. As the *"foundation"* stiffness increased, the energy-absorption capability of the E-Gl reinforced tubes increased even though the *"column"* stiffness decreased. The energy-absorption capability increased for the E-Gl reinforced $[0/\pm75]_4$ and $[\pm75]_6$ tubes even though the *"column"* stiffness decreased to approximately 30 percent of the *"column"* stiffness for the $[0/\pm15]_4$ and $[\pm15]_6$ tubes, respectively. For the $[0/\pm75]_4$ and $[\pm75]_6$ tubes, energy-absorption capability was relatively unchanged as fiber stiffness increased from 74 GPa (E-Gl) to 235 GPa (T300, AS4, and AS6). The crushing response of the E-Gl, T300, AS4, and AS6 tubes is controlled by the *"foundation"* stiffness, hence the lack of change in energy-absorption capability. Energy-absorption capability decreased for the $[0/\pm75]_4$ and $[\pm75]_6$ tubes as fiber stiffness increased from 235 GPa (T300,AS4, and AS6) to 380 GPa (P55S) and 520

GPa (P75S). The decrease in energy-absorption capability is due to the low failure strain of the P55S and P75S fibers.

Effects of Fiber Stiffness in High Failure Strain Matrices (HX205 and F185). The energy-absorption capability of tubes fabricated from AS6-HX205 and E-Gl-HX205 and tubes fabricated from AS6-F185 and E-Gl-F185 were compared to determine the effect of fiber stiffness on energy-absorption capability. The stiffness of the AS6 fiber is three times that of the E-glass fiber. There was little difference in the relative energy-absorption capability of E-Gl and AS6 fiber-reinforced composite tubes using the HX205 and F185 matrices materials for all ply orientations, as depicted in Fig. 21. The E-Gl reinforced tubes typically exhibited equal or higher energy-absorption capability than the AS6 reinforced tubes. The high failure strain of the matrix reduced the interlaminar crack growth causing more of the tube to crush in a brittle fracturing mode than was achieved with lower failure strain matrices. If the matrix failure strain effects are excluded, these results would support the conclusion that fiber stiffness has little effect on energy-absorption capability.

Effects of Fiber Stiffness on Tubes With Crushing Modes Controlled by Fiber Mechanical Properties. The energy-absorption capability of tubes fabricated from T300-5245, AS4-5245, P55S-934, and P75S-934 having a $[0/\pm15]_4$ ply orientation were compared. Unlike in the previous two sections, all of these tubes crushed in modes (transverse shearing and brittle fracturing) that are controlled by the mechanical properties of the fibers. However, the tubes crushed in predominantly brittle fracturing or transverse shearing modes as seen in Fig. 22. The energy-absorption capability of the

63
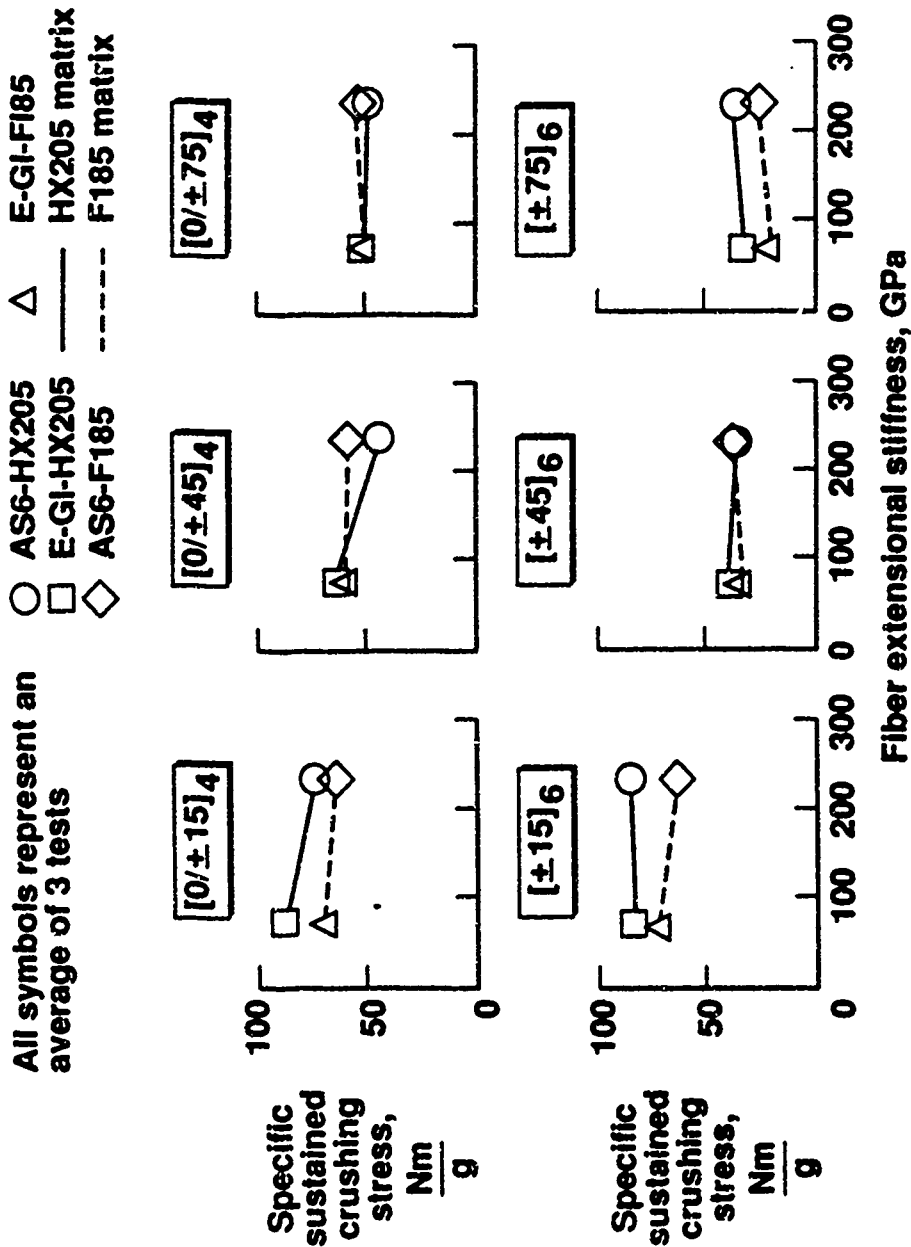
Figure 21. The effect of fiber extensional stiffness on energy-absorption capability of AS6 and E-Gl reinforced HX205 and F185 epoxy composite tubes.

64
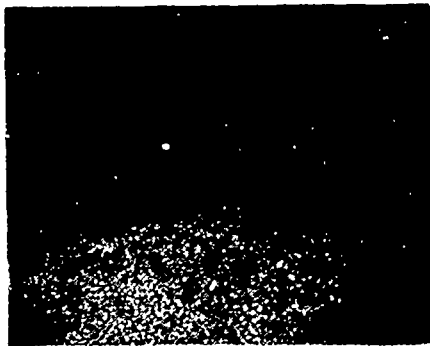
P75S-934

P55S-934

T300-5245

AS4-5245
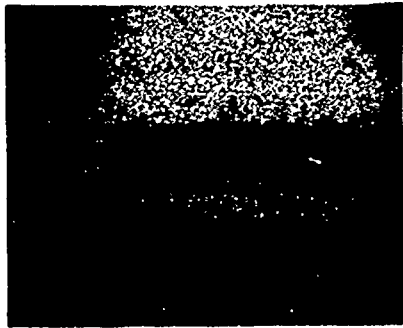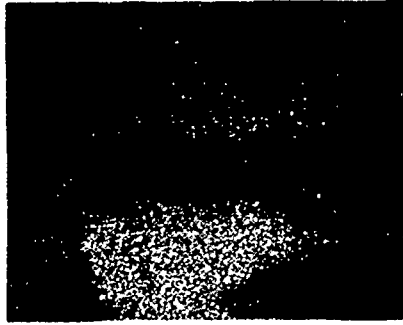
Figure 22. Photomicrographs of $[0/\pm15]_4$ graphite-epoxy tubes.

high-stiffness fiber-reinforced tubes (P55S and P75s) were approximately 25 perce t of the energy-absorption capability of the AS4 fiber-reinforced tubes as seen in Fig. 23. Even though the stiffness of the AS4 and T300 fibers are similar, the AS4-5245 composite tubes had approximately 30 percent higher energy-absorption capability than the T300-5245 composite tubes. The mechanical property that differs between the T300, AS4, P55S, and P75S fibers, besides the differences in fiber extensional stiffness, is fiber failure strain. If the effects of fiber failure strain were omitted, these result suggest energy-absorption capability is inversely proportional to fiber stiffness which is converse to the column analogy.

Summary. The results of the tests presented in the previous three sections provide conflicting evidence on how fiber extensional stiffness affects energy-absorption capability if the effects of fiber failure strain were not included in the interpretation of results. For different combinations of fiber and matrix, energy-absorption capability could increase, decrease, or remain unchanged relative to an increase in fiber extensional stiffness. If a study of a more limited scope were undertaken, it would be obvious how erroneous conclusions could be reached.

The choice of available fibers with increasing modulus had various failure strains. It is suspected that the energy-absorption capability is a stronger function of fiber failure strain than it is of fiber extensional stiffness. It is concluded that for brittle fiber-reinforced tubes an increase in fiber stiffness can, depending upon the matrix properties and ply orientation, produces higher energy-absorption capability.

66
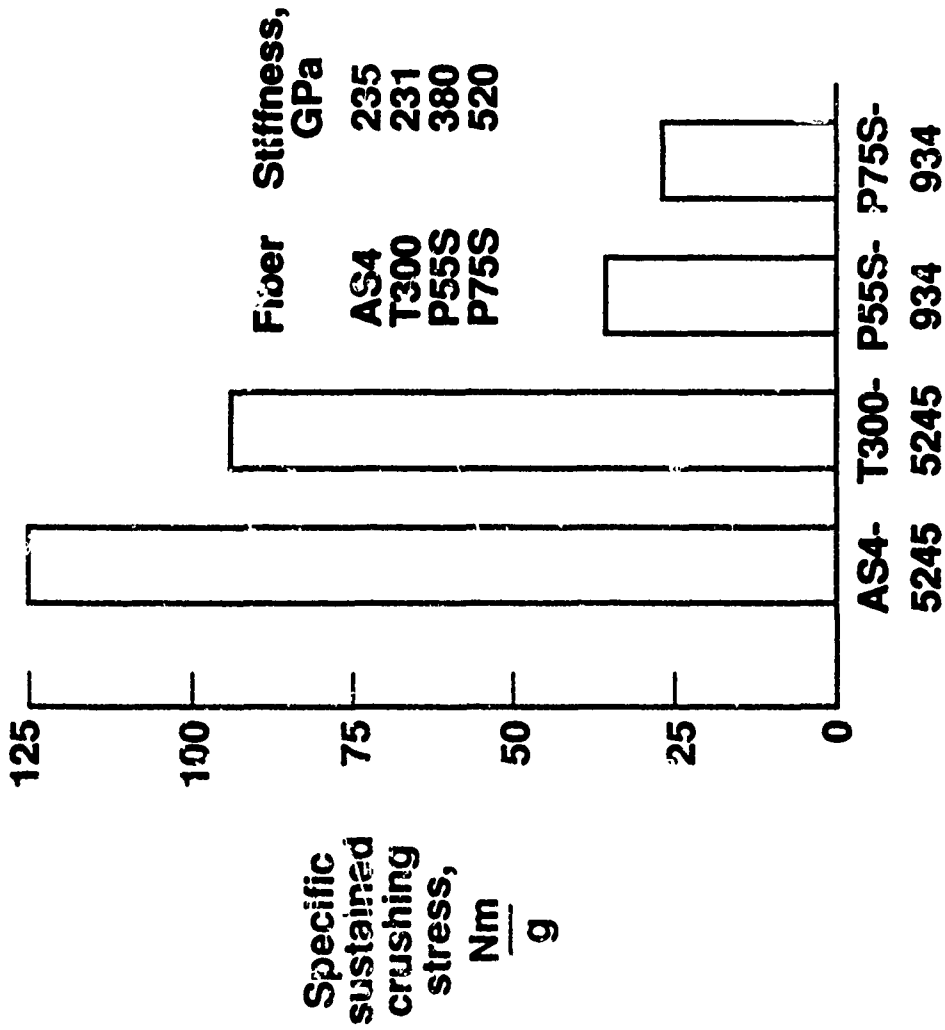
Figure 23. The effect of fiber stiffness on the crushing characteristics of [0/±15]₄ graphite-epoxy tubes.

3.3.2 Effects of Matrix Stiffness on the Crushing Response of

Brittle Fiber-Reinforced Composite Tube Specimens

Tests were conducted to evaluate the effects of changes in matrix extensional stiffness (modulus of elasticity, E) on the crushing response of brittle (graphite and E-Gl) and ductile (Kevlar-49) fiber-reinforced composite materials. In this study, the materials used are T300-934, T300-5245, AS4-934, AS4-5245, AS6-934, AS6-5245, AS6-HX205, AS6-F185, E-Gl-934, E-Gl-HX205, E-Gl-F185, K-934, and K-974.

Effects of Matrix Stiffness on T300-, AS4-, and Kevlar-Fiber-Reinforced Composite Tube Specimens. The effects of changes in matrix stiffness on the energy-absorption capability of $[0/\pm\Theta]_4$ and $[\pm\Theta]_6$ T300, AS4, and K fiber-reinforced composite tubes were addressed. The extensional stiffness of the 934 matrix is 4.0 GPa and the elastic extensional stiffnesses of the 974 and 5245 matrices are 3.9 GPa and 3.8 GPa, respectively. Also, the lowest stiffness matrix material (5245) had twice the failure strain of the highest stiffness matrix (934) material. The influence of matrix failure strain is its effect on interlaminar crack propagation. The higher the matrix failure strain, the greater the load that is required to cause a crack to grow.

Based upon the simple analogy of the column on an elastic foundation, the role of the matrix is to stabilize the axial fibers and to control interlaminar/intralaminar crack growth. In the case where the crushing modes are brittle transverse shearing, fracturing, or lamina bending, interlaminar/intralamina cracks form to separate the lamina bundles. The role of the matrix then becomes to act as an end support for

the lamina bundles and stabilize the axial fibers within a lamina bundle. The energy absorbed is a function of the growth of a crack in the matrix and/or fracture of the lamina bundles. Therefore, increase in matrix stiffness should have a limited effect on the energy-absorption capability of tubes that crush in the transverse shearing, brittle fracturing, or lamina bending crushing mode.

Generally, as matrix stiffness increased for the T300 and AS4 reinforced tubes, the energy-absorption capability decreased, as in Fig. 24. However, this decrease in energy-absorption capability is attributed to the higher failure strain of the low stiffness 5245 matrix material. The high failure strain of the 5245 matrix reduced the length of the interlaminar cracks resulting in a higher energy-absorption capability.

The energy-absorption trends of the Kevlar-reinforced epoxy tubes exhibited a small increase or remained constant in energy-absorption capability as the stiffness of the matrix material increased as in Fig. 24. The *"foundation"* stabilizes the *"column"* to resist buckling. As the matrix becomes stiffer, then the *"foundation"* becomes stiffer (the buckling load increases), hence energy-absorption capability increases. The energy absorbed in the local buckling mode for K-epoxy tubes is primarily a function of the plastic deformation of the fiber and matrix. Brittle fiber-reinforced composite tubes that crush in the local buckling mode absorb energy by plastic deformation of the matrix and the growth of interlaminar cracks at the buckles as the tube folds.

Effects of Matrix Stiffness on the Crushing Response of AS6 Graphite-Reinforced Composite Tubes. The effects of changes in matrix stiffness on the energy-absorption capability

69
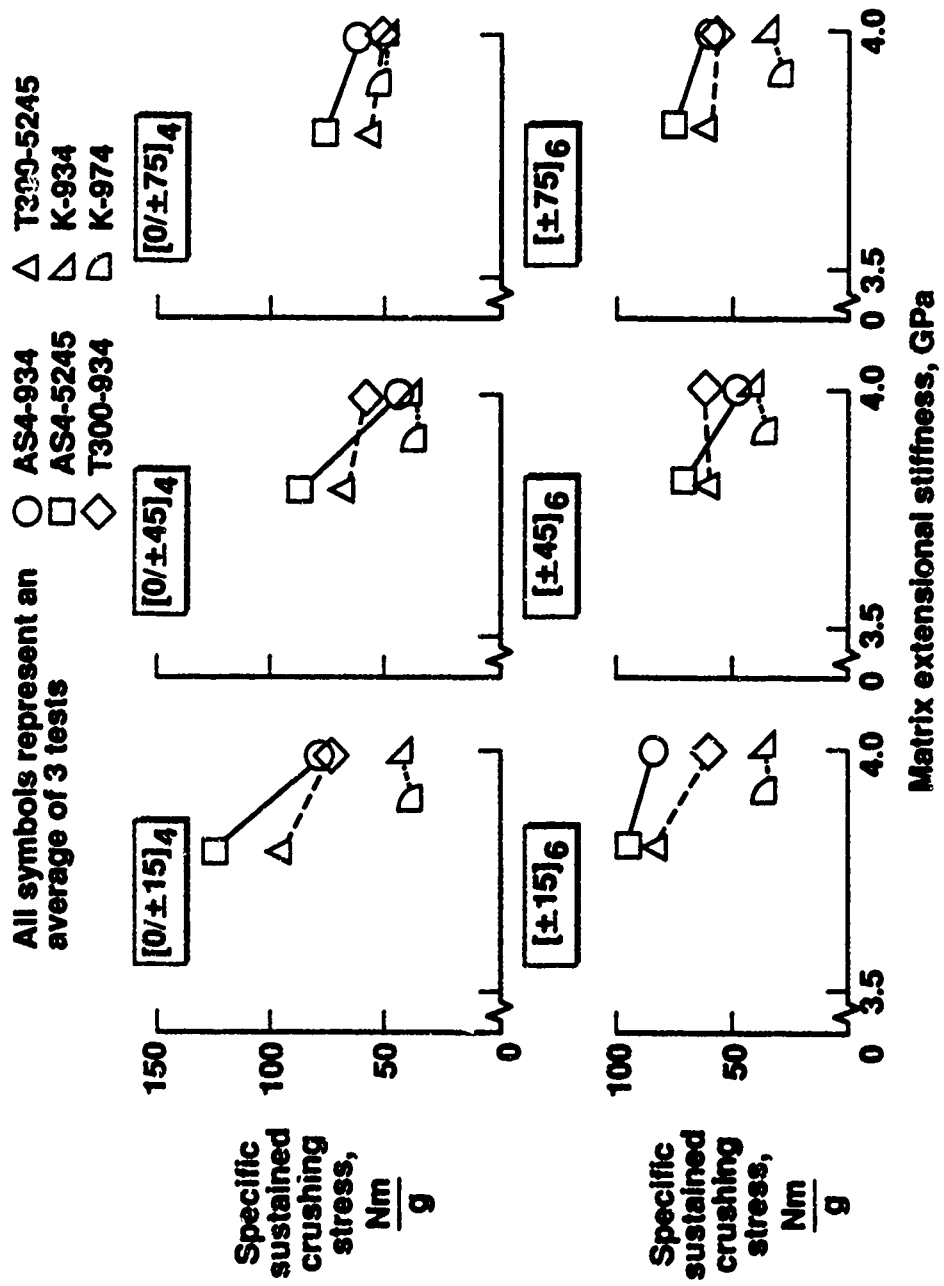
Figure 24. The effect of matrix stiffness on the energy-absorption capability of AS4-, T300-, and K-epoxy composite tubes.

of AS6 graphite-reinforced composite tubes were evaluated using 934, 5245, HX205, and F185 matrices. As previously mentioned, the difference in stiffness of the 934, 5245, and HX205 matrices is less than 5 percent. The stiffness of the F185 matrix is approximately half that of the other matrices. Energy-absorption capability increased between 10 and 15 percent as matrix stiffness increased for tubes having $[0/\pm15]_4$ ply orientations, as seen in Fig. 25. However, for the $[0/\pm\Theta]_4$ tubes, as Θ increases, the circumferential plies provide the major portion of the "foundation" stiffness. The effects of matrix stiffness, as part of the "foundation" stiffness, diminish. As ply angle Θ increases, the contribution of the matrix stiffness to that of the "column" stiffness increase. However, the portion of the "column" stiffness of the $[0/\pm\Theta]_4$ tubes contributed by the matrix is small relative to the fiber stiffness contribution from the 0 degree plies.

The $[\pm\Theta]_6$ tubes exhibited an increase in energy-absorption capability with an increase in matrix stiffness as seen in Fig. 25. The $[\pm15]_6$ tubes exhibited between a 15 and 90 percent increase in energy-absorption capability with an increase in matrix stiffness over the range of materials evaluated. The differences in the energy-absorption capability of tubes made from the 934, 5245, and HX205 matrices are partially attributable to differences in matrix failure strain. The matrix stiffness contributes to both "column" and "foundation" stiffness and is a function of ply orientation. For the $[\pm45]_6$ and $[\pm75]_6$ tubes, the matrix stiffness has an increasing contribution to the "column" stiffness as Θ increases, whereas matrix stiffness has a diminishing effect, with increasing Θ, on "foundation" stiffness.

The $[\pm45]_6$ and $[\pm75]_6$ tubes made from AS6-F185 and AS6-HX205 composite
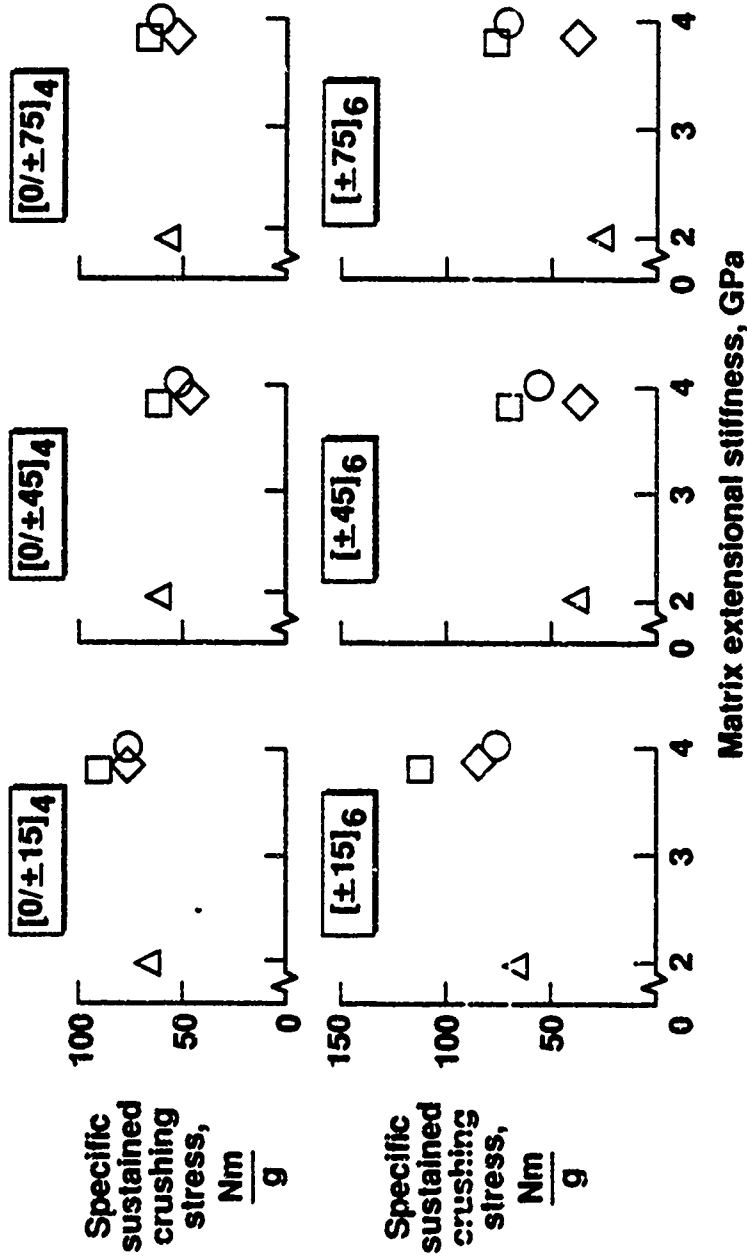
Figure 25. The effect of matrix stiffness on the energy-absorption capability of AS6-epoxy composite tubes.

72

materials crushed in a local buckling crushing mode, whereas the AS6-5245 and AS6-934 tubes crushed in a combined lamina bending and brittle fracturing mode. Energy-absorption capability was relatively constant with increasing matrix stiffness for the $[\pm 45]_6$ and $[\pm 75]_6$ AS6-F185 and AS6-HX205 tubes. This energy-absorption trend occurs because these tubes crushed in a local buckling crushing mode. The dominant term for brittle fiber-reinforced tubes that crush in the local buckling mode is the "foundation" stiffness. The "foundation" stiffness is a stronger function of fiber stiffness than matrix stiffness for $[\pm 45]_6$ and $[\pm 75]_6$ ply orientations. A slight increase in energy-absorption capability occurred as matrix stiffness increased for the $[\pm 75]_6$ tubes. The increase in energy-absorption capability as matrix stiffness increases occurs because for $\Theta=75$ the matrix stiffness makes the major contribution to the "column" stiffness.

The higher energy-absorption capability of the 5245 $[\pm 15]_6$ tubes relative to 934 tubes is attributed to the higher failure strain of the 5245 matrix. This difference in energy-absorption capability decreased between the 5245 and 934 composite matrix tubes as Θ increased. The change in relative energy-absorption capability occurs because the "foundation" stiffness increases as Θ increases. That is, the fibers are making a more significant contribution to the "foundation" stiffness than the matrix as Θ increases. For example, the energy-absorption capability of the $[\pm 75]_6$ 5245 and 934 tubes are essentially equal.

Effects of Matrix Stiffness on E-Glass Fiber-Reinforced Composite Tube Specimens. Tubes fabricated from E-Glass fiber-reinforced epoxy composite material were loaded to

73

determine the effects of matrix stiffness on energy-absorption capability. The epoxy matrices used in this study were 934, HX205, and F185. The E-Gl-934 tubes exhibited lower energy-absorption capability than the E-Gl-HX205 or E-Gl-F185 tubes while the E-Gl-HX205 tubes exhibited higher energy-absorption capability than the E-Gl- F185 material for $[0/\pm15]_4$ and $[0/\pm45]_4$ ply orientations as seen in Fig. 26. However, the energy-absorption capabilities of all three materials were equal for the $[0/\pm75]_4$ ply orientation. The increase in energy-absorption capability as matrix stiffness increased from the F185 tubes to the HX205 tubes was due to matrix stiffness effects. The stiffer HX205 matrix reduced the bending of the lamina bundles due to a stiffer end support of the lamina bundle. Higher end support stiffness produced a slight increase in brittle fracturing, hence the slight increase in energy-absorption capability. However, the decrease in energy-absorption capability between the HX205 and the 934 tubes was due to the lower matrix failure strain of the 934 matrix. The 934 matrix fails at a relatively low strain which produces longer interlaminar and intralaminar cracks than in the HX205 tubes. Generation of long interlaminar cracks typically results in lower energy-absorption capability.

As ply angle Θ increases for the $[0/\pm\Theta]_4$ tubes, the "foundation" stiffness increases because as Θ increases an increasing portion of the "foundation" stiffness is contributed from the fibers. Therefore, the significance of the matrix contribution to the "foundation" decreases as Θ increases. At $\Theta=75$ degrees, the difference in energy-absorption capability of the F185 and HX205 matrices is virtually eliminated.

The energy-absorption capability of the $[0/\pm45]_4$ 934 tubes is less than the energy-absorption capability of the F185 and HX205 tubes. Even with $\Theta=45$
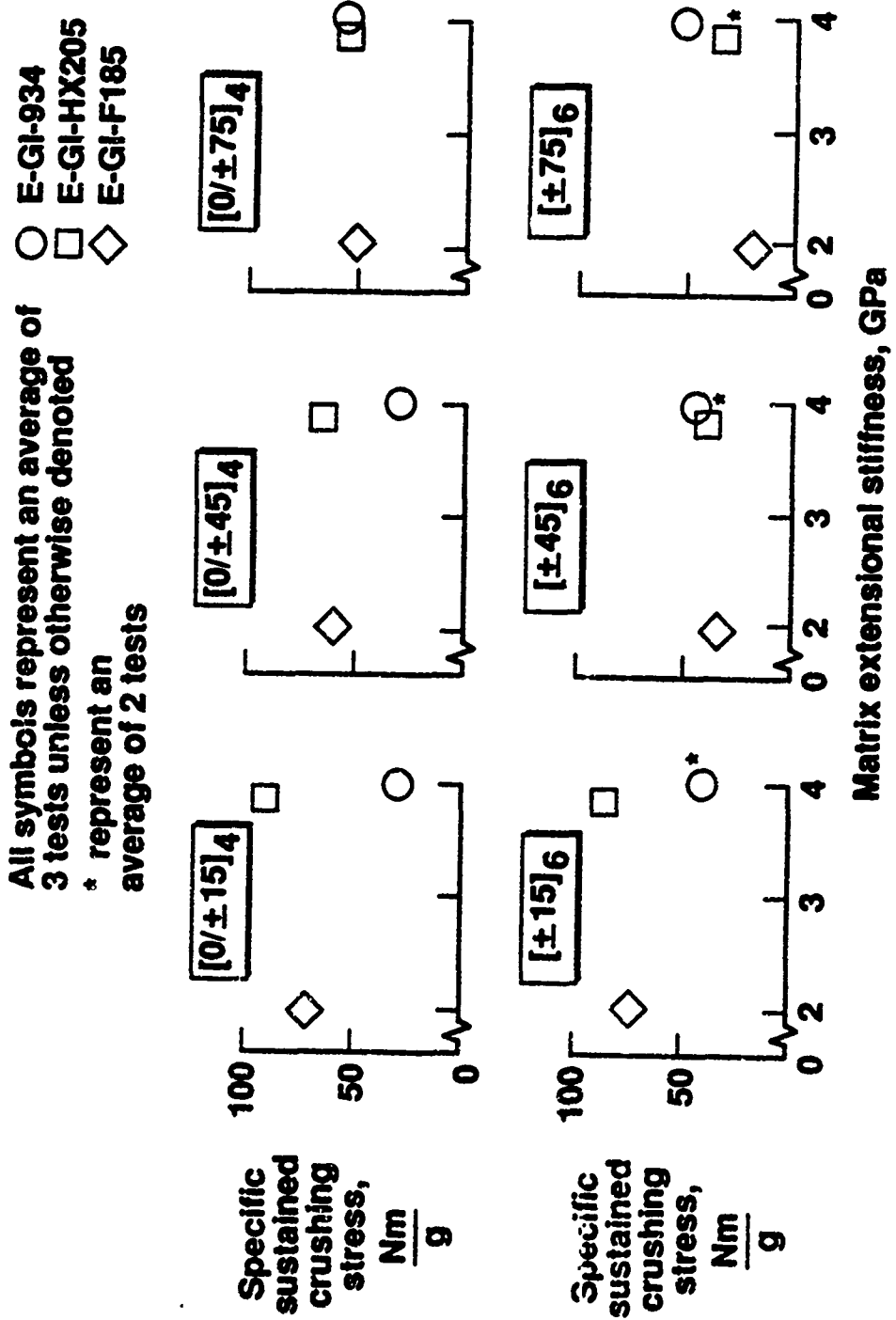
Figure 26. The effect of matrix extensional stiffness on the energy-absorption capability of E-Gl-epoxy composite tubes.

75

degrees, insufficient *"foundation"* stiffness is obtained to significantly increase the percentage of material that exhibited a brittle fracturing crushing mode. At $\Theta=75$ degrees, the circumferential fibers provide equal *"foundation"* support to all materials resulting in equivalent energy-absorption capabilities.

The energy-absorption trends for the $[\pm15]_6$ tubes are the same as described for the $[0/\pm15]_4$ tubes. The mechanisms that control the crushing response of these tubes are also the same. That is, the increase in energy-absorption capability between the F185 and HX205 tubes is due to an increase in matrix stiffness. However, the low energy-absorption capability of the 934 tubes is due to lower matrix failure strain relative to the failure strain of either the F185 or the HX205 matrices. The crushing modes of the $[\pm15]_6$ tubes were predominately lamina bending with some brittle fracturing. These crushing modes changed to local buckling for the $[\pm45]_6$ and $[\pm75]_6$ F185 and HX205 tubes. The crushing mode of the 934 tubes remained combined lamina bending and brittle fracturing.

Energy-absorption capability increased as matrix stiffness increased for the $[\pm45]_6$ F185 and HX205 tubes. This energy-absorption trend occurred because for brittle fiber-reinforced composite tubes that crush in the local buckling mode, as *"foundation"* stiffness increase a higher force is required to buckle the *"column"*; hence, a higher energy-absorption capability is achieved. The difference in energy-absorption capability was even greater for the $\pm75]_6$ F185 and HX205 tubes. The *"foundation"* stiffnesses of $[\pm75]_6$ F185 and HX205 tubes are equal because the *"foundation"* stiffness is essentially controlled by the stiffness of the fibers. However, the difference in *"column"* stiffness is primarily controlled by the stiffness of the

76

matrix and approximately a factor of two difference exists in matrix stiffness between the F185 and HX205 matrices. This difference in "column" stiffness nearly equals the difference in energy-absorption capability between the F185 and HX205 tubes.

The crushing mode of the E-Glass-934 $[\pm\Theta]_6$ tubes was combined lamina bending and brittle fracturing. As ply angle Θ increased, the percentage of material crushing in a lamina bending mode decreased whereas the percentage of mater. that crushed in the brittle fracturing mode increased. Also, as ply angle Θ increased, there was an increase in energy-absorption capability. The change in crushing mode and energy-absorption capability is a result of an increase in "foundation" stiffness as ply angle Θ increases.

3.3.3 Effects of Fiber Failure Strain on Crushing Response of

Brittle Fiber-Reinforced Composite Tube Specimens

Four studies were conducted to evaluate the effect of changes in fiber extensional failure strain on the crushing response of composite tube specimens. The composite materials used in these studies were T300-934, AS4-934, AS6-934, E-Gl-934, T300-5245, AS4-5245, AS6-5245, AS6-HX205, E-Gl HX205, AS6-F185, E-Gl-F185, and K-49-934. Ply orientations of the tubes in studies one through three were $[0/\pm\Theta]_4$ and $[\pm\Theta]_6$. These studies are analogous to those performed in the investigations examining the effects of fiber and matrix stiffness. The first study consisted of comparing the energy-absorption capability of T300, AS4, AS6, and E-Gl reinforcement fiber in a low failure strain matrix (934). The second study consisted of evaluating three graphite reinforcements (T300, AS4, and AS6) in a matrix

having an intermediate failure strain. The effects of failure strain of AS6 and E-Gl reinforcement in two different high failure strain matrices (HX205 and F185) were evaluated in the third study. The fourth study consists of comparing the energy-absorption capability of T300, K-49, and E-Gl reinforced 934 epoxy $[0/\pm45/90]_S$ tubes wherein only the fiber properties were changed, i.e., a common matrix was maintained.

Effects of Fiber Failure Strain in a Low Failure Strain Matrix (934). Composite tubes fabricated from T300, AS4, AS6, and E-Gl fibers in a 934 epoxy were evaluated to investigate the effect of fiber failure strain on energy-absorption capability. Graphite-reinforced tubes with $[0/\pm15]_4$ ply orientation exhibited essentially a constant energy-absorption capability as fiber failure strain increased from 1.1 to 1.7 percent. Energy-absorption capability of the E-Gl reinforced tubes was substantially less than the graphite-reinforced tubes. Tubes with ply orientations of $[\pm15]_6$ exhibited an increase in energy-absorption capability as fiber failure strain increases from 1.1 to 1.5 percent but decreases with further increase in fiber failure strain as depicted in Fig. 27. In these comparisons, the predominant crushing mode of the tubes fabricated from the T300/934 material is brittle fracturing while the tubes fabricated from the AS4 and AS6 fiber-reinforced materials exhibit a combined lamina bending and brittle fracturing crushing mode. Tubes fabricated from E-Gl-934 material exhibit a lamina bending-crushing mode. Fiber failure strain does not control the crushing mechanisms associated with the lamina crushing mode. Therefore, this comparison does not provide a clear representation of how fiber failure strain influences energy-absorption capability.
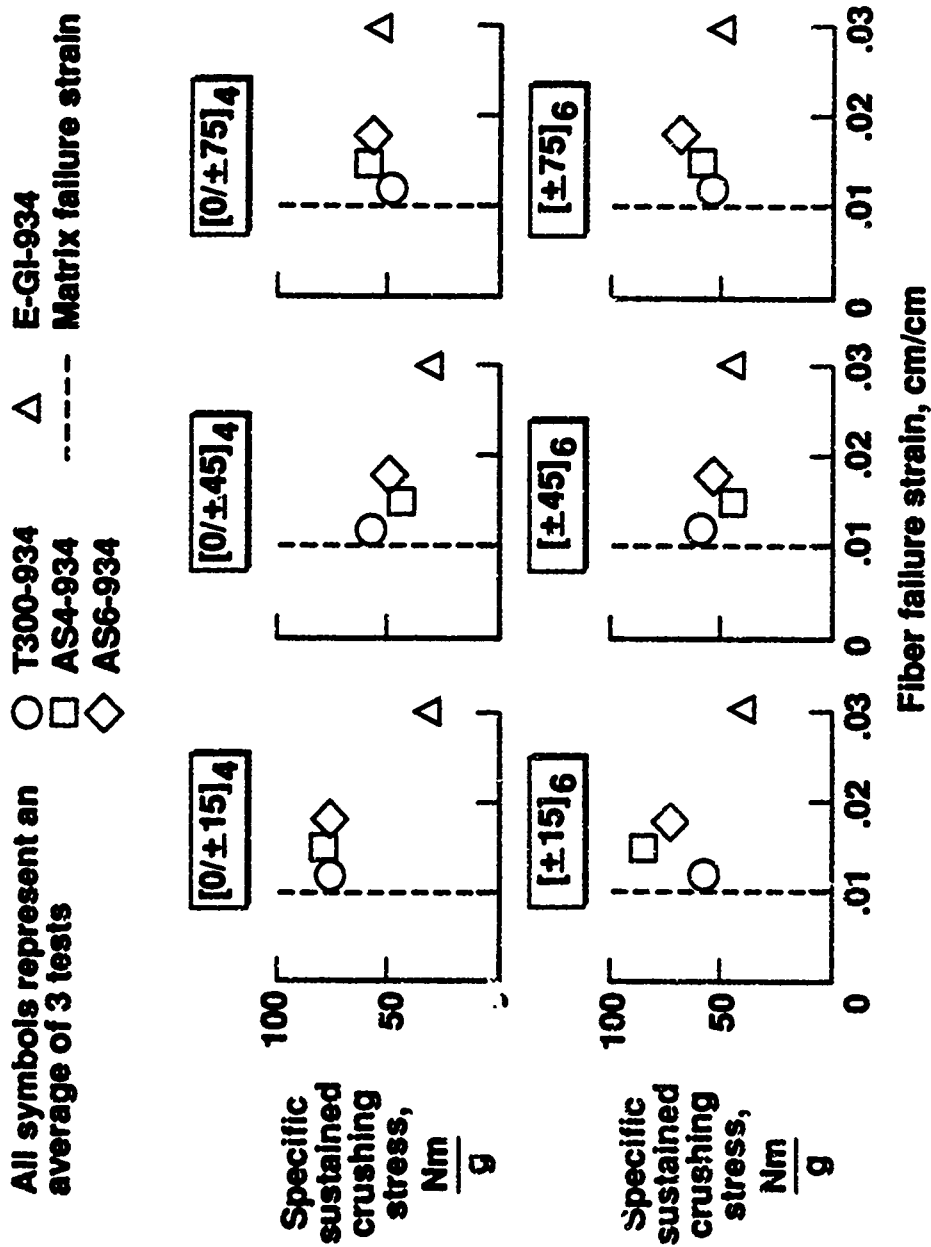
Figure 27. The effect of fiber failure strain on the energy-absorption capability of brittle-fiber-reinforced 934 epoxy composite tubes.

79

As the ply angle Θ increases, the percentage of fibers in the direction of the applied load decreases. The decrease in energy-absorption capability occurs because of a decrease in "column" stiffness. However, as more fibers are oriented in the circumferential direction of the tube, an increase in "foundation" support is provided and a greater percentage of material is crushed in a brittle fracturing mode. The net result is that the energy-absorption capability can increase or decrease as ply angle Θ increases depending upon the material properties of both the fiber and matrix.

This seemingly random change in energy-absorption capability occurred as ply angle increased. The differences in crushing modes suggest that if additional stiffness were provided to the "foundation", then the AS4, AS6, and E-Gl tubes could be crushed in more efficient crushing modes. Even though the AS4 and AS6 reinforced tubes crushed in less efficient crushing modes than the T300 fiber-reinforced tubes, the AS4 and AS6 reinforced tubes have equal or greater energy-absorption capability than the T300 fiber reinforced tubes. Therefore, the energy-absorption potential of the AS4, AS6, and E-Gl tubes is higher than that of the T300 fibers. Hence, an increase in fiber failure strain can produce an increase in energy-absorption capability.

The energy-absorption capabilities of the $[0/\pm 75]_4$ E-Gl-934 tubes are equal to or greater than the graphite-reinforced tubes. The effect of fiber stiffness was established to be small for tubes that crush in a lamina bending crushing mode. Therefore, the increase in energy-absorption capability as Θ increased for the E-Gl-934 tubes relative to the graphite-reinforced tubes is the result of the E-Gl fibers' ability to deform more prior to fracture than was possible with the graphite

80

reinforcements. The crushing modes of the AS4, AS6, and E-Gl still retain a considerable percentage of lamina bending which suggests that even higher energy-absorption capability exists provided more *"foundation"* support is provided to the *"column"* . Hence, fiber failure strain can, depending upon ply orientation, significantly affect energy-absorption capability.

When the failure strain of the fiber exceeds the failure strain of the matrix, then the energy-absorption potential of the tube, depending upon the ply orientation of the tube, can decrease. For example, the crushing modes of the T300-934 tubes were predominantly brittle fracturing. which is an efficient crushing mode. The failure strain of the fiber exceeds the failure strain of the matrix by approximately twenty percent. However, the crushing mode of the E-Gl-934 material is lamina bending, which is an inefficient crushing mode, and the failure strain of the fiber is 200 percent greater than the failure strain of the 934 matrix.

Effect of Fiber Failure Strain in an Intermediate-Failure-Strain Matrix (5245). Similar studies were conducted on the effects of fiber failure strain on the energy-absorption capability of composite material using 5245, HX205, and F185 matrices. Tubes fabricated from T300-, AS4-, and AS6-5245 composite material and with laminate stacking sequences of $[0/\pm\Theta]_4$ and $[\pm\Theta]_6$ were evaluated. As fiber failure strain increased from 1.1 (T300) to 1.5 (AS4), the energy-absorption capability increased as depicted in Fig. 28. However, further increase in fiber failure strain to 1.7 (AS6) percent generally resulted in a decrease in energy-absorption capability. The exception to this trend was the $[\pm15]_6$ tubes which exhibited an increase in energy-absorption capability as failure strain increased to 1.7 percent. The

81
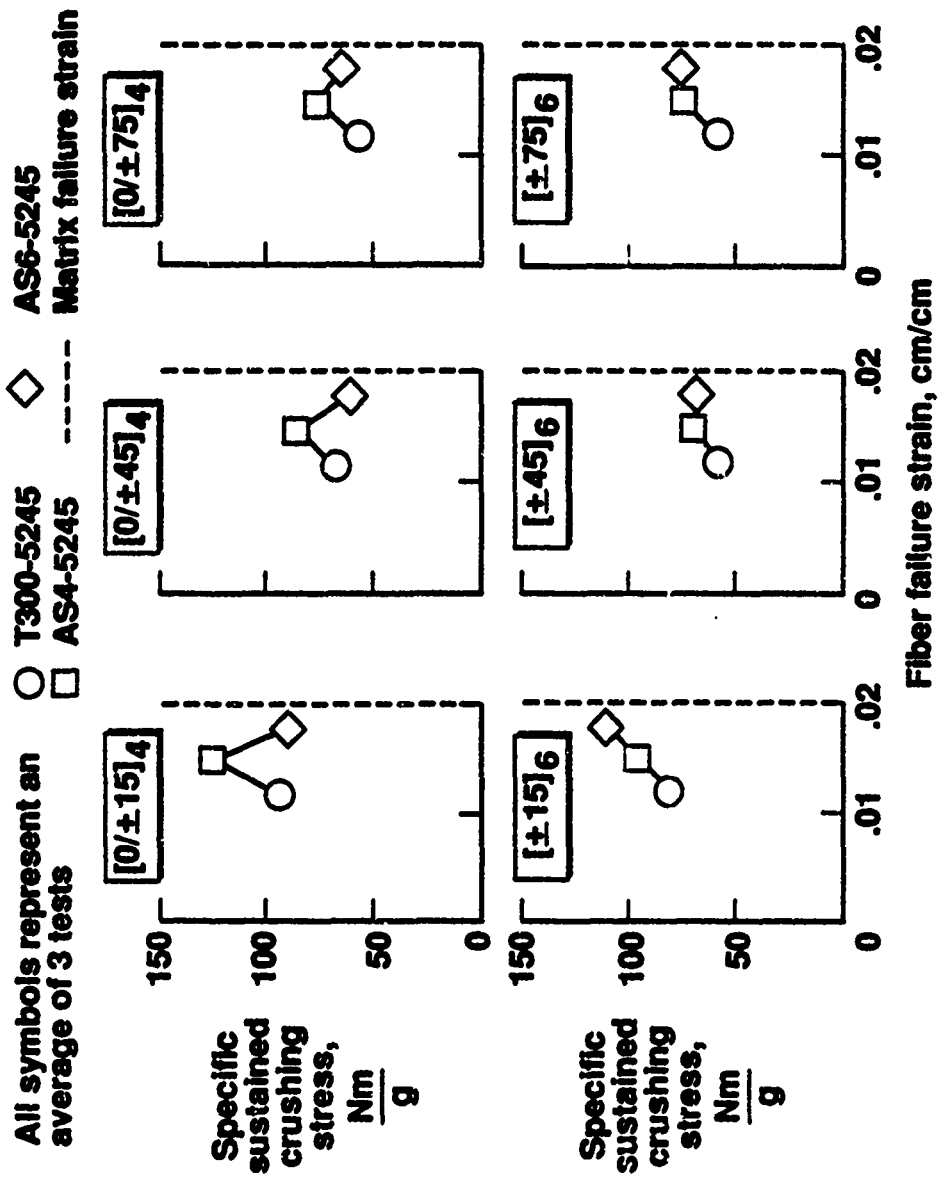
Figure 28. The effect of fiber failure strain on the energy-absorption capability of graphite-fiber-reinforced 5245 epoxy composite tubes.

82

lower energy-absorption capability of the AS6-reinforced tubes occurs because the AS6-reinforced composite materials exhibit a lower compression strength than the AS4-reinforced composite material. The lower compression failure strength occurs because the diameter of the AS6 fiber is smaller than the AS4 fiber which causes a fiber-microbuckling-mode-induced compression failure. As ply angle Θ increased, which increased the *"foundation"* stiffness, more of the material crushed in a brittle fracturing mode. Increasing the *"foundation"* stiffness resulted in increasing the crushing efficiency and energy-absorption capability of the AS6 reinforced composite tubes. An increase in failure strain can result in energy-absorption capability that increases, decreases, or remains constant.

Effects of Fiber Failure Strain in High-Failure-Strain Matrices (HX205 and F185). The effects of fiber failure strain were further investigated through an evaluation of tubes fabricated from AS6 and E-Gl reinforcement fibers in HX205 and F185 matrices for tubes having $[0/\pm\Theta]_4$ and $[\pm\Theta]_6$ ply orientations. The fiber failure strains of the AS6 and E-Gl fibers are 1.7 and 3.0 percent, respectively. Energy-absorption capability remained essentially constant or slightly increased as failure strain increased for either the HX205 or F185 matrices for $[0/\pm15]_6$ or $[\pm15]_6$ as seen in Figs. 29 and 30. The high failure strain of the matrices reduced the interlaminar crack length so that even the E-G reinforced tubes exhibited a partial brittle fracturing crushing mode. The high energy-absorption capability of the E-Gl reinforced tubes was produced even though the stiffness of the E-Gl fiber has only a third the stiffness of the AS6 graphite fiber.

As Θ increased for the $[0/\pm\Theta]_4$ tubes, energy-absorption capability increased or
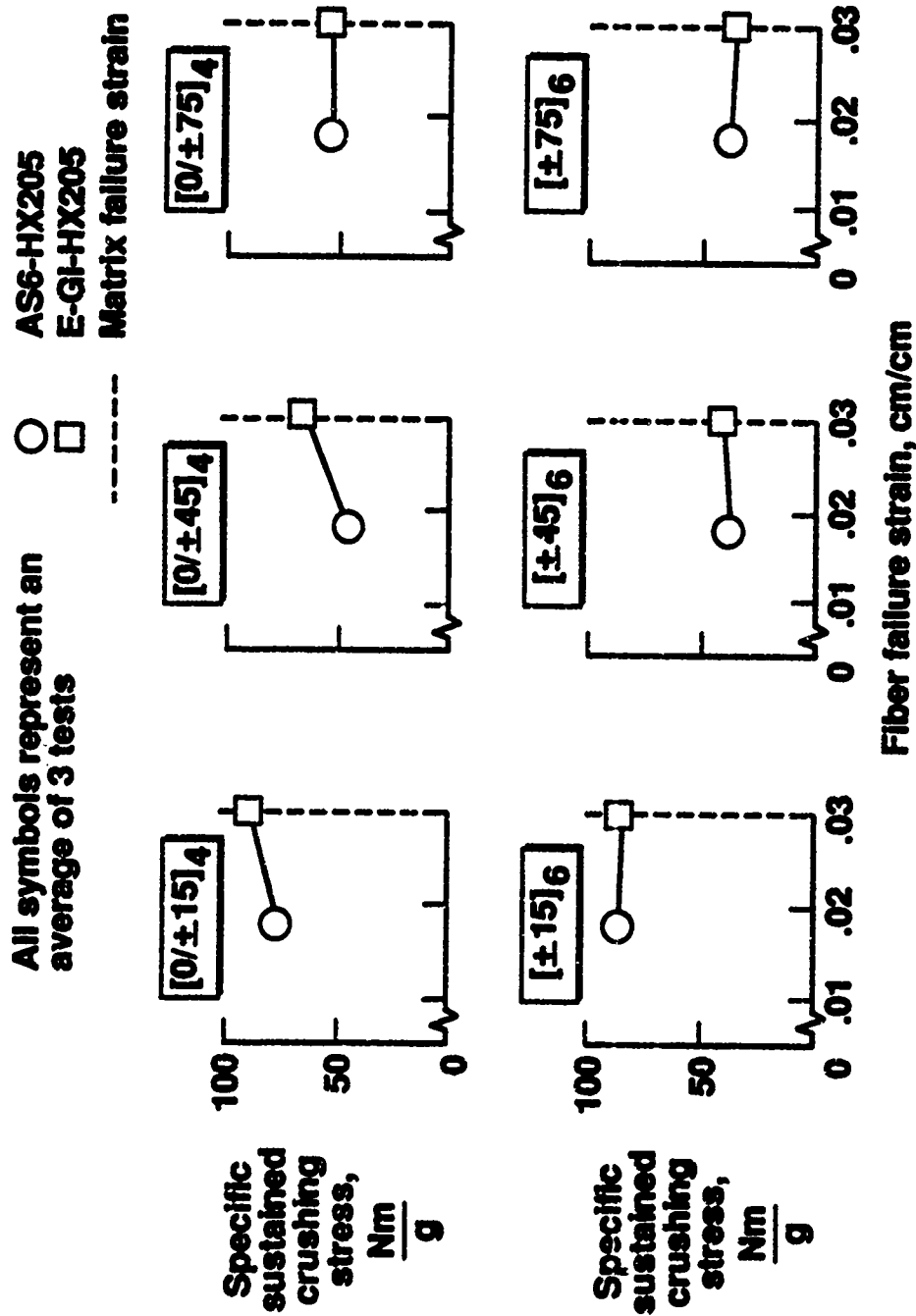
Figure 20. The effect of fiber failure strain on the energy-absorption capability of brittle-fiber-reinforced HX205 epoxy composite tubes.

84
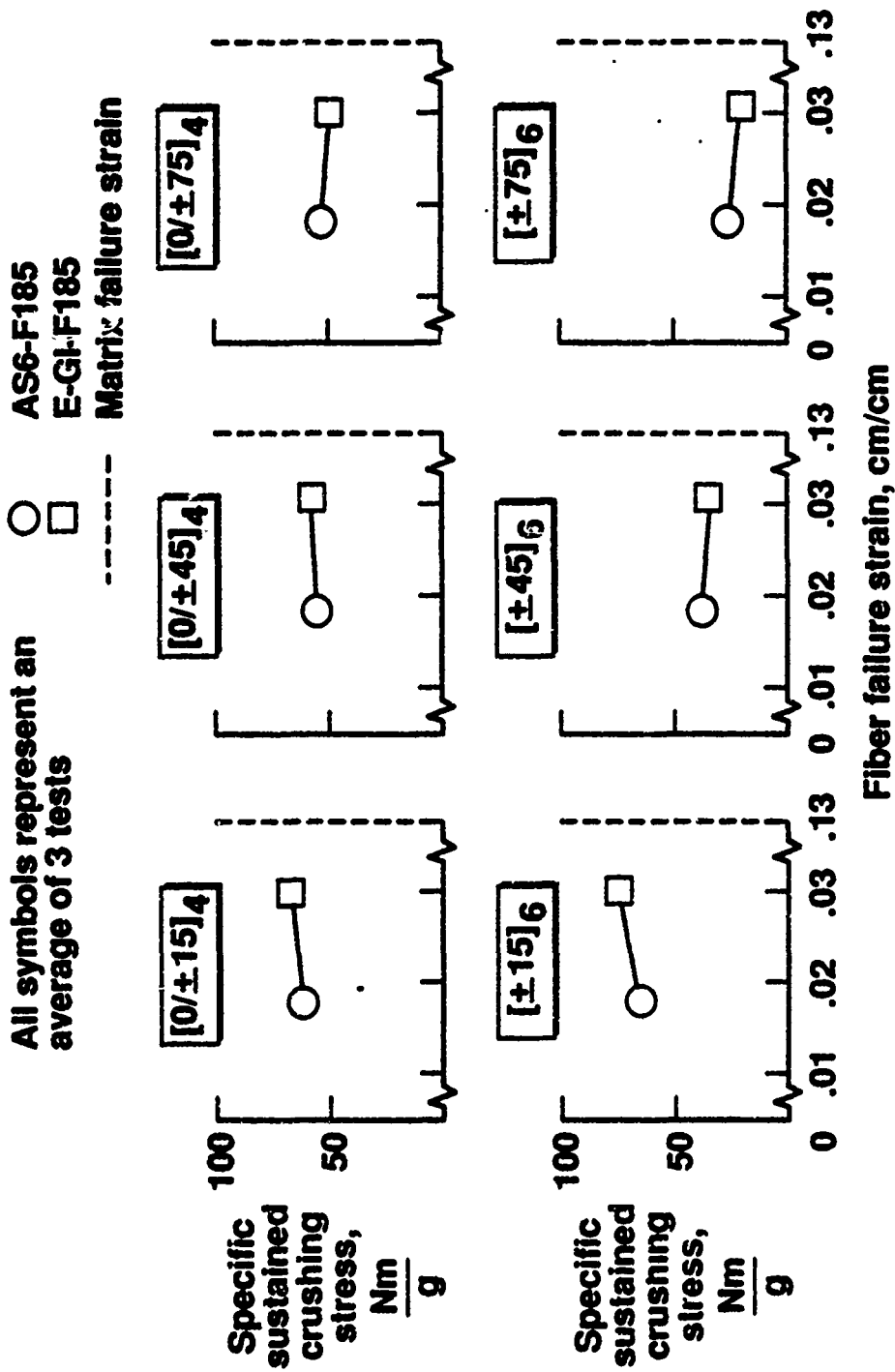
Figure 30. The effect of fiber failure strain on the energy-absorption capability of brittle-fiber-reinforced F185 epoxy composite tubes.

remained constant as fiber failure strain increased. These trends support the finding that as "foundation" stiffness increases, the higher failure strain material, even though it has a lower stiffness, can produce a higher energy-absorption capability than the graphite fibers with a lower failure strain and higher stiffness.

The $[\pm 45]_6$ and $[\pm 75]_6$ HX205 and F185 tubes exhibited an essentially constant energy-absorption capability with respect to an increasing fiber failure strain. These tubes crushed in a local buckling mode. When brittle fiber-reinforced composite tubes crush in a local buckling mode, the most significant parameter that controls energy-absorption capabilities is "foundation" stiffness. The "foundation" stiffness relative to the "column" stiffness is very high for these tubes, and fiber failure strain has no significant effect on this parameter.

Effects of Fiber Failure Strain on Quasi-Isotropic T-300-934, K-934, and E-Gl-934 Tubes. The effects of fiber failure strain on the energy-absorption capability of T300-934, K-934, and E-Gl-934 quasi-isotropic $[0/\pm 45/90]_s$ tubes are examined in the fourth study. The energy-absorption capability of the T300-934 and K-934 tubes were approximately equal while the E-Gl-934 tube had approximately 18 percent higher energy-absorption capability than either the graphite- or Kevlar-reinforced tubes, as depicted in Fig. 31. The higher energy-absorption capability of the E-Gl-934 tubes is due to the larger deformations, prior to fracturing of the lamina bundles, that are achievable with the higher failure strain fiber. The crushing mode for the graphite-reinforced tubes was predominantly brittle fracturing, for the Kevlar was local buckling, and for the E-glass was a combined lamina bending and brittle fracturing, as shown in Fig. 32. Increasing the stability of the axial fibers, such
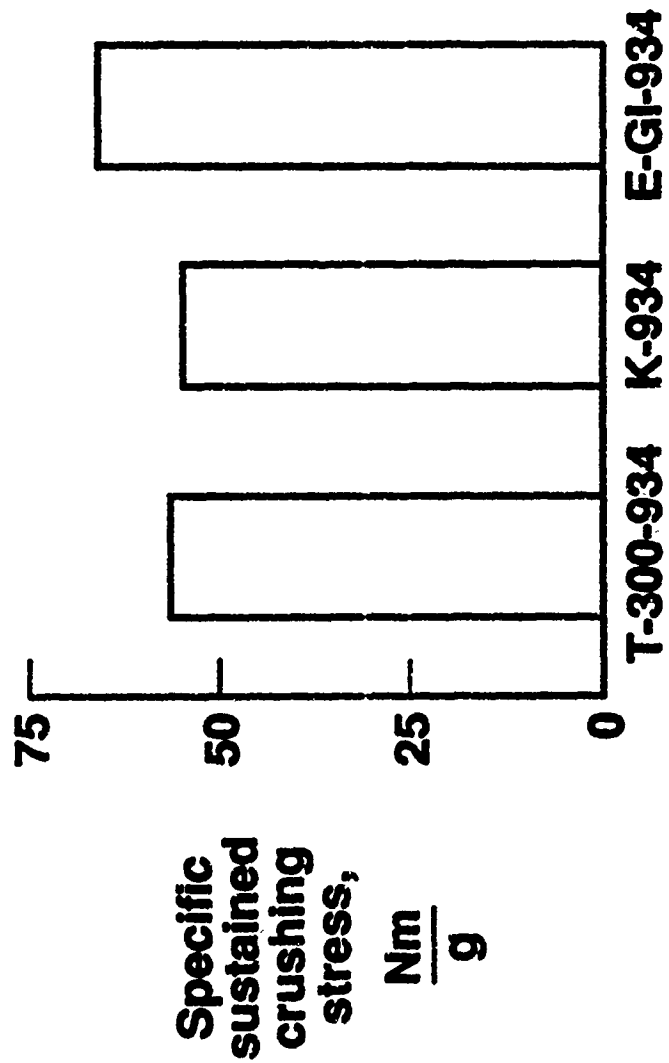
Figure 51. Energy-absorption capability of $[0/\pm 45/90]_S$ composite tubes.

E-G-934

K-934

T300-943
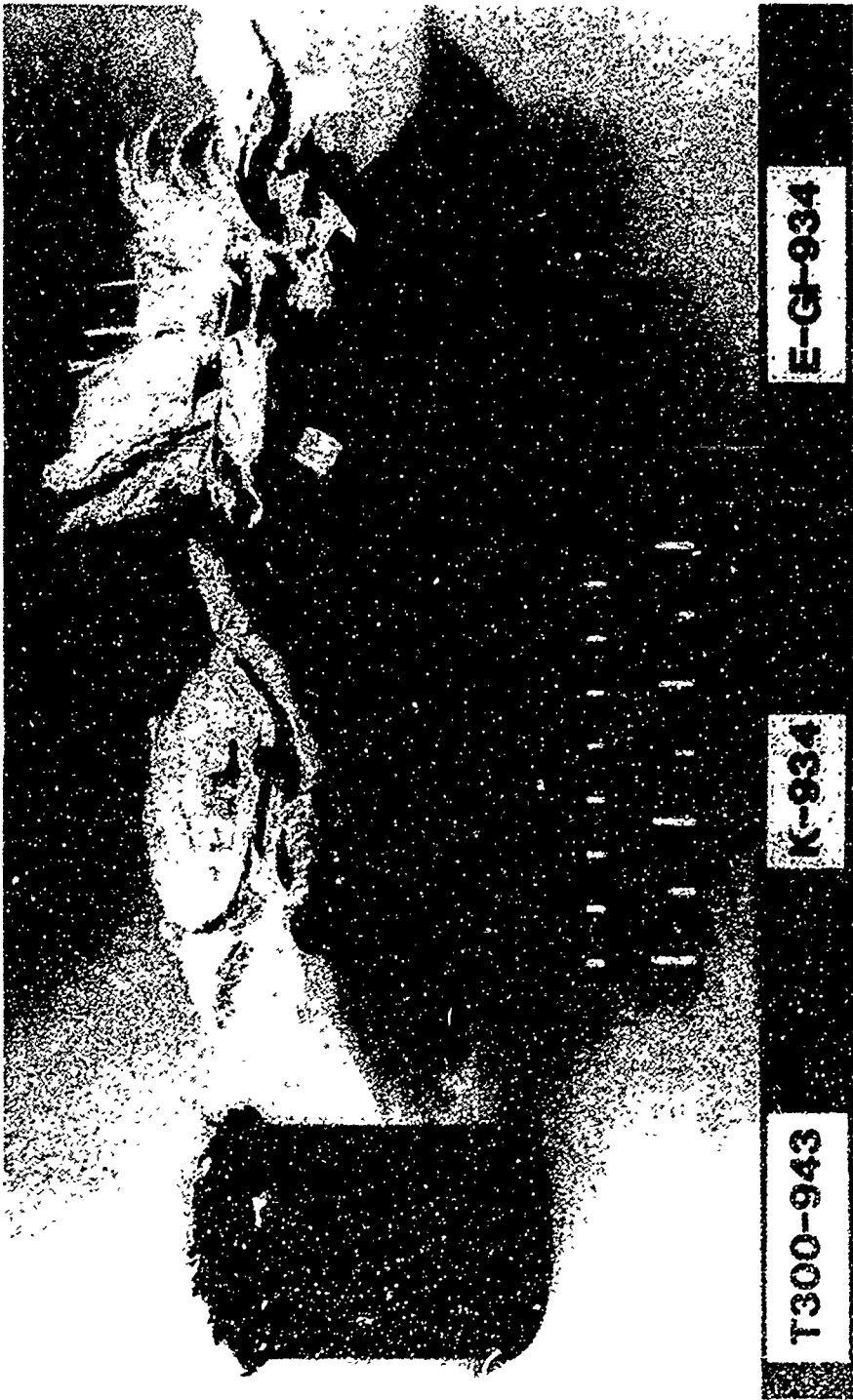
as by increasing the *"foundation"* stiffness, results in increased crushing efficiency, hence increased energy-absorption capability. If additional *"foundation"* stiffness, such as by using a stiffer matrix or reorienting the $\pm$ 45 fibers to 90 degrees, could be provided to the axial fibers of the E-Gl tubes, then further increases in energy-absorption capability could be achieved with the E-Gl reinforced tubes. Furthermore, the energy-absorption potential of the E-Gl reinforced tubes exceeds that of the T300 reinforced tubes.

Summary. As has been the case with many of the other studies, such as the effects of fiber and matrix stiffness on energy-absorption capability, the results are confusing if care is not taken in interpreting the results. An increase in fiber failure strain can increase, decrease, or have no effect on the energy-absorption capability of the tube specimen. However, if adequate *"foundation"* stiffness can be provided to the *"columns"*, then increasing fiber failure strain will result in increasing energy-absorption capability.

3.3.4 Effects of Matrix Failure Strain on Crushing Response of Fiber-Reinforced Composite Tubes

Tests were conducted to evaluate the effects of changes in matrix failure strain on the crushing response of brittle fiber- (graphite and E-Gl) and ductile fiber-(Kevlar) reinforced composite tubes. In this study, the materials used are T300-934. T300-5245, AS4-934, AS4-5245, AS6-934, AS6-5245, AS6-HX205, AS6-F185, E-Gl-934, E-Gl-HX205, E-Gl-F185, K-934, and K-974. The ply orientations of the tubes are $[0/\pm\Theta]_4$ and $[\pm\Theta]_6$.

Effects of Matrix Failure Strain on T300- and AS4-Reinforced Tubes. The effects of matrix failure strain on the energy-absorption capability of T300- and AS4-reinforced tubes were evaluated for $[0/\pm\Theta]_4$ and $[\pm\Theta]_6$ ply orientations. The matrix materials were 934 and 5245 which had 1.0 and 2.0 percent failure strains, respectively. For all ply orientations and reinforcement fibers, energy-absorption capability increased as matrix failure strain increased as depicted in Fig. 33. However, the magnitude of change in energy-absorption capability was a function of ply orientation. As the matrix failure strain increases, the length of the interlaminar cracks and *"column"* decreases. The sustained crushing load is inversely proportional to the length of the *"column"*. Therefore, as the length of the *"column"* decreases, the energy-absorption capability increases.

Effect of Matrix Failure Strain on AS6-reinforced Tubes. A similar series of tests was conducted using AS6 graphite fibers in 934, 5245, HX205, and F185 matrices for tubes with ply orientations of $[0/\pm\Theta]_4$ and $[\pm\Theta]_6$. As matrix failure strain increased from 1.0 (934) to 2.0 (5245) percent, there was a corresponding increase in energy-absorption capability. However, as matrix failure strain increased from 2.0 (5245) to 3.0 (HX205) and 13.0 (F185) percent, energy-absorption capability decreased, as depicted in Fig. 34. For the $[0/\pm15]_4$, $[0/\pm45]_4$ and $[\pm15]_6$ tubes, the decrease in energy-absorption capability is due primarily to the high failure strain matrix's inability to provide sufficient *"foundation"* stiffness to produce a brittle fracturing mode. The AS6-HX205 and AS6-F185 tubes exhibit shorter interlaminar crack lengths, as shown in Fig. 35, than either the AS6-934 or AS6-5245 tubes, but the lamina bundles exhibit little brittle fracturing. The lamina bundles of the AS6-HX205 and AS6-F185 $[\pm15]_6$ tubes seem to bend as if the crushing mode was local
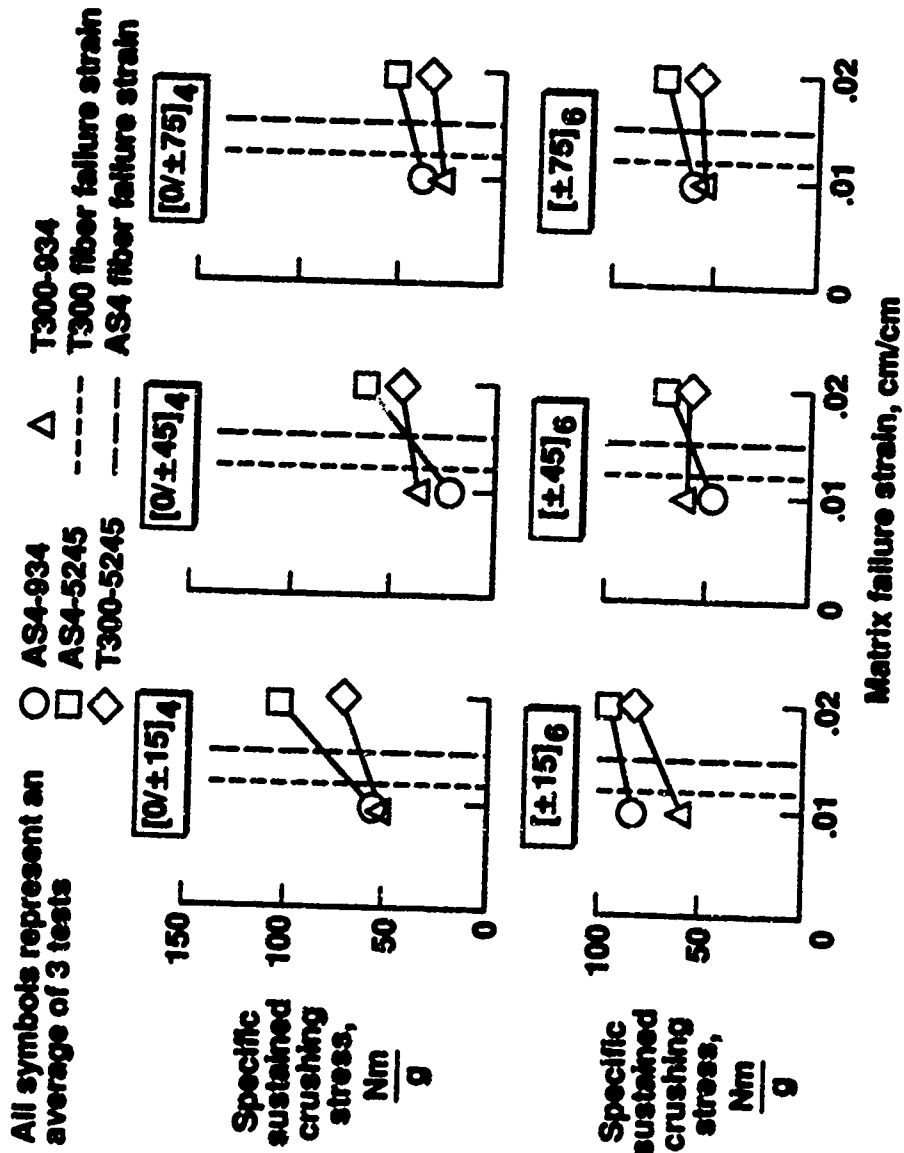
Figure 33. The effect of matrix failure strain on the energy-absorption capability of T300- and AS4-epoxy composite tubes.
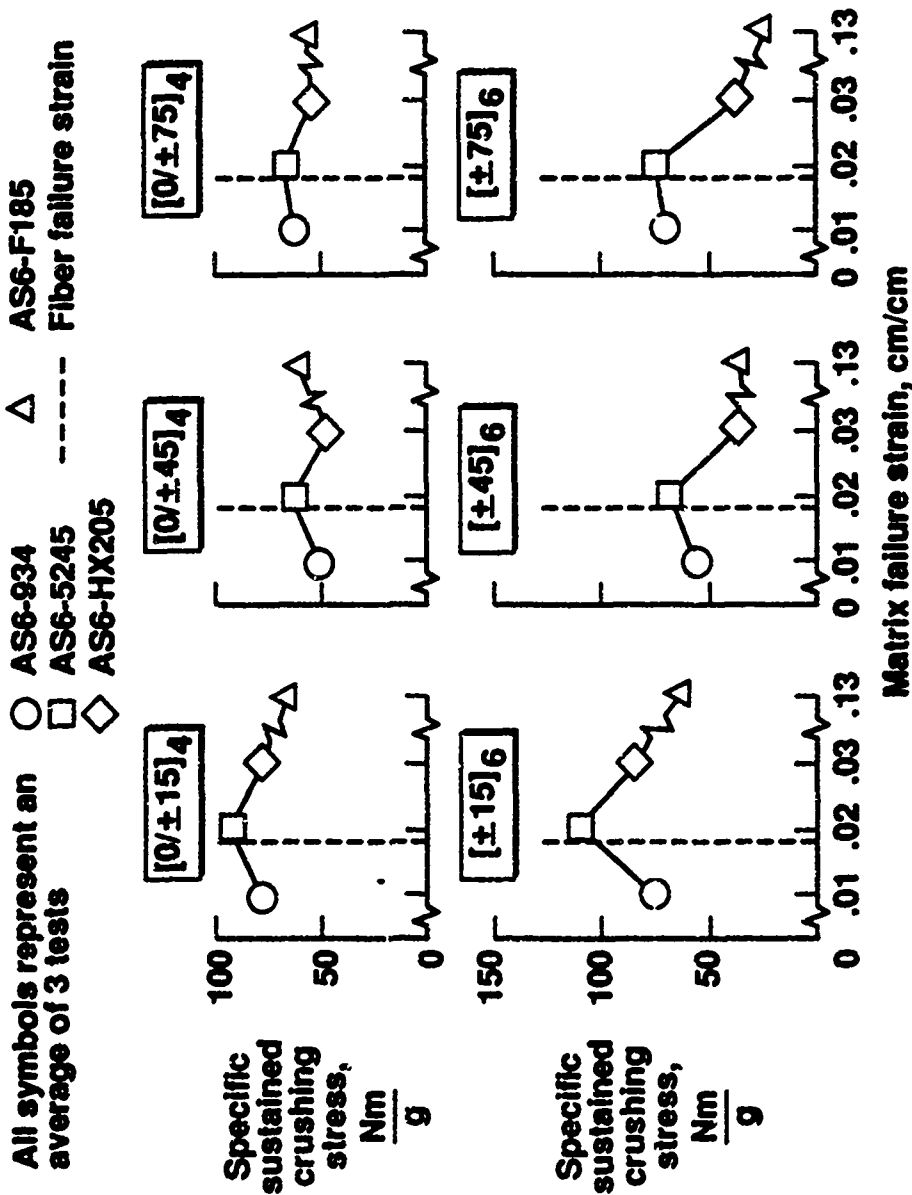
Figure 34. The effect of matrix failure strain on the energy-absorption capability of AS6-epoxy composite tubes.

92
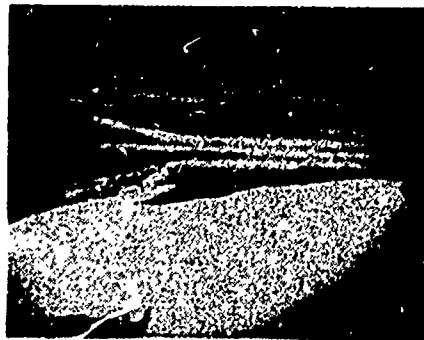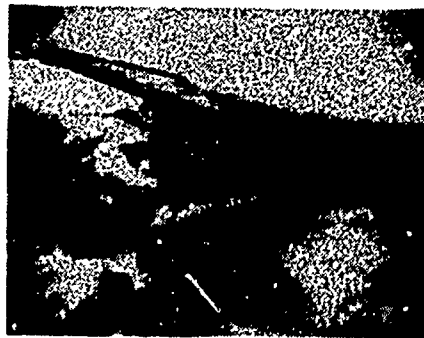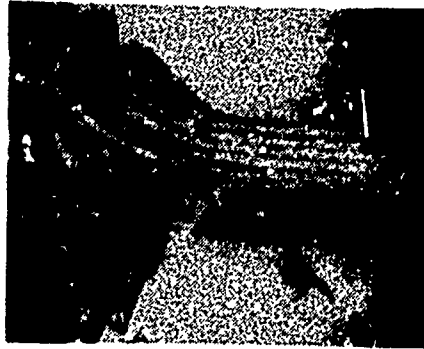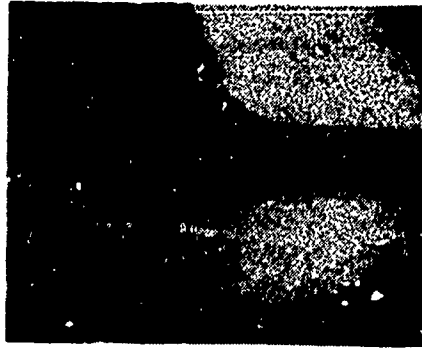
Figure 35. Photomicrographs of cross sections of $[\pm15]_{2}$ graphite-epoxy composite tubes.

AS6-F185

AS6-HX205

AS6-5245

AS6-934

93

buckling, as seen in Fig. 35. Little change in energy-absorption capability occurred for the [0/+75] tubes with increasing matrix failure strain. The $[\pm 45]_6$ and $[\pm 75]_6$ tubes crushed in a local buckling mode. The crushing modes of the $[\pm 45]_6$ tubes are shown in Fig. 36. The local buckling mode is generally a less efficient crushing mode than either brittle fracturing or lamina bending.

Effect of Matrix Failure Strain on E-Gl-Reinforced Tubes. Similar energy-absorption tests were conducted with E-Gl reinforced tubes with 934, HX205, and F185 matrices. The tube ply orientations were $[0/\pm \Theta]_4$ and $[\pm \Theta]_6$. Increasing matrix failure strain from 1.0 (934) to 3.0 (HX205) percent, for the $[0/\pm 15]_4$, $[0/\pm 45]_4$, and $[\pm 15]_6$ tubes, resulted in an increase in energy-absorption capability as seen in Fig. 37. However, as matrix failure strain increased further to 13.0 (F185) percent, energy-absorption capability decreased. The decrease in energy-absorption capability was due to insufficient *"foundation"* stiffness to produce a brittle fracturing crushing mode even though the length of the interlaminar cracks was relatively short. The decrease in energy-absorption capability also occurred for the AS6-F185 tubes described in the previous study.

The $[0/\pm 75]_4$ tubes exhibited essentially a constant energy-absorption capability over the range of materials evaluated. In this case, the *"foundation"* stiffness and the length of the interlaminar cracks is controlled by the circumferentially oriented fibers, and the matrix participates minimally.

In the case of the $[\pm 45]_6$ and $[\pm 75]_6$ tubes, the interlaminar cracks were eliminated and the crushing mode changed from predominately lamina bending with
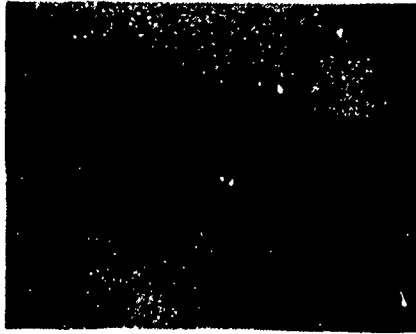
AS6-F185

AS6-HX205

AS6-5245

AS6-934

Figure 36. Photomicrographs of cross sections of $[\pm 45]_6$ graphite-epoxy composite tubes.
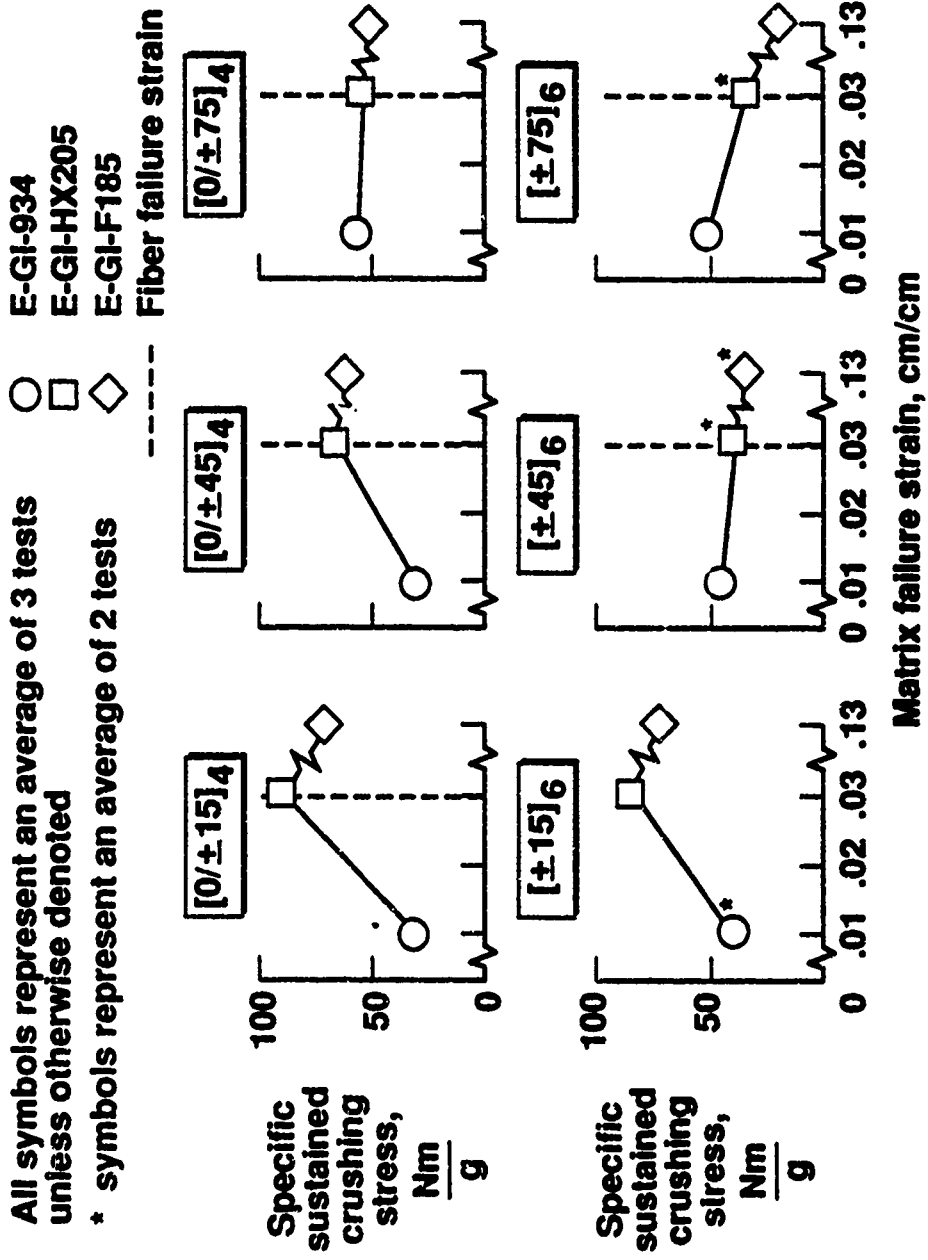
Figure 37. The effect of matrix failure strain on the energy-absorption capability of E-Gl-epoxy composite tubes.

the 934 matrix to local buckling with the HX205 and F185 matrices. Therefore, energy-absorption capability and crushing modes change little with matrix failure strain.

Effect of Matrix Failure Strain on Kevlar-Reinforced Tubes. Tests were conducted using Kevlar fiber in 934 and 974 matrices made into tubes having ply orientations of $[0/\pm\Theta]_4$ and $[\pm\Theta]_6$. In general, as matrix failure strain increases, energy-absorption capability slightly decreases as shown in Fig. 38. This decrease is attributed to the nonlinear stress-strain characteristics of the 974 matrix. That is, at high strain levels, the 974 matrix exhibits considerable nonlinear behavior which results in a reduced matrix stiffness; hence, less *"foundation"* stiffness is provided to the *"column"*. The reduced *"foundation"* stiffness reduces the buckling load of the *"column"* which results in decreased energy-absorption capability.

3.4 Effects of Specimen Structural Variables on Crushing Response

A series of studies was conducted to determine the effects of specimen structural variables on the crushing response of composite tube specimens. The specimen structural variables investigated are ply orientation, fiber volume fraction, stacking sequence, hybridization, and geometry. Isolating the effects of a single structural variable on the crushing response of composite tubes is relatively straightforward as compared to the previous study where changes in one material property (failure strain) could not be uncoupled from another property (stiffness).

All tests were conducted using tubular specimens of either circular, square, or
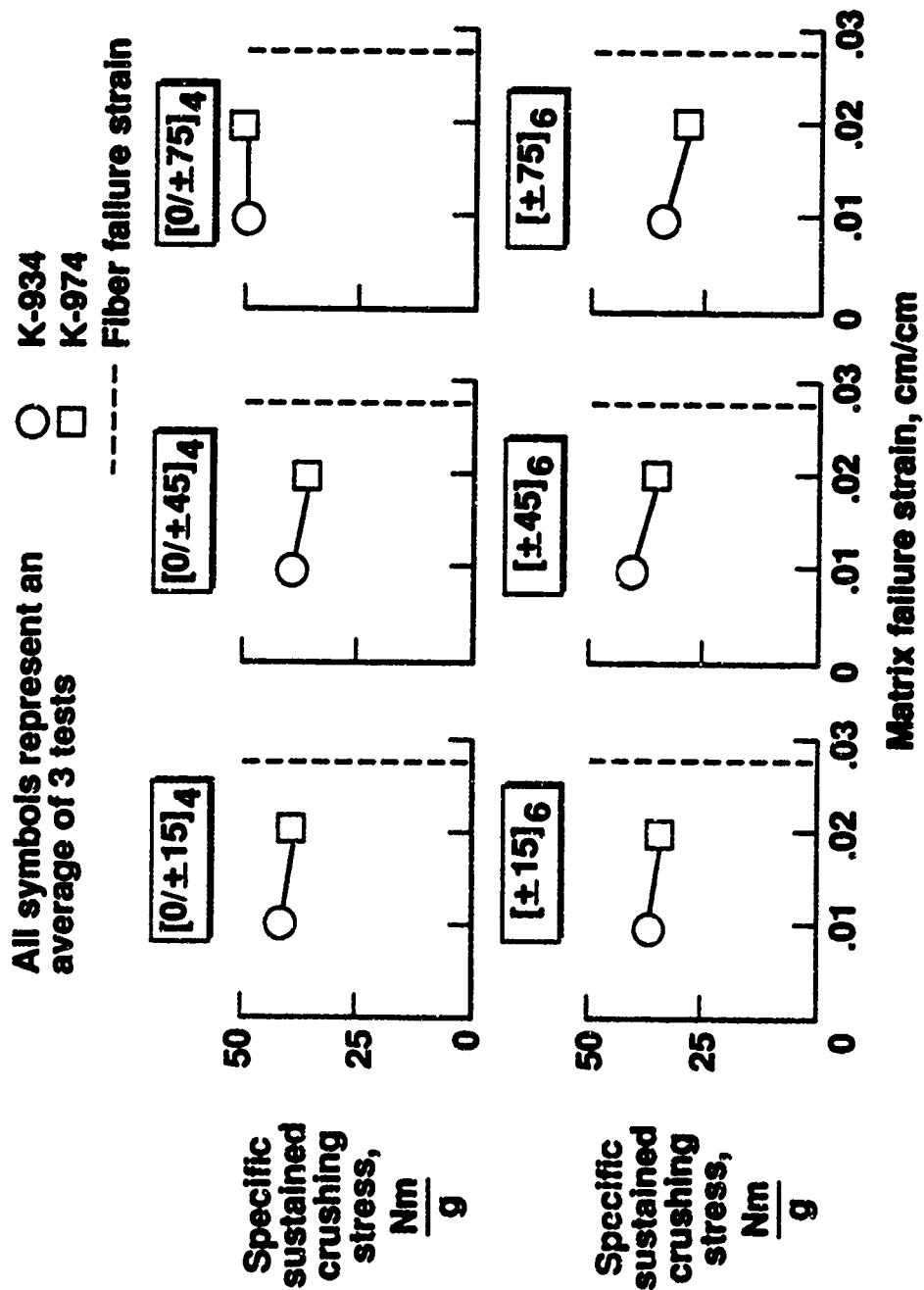
Figure 38. The effect of matrix failure strain on the energy-absorption capability of K-epoxy composite tubes.

"near-elliptic" cross section. All tubes were 10.16 cm in length, 3.81 cm in inside diameter, and were crushed in accordance with procedures described in Chapter 2.

3.4.1 Effects of Tube Ply Orientation on Crushing Response of Composite Tubes

The most widely used structural variable to tailor the response of a composite structure is ply orientation. Extension, bending, shear, and torsional stiffnesses of composite structures are all functions of ply orientation. In this study, tube ply orientations of $[0/\pm\Theta]_4$ and $[\pm\Theta]_6$ were evaluated. Composite materials used in this investigation were T300-934, K-49-934, and E-Gl-934. These materials were chosen because the energy-absorption trends produced by the materials are a result of different crushing mechanisms.

Effects of Tube ply Orientation on Crushing Response of T300-934 Tubes. The energy-absorption capability of the T300-934 tubes generally decreases as Θ increases for both $[0/\pm\Theta]_4$ and $[\pm\Theta]_6$ ply orientation tubes as seen in Fig. 39. The decrease in energy-absorption capability trend follows the same trend as does extensional stiffness with changes in ply orientation. However, there is an anomaly with the $[\pm\Theta]_6$ ply orientations near $\Theta=30$ degrees. The energy-absorption capability, as Θ decreases from $\Theta=5$ degrees, decreases until $\Theta=30$ degrees. Energy-absorption capability begins to increase as Θ increases between $\Theta=30$ and 45 degrees and then decreases as Θ increases from 45 to 60 degrees. At angles greater than 60 degrees, energy-absorption capability decreases as Θ increases. The "bucket" shape formed by the energy-absorption curve, as seen in Fig. 39. near $\Theta=30$ degrees is attributed
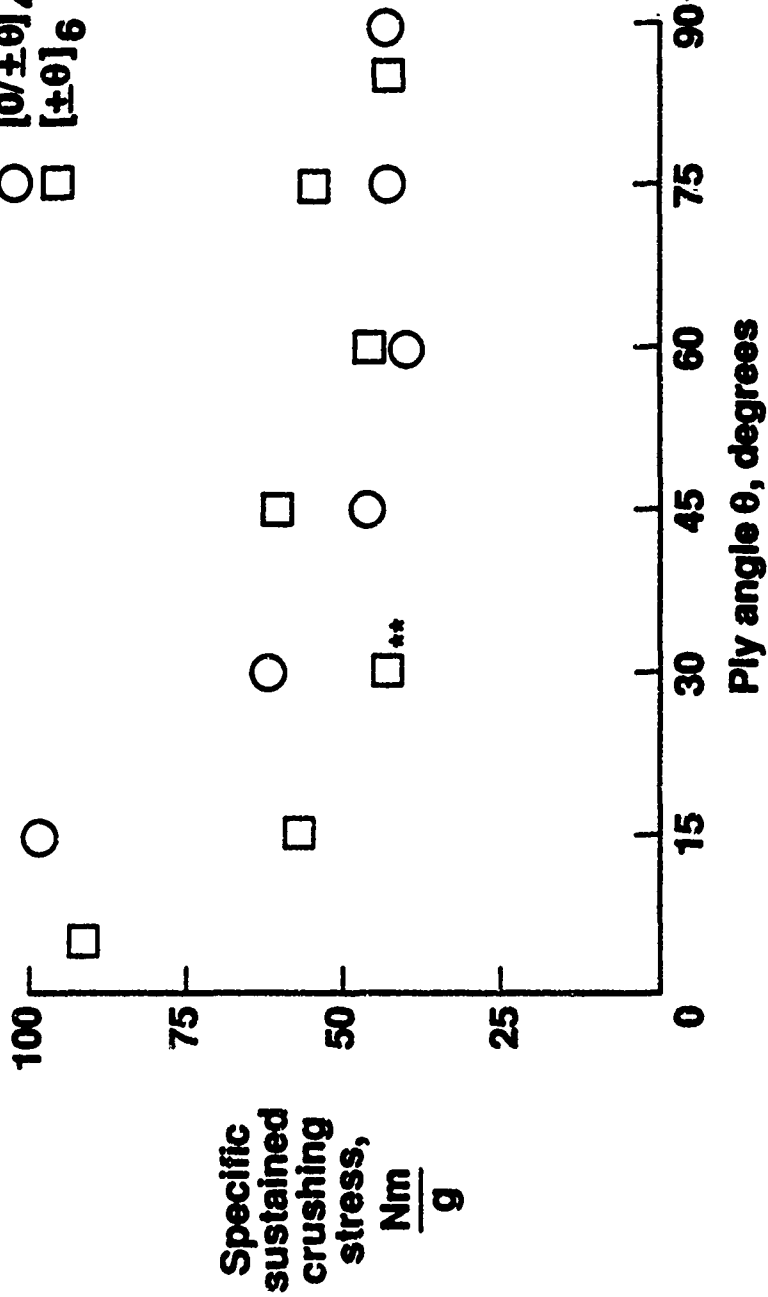
Figure 39. Effect of ply orientation on the energy-absorption capability of T300-934 composite tubes.

to the high Poisson's ratio of the $\pm$ 30 ply orientation. The high Poisson's ratio causes high interlaminar stresses which facilitate interlaminar crack growth. Long crack lengths result in longer lamina bundles and lower the buckling load, and hence reduce the energy-absorption capability.

The length of the interlaminar cracks in the $[\pm 30]_6$ tube is longer than in the $[\pm 15]_6$ or the $[\pm 45]_6$ composite tubes. Typically, the longer the interlaminar cracks, the lower the energy-absorption capability of the tube. The predominant crushing modes for the tubes are combined brittle fracturing and lamina bending. The percentage of material that crushes in each mode changes with ply orientation. Generally, as more circumferential support is provided by the circumferential fibers, more of the material crushes in a brittle fracturing mode. However, as more of the fibers are oriented in the circumferential direction and the crushing efficiency improves, the longitudinal stiffness of the lamina bundles decreases. The net result is a change of crushing modes, and the energy-absorption capability can increase, decrease, or remain unchanged.

Effects of Tube Ply Orientation on Crushing Response of E-Gl-934 Tubes. The energy-absorption trends for both the E-Gl-934 $[0/\pm\Theta]_4$ and the $[\pm\Theta]_6$ tubes in Fig. 40 are considerably different than the energy-absorption trends exhibited by the T300-934 tubes in Fig. 39. The energy-absorption capability of the $[0/\pm\Theta]_4$ E-Gl-934 tubes increases as ply angle Θ increases until approximately $\Theta=60$ degrees. That is, the increase in energy-absorption capability as a function of Θ is larger as a result of increased *"foundation"* support from the circumferentially oriented fibers

101
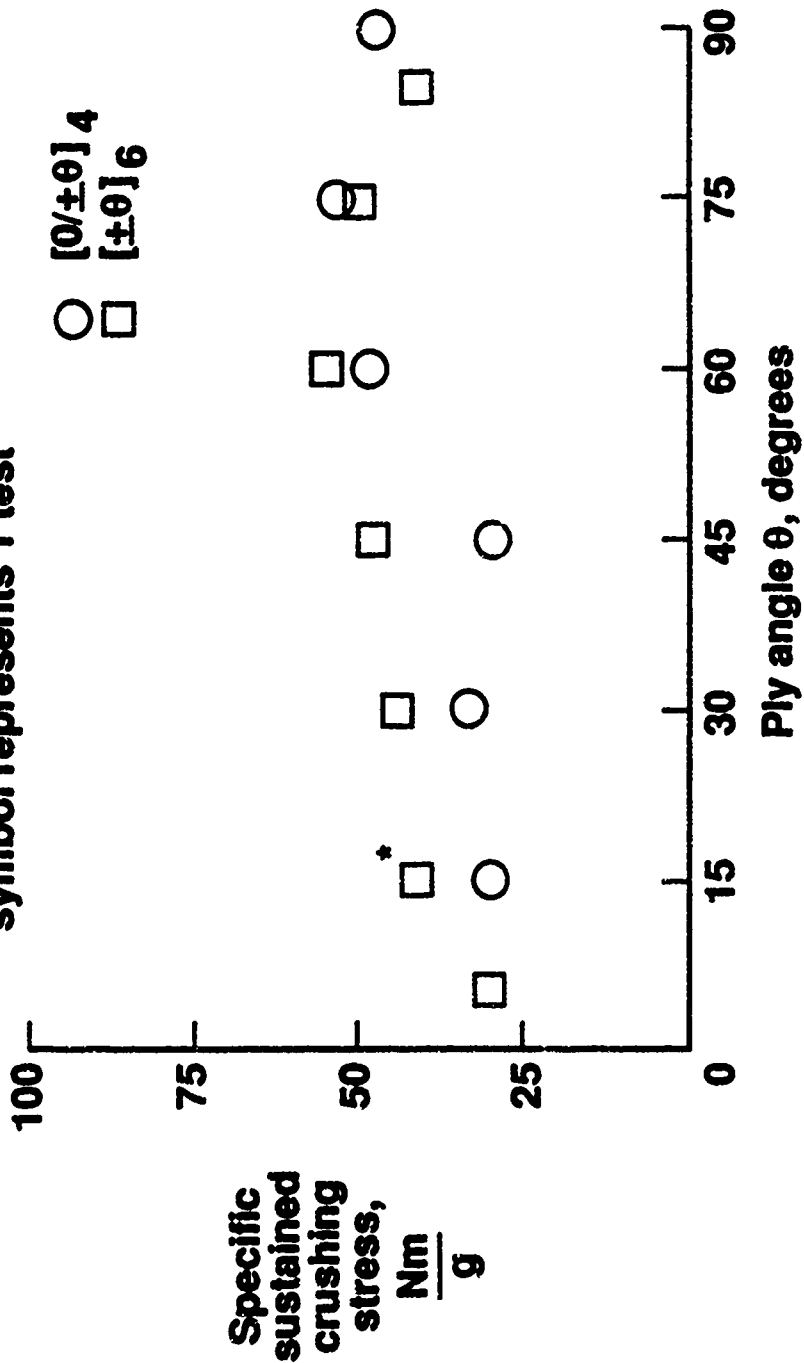
Figure 40. Effect of ply orientation on the energy-absorption capability of E-Gl-934 composite tubes.

than the decrease in energy-absorption capability as a result of decreased "column" stiffness. At ply orientations greater than 60 degrees, the energy-absorption capability decreases as ply orientation increases. As ply angle Θ increases, the decrease in energy-absorption capability is due to the decreased "column" stiffness.

The failure strain of the fiber and matrix significantly affects the crushing characteristics of the composite tube. In the case of the E-Gl-934 composite tubes, the glass reinforcement has a high failure strain and exhibits brittle failure characteristics. The matrix has a lower failure strain than the glass fiber, and the matrix also exhibits brittle failure characteristics. When fibers and matrices with brittle failure characteristics are combined. then the predominant crushing mode will be lamina bending. A brittle fracturing mode can be achieved if circumferentially oriented fibers can stiffen the "foundation" and stabilize the "column" . In the case with the E-Gl-934 tubes, the matrix alone can not stabilize the axially oriented fibers. Therefore, tubes with near 0 degree ply orientations can have lower energy-absorption capability than tubes with a mixture of 0 degree and circumferentially oriented fibers. As ply angle Θ increases and the fibers are able to increase the "foundation" stiffness, then the energy-absorption capability increases. As ply angle Θ increases beyond $\Theta=60$ degrees, further increase in foundation stiffness from the circumferential fibers is minimal. Also, as ply angle Θ increases, the "column" stiffness decreases. Therefore, a slight decrease in energy-absorption capability occurs as Θ increases beyond 60 degrees.

The crushing mode of the E-Gl-934 tubes is predominately lamina bending. Interlaminar crack length generally decreases as Θ increases because, as Θ increases,

103

"foundation" stiffness increases. Ply orientations greater than 60 degrees provided little further reduction in interlaminar crack length.

Effects of Tube Ply Orientation on Crushing Response of K-934 Tubes. The Kevlar-reinforced 934 epoxy matrix material produces energy-absorption trends, in Fig. 41, similar to those of the E-Gl-934 composite tubes in Fig. 40. However, the material mechanical properties that are responsible for these energy-absorption trends are different from the corresponding properties of the E-Gl-934. All of the Kevlar-reinforced tubes crushed in a local buckling crushing mode. The 934 matrix, when combined with the high failure strain and ductile compressive failure characteristic Kevlar fiber, can not provide sufficient *"foundation"* stiffness to stabilize the axial Kevlar fibers. Therefore, when Θ is small, that is, when the fibers are predominantly oriented in the direction of the applied load, the tube crushes at a low applied load, hence a low energy-absorption capability. As Θ increases, the circumferentially oriented fibers contribute to the *"foundation"* stiffness which results in an increase in energy-absorption capability. Beyond $\Theta = 60$ degrees, the energy-absorption capability of the $[0/\pm\Theta]_4$ tubes continues to increase while the energy-absorption capability of the $[\pm\Theta]_6$ tubes decreases. That is, for the $[0/\pm\Theta]_4$ tubes, the increase in energy-absorption capability as a function of increasing Θ is the result of increasing *"foundation"* support. This *"foundation"* stiffness is larger than the decrease in energy-absorption capability due to a decreasing *"column"* stiffness. The axial stiffness of the $[\pm\Theta]_6$ tubes decreases as Θ increases resulting in a decrease in energy-absorption capability. Unlike the situation in which Θ is less than 60 degrees for the $[\pm\Theta]_6$ tubes, further increase in circumferential fibers

104
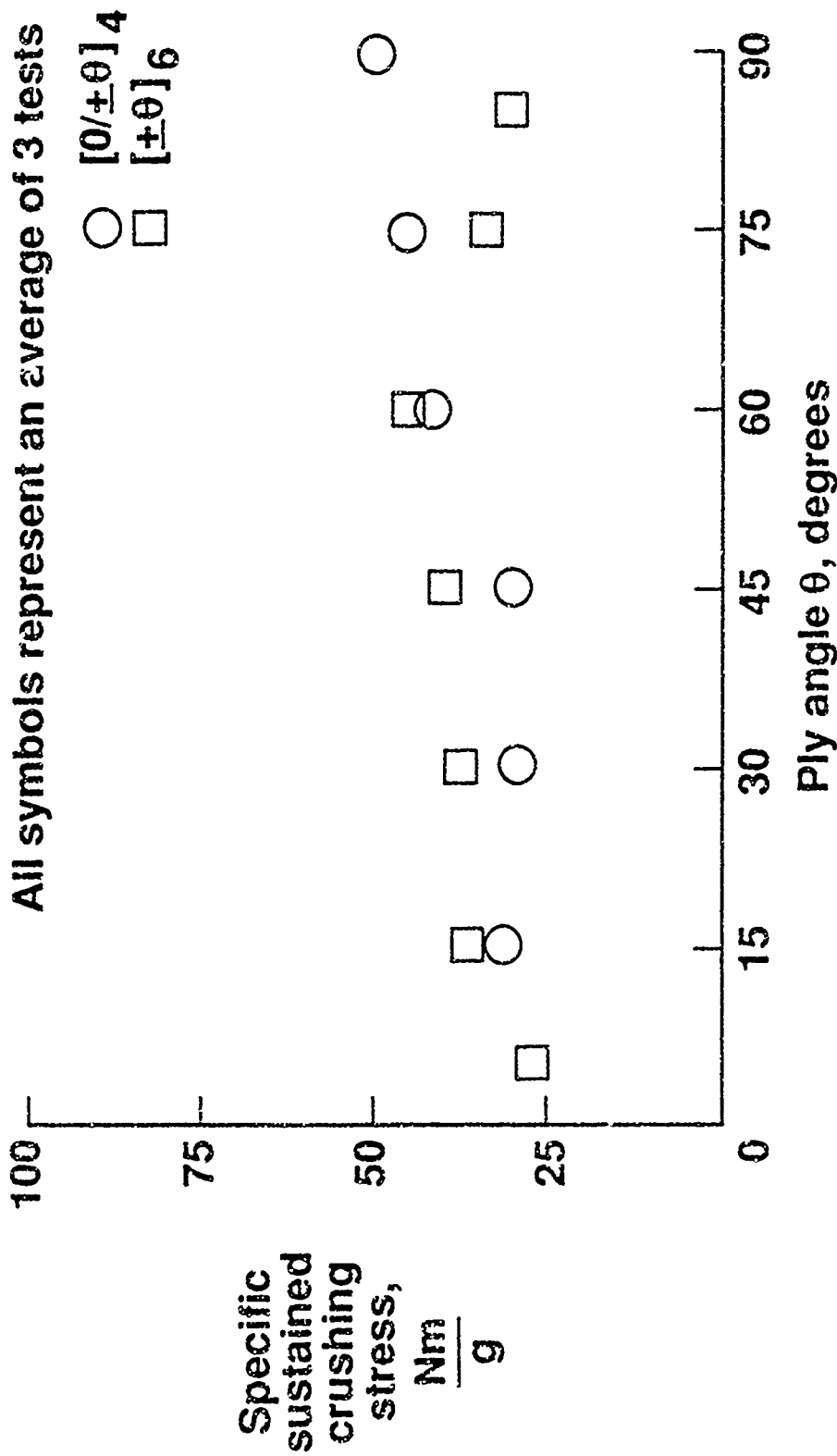
Figure 41. Effect of ply orientation on the energy-absorption capability of K-934 composite tubes.

105

increases the *"foundation"* stiffness proportionally but decreases the axial stiffness of the tube. The reduction of axial stiffness results in a lower buckling load and hence, a decrease in energy-absorption capability.

3.4.2 Effects of Fiber Volume Fraction on Crushing Response of Composite Tubes

Fiber volume fraction is a parameter that is not frequently used to change the mechanical response of a composite structure. Generally, the designer, based upon manufacturing and other design requirements and limitations, is required to use materials having a specific fiber volume fraction. Most aircraft composite primary structures have fiber volume fractions between 55 and 65 percent. Laminate extensional stiffness and strength typically vary linearly with fiber volume fraction because they are fiber dominated. However, to more completely understand the crushing response of composite materials, it is important to understand how the crushing response of the tube changes as a function of fiber volume fraction.

The effect of fiber volume fraction on the energy-absorption characteristics of T300-934 and K-934 composites was investigated. Prepreg material with different percentages, between 40 and 70 percent, of fiber by volume were used to make tube specimens. Fiber volume fraction was determined using a nitric acid digestion technique, Ref. 29, for the graphite-reinforced composites while a DMSO acid digestion technique, Ref. 30, was used for the Kevlar-reinforced composites. Ply orientations used in this investigation were $[\pm 45]_6$, $[0/\pm 15]_4$, and $[0/\pm 75]_4$.

Effects of Fiber Volume Fraction on Crushing Response of T300-934 Tubes. Fiber volume fractions of the T300-934 composite tubes were between 40 and 55 percent. As

106

fiber volume fraction increases, the $[\pm45]_6$ and $[0/\pm15]_4$ tubes exhibited an approximate 10 percent decrease in energy-absorption capability while the $[0/\pm75]_4$ tubes experienced no change in energy-absorption capability, as depicted in Fig. 42.

Energy-absorption capability as defined in this study is inversely proportional to the density of the composite material. The density of the composite material can change as fiber volume fraction changes because the densities of the fiber and matrix material are usually different. Therefore, composite materials composed of the same constituent material but having different fiber volume fractions can exhibit different energy-absorption capabilities even though their average crushing stress are the same. For example, as fiber volume fraction increases, the density of the T300-934 composite material increases while the density of the K-934 is almost unchanged.

As fiber volume fraction increases, the volume of matrix between fibers and adjacent plies decreases resulting in closer fiber spacing. The proximity of adjacent fibers can affect the stress state in the matrix in the following manner. The magnitude of the stresses in the matrix adjacent to a fiber decrease with increasing distance from the fiber. Provided sufficient distance exists between fibers, certain stress components will vanish or reach a constant magnitude at some distance from the fiber. If adjacent fibers are closely spaced, then an interaction exists in the stress state in the matrix between the fibers. This interaction can result in a stress state of a higher magnitude than if the fibers were more widely spaced. These higher matrix stresses as a result of higher volume fraction can allow formation and propagation of cracks at lower load levels than would occur at lower fiber
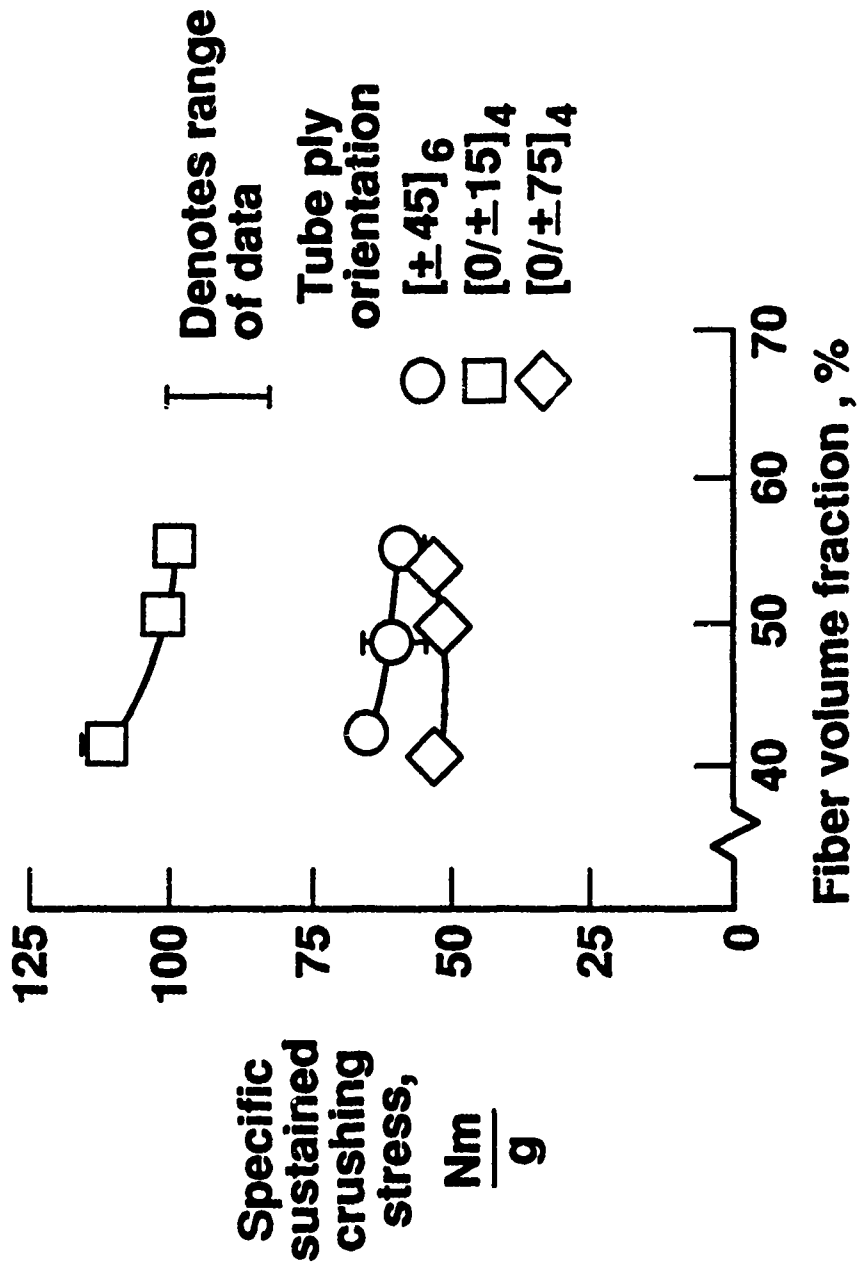
Figure 42. Effect of fiber volume fraction on the energy-absorption capability of T300-934 composite tubes.

volume fractions. As previously discussed, energy-absorption capability is inversely proportional to interlaminar crack length. Therefore, as fiber volume fraction increases, the sustained crushing load decreases and the density of the material increases. The net effect is a decrease in energy-absorption capability for the $[\pm 45]_6$ and $[0/\pm 15]_4$ tubes.

The process of forming interlaminar cracks and their subsequent propagation is also a function of ply orientation. The length and location of interlaminar cracks is a function of the ability of circumferentially oriented fibers to stabilize the axial fibers. As discussed in the subsubsection on *3.4.1 Effects of Tube Ply Orientation on Crushing Response of Composite Tubes*, when there are circumferential fibers, in this case $\Theta=75$ degrees, to stabilize the axial fibers, the circumferential fibers provide most of the *"foundation"* stiffness.

For the case of the $[0/\pm 75]_4$ tubes, a hypothesis of the phenomena that controls the crushing process is as follows: as fiber volume fraction increases, the compliance between the circumferential and axial fibers decreases because there is less matrix between the circumferential and axial fibers. The decrease in compliance, hence an increase in *"foundation"* stiffness results in an increase in the sustained crushing load. Increase in fiber volume fraction results in an increase in density of the T300-934 composite material. Therefore, the increase in sustained crushing load is offset by the increase in material density resulting in little or no change in energy-absorption capability with respect to changes in fiber volume fraction.

Effects of Fiber Volume Fraction on Crushing Response of K-934 Tubes. Energy-absorption capability of K-934 $[\pm 45]_6$, $[0/\pm 15]_4$, and $[0/\pm 75]_4$ tubes as a function of fiber

volume fraction between 46 and 70 percent was investigated. Between fiber volume fractions of 46 and 55 percent, the change in energy-absorption capability was negligible for all ply orientations as seen in Fig. 43. Both the $[\pm 45]_6$ and $[0/\pm 75]_4$ ply orientations exhibited approximately a 10 percent decrease in energy-absorption capability between fiber volume fractions of 54 and 70 percent. The energy-absorption capability of the $[0/\pm 15]_4$ ply orientation increased approximately 10 percent between fiber volume fractions of 55 and 66 percent. Unfortunately, the small magnitude of change in energy-absorption hinders resolution of the governing mechanism.

3.4.3 Effects of Stacking Sequence on Crushing Response of Composite Tubes

A change in stacking sequence can refer to the total description of a laminate or merely to the mean order of predetermined layer orientations. In this study the definition of stacking sequence is the later. A change in laminate stacking sequence is an effective method of changing the bending stiffness of a laminate without altering the in-plane stiffness. This technique of tailoring bending stiffness is used sparingly because more significant changes in bending stiffness can be achieved by the use of stiffeners or utilizing a sandwich construction. Change in stacking sequence is generally dictated by manufacturing considerations. Many companies limit the number of plies of the same fiber direction that are stacked together to reduce problems with laminate consolidation and free-edge stresses.

Effects of Stacking Sequence on Crushing Response of $[\pm 45]_7$ *300-934 and K-934 Tubes.* In this study, the effects of stacking sequence are studied using a family of $[\pm 45]_6$ T300-934 and K-49-934 and a hybrid laminate composed of unidirectional T300-934 and a

110
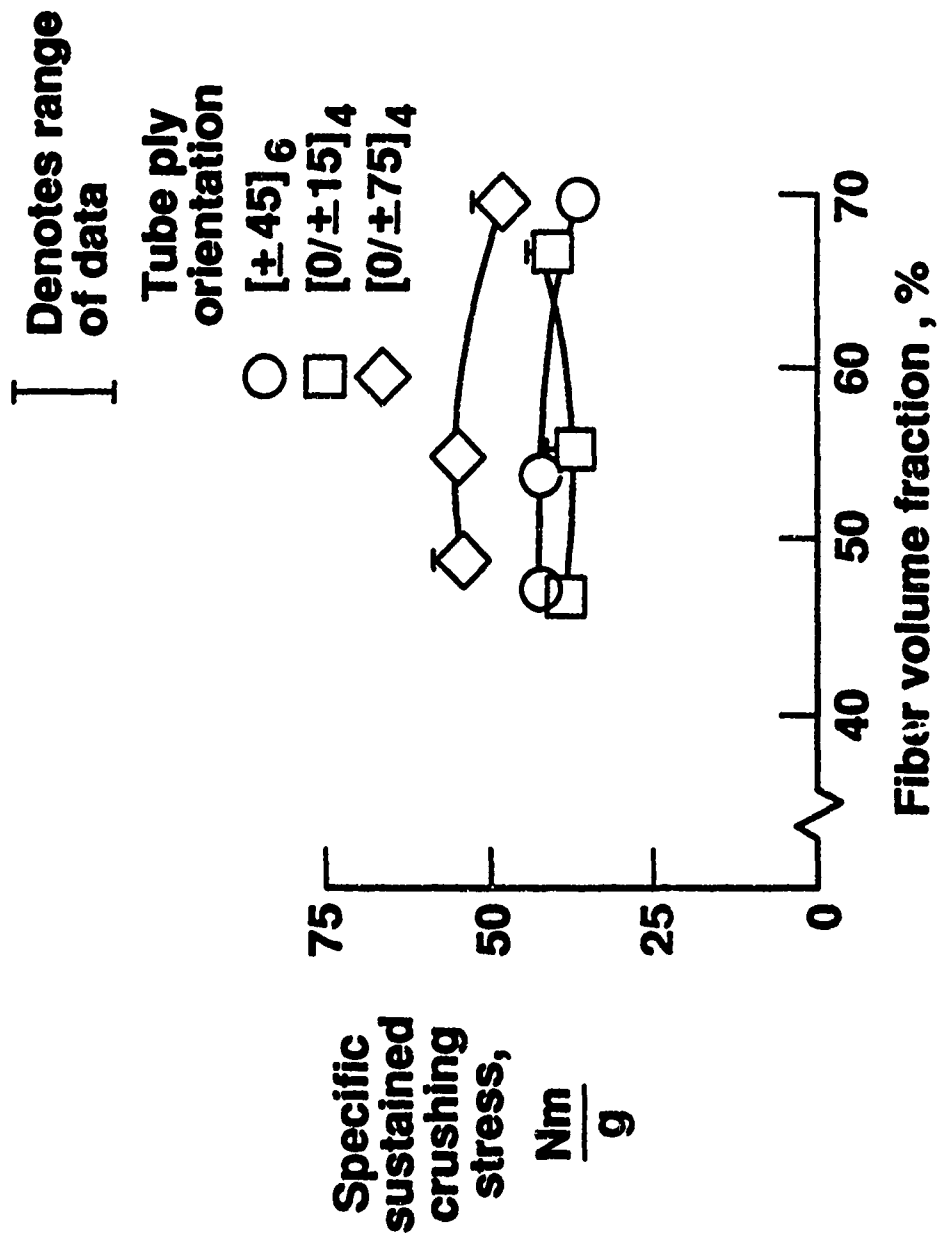
Figure 43. Effect of fiber volume fraction on the energy-absorption capability of K-934 composite tubes.

111

hybrid woven fabric (T300-K) with a 934 matrix. The [±45] ply orientations typify the effects of changes in stacking sequence of most commonly used laminates while the hybrid fabric would represent special layups devised for high energy-absorption capability and post-crushing integrity.

Five different [±45] configurations were investigated to determine the effect of stacking sequence on energy-absorption capability. The two T300-934 and three K-934 stacking sequences investigated were $[\pm 45]_6$ and $[\pm 45]_{3S}$ plus $[\pm 45]_6$, $[\pm 45]_{3S}$, and $[+45_6/-45_6]$, respectively. The differences in energy-absorption capability of the two different T300-934 layups were less than 5 percent as seen in Fig. 44. The crushing modes for both layups were predominately brittle fracturing. The energy-absorption capability of the $[\pm 45]_6$ and $[\pm 45]_{3S}$ K-934 tubes were comparable whereas the energy-absorption capability of the $[+45_6/-45_6]$ K-934 tubes were approximately 30 percent less than the other K-934 tubes in Fig. 44. All of the K-934 tubes crushed in similar local buckling modes. However, the $[+45_6/-45_6]$ K-934 tube exhibited more extensive interlaminar delaminations than the other K-934 tubes. It is doubtful that a designer would prescribe the $[+45_6/-45_6]$ layup because of the segregation of ply orientations. A designer would probably use the $[\pm 45]_{3S}$ ply orientation. Therefore, based upon the [±45] family of ply orientations of T300-934 and K-934 that would typically be used in a structure, the effect of ply orientation is small.

The [±45] layup is not the most efficient with respect to energy-absorption capability. When energy-absorption capability becomes the driving design requirement, then the structural designer will want to employ more efficient ply orientations than

112
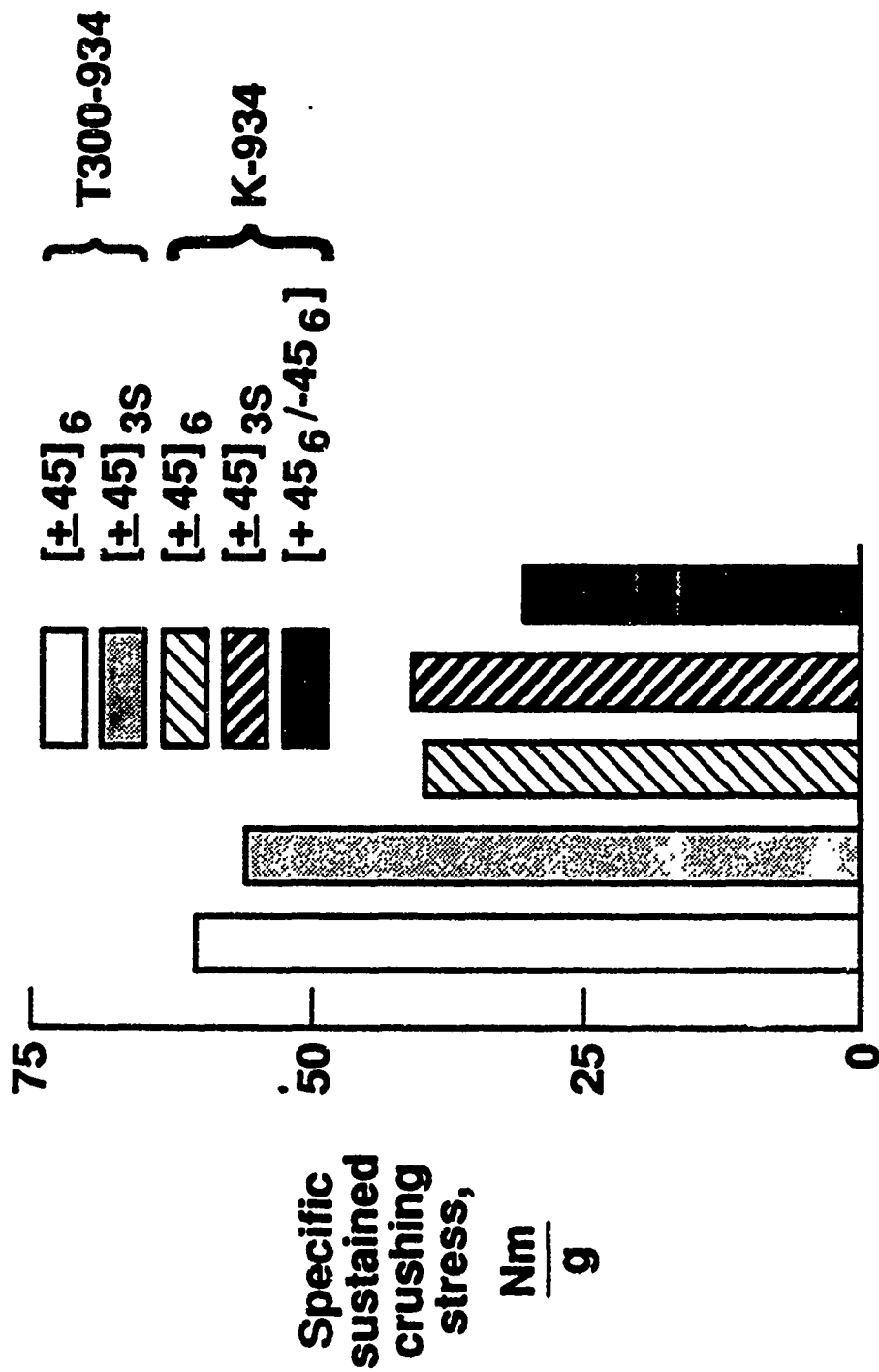
Figure 44. Effect of stacking sequence on the energy-absorption capability of $[\pm 45]_T$ 300- and K-934 composite tubes.

113

[±45] . As shown in previous sections, to increase the energy-absorption capability, a large percentage of fibers should be oriented in the direction of the applied load. The following example will show a major pit fall that could await the designer if stacking sequence considerations were not considered.

Effects of Stacking Sequence on Crushing Response of Hybrid Composite Tube. A hybrid tube composed of unidirectional T300-934 material oriented at a 0 degree ply orientation is combined with a balanced plain weave hybrid fabric material (T300-K-934) oriented at 45 degrees. The ply orientations of the tubes were $\left[+45_F^H/0_{5T}^{Gr}\right]_S$ and $\left[0_{5T}^{Gr}/+45_F^H\right]_S$ where T and F refer to tape and fabric prepreg, respectively, Gr refers to graphite, and H refers to a hybrid material composed of alternate tows of graphite and Kevlar. The $\left[+45_F^H/0_{5T}^{Gr}\right]_S$ tube energy-absorption capability was 300 percent higher than the $\left[0_{5T}^{Gr}/+45_F^H\right]_S$ tubes as seen in Fig. 45. The difference in energy-absorption capability is attributed to the different crushing modes. The tubes that had 0 degree fibers on the outside of the stacking sequence exhibited a lamina bending crushing mode for the 0 degree plies and a local buckling mode for the hybrid fabric as depicted in Fig. 45. As previously discussed, the lamina bending mode is not as an efficient crushing mode as the brittle fracturing mode. The crushing mode of the ply orientation where the 0 degree T300-934 plies are imbedded in the center of the stacking sequence is brittle fracturing of the 0 degree T300-934 plies, and the hybrid fabric on the outer plies tended to peel away from the unidirectional graphite as the tube was crushed. The hybrid fabric, because of the

114
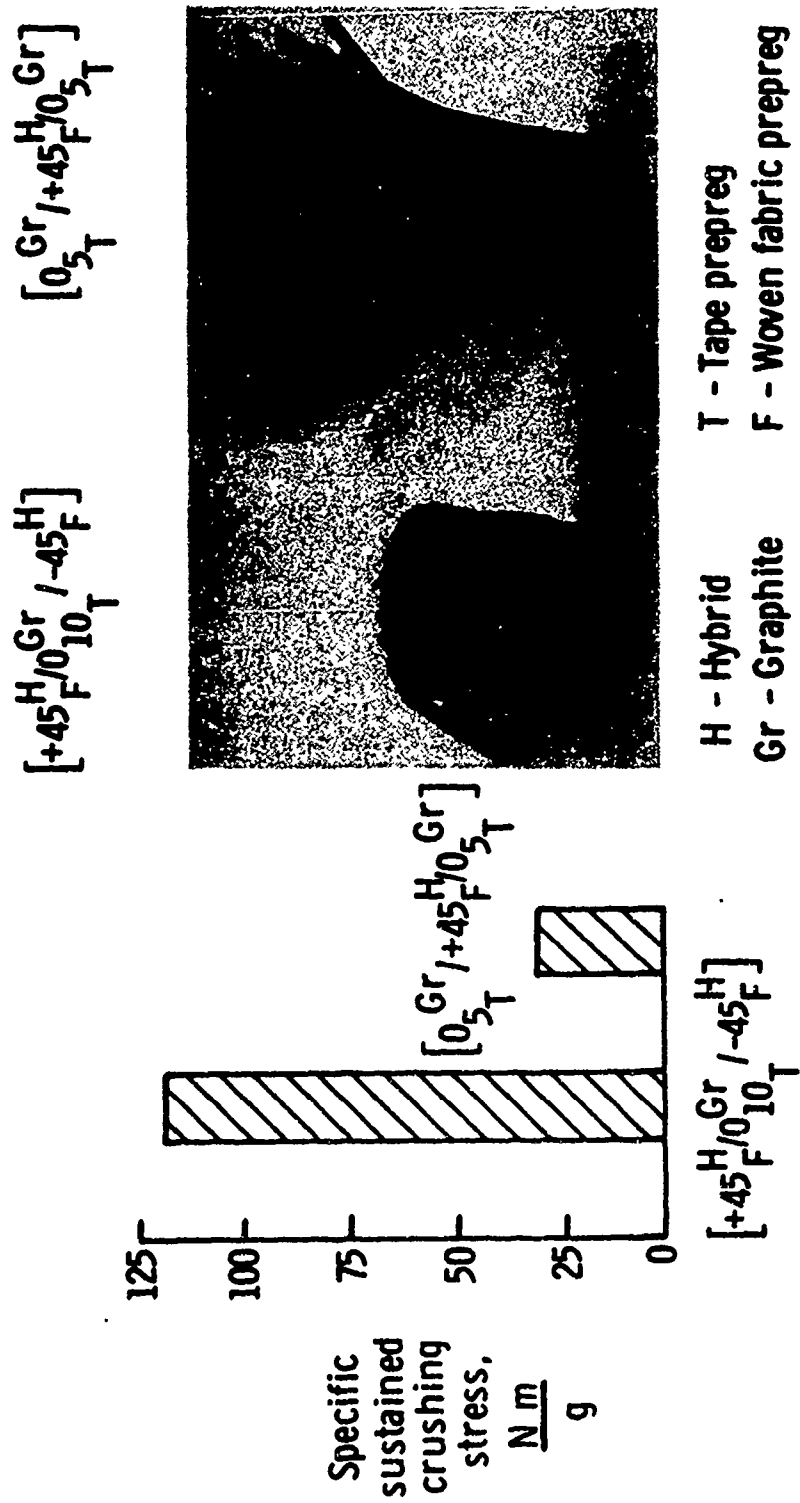
Figure 45. Effect of stacking sequence on the energy-absorption capability of hybrid composite tubes.

high-failure-strain Kevlar fibers, provided the necessary *"foundation"* stiffness to stabilize the 0 degree T300-934 plies to facilitate the crushing in a brittle fracturing mode. The peeling of the hybrid fabric outer ply would not occur in a built-up beam structure because the outer ply would be molded into the beam cap. In a beam composed of these hybrid materials, the outer ply would probably delaminate as the beam was crushed and fold producing a local buckling mode. The folding of the outer ply would provide the beam with post-crushing integrity.

3.4.4 Crushing Response of Hybrid Composite Materials

The term hybrid composite materials encompasses a broad category of materials and material forms. Generally, the term hybrid composite materials is used in reference to combinations of different fiber reinforcements, such as graphite-Kevlar hybrids. Mixed-matrix materials are difficult to cure properly, so mixed-fiber, single matrix hybrid materials are practical examples of hybrid composite materials. Hybrid materials offer the potential of increased energy-absorption capability and post-crushing integrity that is not readily achievable with a single-fiber composite material system.

In this investigation, three examples of hybrid materials will be presented to demonstrate the energy-absorption capability and post-crushing integrity that is achievable with hybrids. The first example is a hybrid balanced woven fabric composed of 50 percent T300 and 50 percent K-49 fibers in a 934 matrix. The ply orientation of the hybrid fabric is $\left[\pm 45\frac{H}{F}\right]_2$. The energy-absorption capability of the hybrid material is compared with the energy-absorption capability of $[\pm 45]_6$

116

T300-934 and K-934 tubes. The energy-absorption capability of the hybrid fabric tube is approximately the average of the T300-934 and K-934 tubes of the same ply orientations in Fig. 46. The crushing mode of the hybrid fabric tube is a local buckling mode as seen in Fig. 47. Based upon these results, the hybrid fabric material could be directly substituted in an energy-absorption application that is currently using an all-Kevlar material without losing the post-crushing integrity capability. The hybrid design would increase the energy-absorption capability and increase the in-plane extensional and shear stiffness.

A second example of hybrid composite materials is a tube with hybrid woven Kevlar and T300 graphite fabric encapsulating unidirectional T300 graphite in the center of the stacking sequence. The ply orientation of this tube is $\left[+45_F^H/0_{5\ T}^{Gr}\right]_S$. The energy-absorption capability of this tube is more than twice that of the $\left[\pm45_F^H\right]_S$ in Fig.45.

The third example of the hybrid composite materials is $[\pm45_K/0_{N\ Gr}]_S$ ply orientations where N=3, 6, 9, and 12. In these specimens, the percentage of 0 degree T300-934 and $\pm$ 45 K-934 was varied to determine the effect on energy-absorption capability. The Kevlar $\pm$ 45 degree plies were used to stabilize the unidirectional graphite plies to produce a brittle fracturing crushing mode. Based upon tests, described in subsubsection *3.4.1 Effects of Tube Ply Orientation on Crushing Response of Composite Tubes*, as the percentage of graphite oriented in the direction of the applied load increases, the energy-absorption capability should increase. However, the opposite energy-absorption trend occurred. As the percent of graphite increased,

117
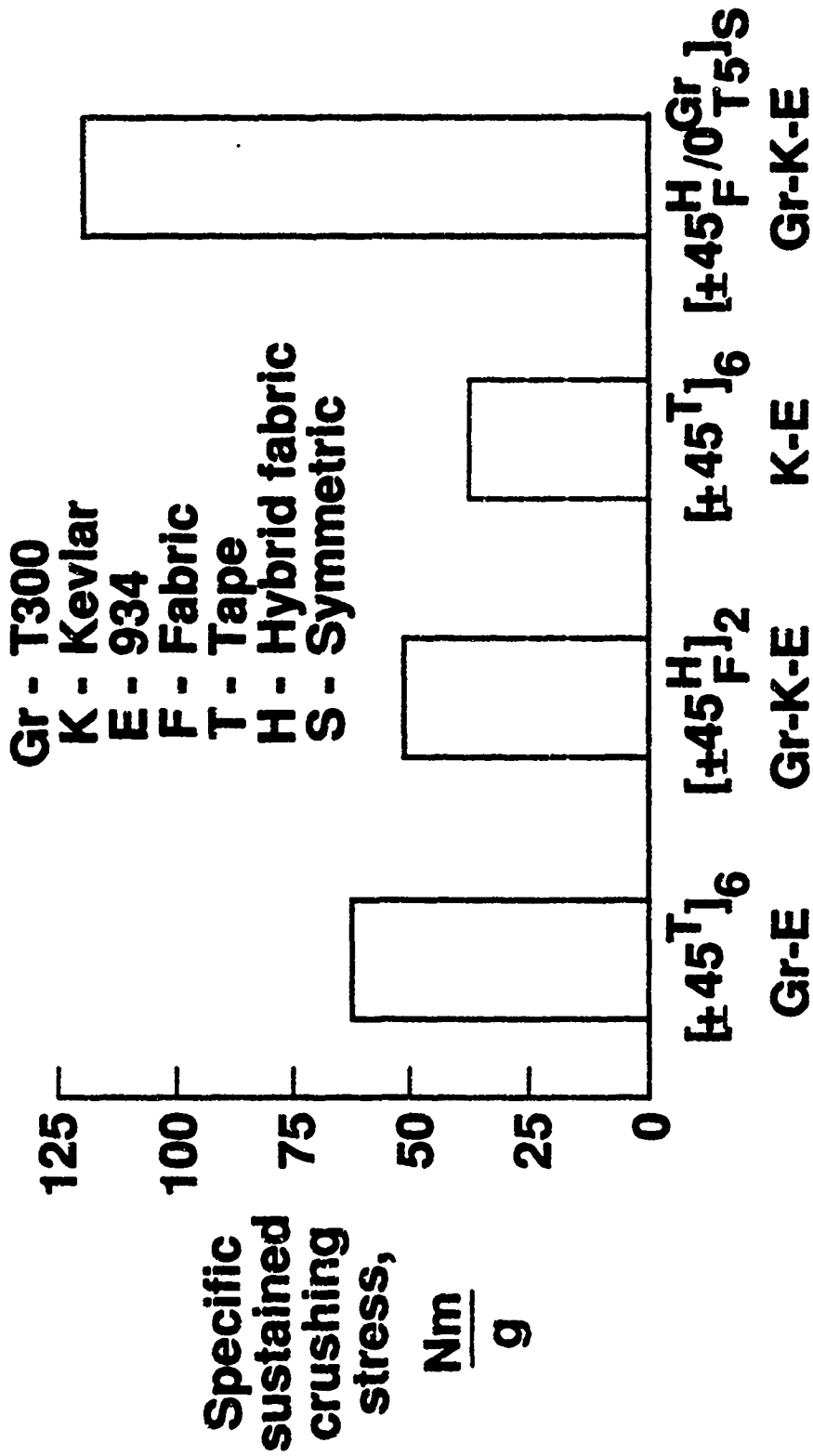
Figure 46. Energy-absorption capability of hybrid composite tubes.

118

Figure 47. Crushing mode of hybrid woven fabric composite tubes.

the energy-absorption capability slightly decreased as in Fig. 48. Explanation of this trend can be determined by examination of the crushing modes of the tubes shown in Fig. 49. The graphite plies crushed in a brittle fracturing mode for the tubes with N=3. However, as the number of graphite plies increased, the crushing mode gradually changed to predominantly lamina bending, as exhibited by the $[\pm 45_K/0_{12 \ Gr}]_S$ tubes. To achieve a brittle fracturing mode of the 0 degree plies for N=12, circumferentially oriented plies must be interspersed throughout the stacking sequence. The congregation of plies together, such as the 0 degree plies, increased the compliance in the 0 degree lamina bundles resulting in a change in crushing mode to the lamina bending mode.

3.4.5 Effect of Specimen Geometry on Crushing Response

The subfloor structure of a helicopter is composed of a grillwork of beams interconnected to carry the aircraft bending loads. The webs of the subfloor structure are generally composed of flat and circular sections such as that found in sine-wave and integrally stiffened beams. The crushing characteristics of these sections can be represented by three tubular shapes; circular, square, and near-elliptical. The near-elliptical tube, as depicted in Fig. 50, is actually two halves of a circular tube where the radii of curvature of the halves are not coincident. The greater the distance between the two centers, the smaller the included angle (Φ) of the tube.

In this study, the effects of tube geometry for the three different tube cross-sectional shapes are studied. The geometrical parameters varied in this study are diameter (D) to thickness (t) ratio (D/t) for the circular cross-section tubes and the

120
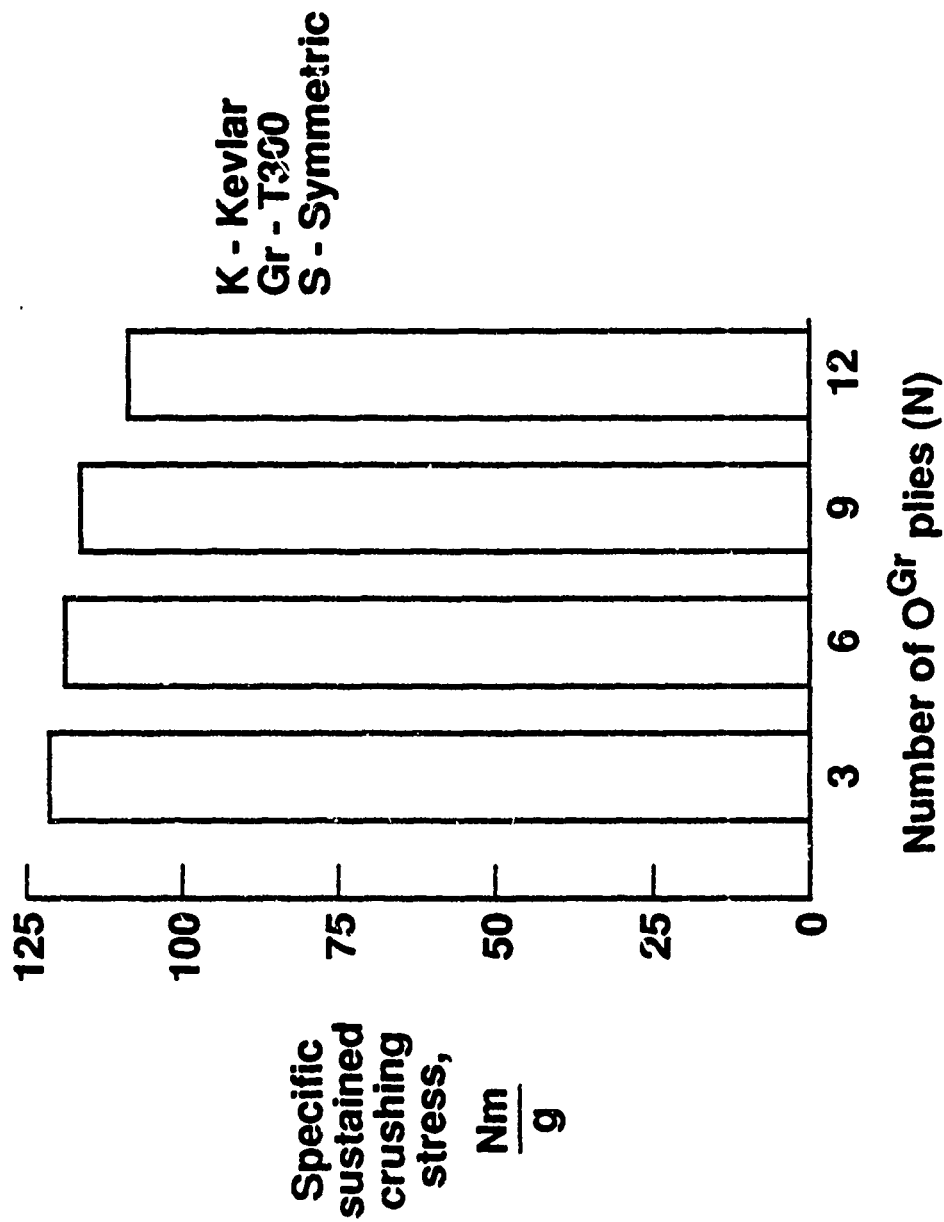
Figure 48. Energy-absorption capability of $\left[\underline{\pm45}^K/0_N^{Gr}\right]_S$ hybrid composite tubes.

$\left[\pm 45^K/0^{Gr}_3\right]_s$ $\left[\pm 45^K/0^{Gr}_6\right]_s$ $\left[\pm 45^K/0^{Gr}_9\right]_s$ $\left[\pm 45^K/0^{Gr}_{12}\right]_s$
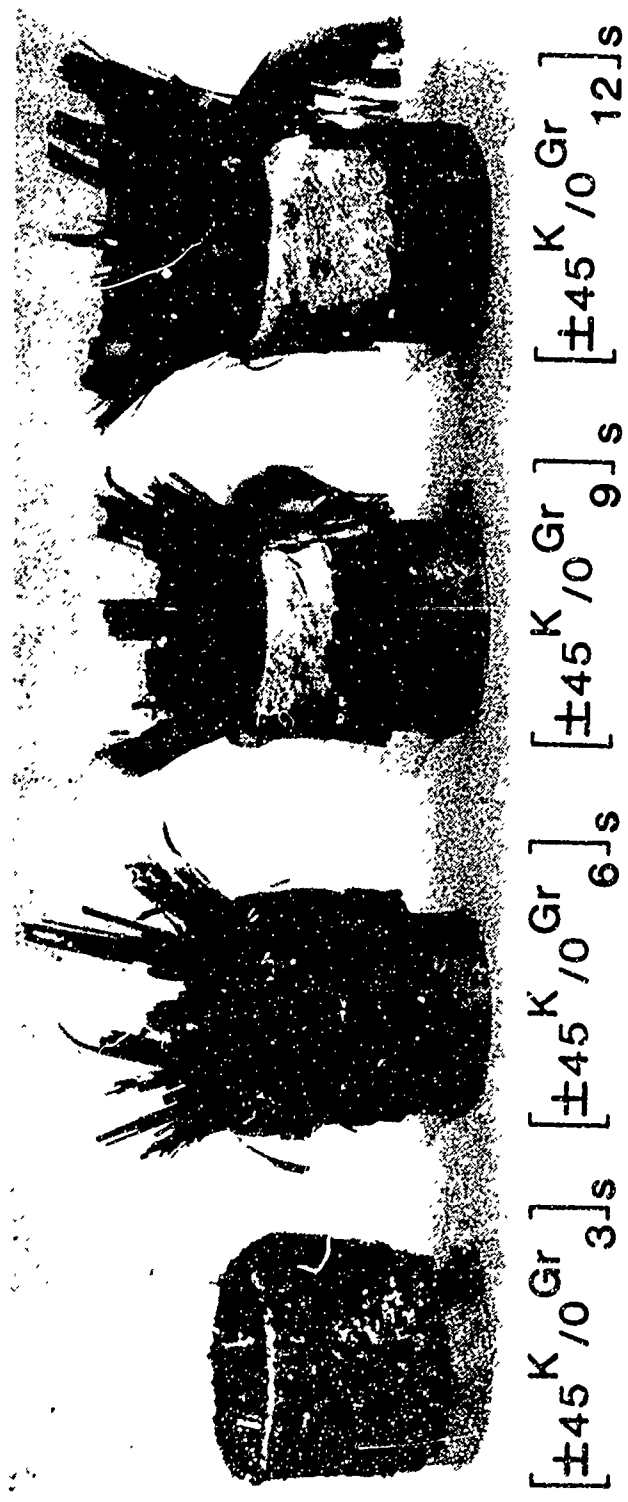
Figure 49. Crushing modes of $\left[\pm 45^K/0^{Gr}_N\right]_s$ hybrid composite tubes.
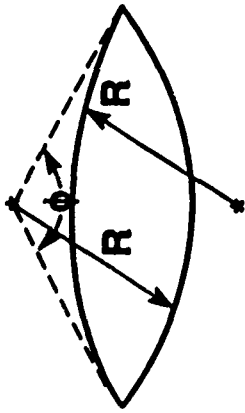
Top view of near-elliptical tube
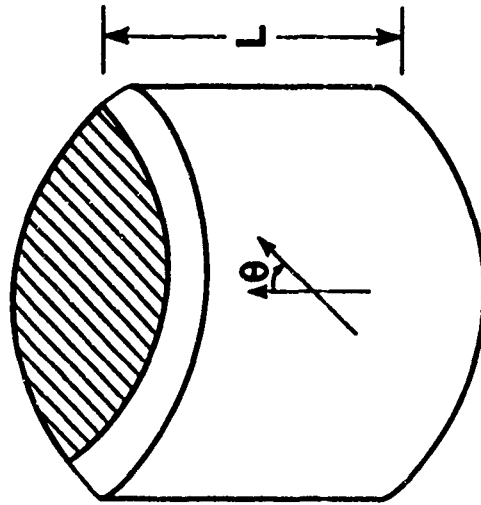
Near-elliptical cross-section tube specimen

Figure 50. Near-elliptical cross-section tube specimen.

near-elliptical tubes and inside tube width (W) to thickness (t) ratio (W/t) for the square cross-section tubes. The diameter (D) of the near-elliptical tubes is "defined" to be actually twice the radius. Another parameter studied of the near-elliptical tubes is the included angle (Φ) as denoted in Fig. 50. Tubes were fabricated from T300-934 and K-934 composite material, and the ply orientations were $[\pm 45]_N$.

Circular Cross-Section Tube Specimens. Circular cross-section composite tubes were fabricated with diameters of 2.54 cm, 3.81 cm, and 7.62 cm. The number of $\pm$ 45 pairs (N) were 2, 4, 6, and 12. The energy-absorption capability of the T300-934 tubes was a nonlinear function of tube D/t ratio. Each diameter tube produced a different nonlinear response. For a given D/t ratio, the energy-absorption capability decreased with increasing tube diameter as in Fig. 51. The crushing modes exhibited by all tubes were combined brittle fracturing and lamina bending as seen in Fig. 52. The differences in energy-absorption capability can be directly related to changes in crushing modes. As tube D/t increases, the percentage of material that crushed in the lamina bending mode decreased. Also at a given D/t ratio, as the tube diameter increased, the percentage of material that crushed in the lamina bending mode also increased. As the percentage of material that crushed in a lamina bending mode increased, a reduction in energy-absorption capability occurred.

The energy-absorption capability of the $[\pm 45]_N$ K-934 tubes is a nonlinear function of D/t ratio as shown in Fig. 53. Unlike the T300-934 tubes, the K-934 energy-absorption test results do not show a different energy-absorption response as a function of tube inside diameter. Between D/t values of 1.4 and 56.0, the

124

Figure 51. Effect of tube D/t ratio on the energy-absorption capability of $[\pm 45]_N$ T300-934 composite tubes.
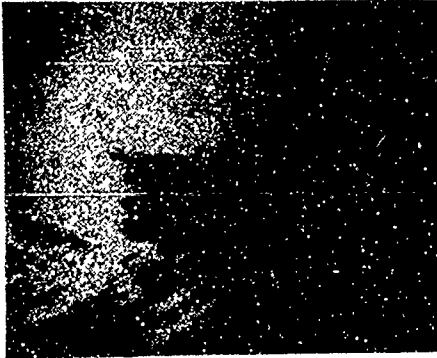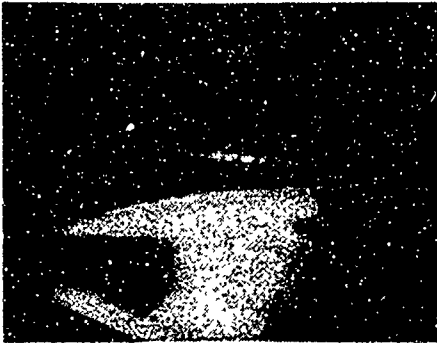
Figure 52. Photomicrographs of cross section of 7.62 cm diameter T300-934 $[\pm 45]_N$ composite tubes.
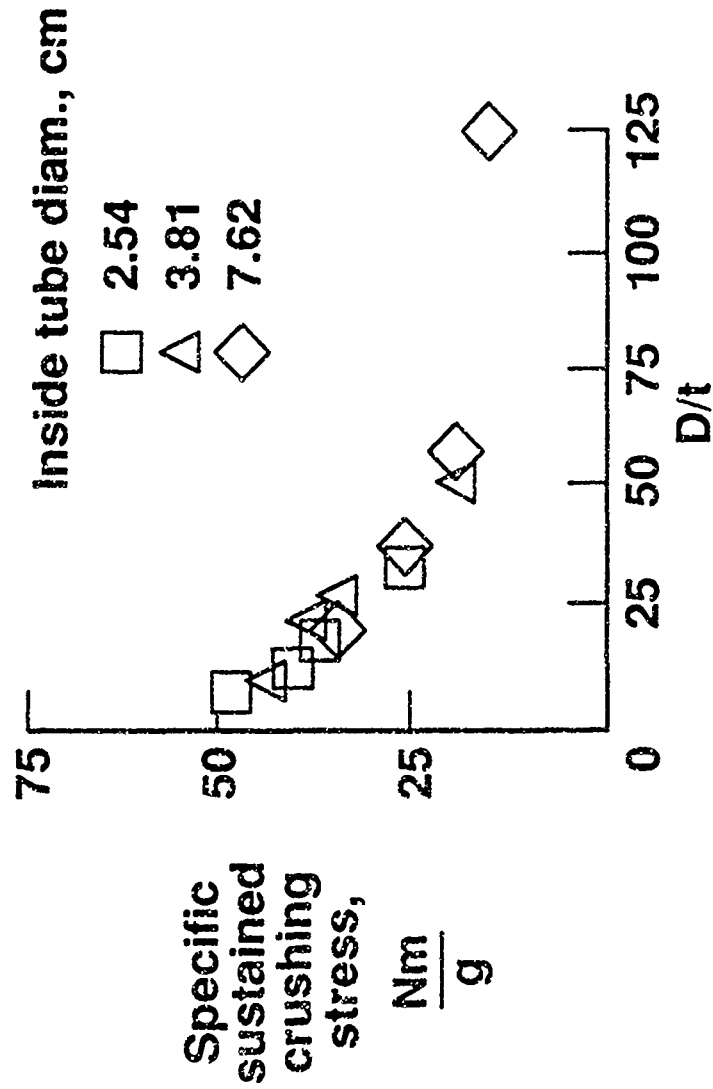
Figure 53. Effect of tube D/t ratio on the energy-absorption capability of $[\pm 45]_N$ K-934 composite tubes.

energy-absorption capability is essentially a linear function of D/t ratio. All of the K-934 tubes crushed in the local buckling mode.

In this series of tests where tube D/t was varied to investigate the effects of specimen geometry on energy-absorption capability, the effects of geometric scaling can also be studied. If the energy-absorption capability of tube specimens can be geometrically scaled, then for a specific D/t, but different diameters and wall thicknesses, the specimen should exhibit similar energy-absorption capability. The D/t=20 T300-934 tube test results for 2.54 cm, 3.81 cm, and 7.62 cm inside diameters tubes exhibited less than a 10 percent difference in energy-absorption capability. There also exists a 25 percent difference in energy-absorption capability at approximately D/t=50 for the 3.81 cm and 7.62 cm diameter tubes. These results suggest that energy-absorption capabilities of T300-934 $[\pm 45]_N$ tubes are not geometrically scalable. The lack of scalability of these tube results is attributed to the change in crushing modes. That is, the percentage of material that crushed in the brittle fracturing and lamina bending-crushing modes changed with tube diameter and tube wall thickness.

The K-934 tubes, for a particular D/t ratio, exhibit little difference in energy-absorption capability for all configurations tested. These results indicate that energy-absorption capability of K-934 $[\pm 45]_N$ tubes can be geometrically scaled. The scalability of K-934 is reasonable because the crushing modes did not change with changes in geometry.

Square Cross-Section Tube Specimens. A series of square-cross section tubes was tested

128

to determine the effect of tube width to thickness ratio (W/t) on energy-absorption capability of T300-934 and K-934 $[\pm 45]_N$ tubes. Inside tube widths were 1.27 cm, 2.54 cm, 3.81 cm, and 7.62 cm. The number of $\pm$ 45 pairs (N) were 2, 4, and 8 resulting in a range of W/t values of between 6.4 and 150.0.

The energy-absorption trend is a nonlinear function of W/t ratio and the energy-absorption capability, generally decreases with increasing W/t ratio. Regardless whether plotted in terms of similar tube internal widths, as in Fig. 54, or similar wall thicknesses, no single nonlinear function represents the overall response. A family of unique curves representing the effects of W/t ratio on energy-absorption capability for tubes having similar internal widths or wall thicknesses is shown in Fig. 55. With respect to tubes of similar internal widths at small values of W/t, energy-absorption capability increases with increasing W/t until a maximum is reached. Energy-absorption capability then decreases nonlinearly as W/t increases. At sufficiently large W/t values, the walls of the tube will buckle and the tube will not crush but fails catastrophically. The W/t value corresponding to the maximum sustained stress increases with increasing tube width. For tubes having similar wall thickness, energy-absorption capability decreases nonlinearly with increasing W/t as in Fig. 55.

The square cross-section tubes exhibit lamina bending or a combined brittle fracture and lamina bending mode coupled with laminate tearing at the corners of the tubes, as shown in Fig. 56. As the W/t ratio increases, less brittle fracturing occurs and, for W/t=125 ($[\pm 45]_2$ with W=7.62 cm), the $[\pm 45]$ tubes exhibit mostly a lamina bending mode. As the number of plies increases, the tubes still exhibit

129
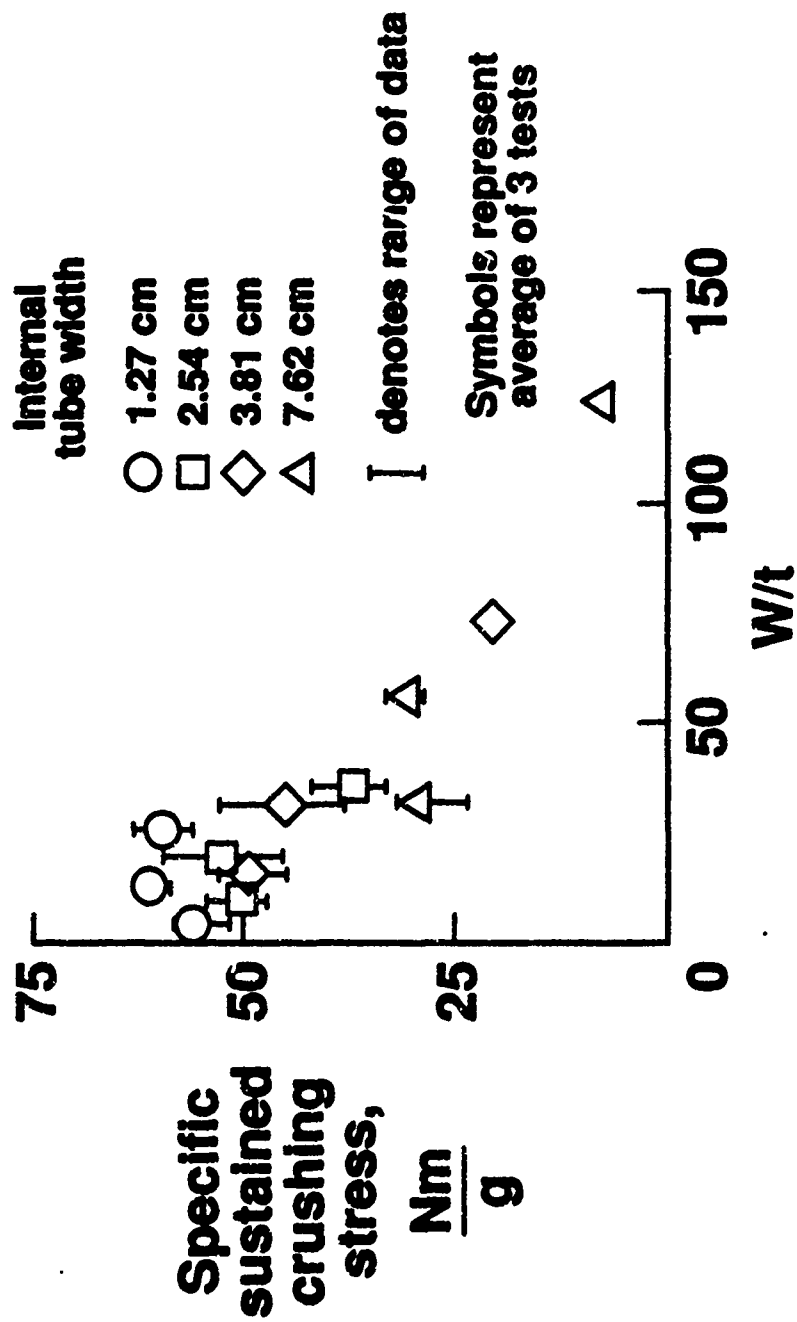
Figure 54. Effect of tube W/t ratio on the energy-absorption capability of T300-934 square cross-section composite tubes.
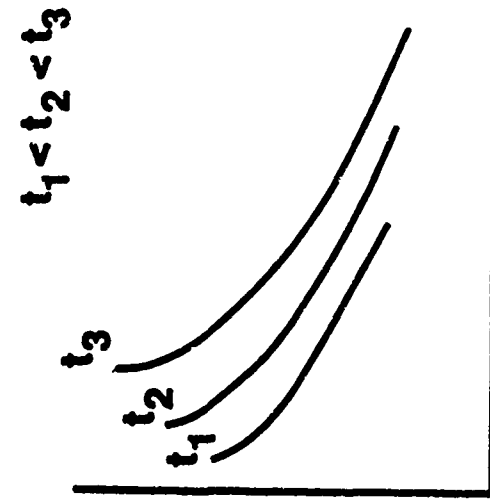
Figure 55. Energy-absorption trends of square cross-section T300-934 composite tubes.
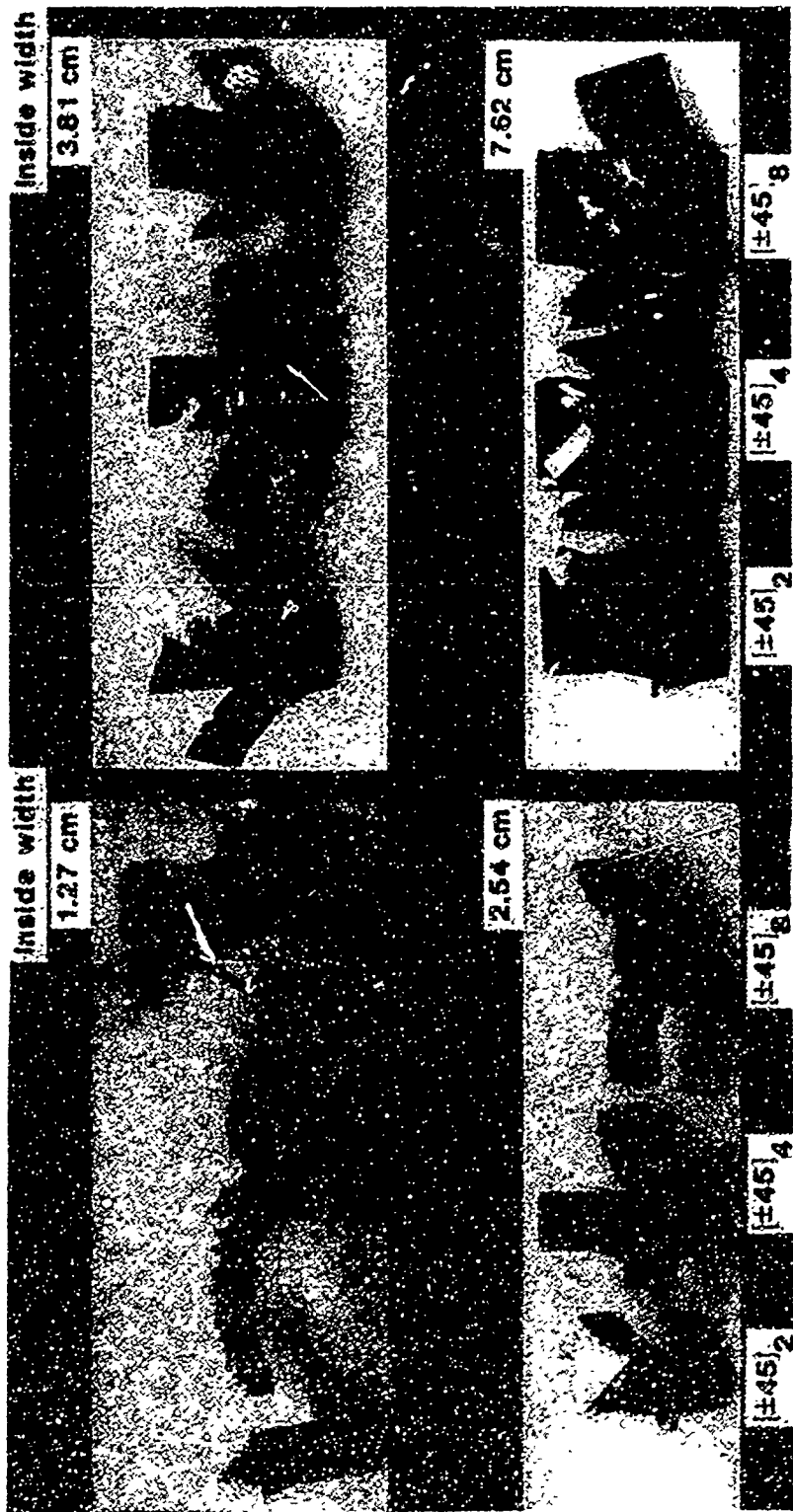
Figure 56. Crushing modes of square cross-section T300-934 composite tubes.

132

the lamina bending mode, however, with an increased amount of interlaminar crack formation. Also, as the number of plies increases, for a constant tube width, the percentage of material that crushes in the brittle fracturing mode increases. As the percentage of material that crushes in the brittle fracturing mode increases. there is a corresponding increase in energy-absorption capability. As W/t further decreases, more secondary interlaminar cracks are formed which results in a reduction in local bending stiffness and a decrease in energy-absorption capability.

The energy-absorption capability of square cross-section K-934 tubes were evaluated in a similar manner to the square cross-section T300-934 tubes described in this section. The energy-absorption trends of the K-934 tubes correspond to a bilinear function with the two linear regions between W/t of 0 and 60 and the second linear region between W/t of 60 and 150, as in Fig. 57. These energy-absorption trends are similar to that described for circular cross-section tubes. The increase in energy-absorption capability with decreasing W/t ratio is related to the reduced interlaminar cracking and the buckling load of an equivalent edge-supported plate. This increase in energy-absorption capability as W/t decreases is consistent with the buckling load characteristic of edge-supported, flat plates. All of the K-934 tubes crushed in the local buckling mode as shown in Fig. 58. The buckle wave length is a function of tube geometry (width and wall thickness).

For the tests conducted on the square cross-section tubes, the energy-absorption capabilities of the T300-934 tubes were not geometrically scalable. As the tube width W changed, the percentage of material that crushes in the lamina bending and brittle fracturing mode changes. However, t ie energy-absorption capabilities

133
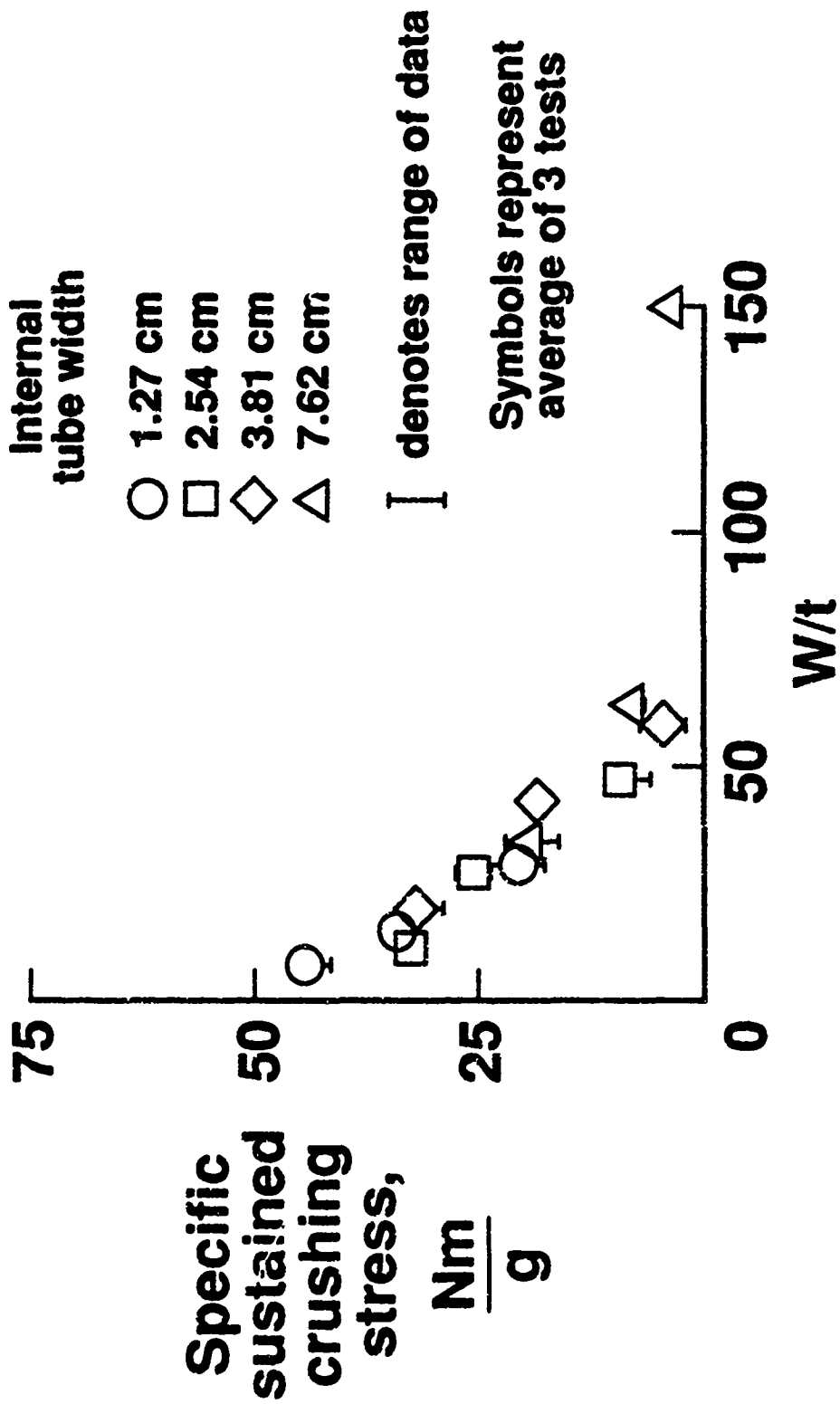
Figure 57. Effect of tube W/t ratio on the energy-absorption capability of K-934 square cross-section tubes.

Figure 58. Crushing modes of square cross-section K-934 composite tubes.

135

of the K-934 tubes were geometrically scalable. These results are consistent with those found for the circular cross-section tubes.

Near-Elliptical Cross-Section Tube Specimens. A series of "near-elliptical" cross-section tubes were tested to determine the effect of tube included angle (Φ) on energy-absorption capability of T300-934 and K-934 $[\pm 45]_N$ tubes. Inside tube diameters were 2.54 cm, 3.81 cm, and 7.62 cm. Included angles (Φ) were 180, 160, 135, 115, and 90 degrees. Tubes having an included angle of 180 degrees are circular in cross-sectional shape. The number of $\pm$ 45 pairs (N) were 2, 4, 6, and 12 plies resulting in a range of D/t values between 7 and 135.

The energy-absorption trend is a nonlinear function of D/t value for all values of included angle and internal diameters (2.54, 3.81, and 7.62 cm) for graphite-reinforced materials as seen in Figs 59 thru 61. Combining the energy-absorption data contained in Figs. 59 thru 61 and depicted in Fig. 62 produces a single continuous nonlinear curve representing the energy-absorption capability as a function of D/t value. For values of D/t between 0 and 30, the energy-absorption capability is a nonlinear function of D/t value. Between D/t values of 30 and 135, a near-linear relationship exists between energy-absorption capability and D/t value. Energy-absorption capability increased between 10 and 30 percent as included angle decreased from 180 to 90 degrees. The variation in energy-absorption capability as a function of included angle increased as tube diameter decreased.

These energy-absorption trends can be explained by examination of the crushing modes. The crushing mode of the "near elliptical" tubes, as seen in Fig. 63, near
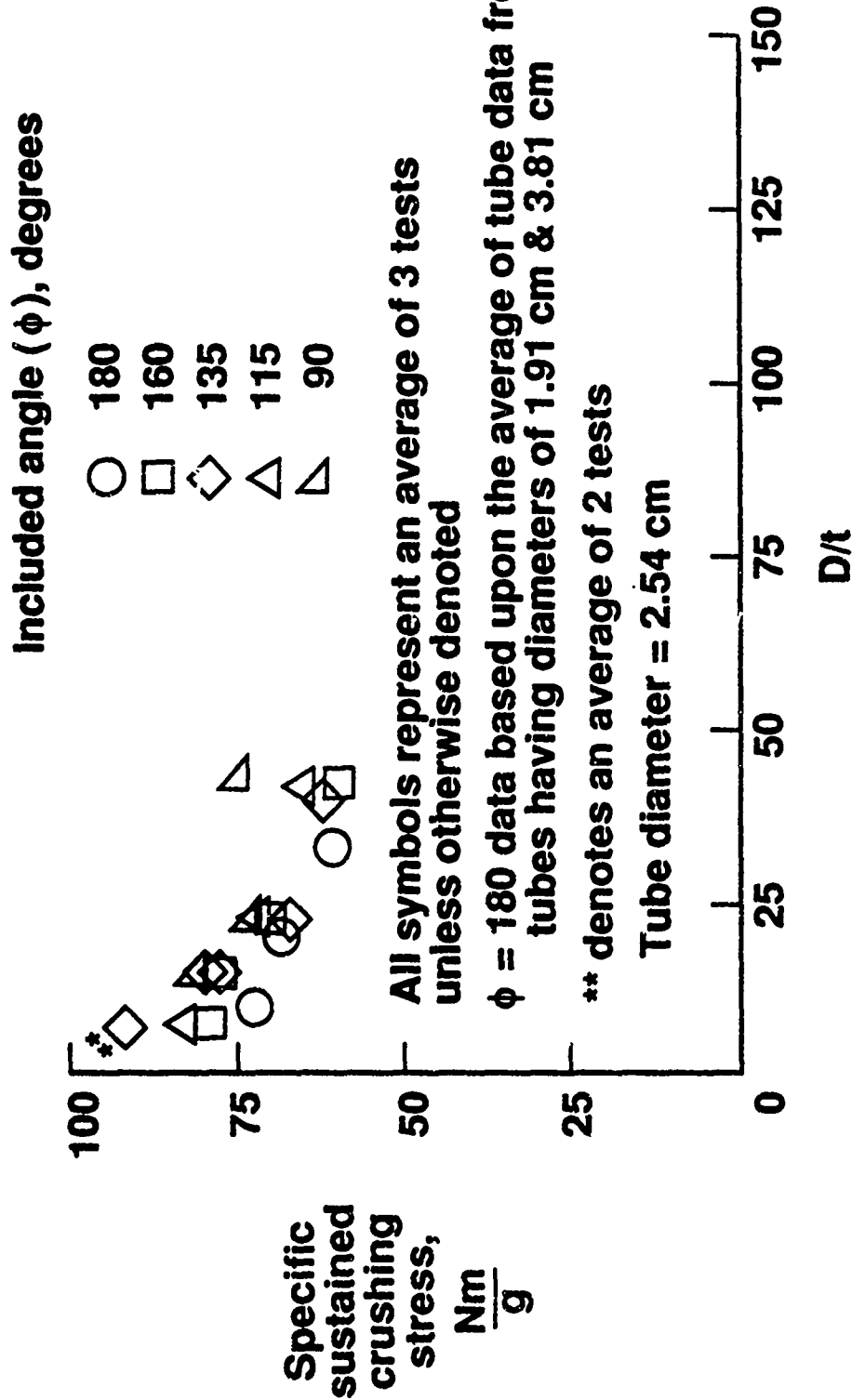
Figure 59. Effect of tube included angle (Φ) on energy-absorption capability of T300-934 $[\pm 45]_N$ 2.54 cm diameter tube specimens.

137
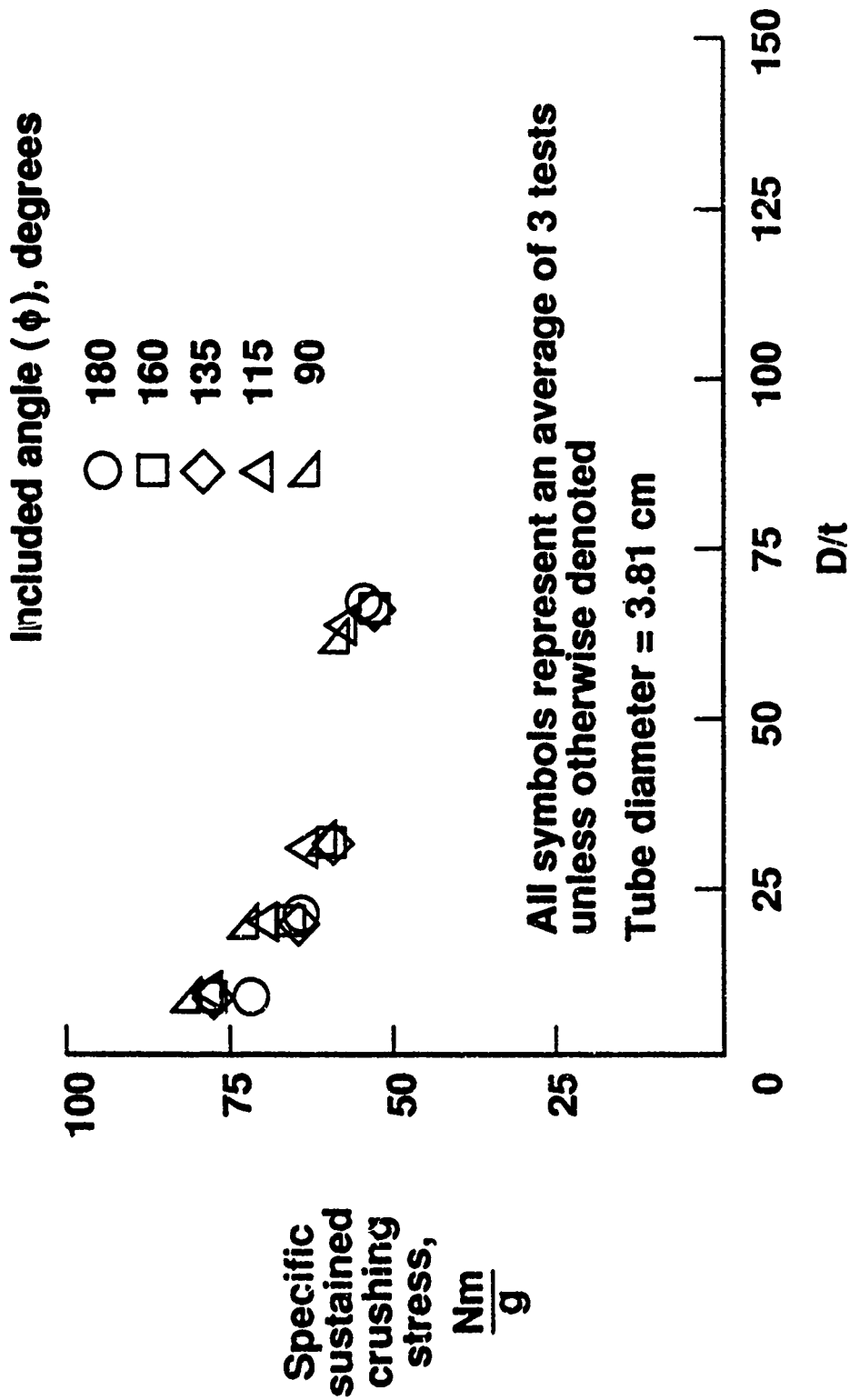
Figure 60. Effect of tube included angle (Φ) on energy-absorption capability of T300-934 $[\pm 45]_N$ 3.81 cm diameter tube specimens.

Figure 61. Effect of tube included angle (Φ) on energy-absorption capability of T300-934 $[\pm 45]_N$ 7.62 cm diameter tube specimens.

139
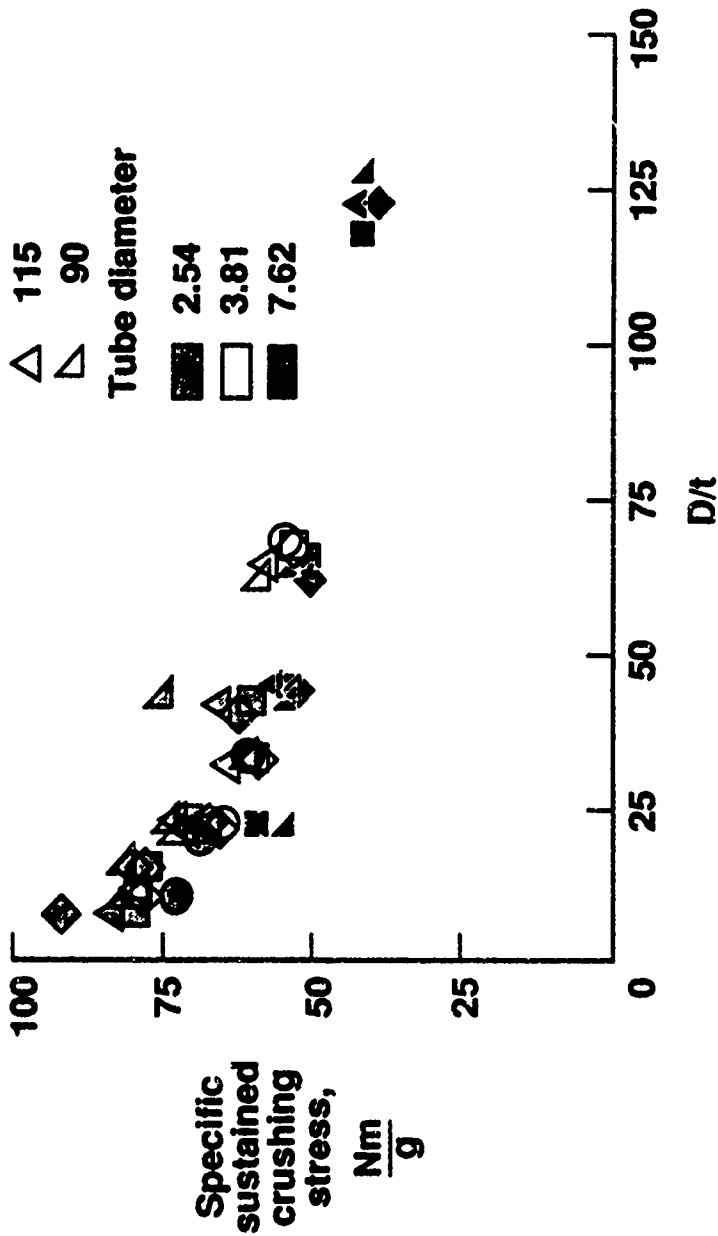
Figure 62. Effect of tube included angle (Φ) on energy-absorption capability of T300-934 $[\pm 45]_N$ 2.54, 3.81, and 7.62 cm diameter tube specimens.

140

the "corner" is different than the crushing mode away from the "corner". The crushing mode near the "corner" of the tube that has an included angle of 90 degrees is predominately brittle fracturing whereas, away from the "corner", the crushing mode is predominately lamina bending. The crushing mode of the tube having an included angle of 180 degrees, as in Fig. 63. is similar to the crushing mode away from the "corner" of the tube having an included angle of 90 degrees. Therefore, as included angle decreases, a greater percentage of the tube crushes in the more efficient crushing mode and hence energy-absorption capability increases.

Energy-absorption capability of the Kevlar-reinforced tubes was a nonlinear function of tube D/t value for all included angles and all tube inside diameters evaluated. Energy-absorption capability was a single nonlinear function for tube D/t value and included angle for tubes having an inside diameter of 2.54 cm, as seen in Fig. 64. However, for tubes with inside diameters of 3.81 cm and 7.62 cm, energy-absorption capability seemed to be a function of included angle, as in Figs. 65 and 66. For tubes of 3.81 cm and 7.62 cm inside diameters, energy-absorption capability generally increased with decreasing magnitude of included angle. The magnitude of these changes in energy-absorption capability is between 10 and 30 percent. If all of the data contained in Figs. 64 thru 66 were plotted together, a single nonlinear curve would result representing energy-absorption capability as a continuous nonlinear function of tube D/t value as in Fig. 67. All Kevlar-reinforced tubes crushed in the local buckling mode.

3.5 Effects of Crushing Speed on Crushing Response of Composite Tubes
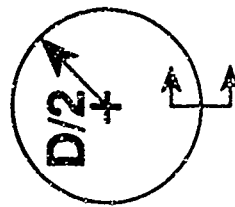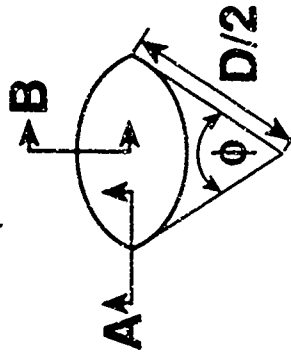
Figure 63. Photomicrographs of $[\pm 45]_6$ graphite-epoxy 3.81 cm diameter tubes with included angle (Φ) of 180 and 90 degrees.

142
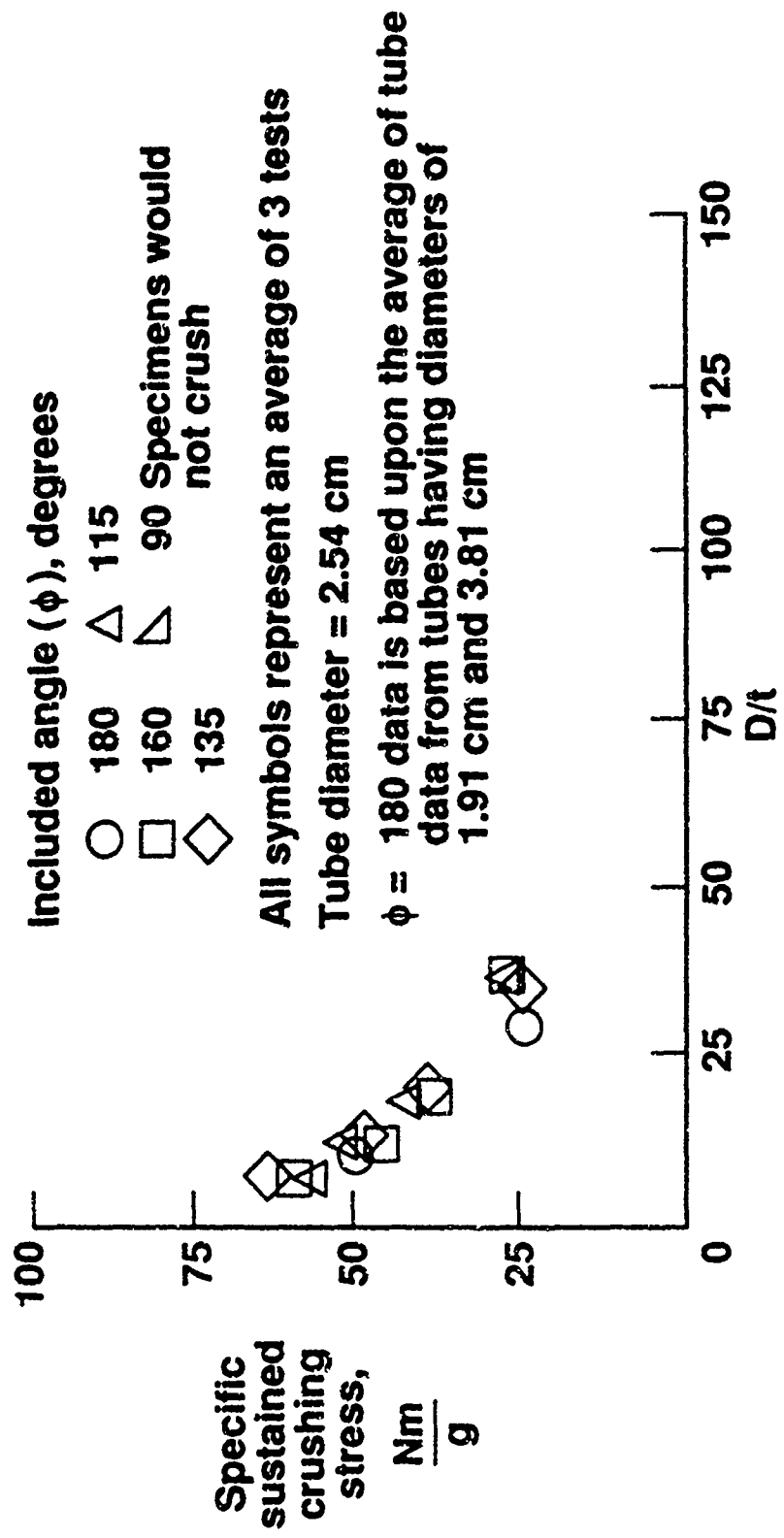
Figure 64. Effect of tube included angle (Φ) on energy-absorption capability of K-934 $[\pm 45]_N$ 2.54 cm diameter tube specimens.

143
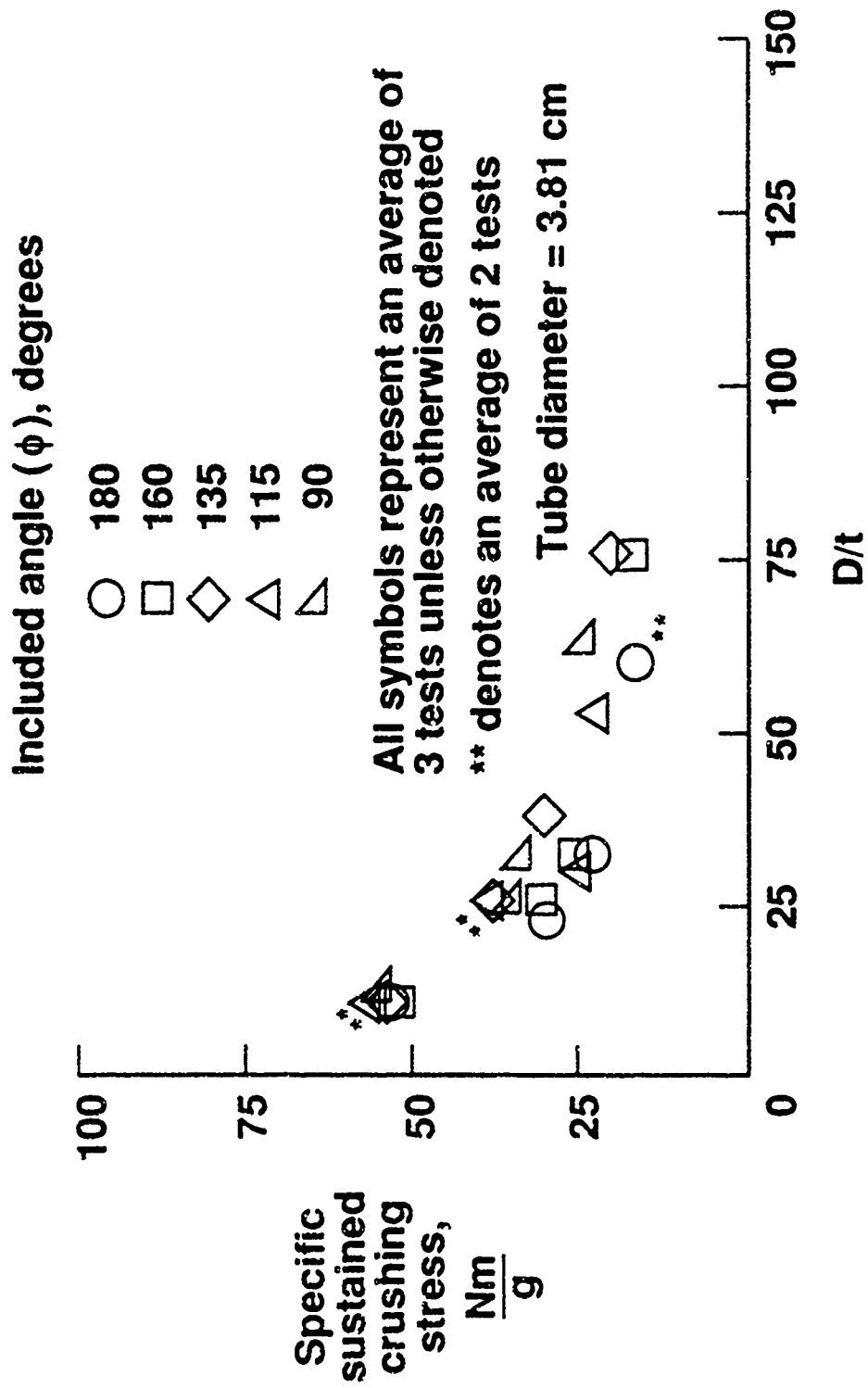
Figure 65. Effect of tube included angle (Φ) on energy-absorption capability of K-934 $[\pm 45]_N$ 3.87 cm diameter tube specimens.

144
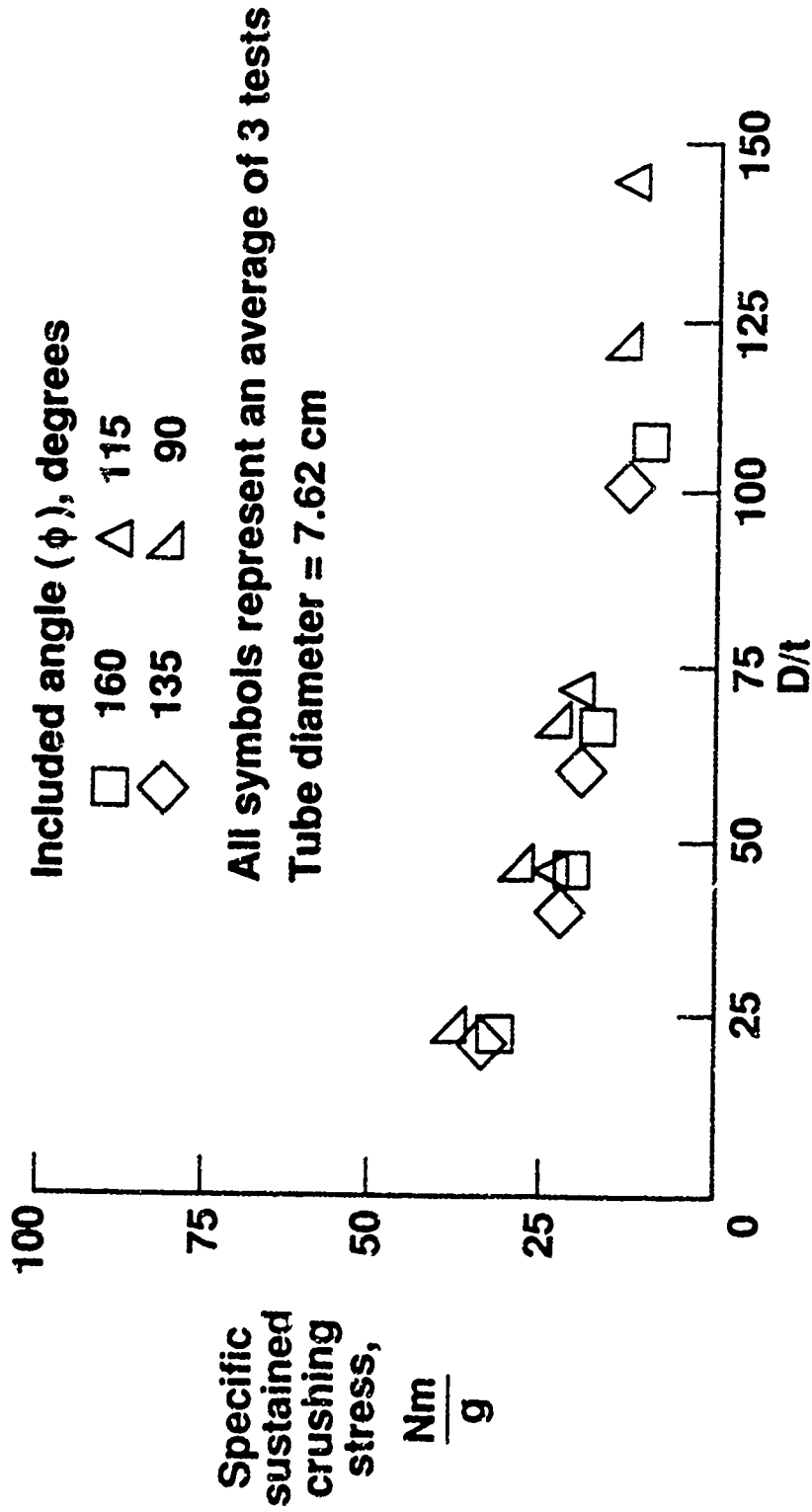
Figure 66. Effect of tube included angle (Φ) on energy-absorption capability of K-934 [±45]$_N$ 7.62 cm diameter tube specimens.

145
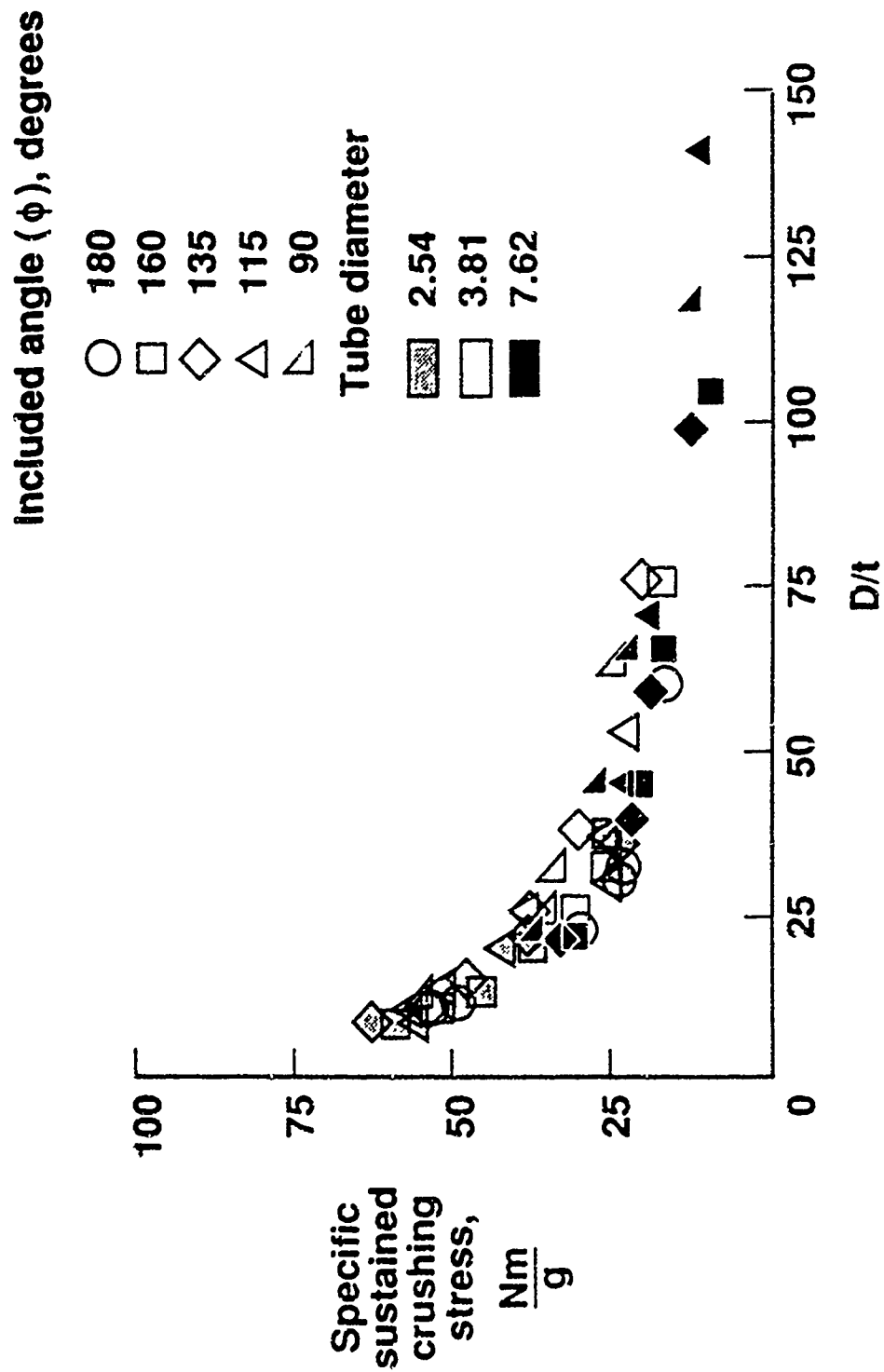
Figure 67. Effect of tube included angle (Φ) on energy-absorption capability of K-934 [$\pm$45]$_N$ 2.54, 3.81, and 7.62 cm diameter tube specimens.

All of the previously described tests in Chapter 3 were conducted at a quasi-static crushing rate to facilitate the understanding of the crushing process and so that the influence of crushing rate was not a factor in interpreting the crushing response. However, the actual crash environment is dynamic, so it is important to understand if and how crushing rate influences the crushing process. In this study, tubes were fabricated from T300-934 and K-934 prepreg material having ply orientations of $[0/\pm\Theta]_2$ and $[\pm\Theta]_3$ where $\Theta=15$, 45, and 75 degrees. T300-934 tubes having ply orientations of $[0/\pm15]_2$ and $[\pm15]_3$ could not be evaluated because the magnitude of the sustained crushing load of these tubes were higher than the capability of the test machine. Crushing speeds was between 10^{-2} m/sec and 12 m/sec.

3.5.1 Effects of Crushing Speed on Crushing Response of T300-934 Tubes

The average energy-absorption capability of the $[0/\pm45]_2$ T300-934 tubes increased between crushing rates of 10 m/sec and 6 m/sec. Then, energy-absorption capability decreased between crushing speeds of 6 m/sec and 12 m/sec as seen in Fig. 68. Although this change in energy-absorption capability seems to be a function of crushing speed, the energy-absorption capability at a crushing speed of between 6 and 12 m/sec is within the data range of the data produced at a crushing rate of 10^{-2} m/sec. Without further data, the energy-absorption capability of $[0/\pm45]_2$ T300-934 tubes can not be conclusively identified as a function of crushing speed. The energy-absorption capability of the $[0/\pm75]_2$ T300-934 tubes exhibited a slight variation with respect to crushing speed. However, this variation in crushing speed may be within nominal data scatter.

147
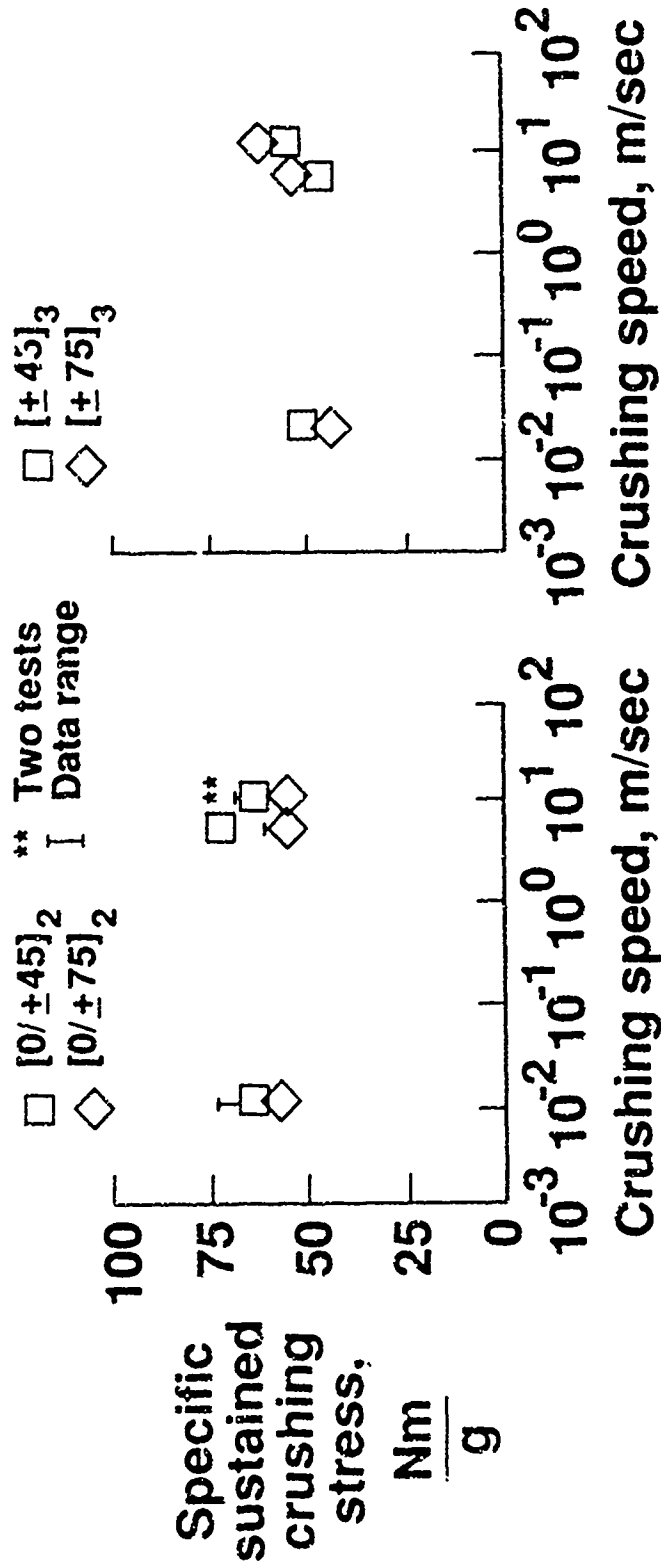
Figure 68. Effect of crushing speed on the energy-absorption capability of T300-934 composite tubes.

148

All the T300-934 tubes crushed in a brittle fracturing mode with some lamina bending. The circumferential orientation of the ± 45 and ± 75 plies provides increased "foundation" support to the axial fibers. In both the $[0/\pm45]_2$ and $[0/\pm75]_2$ tubes, the fiber has the dominant role as both the "column" and the "foundation". Therefore, because the mechanical properties of the fiber are not strain-rate sensitive, then the energy-absorption capability should not be a function of crushing speed. The results in Fig. 64 are consistent with this description of the crushing mechanisms.

The energy-absorption capability of $[\pm\Theta]_3$ T300-934 tubes was a function of crushing speed as shown in Fig 68. As ply orientation angle Θ increased from 45 to 75 degrees, the magnitude of the effects of crushing speed on energy-absorption capability increased. Energy-absorption capability increased as much as 25 percent over the speed range tested for the $[\pm75]_3$ tubes. All $[\pm\Theta]_3$ tubes crushed in a combined brittle fracturing and lamina bending mode. As the ply orientation angle increased from 45 to 75 degrees, the mechanical response of the lamina bundles became more strongly influenced by the matrix properties than the fiber properties. The percent of the total energy absorbed by the fracturing of the axially oriented fibers decreased. Therefore, the energy absorbed by the interlaminar crack growth relative to the total energy absorbed increased. Thus, the energy-absorption capability of the specimen is a function of crushing speed because the mechanical properties of the matrix are a function of strain rate.

3.5.2 Effects of Crushing Speed on Crushing Response of K-934 Tubes

The energy-absorption capability of all $[0/\pm\Theta]_2$ and $[\pm\Theta]_3$ K-934 tubes

evaluated was a function of crushing speed as seen in Fig. 69. The percent change in energy-absorption capability as a function of crushing speed was most significant between speeds of 6 m/sec and 12 m/sec. Energy-absorption capability increased most as a function of crushing speed for the $[\pm 15]_3$ and $[0/\pm 15]_2$ tubes relative to the $[\pm 45]_3$, $[\pm 75]_3$, $[0/\pm 45]_2$, and $[0/\pm 75]_2$ tubes, respectively. Between the 10^{-2} m/sec and 12 m/sec crushing rates, energy-absorption capability increased 25 and 66 percent for the $[0/\pm 15]_2$ and $[\pm 15]_3$ tubes, respectively. The percentage increase in energy-absorption capability decreased as Θ increased for both K-934 $[0/\pm \Theta]_2$ and $[\pm \Theta]_3$ tubes. The $[0/\pm \Theta]_2$ T300-934 tubes exhibited no change in energy-absorption capability as a function of crushing speed while the K-934 $[0/\pm \Theta]_2$ tubes did exhibit such characteristics. In the case of the T300-934 $[\pm \Theta]_3$ tubes, as Θ increased, the percentage change in energy-absorption capability increased. This energy-absorption trend for the T300-934 $[\pm \Theta]_3$ tubes was the opposite for the K-934 $[\pm \Theta]_3$ tubes.

The principal mechanism that is responsible for the crushing speed effects on the energy-absorption capability of the K-934 tubes is related to the origin of the Kevlar fiber. The Kevlar fiber is a polymer-based fiber. The mechanical properties of most polymers are strain-rate sensitive. For both the $[0/\pm \Theta]_2$ and $[\pm \Theta]_3$ K-934 tubes, the change in energy-absorption capability with respect to change in crushing speed was greater for tubes having ply orientation of $\Theta=15$ degrees than for tubes having ply orientation of $\Theta=75$ degrees.

All K-934 tubes exhibited the characteristic local buckling mode. No noticable change in crushing modes was evident between different crushing speeds.

150

Figure 69. Effect of crushing speed on the energy-absorption capability
of K-934 composite tubes.

151

3.6 Summary

The crushing energy-absorption process of composite tubes consists of a complicated series of events. The phenomena that occur consist of crack growth, progressive failure of material, strain-rate sensitivity, and large strains and rotations. Few mechanics problems are as complicated as the crushing process of composite tubes.

In Chapter 3 the four characteristic crushing modes in descending order of crushing efficiency were identified: transverse shearing, brittle fracturing, lamina bending, and local buckling. The crushing mechanisms for each of these modes were identified along with the constituent materials' mechanical property that controls the crushing mechanism. A method was identified to determine whether a tube's crushing response would be a function of crushing speed.

A simple analogy was presented to identify how certain material and specimen geometry variables affect the energy-absorption capability of the tube. The analogy does not include all of the material and geometrical variables that were evaluated in Chapter 3. However, the simple analogy was very useful in the interpretation of the crushing results.

Crushing tests were conducted to evaluate the effects of fiber and matrix extensional stiffness and extensional failure strain on the energy-absorption capability of ductile and brittle fiber-reinforced composite materials. The magnitude of the effects of these material properties on the energy-absorption capability of composite tubes was a function of the mechanical properties of the constitutent materials and the structure of the tube specimen. It is virtually impossible to formulate any

152

broad conclusion of how any one of these variables affects energy-absorption capability without focusing on a specific tube configuration. Through understanding how the numerous material and structural parameters influence the crushing response, it is possible to rationally choose material and structural parameters.

The mechanical properties of the constituent materials were also measured to find how different geometrical variables affect the energy-absorption capability. The specimen variables evaluated are; ply orientation, fiber volume fraction, hybrid materials, stacking sequence, and specimen geometry. Just as ply orientation has an effect on the mechanical properties of composite laminates, it also has a significant effect on energy-absorption capability. The energy-absorption trend as a function of ply orientation does not necessarily follow the same trends as the laminate mechanical properties. Fiber volume fraction is another variable where the effect on the mechanical response of a laminate is reasonably well understood. However, the energy-absorption trends as a function of fiber volume fraction does not coincide with the laminate response. Hybrid materials were found to be excellent vehicles to produce high energy-absorption capability while still having post-crushing integrity. Ply stacking sequence was shown to be a potentially serious pit fall for the designer of energy-absorbing structure. The effects of minor changes in stacking sequence were found to be negligible. However, the effects of stacking sequence for the $\left[+45^H_F / 0^{Gr}_{5T} \right]_S$ tube was determined to be significant. If the plies are rearranged such that the 0 degree plies were the outer layers, then the energy-absorption capability decreased to a third of its original value. Tube geometry was found to be a nonlinear function of tube characteristic dimension (D/t or W/t) for both graphite-

and Kevlar-reinforced tubes. Dynamic crushing tests were conducted to evaluate the effects of crushing speed on energy-absorption capability. Tubes fabricated from the same material, although with a different ply orientation, produced conflicting results. The effects of crushing speed on energy-absorption capability were found to be a function of the strain-rate sensitivity of the material property that controls the crushing mechanism of the tube.

Chapter 4 - THEORETICAL PREDICTION OF
THE ENERGY-ABSORPTION CAPABILITY
OF TUBULAR SPECIMENS

It is important for several reasons to be able to predict the response of a structural element. (1) Once the fundamental mechanisms that control the response of a structural element are understood, a predictive capability generally reduces the expense associated with investigating how material and geometric variables influence a response. (2) An accurate predictive capability also provides an effective alternative in a trade-off study to performing additional experiments. (3) Finally, response predictions for a structural element are the mechanistic relations that are essential in structural design.

In this Chapter, the method of predicting the energy-absorption capability of composite tubular specimens is discussed. These discussions will include a description of the phenomena inherent to the crushing process, calculation of energy-absorption capability, numerical considerations and finite element modeling, and a discussion of the results.

4.1 Phenomena Inherent to the Crushing Process

Four different crushing modes occur in continuous fiber reinforced composite tubes; they are transverse shearing, brittle fracturing, lamina bending, and local buckling. The phenomena that make up these different crushing modes are quite complex. The phenomena include interlaminar, intralaminar, and in-plane

155

crack initiation and propagation; local fracturing of lamina bundles; and large deformations including large strains and large geometric rotations.

The interlaminar/intralaminar cracks form at the interface between plies and within a ply, respectively. Interlaminar cracks predominately occur in specimens that crush in the transverse shearing, brittle fracturing, and lamina bending crushing modes. Interlaminar cracks can also occur in brittle fiber-reinforced composite specimens that exhibit the local buckling-crushing mode. Interlaminar cracks are not as prevalent in ductile fiber-reinforced composite specimens as in brittle fiber-reinforced composite specimens. The interlaminar cracks in the specimens that crush in the transverse shearing, brittle fracturing, and lamina bending crushing modes are Mode I, the opening mode, as depicted in Fig. 70. The interlaminar cracks that form in specimens that crush in the local buckling mode are a combination of Modes I and II, where Mode II is the forward shear mode as in Fig. 70. The length of the interlaminar cracks is a function of the mechanical properties of the fibers and matrix and the structure of the specimen.

Intralaminar cracks in crushed tubes are a Mode II type of crack and primarily form in specimens that exhibit a lamina bending-crushing mode. Tubes having intralaminar cracks generally exhibit a central interlaminar crack forming two main lamina bundles. Within each lamina bundle, secondary interlaminar cracks form. The length of these secondary interlaminar cracks is less than the central interlaminar crack. Intralaminar cracks are generally formed where the lamina bundles experience the highest bending-induced strains. This region of high bending induced strains typically occur where the lamina bundles come into contact with
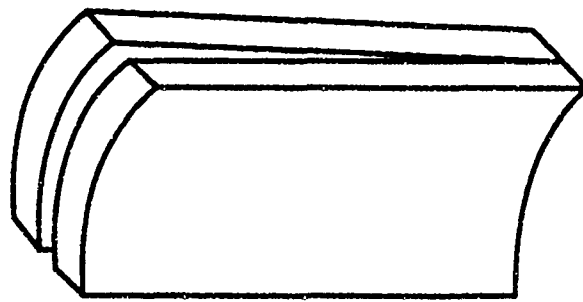
Mode I
Opening mode
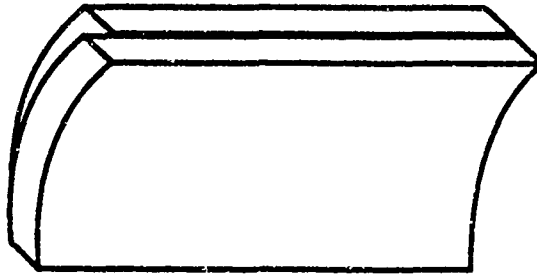
Mode II
Forward shear mode

Figure 70. Sketch of crack propagation modes.

the load platen as shown in Fig. 71. The radius of curvature of the lamina bundle is the smallest on the outer surface, opposite the side of the lamina bundle making contact with the load platen. Interlaminar and intralaminar strains are higher at the outer surface due to the smaller radius of curvature of the lamina bundle. As the load platen is moved, crushing the tube, secondary interlaminar and intralaminar cracks grow. The length of the secondary interlaminar and intralaminar cracks are typically longer at the outer surface than on the inside surface of the main lamina bundle.

Two types of in-plane cracks form in composite specimens: longitudinal cracks and parallel-to-fiber cracks. The longitudinal cracks occur in tubes that crush in transverse shearing and brittle fracturing-crushing modes. Longitudinal cracks extend through the thickness of the lamina and have length, along the longitudinal axis of the tube, on the order of the thickness of a single ply as depicted in Fig. 72. As a result of the formation of the longitudinal cracks, the surface of the crushed region is scalloped in an irregular manner along the crushing surface as depicted in Fig. 73. The height of the scallops varies but is on the order of the thickness of a lamina. When the specimen is being crushed, the load platen pushes against these scallops. Load is introduced into the scallops across the crushing surface of the tube. The scalloped region in the crush zone is typically the points of the highest stresses and is the site of local failures. As one set of scallops fail, a new set of scallops is formed.

Parallel-to-fiber cracks occur parallel to the fibers in a single ply or in a group of plies that are oriented in the same direction. The parallel-to-fiber cracks generally
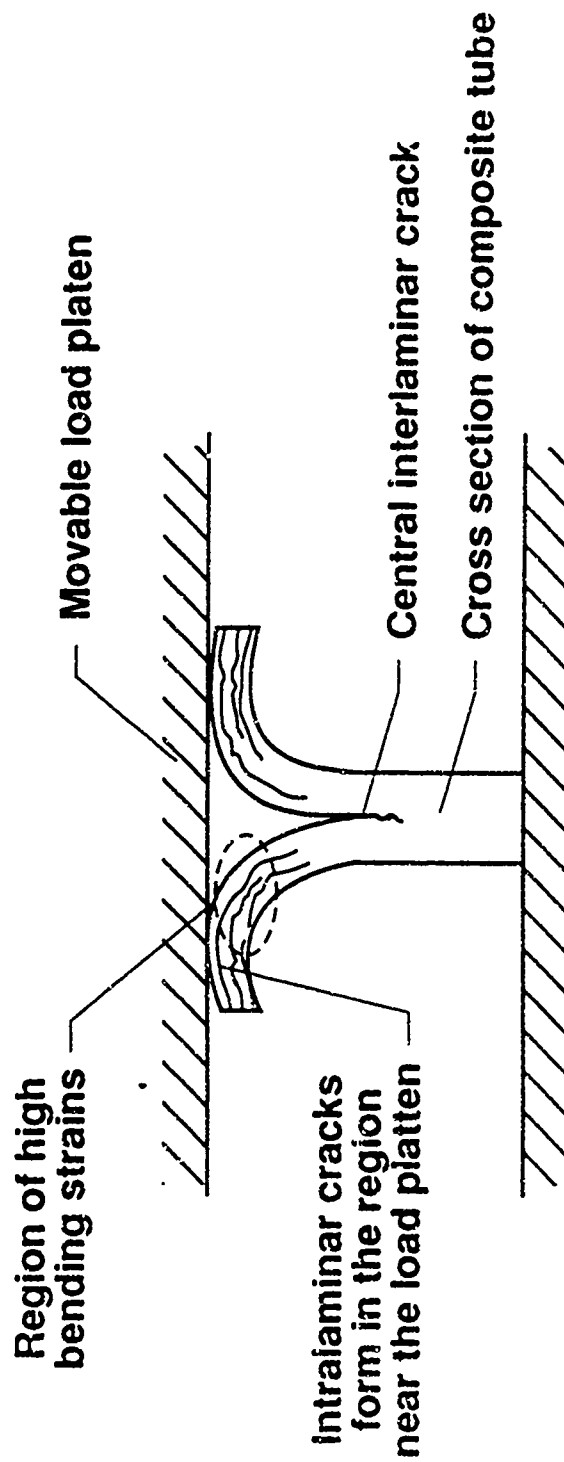
Figure 71. Schematic of formation of intralaminar cracks of tube that exhibits a lamina bending crushing mode.

159
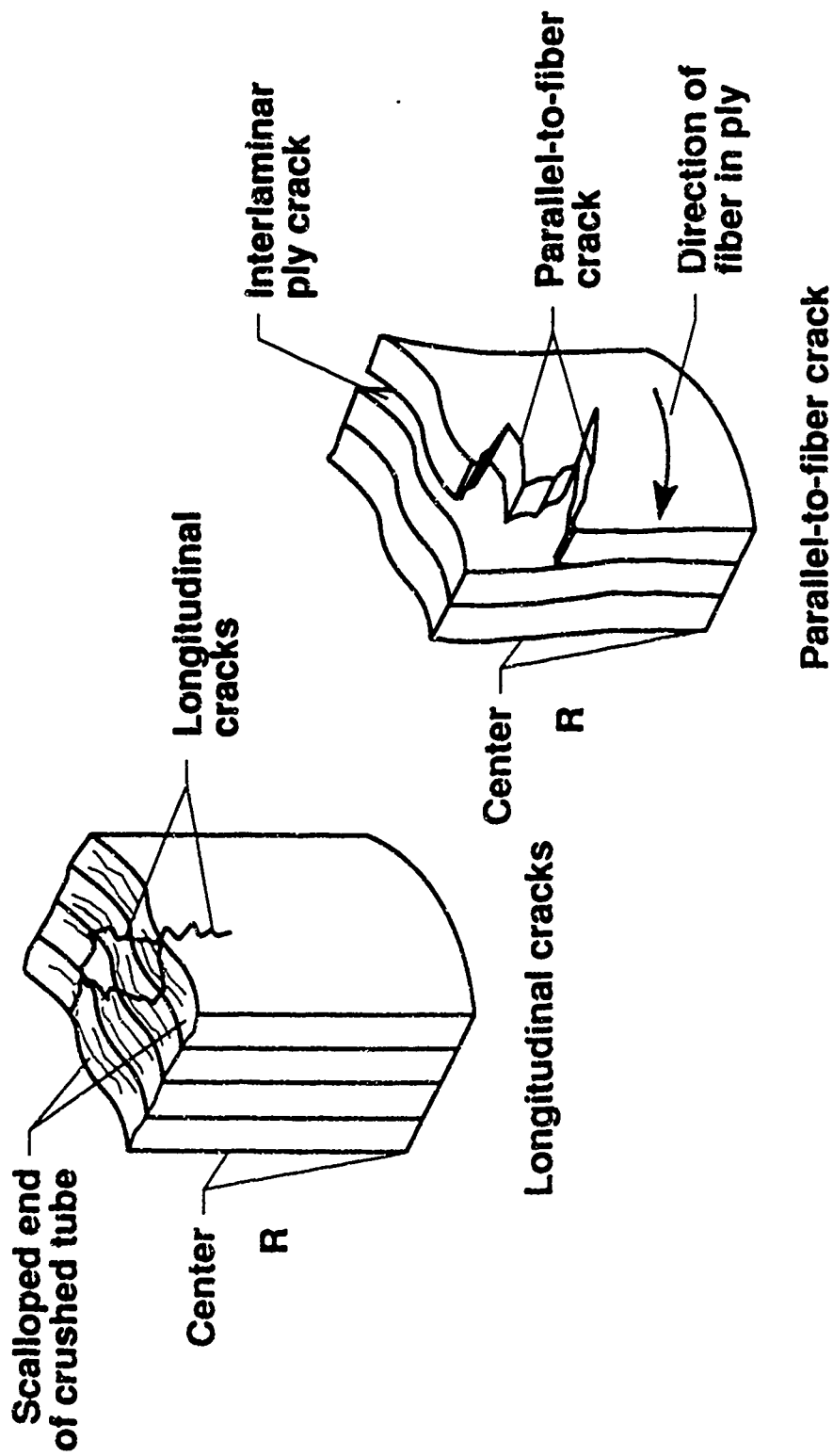
Figure 72. Section of tube specimen showing parallel-to-fiber cracks, longitudinal cracks, and scalloped end.
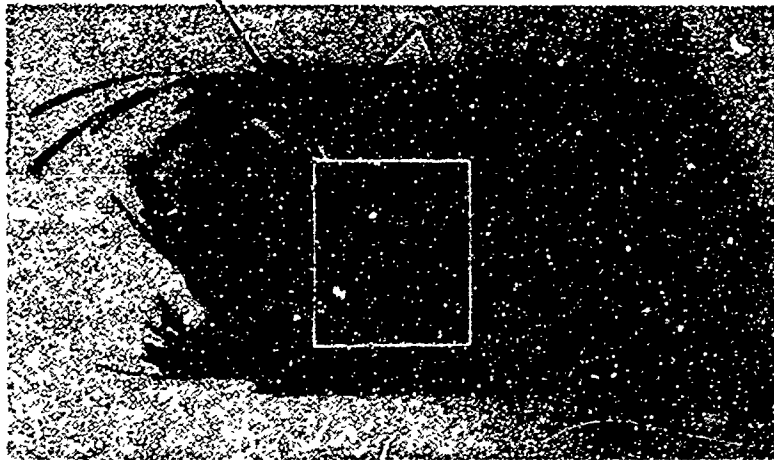
Crush zone
(high strains)

Repeating
element

Crushed tube
specimen
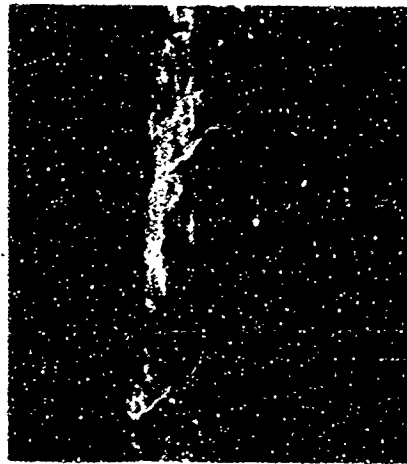
Figure 73. Scalloped material of the crushing surface.

occur in the outer ply of a tube. as in Fig. 72, or in a tube whose ply orientation is primarily unidirectional and crushes in a lamina bending-crushing mode. Parallel-to-fiber cracks consist of an interlaminar crack component and an in-plane crack component that propagates parallel to the fibers. The interlaminar crack component of the parallel-to-fiber cracks can result in a significant amount of energy absorption because the surface area of the crack is large. However, the component of energy absorbed by the in-plane crack propagation parallel to the fibers is small because the crack surface area is small.

As the interlaminar, intralaminar, and in-plane cracks are formed, the subsequently formed lamina bundles can undergo large in-plane strains and large geometric rotations. These large deformations result in nonlinear material and nonlinear geometric responses. When the deformations get large, the lamina bundles can also fracture. The specimens that crush in the local buckling-crushing mode exhibit large deformations consisting of large geometric rotations and nonlinear material response at the folds in each buckle. Interlaminar cracks can also form at the buckles of the specimen.

4.2 Definition of the Energy-Absorption Capability

The measure of energy-absorption capability of tube specimens, as defined in Chapter 2, is the specific sustained crushing stress. The specific sustained crushing stress is the sustained crushing load (average crushing load) divided by the product of the cross-sectional area of the specimen and the density of the material. The progressive crushing process is a cyclic series of failure events which produces a fluctuating crushing force. However, the average crushing force for any cycle is

162

relatively constant, as shown in Fig. 74. Therefore, to determine the average crushing force, only the predicted maximum and minimum crushing force of a representative cycle of the crushing process need be determined. A representative cycle of the crushing force-deflection response is the high-low-high cycle of force as depicted in Fig. 74. The average crushing force is the average of the maximum and minimum crushing forces of a representative crushing cycle.

To determine the maximum and minimum crushing force in a representative cycle, an end-shortening displacement is applied in an incremental process to the model to represent load introduction into the specimen. Displacements, strains, and reaction forces of the model are calculated at each increment of applied end-shortening displacement (load step). At each load step, the total strains are calculated and material properties are updated to account for any material nonlinear behavior. The initiation and growth of interlaminar and intralaminar cracks are also accounted for at each load step.

Specimens that crush in the transverse shearing, brittle fracturing, or lamina bending-crushing modes exhibit different crushing mechanisms that are related to the formation and growth of cracks. As the load is applied, interlaminar and intralaminar cracks initiate and grow. The formation of the cracks produces lamina bundles. As the crack lengths increase, the lamina bundles bend producing large local strains. The cyclic process of increasing the load step and the calculation of model displacements, strains, and reaction forces during crack growth is repeated until the strains in a lamina bundle reach the failure strain of the material.

For tubes that crush in the transverse shearing or brittle fracturing crushing

163

Figure 74. Typical force vs. deflection plot depicting a representative cycle of the crushing process.

modes, the maximum crushing force used in calculating the average crushing force is defined as the maximum reaction force when lamina fail. The minimum crushing force is the minimum reaction force calculated from the model in the failure process of the lamina. The maximum crushing force for specimens that crush in a lamina bending mode corresponds to the maximum reaction force when the crack grows. The minimum crushing force corresponds to the reaction force when the crack stopped growing after unstable crack growth occurs.

For specimens that crush in the local buckling-crushing mode, the reaction forces will increase with each load step until a maximum crushing force is reached. When the maximum load is reached, the reaction forces will decrease with further application of the end shortening displacement. The decrease in the reaction force corresponds to the collapse of the wall of the specimen. When the formed local buckle of the wall has collapsed upon itself, the reaction forces will increase with further increase in applied end shortening displacement. The cycle then repeats itself.

4.3 Numerical Considerations and Finite Element Modeling

The finite element method was chosen as the general analysis method to calculate energy-absorption capability. The finite element method provides inherent flexibility in modeling a relatively complex structure. Enhancements, including material nonlinearities, crack initiation and propagation, and failure of elements, were incorporated as external processors to an existing general-purpose geometric nonlinear finite element program, ref. 32 (Engineering Analysis Language, EAL).

The factors relative to the modeling of the response of a structure that must be evaluated prior to conducting the analysis are; 1) crack initiation and growth, 2) material and geometric nonlinear response, 3) fracture of an individual lamina or laminae, 4) numerical considerations, and 5) element type and level of discretization. Each of these factors will be addressed.

4.3.1 Crack Initiation and Growth

The strain energy release rate, G, was calculated to determine crack initiation and growth. Interlaminar crack growth is modeled by disconnecting coincident nodes of adjacent elements along an interface and calculating the strain energy associated with the resulting deformation state, as depicted in Fig. 75. However, calculation of the strain energy of the entire model includes the effects of all components of crack growth, provided all of the components are present. Only crack growth Modes I and II are assumed to be significant for the crushing of composite tubes.

The strain energy release rate is calculated as the difference in strain energy between the previous state and the present state (which has a larger crack area) divided by the change in crack area. The strain energies associated with the previous state and present state were calculated using a geometrical and material nonlinear-elastic analysis. If G is greater than a critical value, G_c , then the crack grows. If G is smaller than G_c, then additional load must be applied to the specimen to force crack growth.

4.3.2 Geometric and Material Nonlinear Modeling

Large deformations (deflections and strains) are modeled in the crushing of
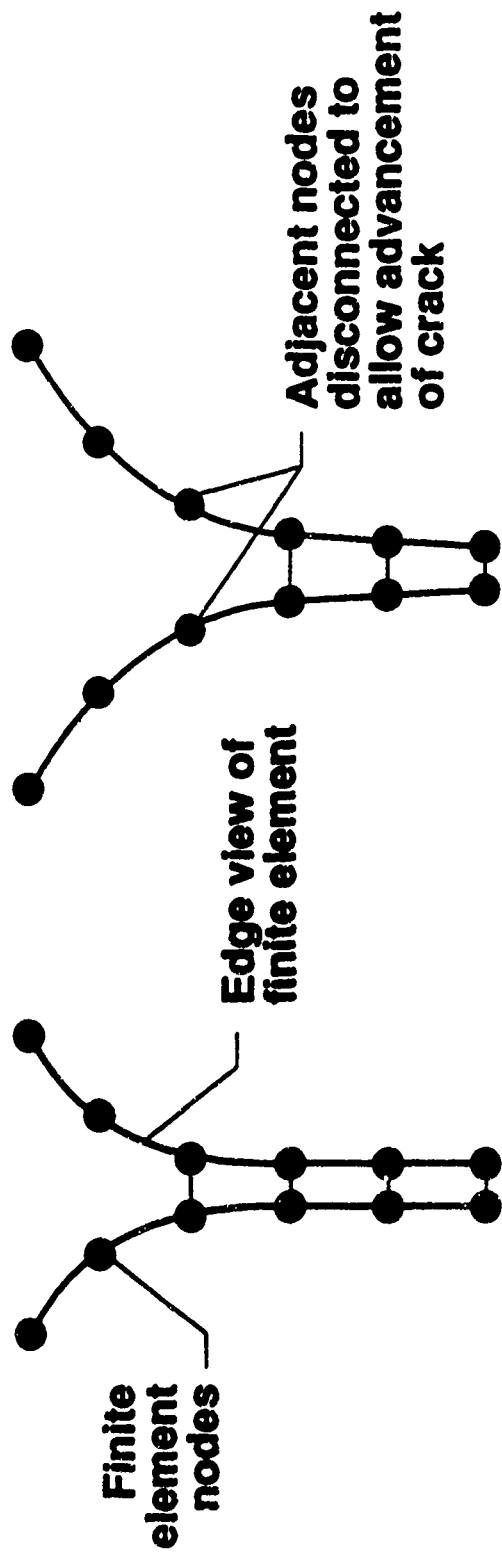
Figure 75. Method of interlaminar/intralaminar crack growth in finite element model.

composite tubes. Geometric nonlinear response is modeled in an incremental manner using a Newton-Raphson iterative solution scheme, ref. 33, to ensure convergence of the solution to the equilibrium condition. The nonlinear system of equations to be solved is :

$$R = F(x,r) + P \qquad (3)$$

where R is the force imbalance term of the system of equations. If the solution is converged to the equilibrium condition, then R equals zero. The sum of all internal point forces (F) exerted by the element joints on the system joints is a function of model displacements (x) and reaction forces (r). The parameter P represents the external forces acting on the joints of the model. The objective is to determine the values of x that will make R equal to zero. The approach taken to make R equal to zero is to use the Newton-Raphson method. For a single degree-of-freedom system, the displacements x are determined in an incremental manner where the ith value of the displacement x is:

$$x_i = x_{i-1} - R(x_{i-1}) * R'(xi-1)^{-1}. \qquad (4)$$

Successive x's are calculated until R equals zero.

The EAL finite element program has no material nonlinear solution scheme for 2-D orthotropic finite elements. Therefore, a solution strategy had to be devised utilizing the mathematical utility processors existing in EAL. Material nonlinear behavior was modeled using a direct iteration solution procedure, ref. 33. Incorporation of the direction iteration solution strategy consists of 1) updating the material properties of each element and 2) repeating the analysis using the updated

material properties. This process of recalculating the material properties and performing another analysis is repeated until the change in deformations becomes small.

The nonlinear material stress-strain data are represented as piece-wise linear segments. It was assumed that the material is nonlinear elastic. That is, no permanent deformation of the material occurs and any unloading occurs along the initial nonlinear stress-strain curve as depicted in Fig. 76.

In the modeling of the crushing process, the load-deflection response of the tube was solved for in an incremental fashion. The nonlinearity of the load-deflection curve is a function of both the material and geometric nonlinear response. A series of geometric nonlinear analyses were performed to advance the solution from load point i to i+1, as in Fig. 77. This series of analyses were performed in an iterative manner. In each geometric nonlinear analysis, between point i and i+1, the material properties of the finite elements were constant. The strains in the finite elements were calculated at point i+1 for each iteration and the material properties of the finite elements were updated in accordance with the strain state in each element. The difference between the strains in the finite elements at point i+1 for each successive iteration decreased. When the difference in strains between successive iterations produced no change in the material properties, the analysis was assumed to be converged. For the composite tubes analyzed, the number of iterations between points i and i+1 was typically less than 4. This process of iterative analyses was repeated at each load step.

The procedure for modeling the geometric and material response of the tube

169
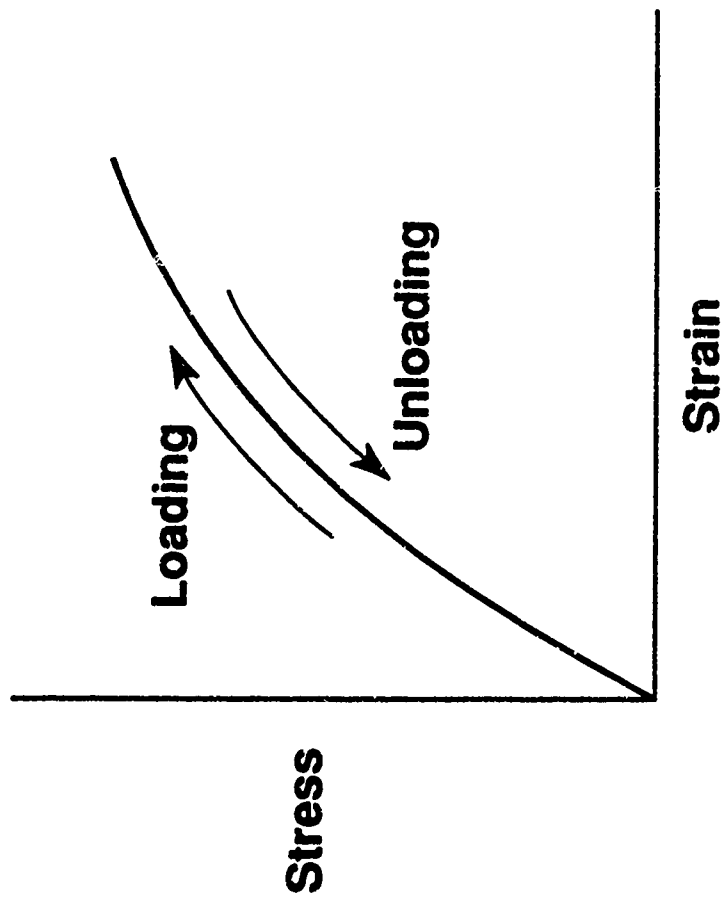
Figure 76. Loading-unloading path of nonlinear elastic material.

170
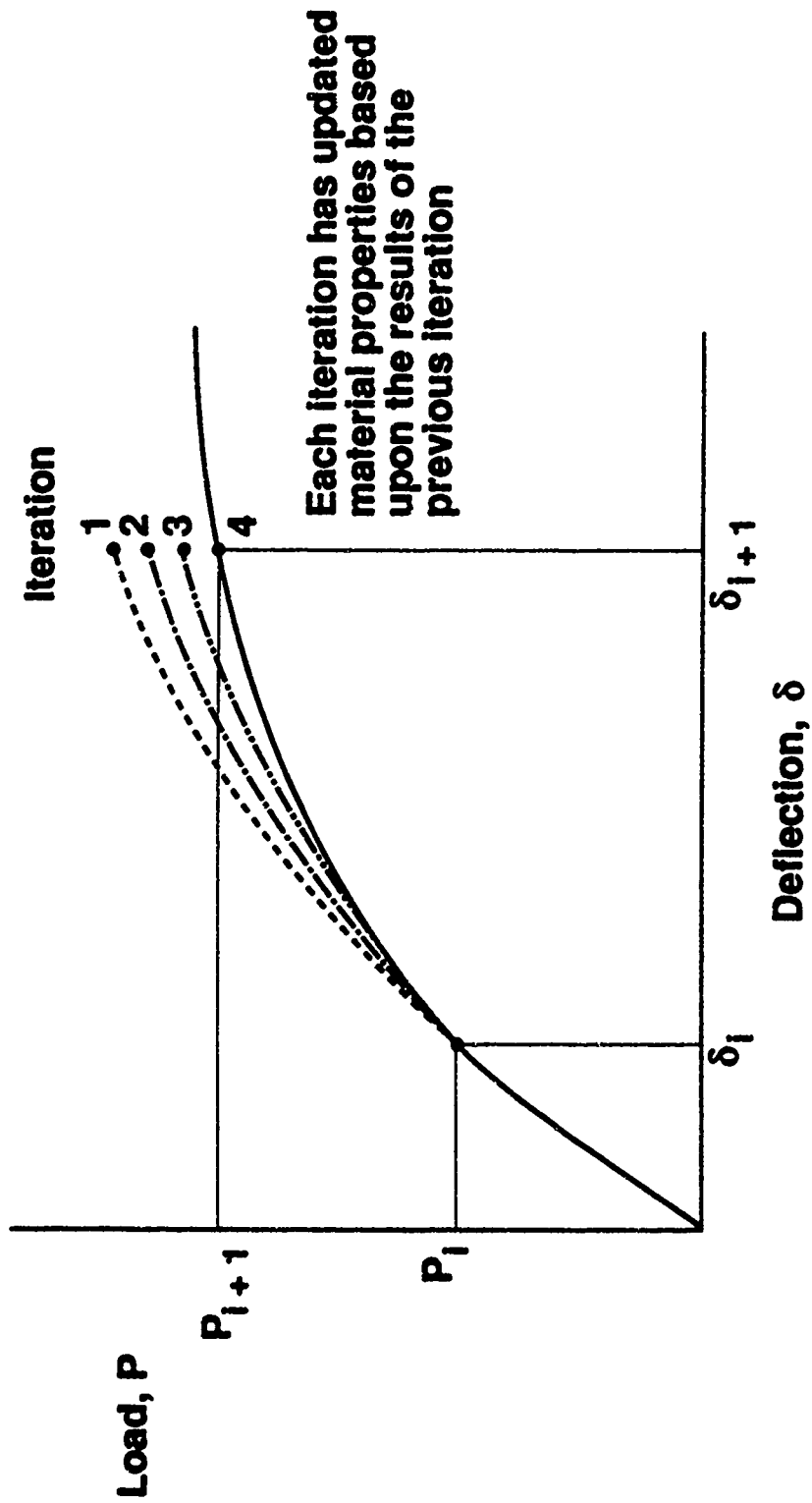
Figure 77. Iterative convergence process for material nonlinearities.

171

is clearly less than optimal. Compromises in the formulation of the analysis were necessary because of the unavailability of suitable commercial computer codes and because the development of a new computer program tailored to modeling the crushing response of composite tubes was beyond the scope of this research activity. For example, the modeling of the material nonlinear response requires an excessive number of iterations of the geometrically nonlinear finite element analysis. These additional analyses result in increased computer cost and increased amount of time required to complete an analysis of a tube. The actual dollar cost and the through put of the individual analyses is a function of the computer hardware, software, and work load of the computer. The analyses, described in this study, each required approximately four man-days of effort to complete.

4.4.3 Fracture of Lamina Bundles

Fracturing of lamina bundles produces a significant amount of energy-absorption capability. Unlike the failure characteristics of some composite structures which tend to be catastrophic, the fracturing process associated with energy absorption is progressive and benign. The progressive fracturing process, as modeled for the crushing of composite tubes, is a series of local failures. These failures can be either matrix- or fiber-controlled failures depending upon the ply orientation and the local stress state. At the convergence of each load step, the stress-strain state of each lamina is calculated, and a failure determination is performed. If a failure has been determined to have occurred in an element, then the mechanical properties relative to the failure mechanism are reduced appropriately to simulate a failed element. For example, if a failure in the fiber direction occurred, then the Young's Modulus

172

(E_{11}) parallel to the direction of the fiber is reduced two orders of magnitude. If the modulus were reduced to zero, then the finite element stiffness matrix could become singular and EAL would abort the analysis. The analysis with the reduced material properties is repeated and the failure analysis of other elements is repeated. If additional elements are determined to have failed, then the appropriate mechanical properties are reduced, and the analysis is repeated. After all the elements in the lamina bundles fail or exhibit a lamina bending crushing mode, then the next increment in load is applied. The modeling of the failure process is continued until a maximum and minimum crushing force in a representative cycle have been determined.

Lamina failure is based upon the maximum allowable strains in the principal material directions. The allowable failure strains are represented as the ultimate values of the material stress-strain data curves shown in Figs. 78, 79, and 80 for T300-934, K-934, and aluminum, respectively. Allowable strains refer to both tensile and compressive strains. When the strains along the principal material directions of a lamina exceed the allowable strains of the material, the lamina is assumed to have failed.

4.3.4 Numerical Considerations

Modeling the axial collapse of tubes poses numerical problems related to the existence of bifurcation buckling loads that are within the load range of interest. At the bifurcation loads, the finite element stiffness matrix is singular. In the current implementation of the nonlinear solution strategy of the finite element code used to model the crushing response of the tubes, there is no direct method for the
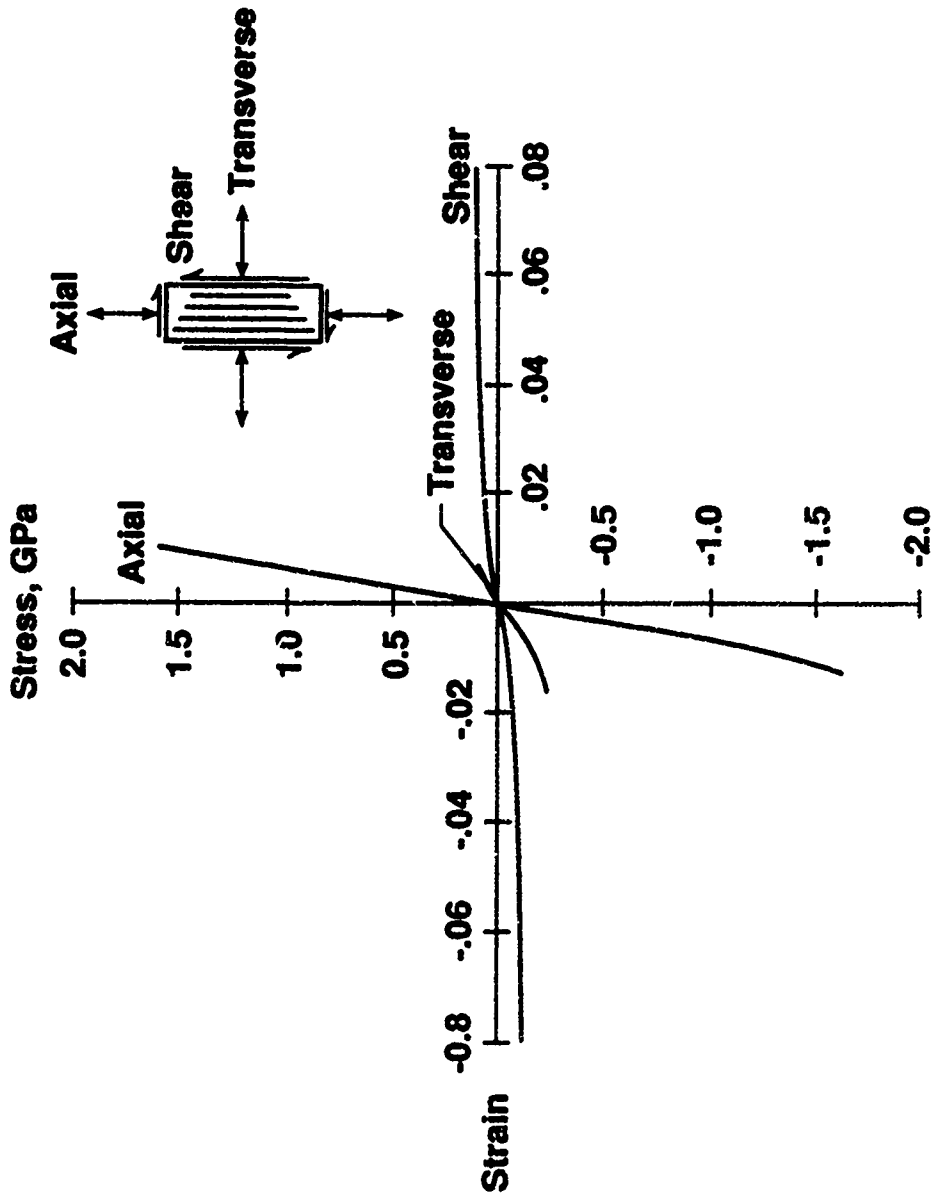
Figure 78. Stress vs. strain data for T300-934 composite material.
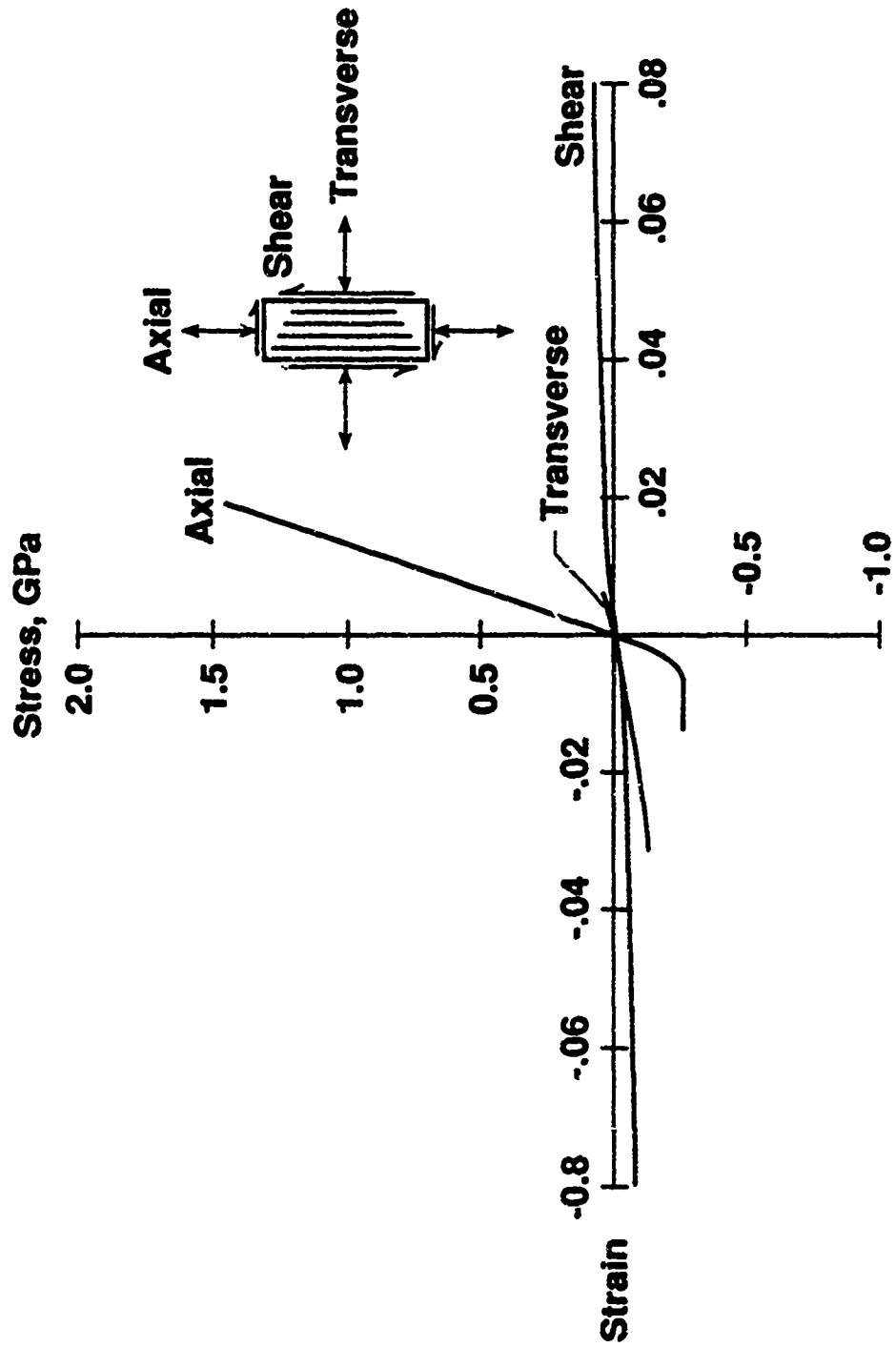
Figure 79. Stress vs. strain data for K-934 composite material.

175
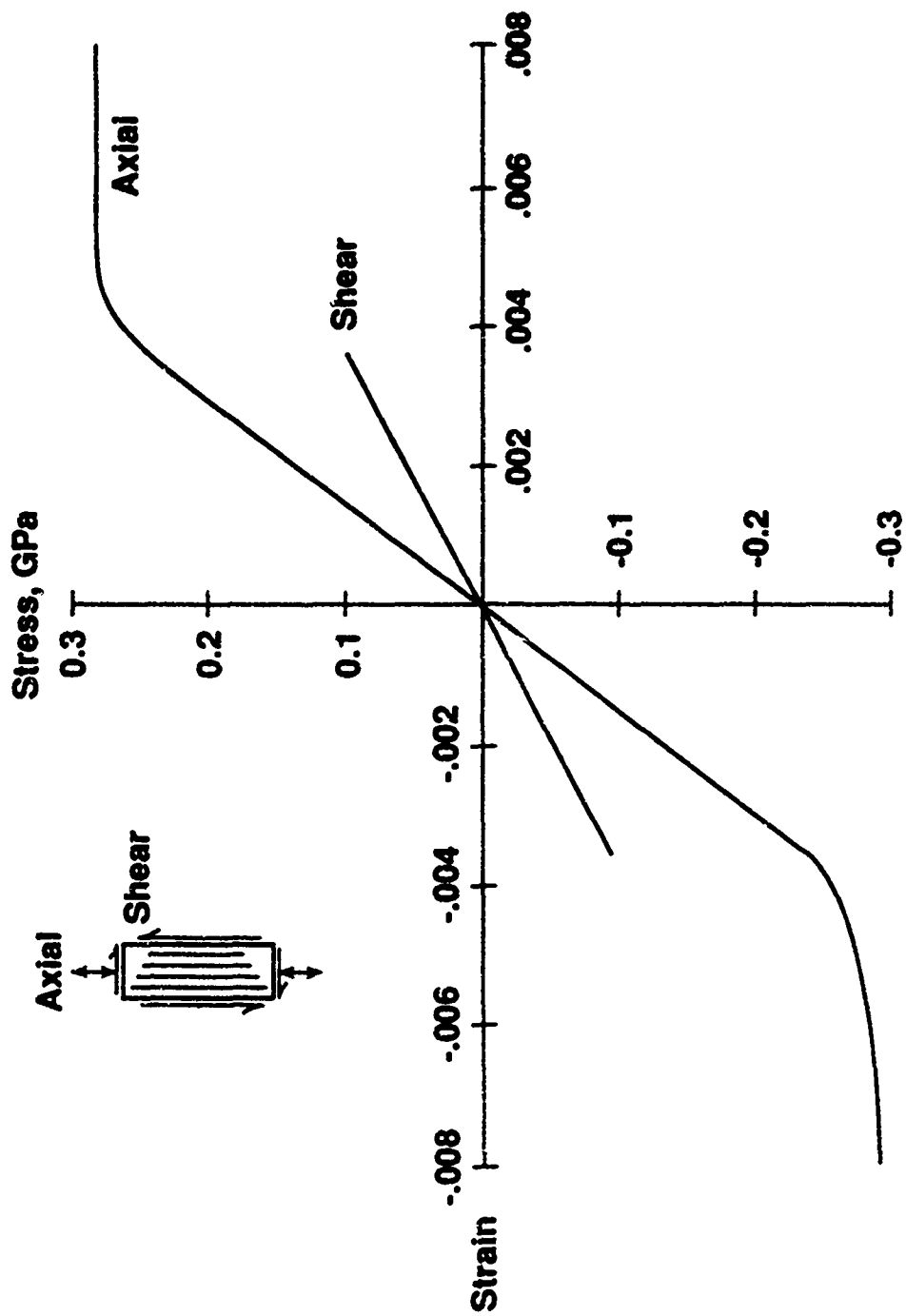
Figure 80. Stress vs. strain data for 6061 T6 aluminum material.

solution to proceed past these singularities. An alternative approach is to make the singularities occur beyond the load range of interest. Creating a situation where the singularities occur beyond the load range of interest can be accomplished by the application of concentrated forces that correspond to local imperfections in the structure. Another approach is to incorporate an imperfection in the original geometry of the structure. The choice of the type of imperfection and the magnitude of the imperfection is based upon experience. Ideally, the chosen imperfection would eliminate numerical difficulties without adversely affecting the original response of the structure.

A half sine-wave radial imperfection along the length of the tube was incorporated in the model to produce a geometrical imperfection. An exagerated example of this type of imperfection is shown in Fig. 81. The maximum increase in the radius of the tube model was 0.0025 cm and occurred at the mid-length of the tube. Based upon preliminary analysis, the computed maximum crushing force used to calculate energy-absorption capability was very sensitive to the magnitude of the imperfection. For example, when the magnitude of the imperfection was on the order of the thickness of the tube wall the maximum crushing force was reduced by more than 50 percent.

Numerical problems occurred in modeling the unloading portion of the load-deflection curve associated with tubes that crush in the local buckling mode. The linear and initial nonlinear response of the load-deflection response was predicted using EAL. The linear and initial nonlinear response region is representative of small deflections in the tube. When the slope of the load deflection response, as in
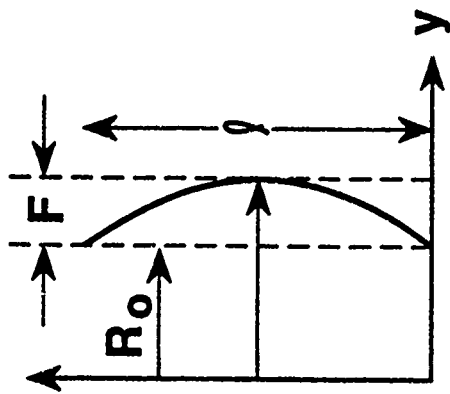
Quarter-symmetric tube

Edge view of tube

$$R = R_o + F * \sin(2z/\ell)$$

Figure 81. Half sine-wave radial tube imperfection.

178

Fig. 82, decreases to zero, EAL's solution algorithm would not reliably converge and EAL aborted. The unloading portion of the load-deflection curve occurs as a buckle forms. During the unloading portion of the load-deflection response the slope of the load-deflection curve is negative. The slope of the load-deflection curve is zero when the walls of the buckle collapse upon themselves. Further loading of the tube produces an increase in load and the hill and valley load-deflection response of the formation of the next buckle repeats.

The Newton-Raphson interative solution method, as implemented in the EAL finite element program, had difficulties in converging near the peak of the load-deflection curve. Techniques for advancing the solution beyond numerically difficult points have yet to be implemented in the EAL finite element code. Therefore, the calculation of the unloading portion of the load-deflection curve was not possible.

Calculation of the energy-absorption capability requires determination of the maximum and minimum crushing force for a representative crushing cycle. For those specimens that crush in the local buckling mode, it was impossible to calculate the minimum crushing force. Therefore, for the sake of this study, the mimimum crushing force was considered to equal the maximum crushing force for tubes that crushed in the local buckling-crushing mode. The difference in maximum and minimum crushing forces is typically less than 15 percent of the average crushing force, ref. 24. Assuming the maximum, the minimum, and hence the average crushing forces are equal results in an error of typically less than 8 percent.

4.3.5 Element Type and Level of Discretization

The phenomena that must be modeled generally define the type of elements that
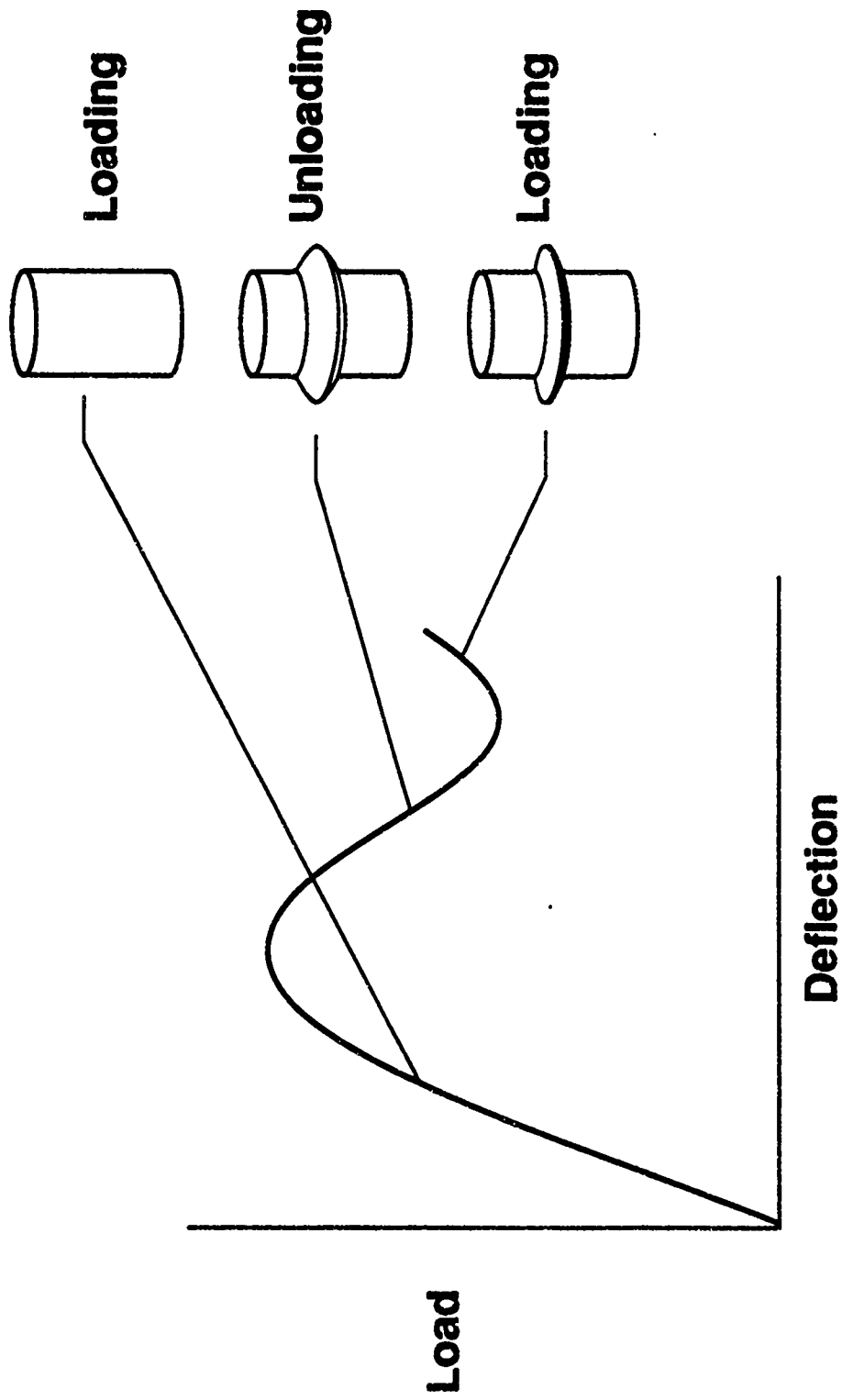
Figure 82. Typical load-deflection response of tubes that crush in the local buckling crushing mode.

are required in the model and the level of discretization that must be used. Prior to the analysis of the crushing process, the length and location of interlaminar, intralaminar, and in-plane cracks are unknown, and the crushing surface of the tube can be scalloped and irregular in shape. Therefore, to separately model these geometrical changes, it is necessary to model each layer of the specimen. Adjacent layers are mathematically attached at coincident element nodes as depicted in Fig. 75. As a crack grows along an interface, the mathematical connections between element nodes (layers) are removed.

The next issue that must be addressed is whether each layer must be modeled with two-dimensional (2-D) planar elements that have membrane, bending, and membrane-bending coupling, or three-dimensional (3-D) solid elements. If 3-D solid elements were used, then the interlaminar stress components can be calculated. However, it is not mandatory to model these interlaminar stresses when using the strain energy release rate to predict crack initiation and growth. If 3-D solid elements were used, then the level of element discretization within a layer to maintain an aspect ratio on the order of one would require substantially more elements than would be required if 2-D elements were used. Therefore, 2-D elements were used in the finite element modeling of the tubes.

The progressive nature of the crushing process results in a relatively constant crushing load, as in Fig. 74. The crushing load varies as the tube is crushed as a result of different local failure events occurring in the crushing process. These failure events are cyclic, and the crushing loads for most materials are relatively constant.

181

The region of the tube that is involved during the progressive crushing of a composite tube is small relative to the entire tube. The strain level in the tube outside of the crush zone is small relative to the corresponding strains required to induce local buckling of the tube wall or small relative to the failure strain of the material. Modeling the progressive crushing process requires modeling of the crush zone and a sufficient portion of the uncrushed tube so that boundary condition effects do not influence the crushing response. The cyclic nature of the crushing response facilitates determination of the energy-absorption capability from a representative cycle of the crushing process. Based upon the cyclic nature of the crushing process, only a section of tube of a length representative of a crushing cycle must be modeled. Therefore, the length of tube that must be modeled is the greater of either of (1) the length requirements to satisfy boundary condition effects or (2) crushing cycle distance.

Whenever possible, it is desirable to take advantage of any symmetry conditions or other repetitive features of the structure being modeled to reduce the number of degrees of freedom in the finite element model. The circular cross-section tube specimen, an axisymmetric structure, lends itself to significant simplication through the use of axial symmetry.

Utilizing a portion of the tube instead of the entire tube can result in exclusion of important failure modes. An example where exclusion of important failure modes can occur is in the modeling of the buckling of a cylinder. Modeling a portion of the cylinder using symmetric boundary conditions excludes any unsymmetrical buckling modes. If the effects of the symmetric and unsymmetric buckling modes

need to be quantified, then an analysis with each type of boundary condition must be performed. However, based upon the crushing of similar metallic tubes that crushed in both symmetrical and unsymmetrical local buckling modes, the difference in energy-absorption capability between the tubes that crushed in symmetric and unsymmetrical buckling modes was small. Therefore, modeling only a portion of the tube using symmetrical boundary conditions is a reasonable approximation.

The finite element representation used in this study was a one-quarter symmetric four-layer model with one layer for each ply of the composite tube. The metallic tube was also modeled with four layers to account for through-the-thickness plastic deformation. Each layer of the tube, as depicted in Fig. 83, was modeled with five elements in the circumferential direction and fourteen elements along the length. The model had 360 nodes and 2160 degrees of freedom. Finite element nodes for each layer were coincident with adjacent layers. The finite element model depicted in Fig. 83 shows the different layers a finite distance apart. However, the layers as modeled are coincident. Mathematical "zero-length" springs with axial and rotational stiffness were used to connect adjacent layers. The "zero-length" springs are shown as axial springs in Fig. 83; however, these springs have axial and rotational stiffnesses in all three coordinate directions. Interlaminar crack growth was represented by the removal of the "zero-length" springs between layers, as in Fig. 75.

Two-dimensional plate finite elements that had membrane, bending, and membrane-bending coupling stiffness were used. The neutral axis of each layer of elements was shifted radially to account for its relative through-the-thickness position. The tube finite element model was 1.27 cm in length. A half sine-wave radial

183

Zero-length springs for
layer interconnection

Discrete modeling
of each layer

Section A-A

Zero-length springs have 3 axial and
3 rotational stiffness components
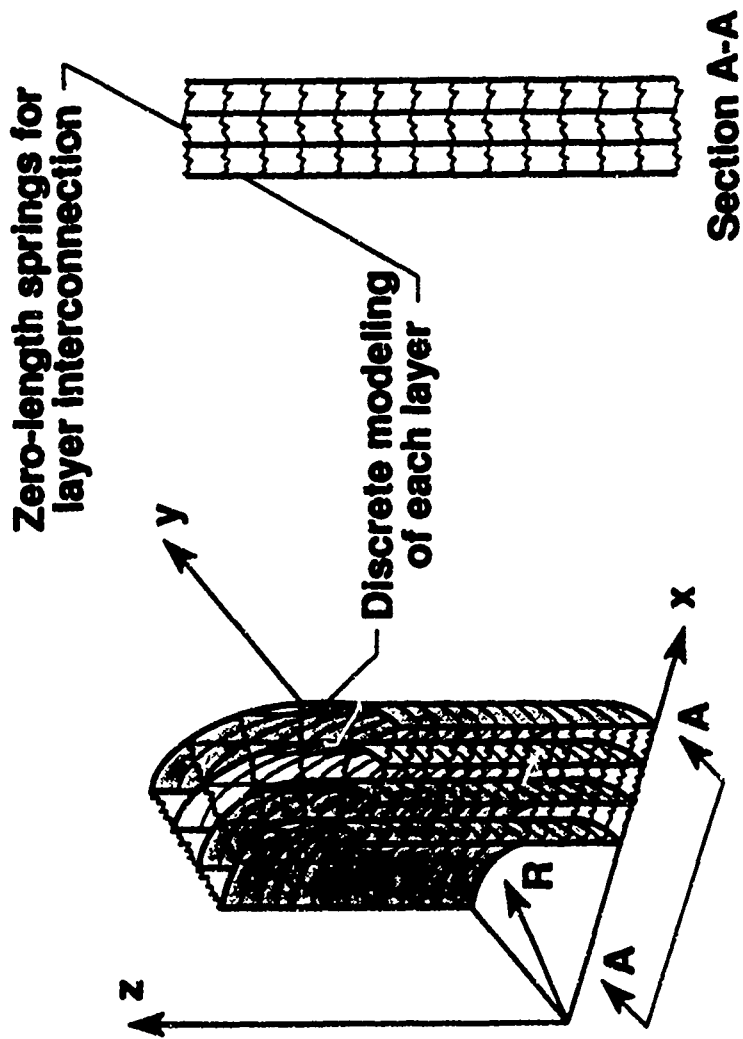
Figure 83. Finite element model.

184

imperfection along the length of the tube, as depicted in Fig. 81, was incorporated with a maximum increase in radius of 0.0025 cm located at the mid-length of the tube.

4.4 Results of Finite Element Studies

Three different computer studies were performed to verify the energy-absorption prediction capability of the analysis. The first study was of a 6061-T6 aluminum tube that was 3.81 cm in inside diameter with a nominal wall thickness of 0.25 cm. The second and third studies were of K-934 and Gr-934 $[\pm\Theta]_S$ tubes, where $\Theta=15$, 45, and 75 degrees. Tube inside diameter was 3.81 cm and wall thickness was 0.24 cm.

The T300-934, K-934, and aluminum material mechanical properties used in these case studies are shown in Figs. 78, 79, and 80. The Mode I critical strain energy release rate, G_c, used to evaluate crack growth for the T300-934 material was 142 Nm/m^2.

4.4.1 Aluminum Tubes

Predicted and measured energy-absorption capabilities for the aluminum tube were 68.2 and 79.2 Nm/g, respectively. The predicted value was 16 percent less than the measured value. The lack of agreement between the predicted and measured energy-absorption capability is attributed to the lack of integrated methods for modeling material stress-strain nonlinearities, the coarseness of the finite element mesh, and the inability to predict the unloading portion of the load-deflection curve.

The aluminum tube crushed in the local buckling mode, and the mechanism for energy-absorption was plastic deformation. Plastic deformation or yielding initially occurred along the inside of the tube at the point of maximum imperfection. As the tube is crushed, the plastic region progressively increased along the length of the tube and through the thickness of the tube with increasing applied load.

4.4.2 Kevlar-Reinforced Tubes

In the second study, the $[\pm\Theta]_S$ K-934 tubes also crushed in the local buckling mode. No interlaminar cracks were initiated. Predicted energy-absorption trends were similar to the experimentally determined trends as seen in Fig. 84. The predicted energy-absorption capability slightly increased between $\Theta=15$ and 45 degrees and decreased between $\Theta=45$ and 75 degrees. The predicted energy-absorption capability was less than 25 percent higher than the experimental values.

The characteristic crushing length, based upon this analysis, is probably inaccurate. The type of imperfection defines the characteristic crushing length. That is, if a full sine-wave imperfection were used, then the characteristic crushing length would be half the length in the current model where a half sine-wave was incorporated. If a crushing initiator, such as a chamfered end, were included in the model, then it might be possible to eliminate an imperfection in the model. Inclusion of the crushing initiator would also provide a mechanism to investigate the effects of initiator design on energy-absorption capability. Unfortunately, the inclusion of an initiator in the finite element model would increase the size of the finite element model. Any increase in model size and complexity, such as would occur with the

186
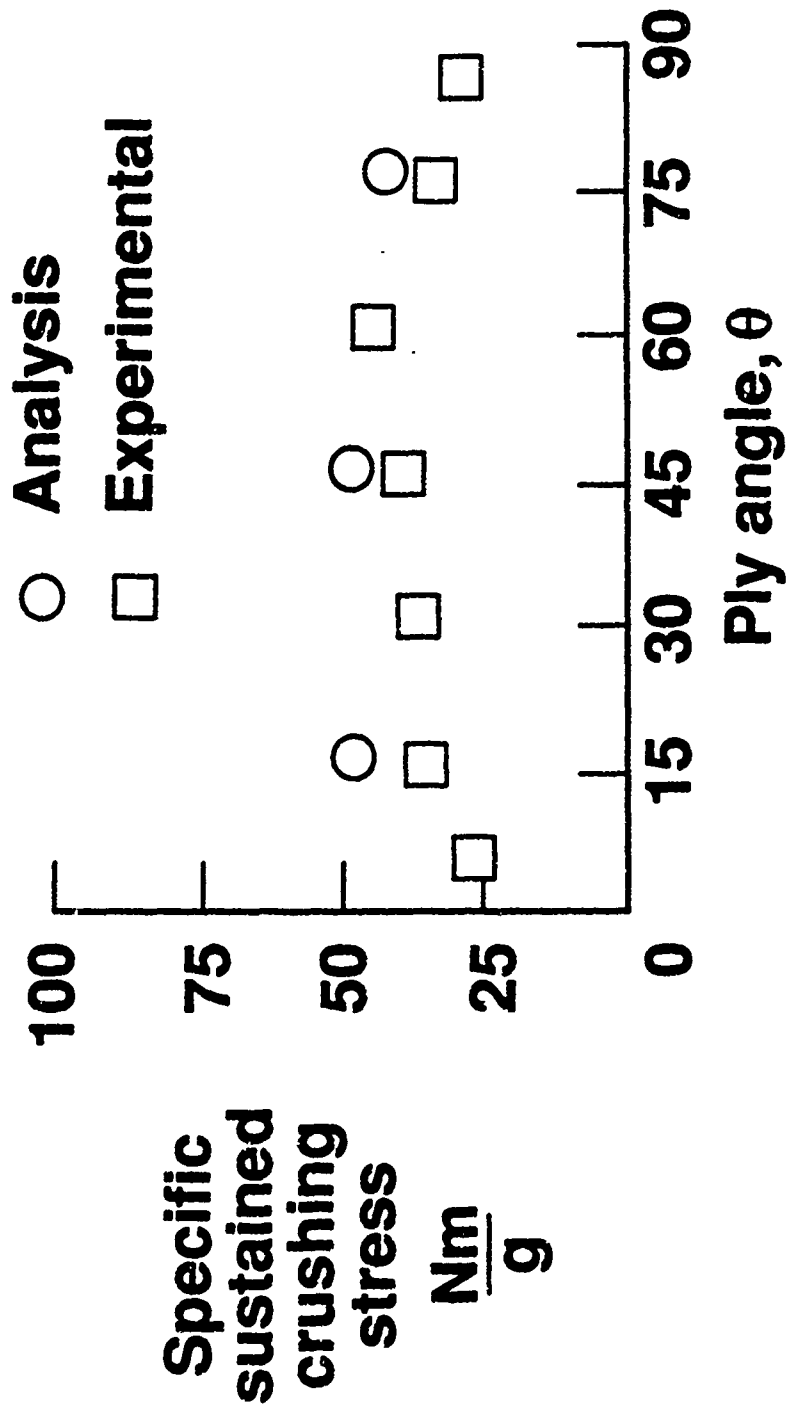
Figure 84. Comparison of predicted and experiment energy-absorption capability of K-934 composite tubes.

inclusion of an initiator, would require additional computational load steps and computational time per load step to obtain a solution.

4.4.3 Graphite-Reinforced Tubes

The third study was of T300-934 $[\pm\Theta]_S$ tubes. The predicted energy-absorption trend, except for the $[\pm75]_S$ tube, was in agreement with the experimental trends as seen in Fig. 85. For the range of ply orientations analyzed, the predicted energy-absorption capability was highest at $\Theta=15$ degrees and decreased in a near-linear manner as Θ increased. The predicted energy-absorption capabilities were less than 28 percent higher than the experimental values at $\Theta=15$ degrees while at $\Theta=75$ degrees the predicted value was only 22 percent of the experimental value. The crushing modes were lamina bending for the $[\pm15]_S$ and $[\pm45]_S$ tubes and brittle fracturing for the $[\pm75]_S$ tubes. The location of the interlaminar cracks was between layers 2 and 3 for both $[\pm15]_S$ and $[\pm45]_S$ tubes. Based upon lamina strains in the principal material coordinate system, the ± 15 laminae were not likely to fracture when crushed. However, lamina failure strains in the fiber direction of the ± 45 laminae were approximately 80 percent of the fiber-direction failure strain at the maximum crushing force. It is possible that with more detailed modeling of the tube, i.e., more layers and a finer finite element mesh, some brittle fracturing of plies would be predicted in addition to the predicted lamina bending. This possible crushing mode scenario is consistent with the experimentally observed crushing response for the $[\pm45]_S$ tubes. The brittle fracturing crushing mode that was predicted for the $[\pm75]_S$ tubes was a compressive failure of the matrix transverse
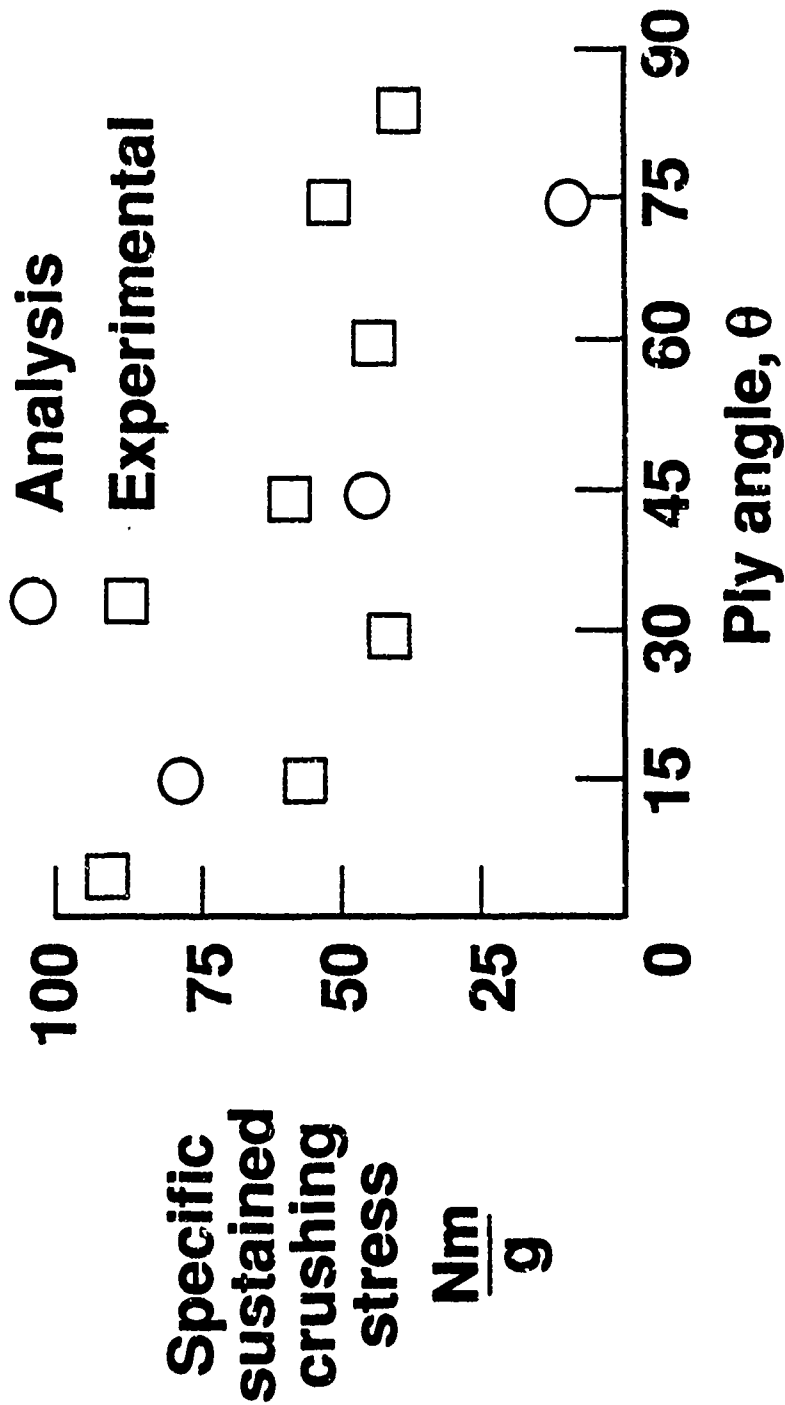
Figure 85. Comparison of predicted and experiment energy-absorption capability of T300-934 composite tubes.

to the longitudinal axis of the fiber. Interlaminar cracks in the $[\pm 75]_S$ tubes also occurred between layers 1 and 2 and layers 2 and 3.

The low predicted energy-absorption capability for the $[\pm 75]_S$ tube could be due to unrealistically low allowable compressive strains transverse to the fiber. The author does not believe there currently exists an acceptable material compression test. He further feels that the different compression test methods currently used in the composite materials industry produce very conservative results for unidirectional material in the transverse-to-the-fiber direction.

4.6 Summary

The predicted energy-absorption trends, crushing modes, and crushing mechanisms presented in this study provide sufficient evidence that the basic approach to predicting the crushing response of composite tubes is reasonable. The agreement between analysis and experiment suggests that the important phenomena of the crushing process have been included in the model. Improvements in the iterative solution strategy, incorporation of crushing initiators, and enhancement of other modeling details should produce even better agreement between experiment and analysis. Further improvements between the predicted and measured energy-absorption capability could be realized if material used to produce the tubes and the material test specimens were of the same batch. This analysis should be applied to tubes having other ply orientations, material combinations (hybrids), and geometries.

Chapter 5 - EXPERIMENTAL AND THEORETICAL EVALUATION OF SUBFLOOR BEAM CONCEPTS

Crash-energy absorbing helicopter subfloor beams consist of the beam caps, the crushing initiator, and the energy-absorbing web, as shown in Fig. 86. The beam caps provide bending-load-carrying capability and the mechanism for attachment of the beam to the floor and the outer fuselage skin. The beam caps do not directly contribute to the energy-absorption process. The crushing initiator produces a local failure of the beam web at a predetermined load. The non-crash loads in the web must be transferred into the caps of the beam through the crushing initiator. The crushing initiator depicted in Fig. 86 is a "J", ref. 34. When a crushing load is applied to the beam a local-bending moment is produced in the radius portion of the "J". The initial failure of the beam occurs at the point in the "J" where the bending moment is the the highest in magnitude. The failure load of the "J" can be tailored by changing the radius of curvature of the "J". In a crash, when the fuselage lower skin impacts the ground, the crushing initiator transfers these loads into the beam webs, without failure, until the design failure load is reached. When the failure load of the initiator is reached, the initiator fails and the crushing process of the beam web begins. Typically, the design failure load of the crushing initiator is less than or equal to the sustained crushing load of the beam web. The energy absorbed by the crushing initiator is small relative to the energy absorbed by the beam web. Therefore, in the investigation of the energy-absorption characteristics of beams, it is only necessary to evaluate the energy-absorption characteristics of the beam webs.

Beam caps

Beam web

"J" crushing initiator
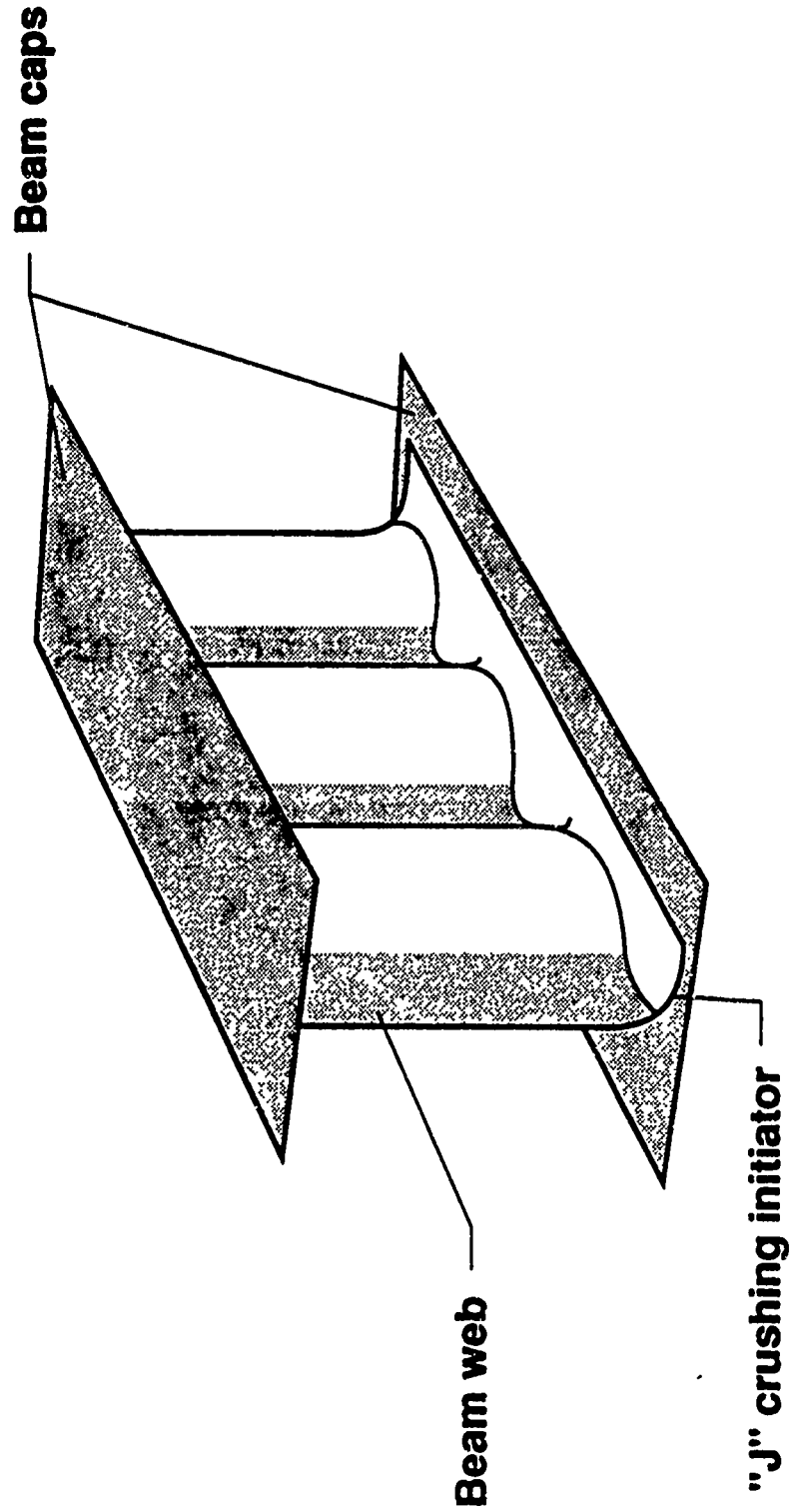
Figure 86. Typical energy-absorbing sine-wave beam.

192
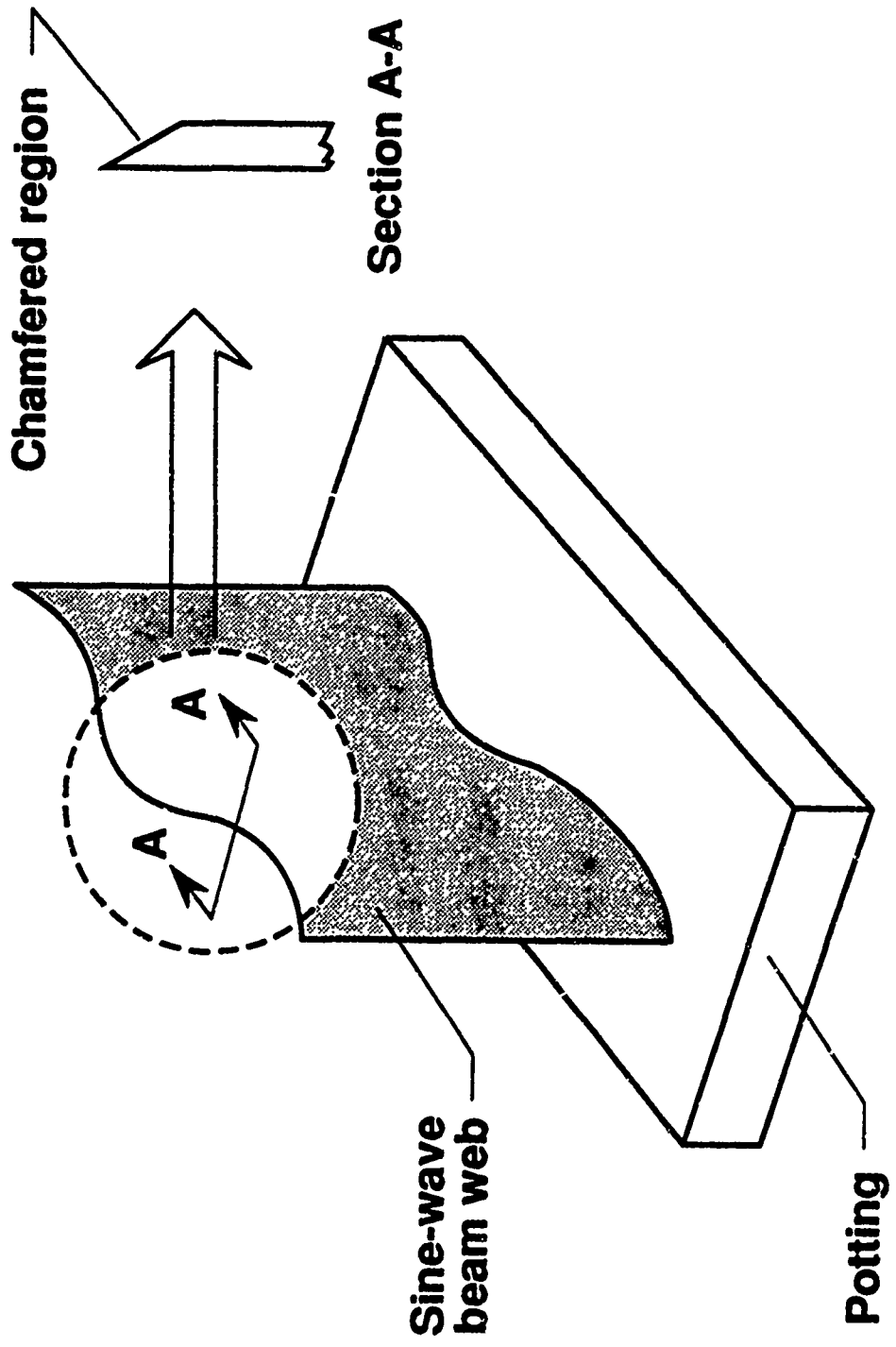
Figure 87. Typical sine-wave beam web specimen showing chamfered end.

The beam webs evaluated in this study incorporate no beam cap or beam intersection structural details. A chamfer crushing initiator was incorporated along the top edge of each beam web as depicted in Fig. 87. The chamfer crushing initiator is suitable for laboratory evaluation purposes. However, chamfering is an inappropriate crushing initiator for flightworthy structure. The bottom edge of the beam web opposite the chamfered top edge of the beam web is mounted in a room-temperature-curing-epoxy base. Each end of the beam webs was unsupported in these tests. Typical sine-wave and integrally stiffened beam webs are shown in Fig. 88. The sine-wave beam web is a continuous series of tangent-half-circle tubes. The centers of each of the half tubes are positioned along the center line of the beam. The circular-tube- and rectangular-tube-stiffened beams resemble beams where circular and rectangular tubes are attached with flat webs between tubes. The stiffened beams are fabricated in halves and bonded together along the centerline of the beam.

In this chapter, the crushing response of composite sine-wave and integrally stiffened beam webs is discussed. Included is the energy-absorption capability of the different beam concepts and how different structural and material variables influence the crushing response. A method of predicting the energy-absorption capability of the beam web concept is also presented.

5.1 Experimental Evaluation of Sine-Wave and Integrally Stiffened Beam Web Specimens

Sine-wave, circular, and rectangular cross-section tubular stiffened beam webs were statically crushed with the test procedure used on the tubular specimens described in Chapter 2. In these tests, the energy-absorption capabilities were
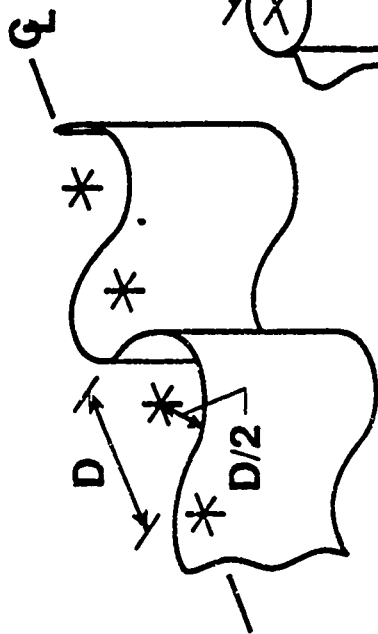
194
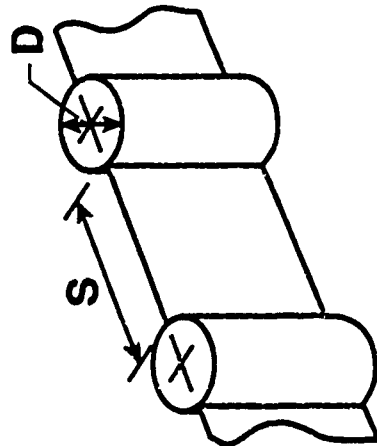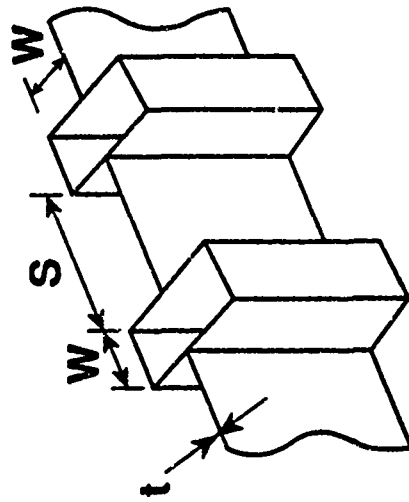
Figure 88. Typical sine-wave and integrally stiffened beams.

195

determined, and the crushing modes of the beams were identified. The variables evaluated include geometry, ply orientation, and material properties.

5.1.1 Effects of Beam Geometry on Energy-Absorption Capability

The effects of beam geometry on the energy-absorption capability of sine-wave and integrally stiffened beams were investigated. Beams were fabricated from T300-934 and K-934 composite material. The ply orientation of the composite beams was $[\pm 45]_N$. The beams were not always fabricated using a symmetric stacking sequence. No noticable warping of the beam occurred due to the unsymmetric stacking sequence. One circular tube and one rectangular tube integrally stiffened aluminum beam were also fabricated for purposes of comparison with composite beams of comparable geometry. In this study, sine-wave beams with different diameter (D) to wall thickness (t) ratios (D/t) were experimentally evaluated. The ply orientations, material, diameter, thickness, length, and height of the sine-wave beam specimens are presented in Table 3. The integrally stiffened beams evaluated in this study had elements of the beam with different geometry (i.e., stiffener cross-sectional shape, wall thickness, diameter or width, and spacing between stiffeners) to facilitate understanding how geometry influences energy-absorption capability. The ply orientation, material, stiffener geometry, length, and height of the integrally stiffened beams are presented in Tables 4 and 5.

Sine-Wave Beam Webs. Graphite- and Kevlar-reinforced epoxy sine-wave beams were loaded with a crushing force, and the energy-absorption results were compared to energy-absorption results from tube specimens of comparable geometry. The

Table 3. Sine-wave beam geometry.

Ply Orientation	Material	Diameter, cm	Thickness, cm	Length, cm
$[\pm45]_{6S}$	T300-934	7.62	0.36	27.9
$[\pm45]_{4S}$	T300-934	7.62	0.23	27.9
$[\pm45]_{2S}$	T300-934	7.62	0.09	27.9
$[0/\pm15]_4$	T300-934	3.81	0.07	22.2
$[0/\pm45]_4$	T300-934	3.81	0.07	22.2
$[0/\pm75]_4$	T300-934	3.81	0.07	22.2
$[\pm45]_{6S}$	K-934	3.81	0.32	27.9
$[\pm45]_{4S}$	K-934	3.81	0.25	27.9
$[\pm45]_{2S}$	K-934	3.81	0.11	27.9
$[\pm45]_S$	K-934	3.81	0.06	27.9
$[\pm45]_{6S}$	K-934	7.62	0.41	22.2
$[\pm45]_{4S}$	K-934	7.62	0.30	22.2
$[\pm45]_S$	K-934	7.62	0.06	22.2
$[0/\pm15]_4$	K-934	3.81	0.07	22.2
$[0/\pm45]_4$	K-934	3.81	0.07	22.2
$[0/\pm45]_4$	K-934	3.81	0.07	22.2
$\left[\pm45_H^F\right]_S$	T300-K-934	3.81	0.06	22.2
$\left[45_H^F/0_{Gr\ 3}^T\right]_S$	T300-K-934	3.81	0.06	22.2

The height of all beams was 15.2 cm.

Table 4. Circular cross-section tube stiffened beam geometry.

Ply Orientation	Material	Diameter of tube, cm	Distance between tubes, cm	Thickness of web, cm	Length, cm
$[\pm 45_4]_S$	T300-934	1.27	2.54	0.08	22.8
$[\pm 45_4]_S$	T300-934	2.54	3.81	0.08	25.4
$[\pm 45_4]_S$	T300-934	7.62	2.54	0.08	30.9
$[\pm 45_4]_S$	K-934	1.27	2.54	0.08	22.8
$[\pm 45_4]_S$	K-934	2.54	3.81	0.08	25.4
$[\pm 45_4]_S$	K-934	7.62	2.54	0.08	30.9
N.A.	Aluminum	2.54	3.81	0.09	25.4

The height of all beams was 15.2 cm.

N.A. = not applicable

Table 5. Rectangular cross-section tube stiffened beam geometry

Ply Orientation	Material	Width of rectangular tube, cm	Distance between tubes, cm	Thickness of web, cm	Length, cm
$[\pm 45_4]_S$	T300-934	1.27	3.81	0.08	30.5
$[\pm 45_4]_S$	T300-934	2.54	3.81	0.08	25.4
$[\pm 45_4]_S$	T300-934	7.62	2.54	0.08	30.5
$[\pm 45_4]_S$	K-934	1.27	3.81	0.08	30.5
$[\pm 45_4]_S$	K-934	2.54	3.81	0.08	25.4
$[\pm 45_4]_S$	K-934	7.62	2.54	0.08	30.5
N.A.	Aluminum	2.54	3.81	0.09	25.4

The height of all beams was 15.2 cm.

N.A. = not applicable

198

inside tube diameter of the graphite-reinforced sine-wave beams was 7.62 cm, and the range of D/t values was between 21 and 83. The energy-absorption capability of the sine-wave beams was similar to the energy-absorption capability of tubular specimens of similar geometry, as shown in Fig. 89. In Fig. 89 the solid symbols represent the energy-absorption capability of the sine-wave beams. A slight decrease in energy-absorption capability was obtained as beam D/t value increased which was also consistent with the energy-absorption trends of the tubular specimens. All graphite-reinforced beams crushed in a combined brittle-fracturing and lamina-bending crushing mode as in Fig. 90.

Inside tube diameter of the Kevlar-reinforced sine-wave beams was either 3.81 or 7.62 cm. The range of D/t values was between 11 and 113. The magnitude of the energy-absorption capability of the beams was typically the same as the energy-absorption capability of tubes of similar geometry, as shown in Fig. 91. Energy-absorption capability of the beams decreased as D/t increased. This energy-absorption trend is consistent with the tubes' energy-absorption trend. However, three beams with D/t values between 15 and 25 exhibited slightly lower energy-absorption capability than tubes of comparable geometry. All of the Kevlar-reinforced beams exhibited a local buckling crushing mode as depicted in Fig. 92. At the unsupported ends, the characteristic crushing length was much longer than the characteristic crushing length at the center of the beam. The longer the characteristic crushing length, the lower the energy-absorption capability. The three beams having D/t values between 15 and 25 exhibited a larger region of long characteristic crushing length than the other beams and hence their lower energy-absorption capability.
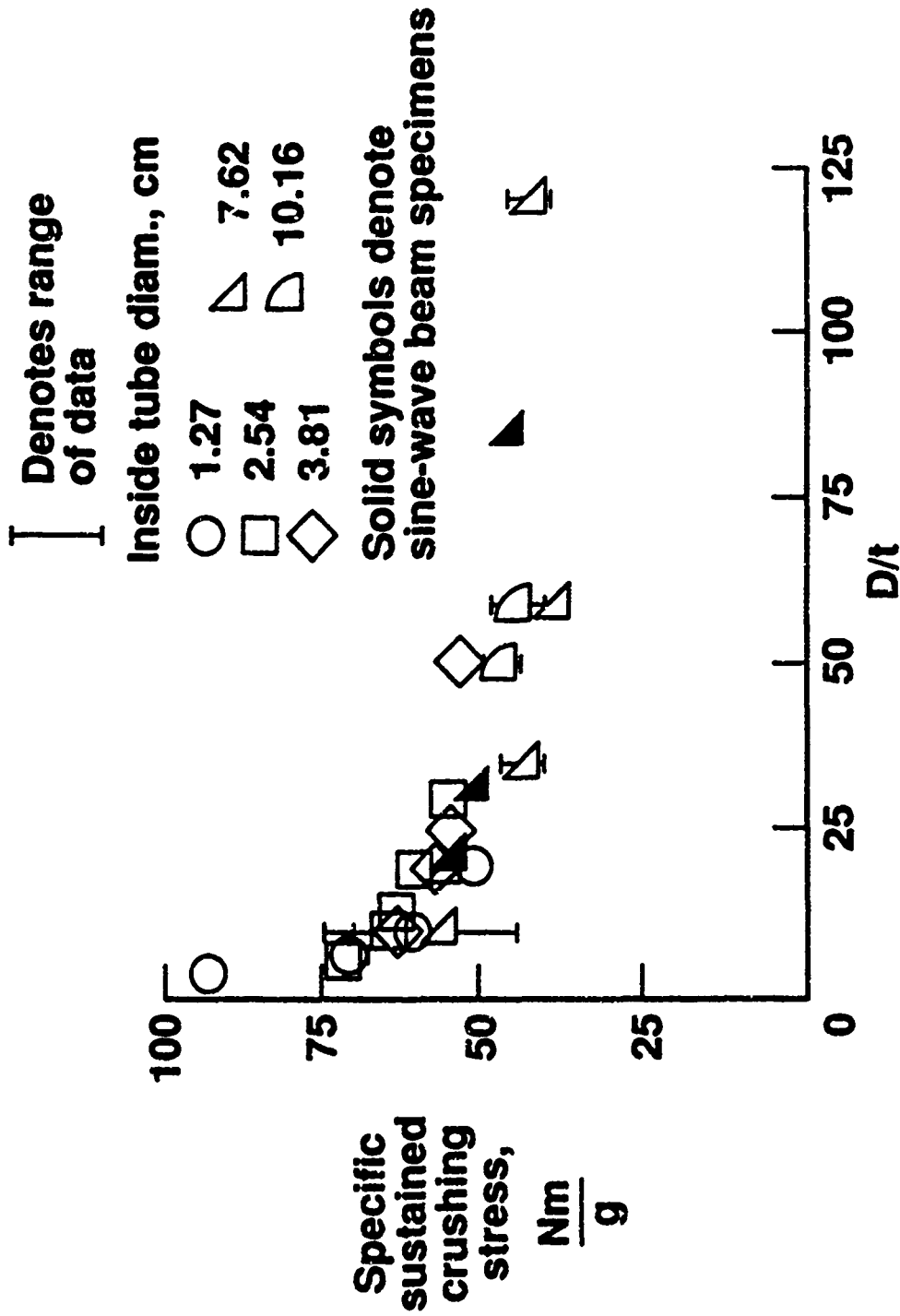
Figure 89. Effects of D/t ratio on the energy-absorption capability of $[\pm 45]_N$ Gr-E tubes and sine-wave beams.
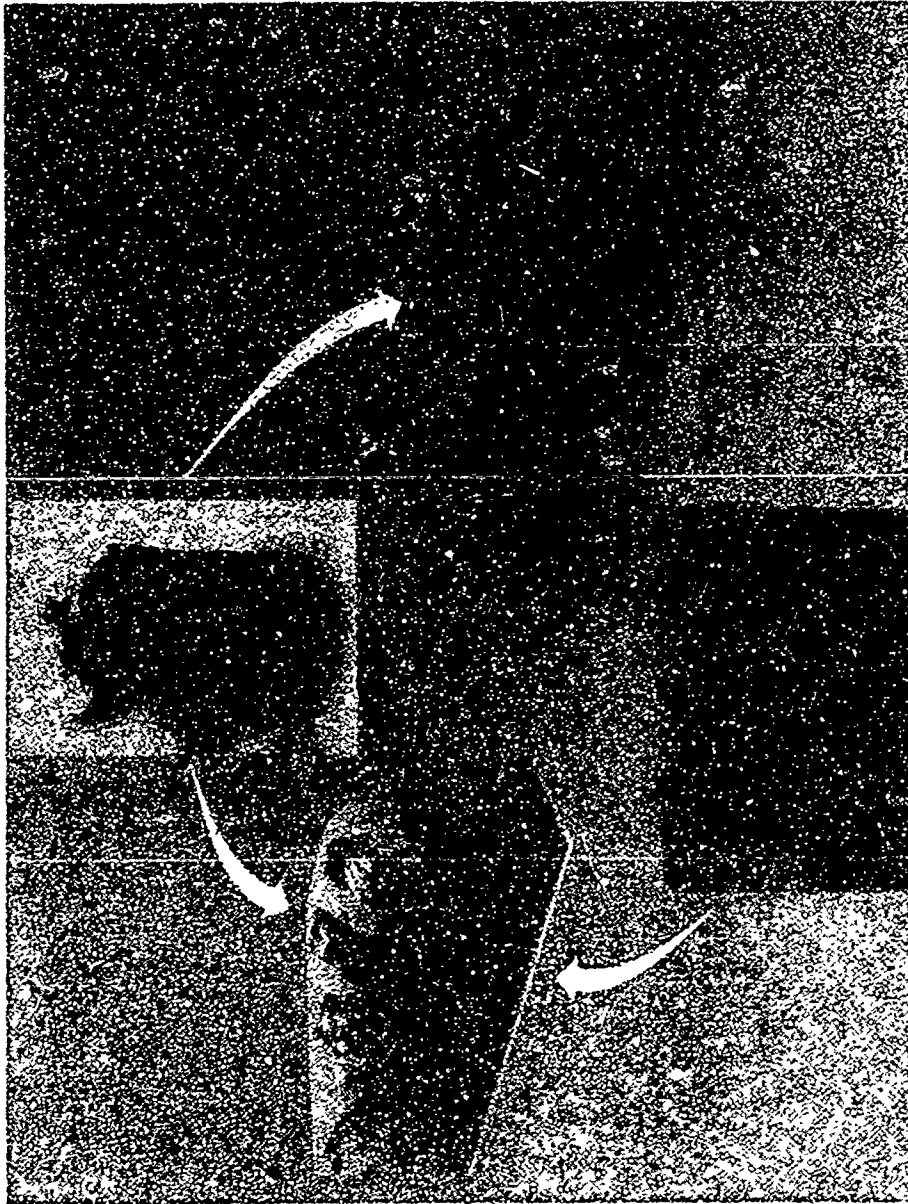
Figure 90. Similarity in crushing modes of Gr-E tubes and beams.
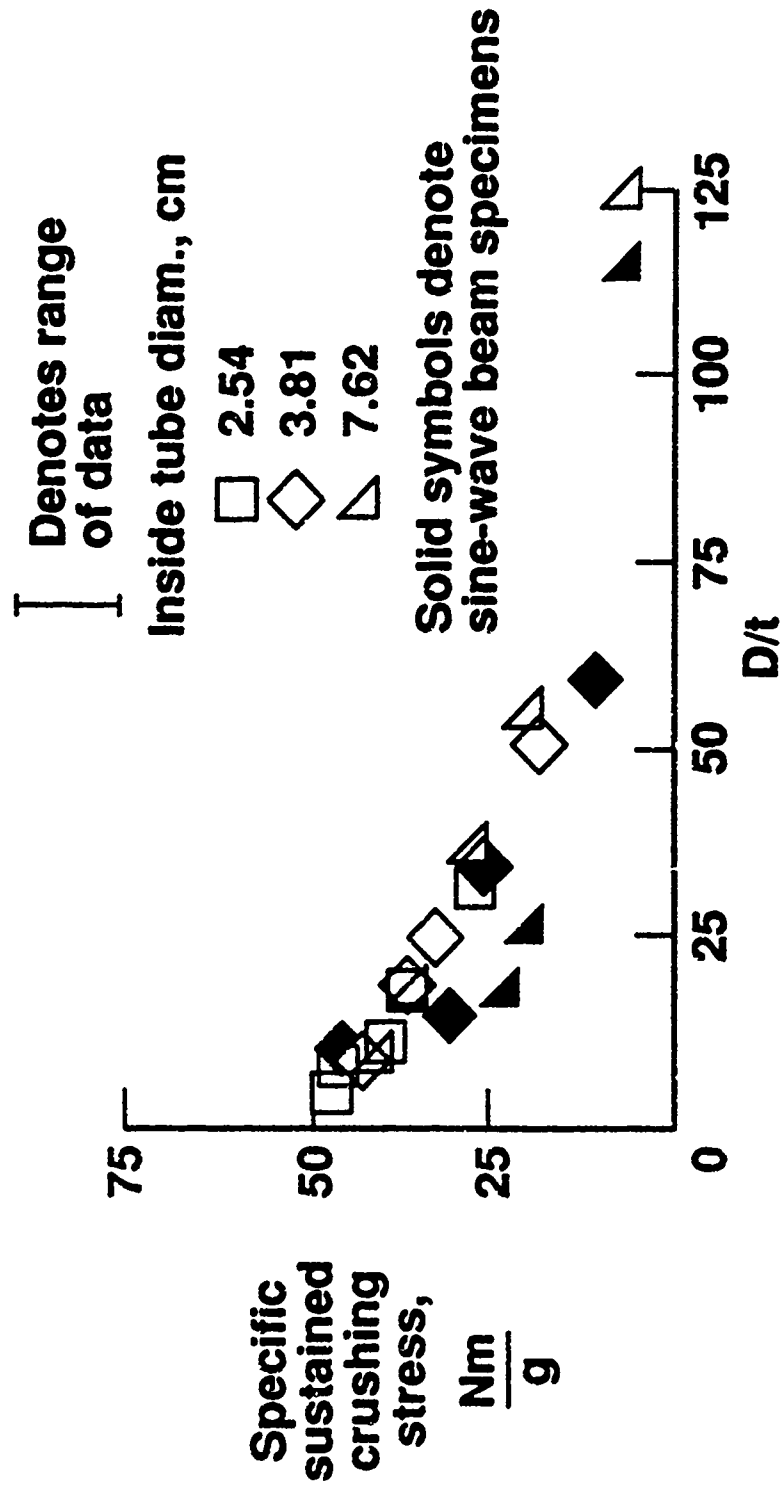
Figure 91. Effects of D/t ratio on the energy-absorption capability of $[\pm 45]_N$ K-E tubes and sine-wave beams.

Figure 92. Similarity in crushing modes of K-E tubes and beams.

Integrally Stiffened Beam Webs. A direct comparison of energy-absorption data for tubes and integrally stiffened beams can not be made because the integrally stiffened beams are composed of multiple elements of different geometry instead of a single continuously repeating element. However, the energy-absorption trends of the beams can be compared with energy-absorption characteristics of tube specimens.

The energy-absorption trends of the circular and rectangular cross-section tube integrally stiffened beams are similar to those found for circular and square cross-section tube specimens. As the tube diameter D or width W increases, and hence the D/t and W/t values increase, the energy-absorption capability decreased, as depicted in Figs. 93 and 94. In both Figs. 93 and 94, the distance between stiffeners is denoted as S. The web between the stiffeners crushes in a similar mode to that of a side of the rectangular tube stiffener. Therefore, interpretation of the effects of stiffener spacing on energy-absorption capability stiffener spacing, the distance between stiffeners S is equivalent to the wall width W of a tube. As the distance between stiffener increases, the corresponding W/t of the web between stiffeners increases, and the energy-absorption capability of the beams decreases. This energy-absorption trend is consistent for both graphite- and Kevlar-reinforced beams.

The crushing modes for the composite beams were also consistent with the crushing modes of the tube specimens. The flat elements of the graphite-reinforced beams crushed in a predominantly lamina bending mode with some brittle fracturing as in Fig. 90. Curved elements of the graphite beams crushed in a predominantly brittle fracturing mode with some lamina bending as in Fig. 90. Both the flat and curved

204
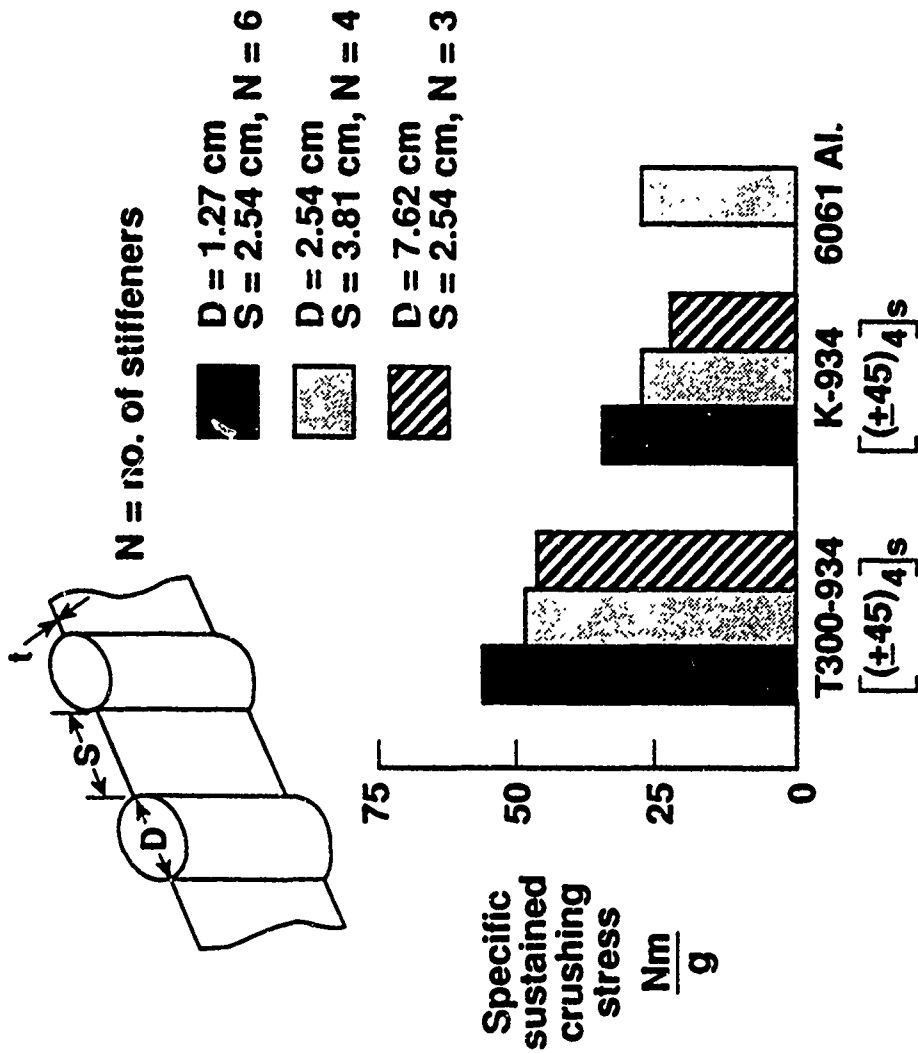
Figure 93. Energy-absorption capability of circular tube stiffened beams.
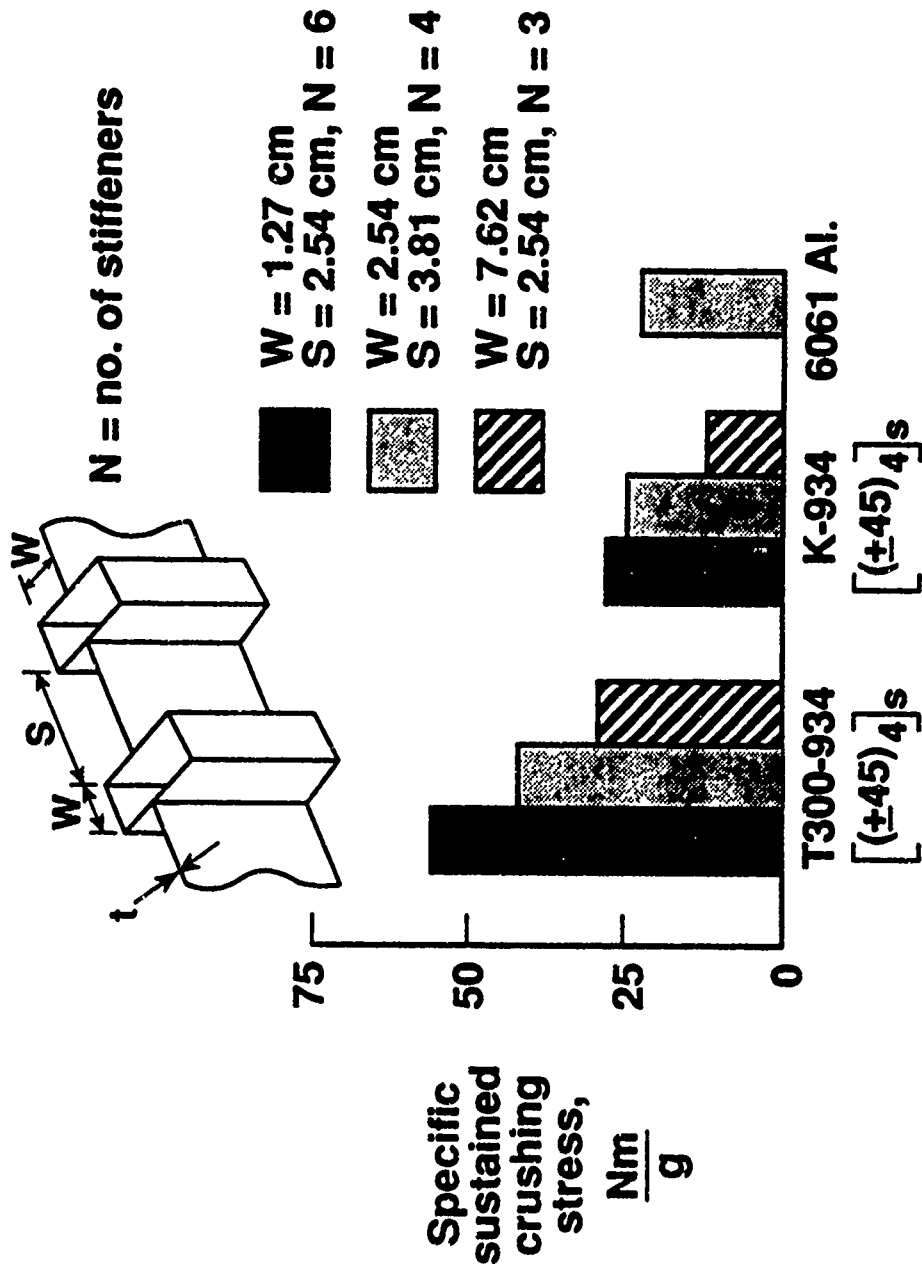
Figure 94. Energy-absorption capability of rectangular tube stiffened beams.

elements of the Kevlar-reinforced beams crushed in a local buckling mode as in Fig. 92.

The geometry of the Aluminum integrally stiffened beams were fabricated comparable to one configuration of graphite- and Kevlar-circular-tube- and rectangular-tube-stiffened beams. The energy-absorption capability of the aluminum beam was equal to the energy-absorption capability of a comparable geometry K-reinforced beam as shown in Figs. 93 and 94. However, the energy-absorption capability of the aluminum beams was approximately half the energy-absorption capability of the graphite-reinforced beam. These results demonstrate that K-reinforced composite beams have equal energy-absorption capability to aluminum beams whereas graphite-reinforced beams are substantially superior energy absorbers. Based upon tube energy-absorption capabilities, alternative composite materials and ply orientations could more than double the energy-absorption capability of the graphite-reinforced composite beams in Figs. 93 and 94.

5.1.2 Effects of Ply Orientation on the Crushing Response

of Composite Sine-Wave Beams

Sine-wave beams fabricated from T300-934 and K-934 prepreg were crushed to determine the effect of ply orientation on the crushing response of composite beam specimens. The laminate stacking sequence of the beams was $[0/\pm\Theta]_4$, where $\Theta=15$, 45, and 75 degrees. Energy-absorption capabilities of tube specimens that had the same laminate stacking sequence and material are also presented for comparative purposes.
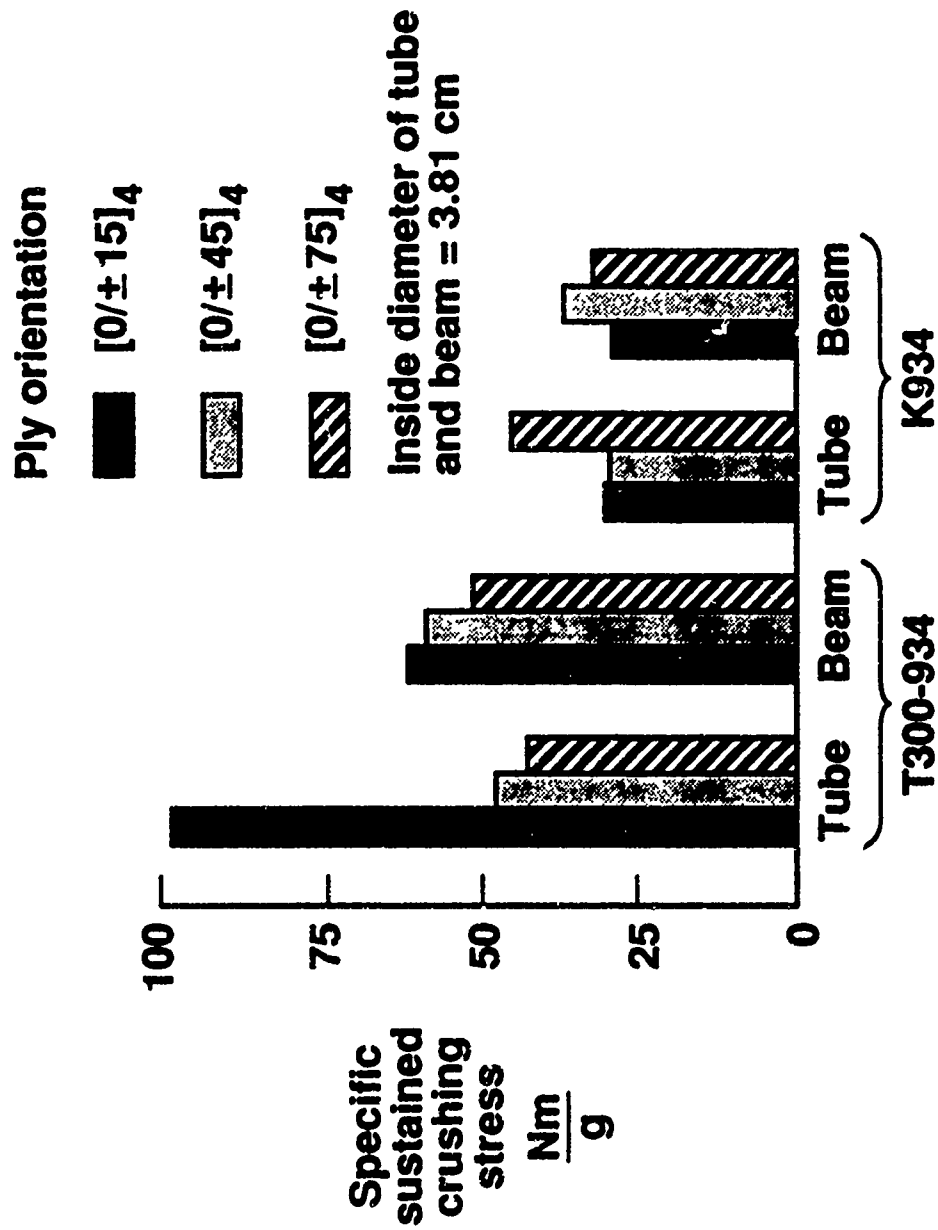
Figure 95. Effects of ply orientation on the energy-absorption capability of sine-wave beams.

The crushing modes of all beams were observed to be the same as the tubes with the same laminate stacking sequence and geometry. The energy-absorption capability of the beam specimens, presented in Fig. 95, was generally less than 10 percent different from the tube specimens of the same ply orientation except for the $[0/\pm 15]_4$ T300-934 and $[0/\pm 75]_4$ K-934 beams. In both cases, the energy-absorption capability of the beam was less than the tube specimens. The crushing modes of the $[0/\pm 15]_4$ T300-934 and $[0/\pm 75]_4$ K-934 beams near the unsupported ends significantly differed from the central part of the beam. The differences in crushing mode, hence, the lower energy-absorption capability, are attributed to the unsupported ends of the beam. It is suspected if either of these beams were part of a built-up structure in which there are no unsupported ends, the changes in crushing mode and lower energy-absorption capability would not occur. Good agreement in energy-absorption capability was obtained between tube and beam specimens, except for beams which exhibited crushing modes at the unsupported ends that were different than tubes of the same ply orientation and geometry.

5.1.3 Effects of Graphite-Kevlar Hybrid Material on the Crushing Response of Sine-Wave Beams

Sine-wave beams were fabricated from T300-K-934 hybrid woven fabric and a combination of a T300-K-934 hybrid woven fabric and T300-934 tape prepreg. The laminate stacking sequences for these two beams are $\left[\pm 45_H^F\right]_S$ and $\left[45_H^F/0_{Gr\ 3}^T\right]_S$. The $\left[45_H^F/0_{Gr\ 5}^T\right]_S$ tube has more 0 degree T300-934 plies than the $\left[45_H^F/0_{Gr\ 3}^T\right]_S$ beam. However, the crushing modes were observed to be similar, and, for compar-

ison purposes, the tube should have a slightly higher energy-absorption capability because the tube has more 0 degree T300-934 material.

The energy-absorption capabilities of the hybrid sine-wave beams compare favorably with results from tubes of similar structure as seen in Fig. 96. The energy-absorption capability of the $\left[\pm 45_H^F\right]_S$ sine-wave beam was approximately 20 percent less than the tube of the same ply orientation. The difference in energy-absorption capability between the tube and beam is partially attributable to the unsupported ends of the beam. These unsupported ends allowed the ends of the beam to buckle in a mode that was not consistent with the central portion of the beam as depicted in Fig. 97. The energy absorbed near the unsupported ends was less than elsewhere on the beam. The energy-absorption capability of the $\left[45_H^F/0_{Gr\ 3}^T\right]_S$ beam was approximately 5 percent less than the $\left[45_H^F/0_{Gr\ 5}^T\right]_S$ tube. The crushing mode of the $\left[45_H^F/0_{Gr\ 3}^T\right]_S$ beam was brittle fracturing for the 0 degree T300-934 plies whereas the outer plies of hybrid woven fabric delaminated and rolled up as depicted in Fig. 98. The crushing modes of both of these hybrid composite beams were identical to those of the tube specimens. Both $\left[\pm 45_H^F\right]_S$ and $\left[45_H^F/0_{Gr\ 3}^T\right]_S$ beams exhibited post-crushing integrity similar to the tube specimens, as seen in Figs. 97 and 98. The energy-absorption capability of the $\left[45_H^F/0_{Gr\ 3}^T\right]_S$ beam exceeds the energy absorption capability of other all-graphite-reinforced tube specimens and aluminum tube specimens evaluated in this study.
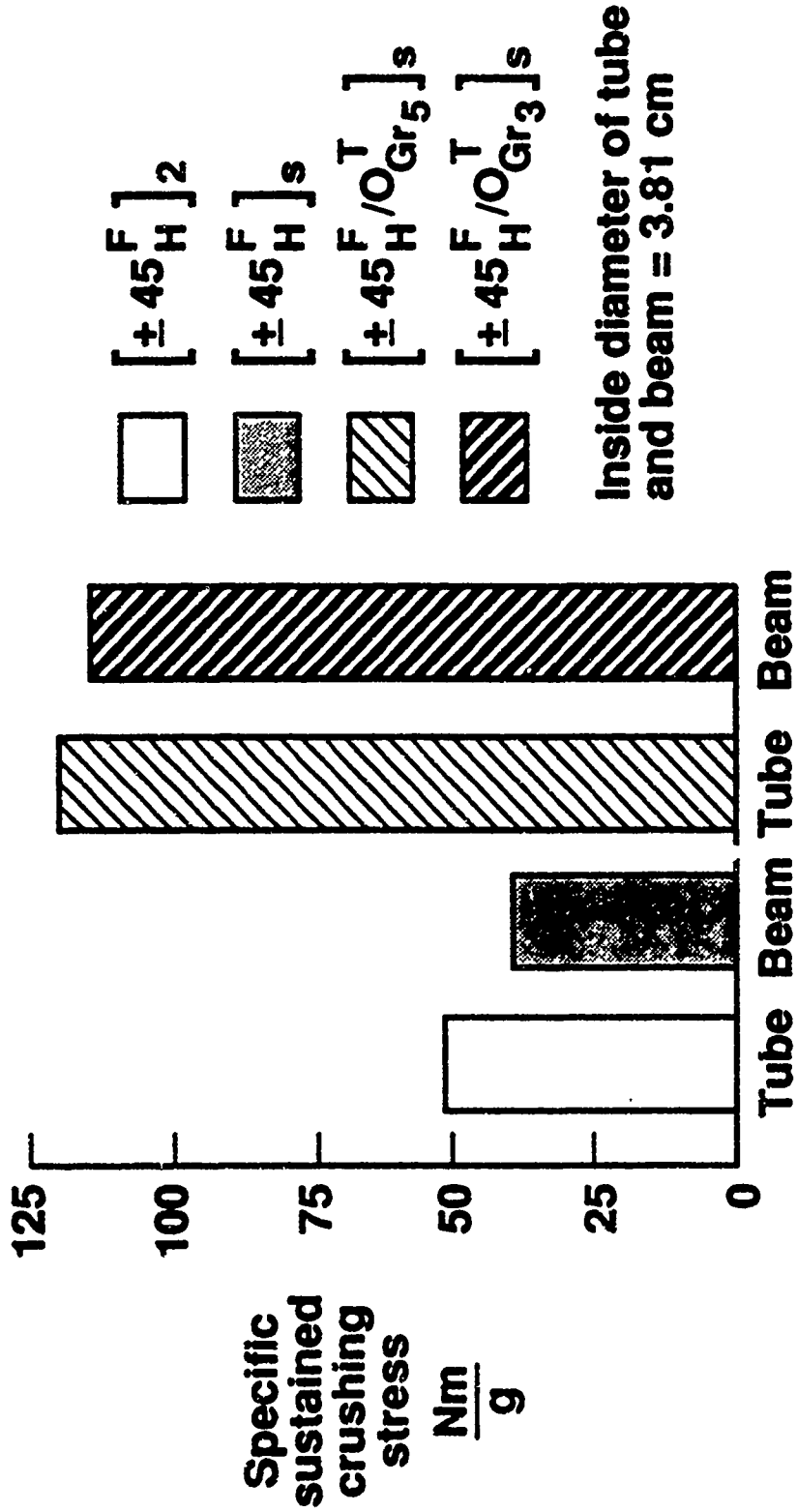
Figure 96. Energy-absorption capability of hybrid composite of hybrid composite sine-wave beams and tubes.

211

Figure 97. Crushed hybrid woven fabric sine-wave beam.

212
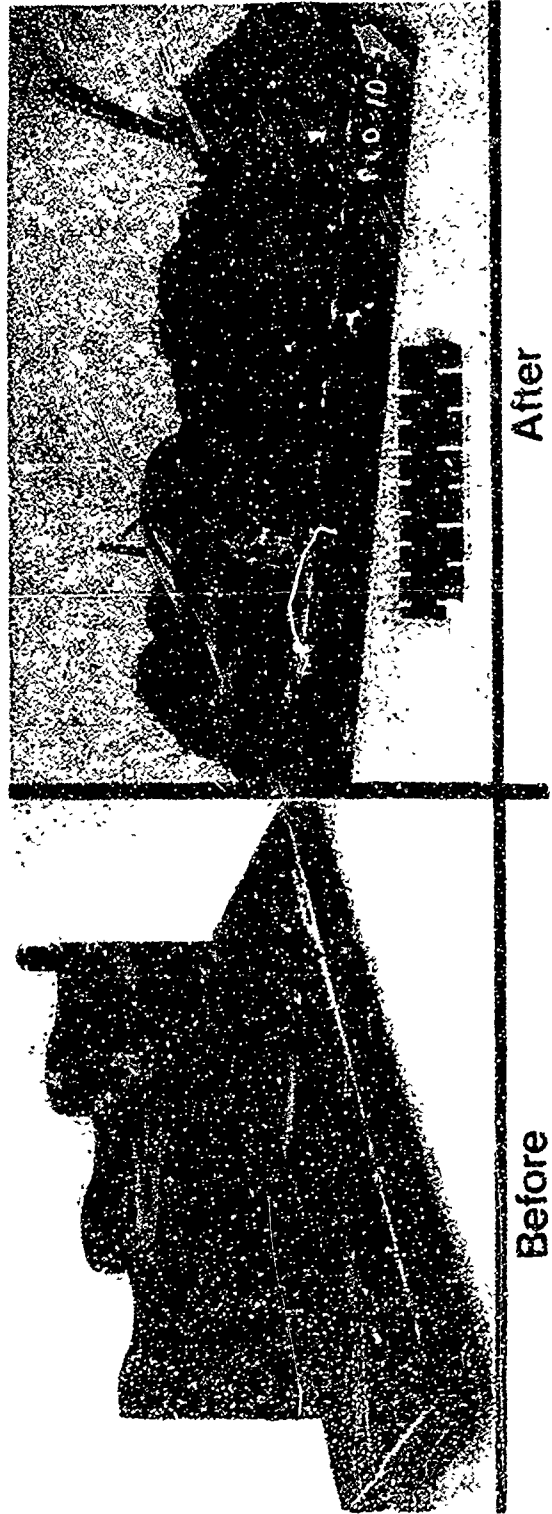
Figure 98. Crushed hybrid composite sine-wave beam.

213

5.2 Theoretical Evaluation of Subfloor Beam Concepts

At present, the state-of-the-art systems-design procedure for crashworthy structure relies heavily on a limited empirically determined data base. A test data base approach has been employed because no other method existed for predicting the energy-absorption capability of a structural concept. These structural concepts are therefore point designs, and thus limited guidance has been developed with respect to the effect of changes in material and test specimen structure. Utilization of a test data base for the design of energy-absorbing structure generally results in a heavy design. A heavy design is produced because test data bases are typically based upon a limited number of material and structural variables. The development of any experimental data base is expensive and the cost of creating an experimental data base is an increasing nonlinear function of the number of variables. Ideally, the designer would conduct concept trade-off studies to investigate the effects of changing material and geometric variables to achieve the optimal design. However, the designer has no established basis of mechanistic relations to conduct such studies.

The subfloor beam webs consist of an assemblage of flat and circular elements as depicted in Fig. 99. As has been shown in the previous sections on the crushing characteristics of beams as a function of beam geometry, ply orientation, and material, the crushing characteristics of beam webs are similar to those of tubular specimens. Energy-absorption trends and crushing modes have been shown to be similar for beam and tube specimens of similar characteristic geometry and material.

The following hypothesis was formulated for predicting the energy-absorption capability of structural elements: the crash energy-absorption capability of a

214
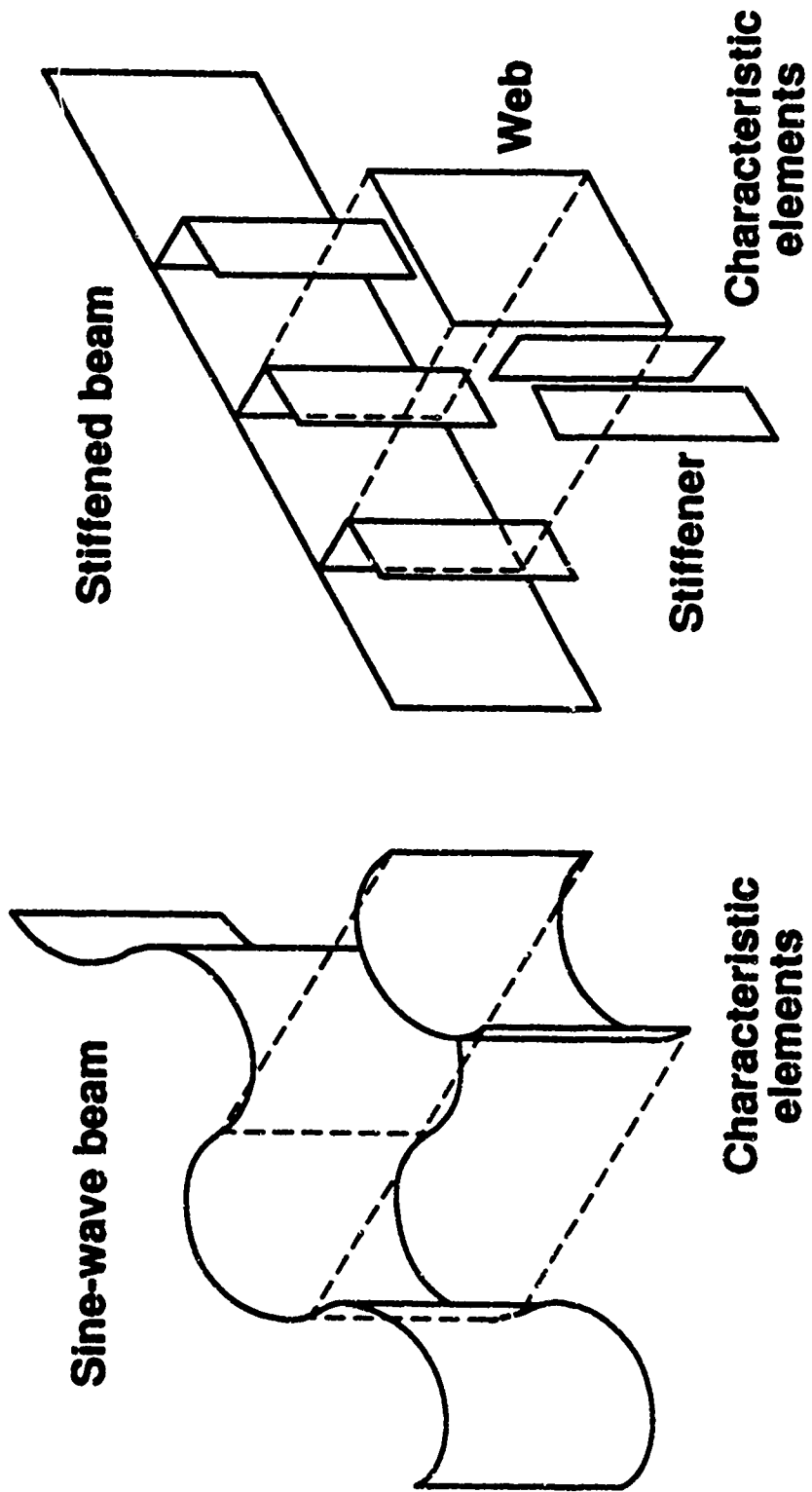
Figure 99. Characteristic elements of an integrally stiffened beam.

structural element is the sum of the area-weighted average of the energy-absorption capabilities of its characteristic elements. Mathematically, in terms of the specific sustained crushing stress (σ/ρ), where (σ) is the sustained crushing stress and (ρ) is the density of the material, the energy-absorption capability can be expressed as:

$$(\sigma/\rho)_{s.e.} = \sum_{i=1}^{n} \left[\frac{A_{i\ c.e.}}{A_{s.e.}} * (\sigma/\rho)_{i\ c.e.} \right]$$ (5)

The terms $A_{i\ c.e.}$ and $A_{s.e.}$ are the cross-sectional areas of the ith characteristic element (c.e.) and the structural element (s.e.), respectively. The $(\sigma/\rho)_{i\ c.e.}$ and $(\sigma/\rho)_{s.e.}$ are the specific sustained crushing stress of the ith characteristic element and the structural element, respectively.

In this hypothesis, the structure is assumed to be properly designed to progressively crush prior to catastrophic failure. Other requirements are that the tube specimens must have the same geometrical characteristics as the characteristic elements of the beam (i.e., the same D, W, and t), the same stacking sequence, material, and have the same material form (e.g., tape, woven, or filament-wound).

The energy-absorption capabilities of a beam's characteristic elements are based upon the energy-absorption capabilities of tubular specimens. The energy-absorption capabilities of flat characteristic elements of a beam are determined from square cross-section tube specimens. Similarly, the energy-absorption capability of half or complete circular characteristic elements can be determined from circular cross-section tubes.

216

An example of the prediction method is given for a circular cross-section-tube-stiffened beam fabricated with K-epoxy. Web width between tube stiffeners was 2.81 cm, and web thickness was 0.20 cm resulting in a W/t value of 19. The cross-sectional area of each web was 0.76 cm . The web extended beyond the stiffeners 1.27 cm on each side of the beam. The W/t value of the web beyond the stiffeners was 6 and the cross-sectional area was 0.25 cm^2. The composite layup in the web region was $[\pm 45]_{3S}$. The stiffener was a circular tube with an inside diameter of 2.54 cm and a wall thickness of 0.09 cm resulting in a D/t of 28.2. The layup of the tube was $[\pm 45]_3$, and the cross-sectional area was 0.78 cm^2. Using equation 5 to compute the energy-absorption capability of the beam with the appropriate circular and square cross section tube data results in:

$$(\sigma/\rho)_{s.e.} = [4 * A_{Tube} * (\sigma/\rho)_{Tube} + 3 * A_{Web} * (\sigma/\rho)_{Web}$$
$$+ 2 * A_{End\ of\ Web} * (\sigma/\rho)_{End\ of\ Web}] / A_{s.e.} \tag{6}$$

$$(\sigma/\rho)_{s.e.} = 30\ Nm/g \tag{7}$$

The measured energy-absorption capability of the beam was 28 Nm/g. The difference between the predicted and measured values was approximately 7 percent which is excellent agreement for an analysis of this level of sophistication.

This prediction method was verified using the previous example for the integrally stiffened circular-cross section tube stiffened K-934 beam, a sine-wave T300-934 beam, and a rectangular tube stiffened T300-934 beam. The differences between the experimentally determined and the predicted energy-absorption capabilities for the composite beams were less than 10 percent as seen in Fig. 100.

217
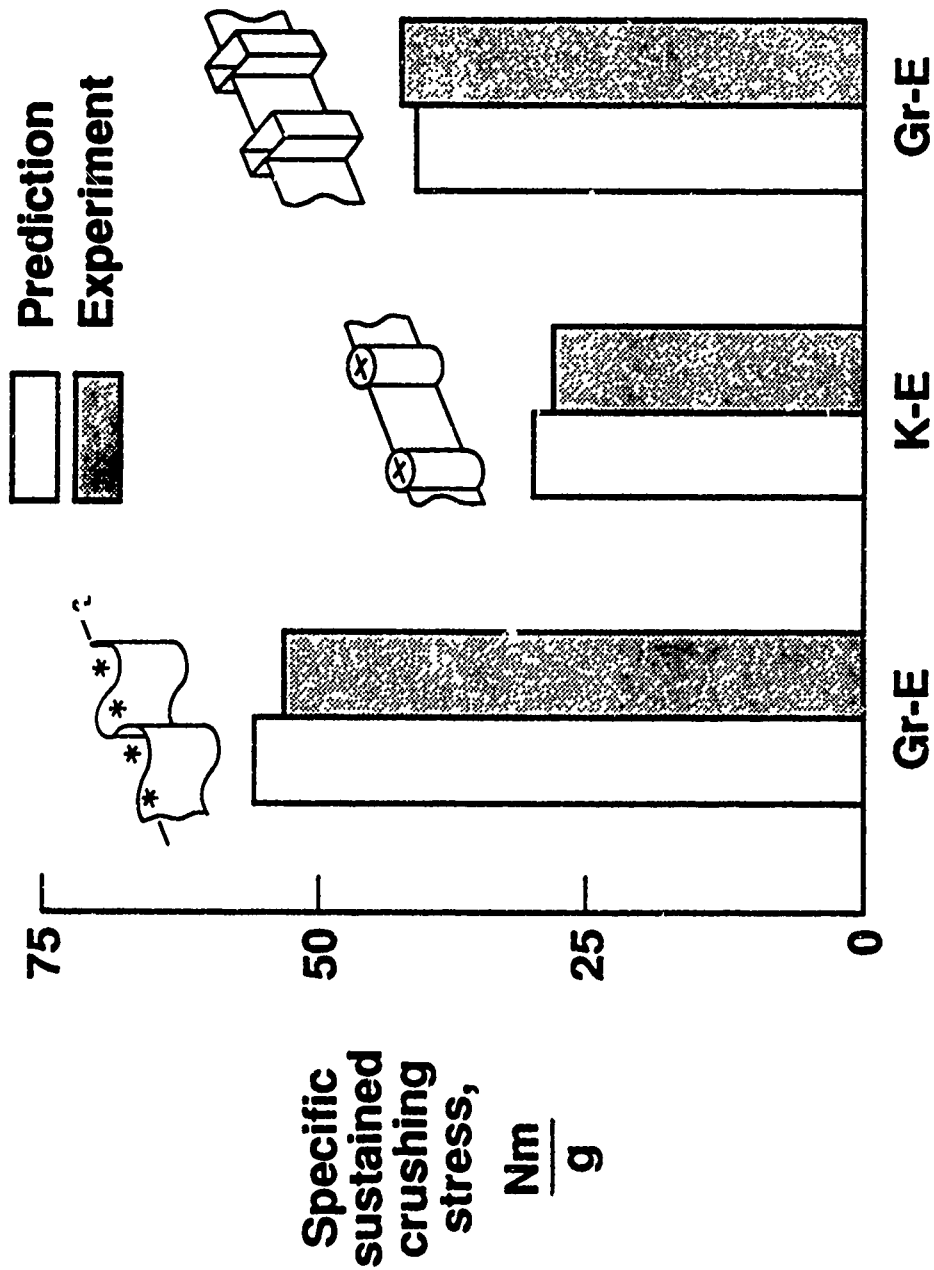
Figure 100. Comparison of predicted and experimentally determined energy-absorption capability.

5.3 Discussion of Beam Experimental and Theortical Results

Based upon the experimental energy-absorption results, properly designed composite beams are more efficient energy absorbers than metallic beams of comparable geometry. Sine-wave beams are more efficient energy absorbers than integrally stiffened beams.

Energy-absorption capability is not the only design driver of the subfloor structure of helicopters. Non-crash flight loads must also be reacted by the subfloor structure. It is not uncommon that the crash and non-crash loading conditions drive the design in opposite directions. The problem of opposing design requirements is most prevalent with sine-wave or honeycomb sandwich subfloor beam concepts. Integrally stiffened subfloor beams can be used to uncouple, to some extent, the effects of these design conditions. The in-plane shear carrying capability of the integrally stiffened beams is predominantly provided by the web between the stiffeners whereas the stiffeners would be designed to be the primary energy-absorbing component of the structure. Even though the integrally stiffened beam concept is a less efficient energy absorber than a sine-wave concept, the integrally stiffened concept may prove to be the best concept because of its versatility and it is a more controllable design.

The crushing characteristics (i.e., energy-absorption capability and crushing mode) of the energy-absorbing beam web concepts have been determined to be similar to tubular specimens of similar material and structure. This similarity in crushing characteristics facilitated the development of a simple, yet accurate,

219

method of predicting the energy-absorption capability of more complicated structure. The prediction method requires energy-absorption data obtained from tube specimens. The number of different tube configurations necessary to establish a data base for preliminary design purposes is small. Furthermore, utilizing this prediction method, the designer of energy-absorbing structure, has for the first time, a rationale for selecting material and structural parameters to achieve a prescribed energy-absorption capability. Utilizing this predictive capability can reduce the number of ancillary tests required to validate the response of a structure which should reduce the final design cost and weight of the structure.

Chapter 6 - SUMMARY AND RECOMMENDATIONS

The goal of this study was to develop a method of predicting the energy-absorption capability of composite helicopter subfloor beam structure. To reach this goal, it was first necessary to develop an in-depth understanding of how a multiplicity of parameters influences the crushing response of composite structures. This multiplicity of parameters that is available to the designer of energy-absorbing structure can be both a blessing and a hindrance. A slight change to a parameters can result in significant change in the structure's energy-absorption characteristics. The increase or decrease of a parameter may have a beneficial effect on energy-absorption within a limited range. However, further increase or decrease of the parameter may result in drastically different energy-absorption trends. Therefore, the understanding of how these parameters influence the crushing characteristics of composite materials is paramount.

As discussed in the review of literature section, many researchers have attempted to develop broad conclusions from a limited data base without realizing the limitations of these conclusions. An attempt will be made to quantify the range of applicability of the findings from this study. There still exists some danger of over generalizing the results. For example, the summary of findings for the tube material mechanical properties is based upon the effect of changing a single parameter with all other parameters held constant.

6.1 Summary of Research

Some of the observations and accomplishments developed from this study were:

221

1. The four characteristic crushing modes for tubes, transverse shearing, brittle fracturing, lamina bending, and local buckling, have been identified, and the mechanisms that control the crushing process have been defined.

2. An in-depth understanding has been developed of how the different material properties, structural variables, and loading conditions affect the crushing response of composite tubes. The influence of each of these parameters on the energy-absorption capability of a tube is a function of the design of a specific tube. The effects of these parameters can be quantified only on a case-by-case basis.

3. A simple buckling of a column-on-an-elastic-foundation equation was modified that proved to be very useful in understanding how different material and structural variables influence the energy-absorption capability of a laminated tube.

4. Energy-absorption capability of tubes increases as fiber stiffness increases provided the stiffness of the "*column*" is significantly influenced by the stiffness of the fiber. Increasing fiber stiffness, within the range of materials evaluated, has little influence on energy-absorption capability as a result of increase in "*foundation*" stiffness.

5. Increase in matrix stiffness of tubes increases energy-absorption capability of tubes where "*foundation*" stiffness significantly influences "*column*" buckling. Therefore, specimens that crush in the local buckling mode are affected most by changes in "*foundation*" (hence, matrix) stiffness. Matrix stiffness has a small effect on the energy-absorption capability of specimens that exhibit transverse shearing, brittle fracturing, and lamina bending.

222

6. Fiber failure strain of tubes has a significant effect on energy-absorption capability. The effect of fiber failure strain has different results on the energy-absorption capability depending upon the properties of the matrix and the structure of the tube. Increasing fiber failure strain in a tube that exhibits a lamina bending crushing mode would result in a negligible change in energy-absorption capability. However, increasing the fiber failure strain in a tube that exhibits a transverse shearing or brittle fracturing crushing mode will result in an increase in energy-absorption capability.

7. Matrix failure strain has a similar effect on energy-absorption capability as fiber failure strain. An increase in matrix failure strain can have different results depending upon the properties of the fiber and the structure of the tube. For example, an increase in fiber failure strain of a tube that exhibits a lamina bending crushing mode will result in an increase in energy-absorption capability. However, if a tube exhibits a transverse shearing crushing mode and matrix failure strain is significantly increased, then it is possible to cause catastrophic failure of the tube or force the tube into the local buckling crushing mode. Failure of the tube or crushing in the local buckling mode would result in lower energy-absorption capability than was achieved when the tube crushed in the transverse shearing mode.

8. Tube ply orientation can have a significant effect on energy-absorption capability. The magnitude of the effect of changing tube ply orientation on energy-absorption capability is a function of the crushing mode exhibited. If a tube exhibits predominantly a transverse shearing or brittle fracturing crushing mode, then energy-absorption capability increases as the percentage of fiber oriented in the

223

direction of the applied load increases. If a tube exhibits either a lamina bending or local buckling crushing mode, then the change in energy-absorption capability as a function of a change in ply orientation is not as large as the case where the tube crushed in the transverse shearing or brittle fracturing modes. Energy-absorption capability of tubes that crush in either the lamina bending or local buckling crushing modes does not change monotonically with changes in ply orientation.

9. An increase in fiber volume fraction can result in a decrease, no change, or an increase in energy-absorption capability of tubes. Fiber volume fraction affects material density, interlayer compliance, and *"foundation"* strength. For example, an increase in fiber volume fraction can produce a decrease in energy-absorption capability for tubes that crush in a lamina bending crushing mode. The increase in fiber volume fraction reduces the volume of matrix between fibers. Reducing the matrix between fibers decreases the interlaminar strength and hence reduces the energy-absorption capability.

10. Small changes in stacking sequence generally result in negligible changes in energy-absorption capability of tubes. However, changes in lamina stacking sequence can have a potentially significant effect on energy-absorption capability. For example, two hybrid tubes with different stacking sequences had a 300 percent difference in energy-absorption capability.

11. Hybrid material consisting of graphite- and Kevlar-reinforcements can produce, depending upon the structure of the tube, higher energy-absorption capability than tubes fabricated from either all graphite- or Kevlar-reinforced tubes.

Tubes fabricated from hybrid combinations of graphite and Kevlar reinforcements also exhibit post-crushing integrity.

12. Circular cross-section tube diameter (D) to thickness (t) ratio (D/t) and square cross-section tube width (W) to thickness (t) ratio (W/t) significantly affect energy-absorption capability. As tube D/t and W/t decrease, energy-absorption capability increases. Energy-absorption capability of Kevlar-reinforced tubes are geometrically scalable whereas the energy-absorption capability of graphite- reinforced tubes is not geometrically scalable. Tubes that are geometrically scalable have a one-to-one correspondence between their energy-absorption capability and the characteristic geometrical parameter (i.e., D/t or W/t).

13. Energy-absorption capability of tubes do not seem to be a strong function of tube included angle (Φ). Tube included angle is the angle formed between radial lines originating from the center of curvature of one side of a "near-elliptical" tube and extending to the corners of the tube.

14. Energy-absorption capability of composite tubes is a function of crushing speed. The influence of crushing speed on energy-absorption capability is controlled by the strain-rate sensitivity of the mechanism that controls the crushing process. Tubes, whose crushing response is controlled by mechanisms that are not a function of strain rate, do not exhibit effects of crushing speed on energy-absorption capability. Tubes, whose crushing response is controlled by mechanisms that are a function of strain rate, exhibit effects of crushing speed on energy-absorption capability. Both fiber and matrix mechanical properties can contribute to the strain-rate effects of the crushing mechanisms of the composite tubes.

225

15. A finite element analysis was developed to predict the crushing response of composite tubes. The difference between analysis and experiment was, generally, less than 30 percent.

16. The crushing response of composite beams was evaluated and found to follow the same trends as tube specimens that have similar material and structural characteristics.

17. The energy-absorption capability of graphite-epoxy and Kevlar-epoxy structural elements were found to be equal or superior to aluminum beams of similar geometry.

18. A simple, yet accurate, analysis was developed to predict the energy-absorption capability of composite beams.

6.2 Recommendations for Future Research

The crushing process of composite structures encompasses some of the most complex phenomena related to the mechanics of composite materials and structures. The state of the art of energy-absorbing composite materials and structures has been significantly advanced. However, there are a considerable number of topics that warrant further study. The following comments are offered as guidelines for future work in the area of energy absorption of composite materials and structures.

1. The analysis method to predict the energy-absorption capability of composite tube specimens needs to be improved and more fully validated. Improvements, such as better nonlinear solution strategies, lamina failure criteria, inclusion of crushing initiators, and dynamic crushing effects should be made to the analysis.

226

2. An understanding of dynamic crushing mechanisms needs to be developed. This study should focus on the dynamic mechanical properties corresponding to the different crushing mechanisms.

3. Dynamic crush testing of subfloor beam specimens is needed to assure that the crushing characteristics are similar to those produced by tubes.

4. Realistic crushing initiators need to be developed for subfloor beam structures.

5. Terminology, test methods, and test specimens should be standarized.

Chapter 7 - REFERENCES

1. "Light Fixed and Rotary Wing Aircraft Crashworthiness," Mil-Std-1290, Jan. 1974.

2. Thornton, P. H., "Energy Absorption in Composite Structures," *Journal of Composite Materials*, July 1979, pp. 248-262.

3. Thornton. P. H. and Edwards, P. J., "Energy Absorption in Composite Tubes", *Journal of Composite Materials*, Nov. 1982, pp. 521-545.

4. Thornton, P.H., Harwood, J.J., and Beardmore, P., "Fiber-Reinforced Plastic Composites for Energy Absorption Purposes", *Composite Science and Technology*, 1985, pp. 275-298.

5. Hull, D., "Energy Absorption of Composite Materials Under Crash Conditions". *Proceedings of the Fourth International Conference on Composite Materials*, T. Hayashi, K. Kawata, and S. Umekawa (Editors), Japan Society for Composite Materials, Tokyo. Japan, Oct. 1982, pp. 861-870.

6. Hull, D., "Research on Composite Materials at Liverpool University, Part 2: Energy Absorbing Composite Materials," *Physics Technology*, 1983, pp. 99-112.

7. Berry. J. and Hull, D., "Effect of Speed on Progressive Crushing of Epoxy-Glass Cloth Tubes," *Proceedings of the Institute Physics Conference*. Series No. 70, 1984, pp. 463-470.

8. Fairfull, A.H. and Hull, D., "Effects of Specimen Dimensions on the Specific Energy Absorption of Fibre Composite Tubes," *Proceedings of the Sixth International Conference on Composite Materials*, F. L. Matthews, N. C. R. Buskell, J. M. Hodgkinson, and J. Morton (Editors), Elsevies Applied Science, London, UK, July 1987, pp. 3.36-3.45.

9. Kindervater, C.M., "Quasi-Static and Dynamic Crushing of Energy Absorbing Materials and Structural Components With the Aim of Improving Helicopter Crashworthiness", *Proceedings of the Seventh European Rotorcraft and Powered*

Lift Aircraft Forum, Garmisch-Partenkirchen, Federal Republic of Germany, Sept. 1981.

10. Kindervater, C.M., "Energy Absorbing Qualities of Fiber-Reinforced Plastic Tubes", *Proceedings of the AHS National Specialist Meeting on Composite Materials for Helicopters*, Philadelphia, Pennsylvania, March 1983.

11. Bannerman, D.C. and Kindervater, C. M., "Crash Impact Behavior of Simulated Composite and Aluminum Fuselage Elements", *Proceedings of the Ninth European Rotorcraft Forum*, Stresa, Italy, Sept. 1983.

12. Bannerman, D. C. and Kindervater, C. M., "Crash Energy Absorption Properties of Composite Structural Elements", *Proceedings of the Fourth International Conference SAMPE European Chapter*, Bordeaux, France, Oct. 1983, pp. 155-167.

13. Bannerman, D. C. and Kindervater, C. M.. "Crashworthiness Investigation of Composite Aircraft Subfloor Beam Sections", *Proceedings of the International Structural Impact and Crashworthiness Conference*, J. Morton (Editor), Elsevies Applied Science. London, UK, July 1984, pp. 710-722.

14. Kindervater, C. M., "Crash Impact Behavior and Energy Absorbing Capability of Composite Structural Elements", *Proceedings of the 30th National SAMPE Symposium*, Anaheim, California, March 1985.

15. Kindervater, C. M., "Compression and Crush Energy Absorption Behavior of Composite Laminates", *Proceedings of the E/MRS Conference*, Strasbourg, Federal Republic of Germany, Nov. 1985.

16. Sen. J. K., "Designing for a Crashworthy All-Composite Helicopter Fuselage", *Proceedings of the 40th AHS Forum*, Arlington. Virginia, May 1984, pp. 123-134.

17. Votaw, M. W. and Sen. J. K., "A Systems Approach for Designing a Crashworthy Helicopter Using Program KRASH", *AIAA-84-2448, San Diego, California, Nov. 1984*.

18. *Sen, J. K. and Dremann. C. C., "Design Development Tests For Composite Crashworthy Helicopter Fuselage", SAMPE Quarterly, Oct. 1985, pp. 29-39.*

19. Sen, J.K., "Designing for a Crashworthy All-Composite Helicopter Fuselage," *Journal of the American Helicopter Society*, April 1987, pp. 56-66.

20. Farley, G. L., "Energy Absorption of Composite Materials," *Journal of Composite Materials*, May 1983, pp. 267-279.

21. Farley, G. L., "The Effects of Crushing Speed On the Energy Absorption Capability of Composite Material," *NASA TM89122*, March 1987.

22. Farley, G. L.. "Effect of Fiber and Matrix Maximum Strain on the Energy Absorption of Composite Materials," *Journal of Composite Materials*, July 1986, pp. 322-334.

23. Farley, G. L., Bird. R. K.., and Modlin, J. T., "The Role of Fiber and Matrix in Crash Energy Absorption of Composite Materials," *Proceedings of the AHS National Specialists' Meeting on Crashworthy Design of Rotorcraft*, Atlanta, Georgia, April 1986.

24. Farley, G. L.. "Effect of Specimen Geometry on the Energy- Absorption Capability of Composite Materials," *Journal of Composite Materials*, July 1986, pp.390-400.

25. Farley. G. L.. "Energy Absorption Capability and Scalability of Square Cross Section Composite Tube Specimens," *NASA TM 89087*. March 1987.

26. Farley. G. L., "Crash Energy Absorbing Composite Sub-Floor Structure," Presented at the 27th AIAA/ASME/ASCE/AHS Structures. Structural Dynamics and Materials Conference. May 1986.

27. Farley. G. L.. "A Method of Predicting the Energy-Absorption Capability of Composite Sub-Floor Beams." *NASA TM 89088*. March 1987.

28. Brush, D. O. and Almroth. B. O.. "Buckling of Bars. Plates, and Shells". McGraw-Hill Book Co.. 1975.

29. "Test of Fiber Content of Resin-Matrix Composites by Matrix Digestion, "Annual Book of ASTM Standards." Part 36, D 3171-76. 1982.

230

30. Allred, R. E. and Hall, N. H., "Volume Fraction Determination of Kevlar-49/Epoxy Composites," *Polymer Engineering and Science*, October 1979, pp. 907-909.

31. Devitt, D. F., R. A. Schapery, and W. L. Bradley, "A Method for Determining the Mode I Delamination Fracture Toughness of Elastic and Viscoelastic Composite Materials," *Journal of Composite Materials*, Oct. 1980, pp. 270-285.

32. EISI Reference Manual, Program Execution; Engineering Information Systems Incorporated, San Jose, CA, July 1983.

33. Cook, R. D., "Concepts and Applications of Finite Element Analysis", John Wiley and Sons, Inc., 1974.

34 Cronkhite, J. D., Haas, T. J., Winter, R., Cairo, R. R., and Singley, G. T., "Investigation of the Crash Impact Characteristics of Composite Airframe Structures", *Proceedings of the 34th Annual National Forum of the American Helicopter Society*", May 1978.

Report Documentation Page

1. Report No. NASA TM-101634 AVSCOM TR-89-B-003	2. Government Accession No.	3. Recipient's Catalog No.
4. Title and Subtitle Energy-Absorption Capability of Composite Tubes and Beams		5. Report Date September 1989
		6. Performing Organization Code
7. Author(s) Gary L. Farley Robert M. Jones		8. Performing Organization Report No.
		10. Work Unit No. 505-63-01-06
9. Performing Organization Name and Address Aerostructures Directorate USAARTA (AVSCOM) NASA Langley Research Center, Hampton, VA 23665-5225		11. Contract or Grant No.
		13. Type of Report and Period Covered
12. Sponsoring Agency Name and Address National Aeronautics and Space Administration Washington, DC 20546 and U.S. Army Aviation Systems Command St. Louis, MO 63166		Technical Memorandum
		14. Sponsoring Agency Code

16. Abstract

In this study, the objective was to develop a method of predicting the energy-absorption capability of composite subfloor beam structures. Before it is possible to develop such an analysis capability, an in-depth understanding of the crushing process of composite materials must be achieved. A comprehensive experimental evaluation of tube specimens was conducted to develop insight into how composite structural elements crush and what are the controlling mechanisms. In this study, the four characteristic crushing modes, transverse shearing, brittle fracturing, lamina bending, and local buckling were identified and the mechanisms that control the crushing process defined. An analysis to predict the energy-absorption capability of composite tube specimens was developed and verified.

Composite beams are equal or superior energy absorbers to comparable geometry metallic beams. A simple and accurate method of predicting the energy-absorption capability of composite beams was developed.

17. Key Words (Suggested by Author(s)) Crash Energy Absorption, Composite Materials, Composite Structures, Crushing, Fracture, Post-Crushing Integrity, Helicopters, Automobiles, Graphite/Epoxy, Kevlar/Epoxy, Glass/Epoxy		18. Distribution Statement Unclassified--Unlimited Subject Category 24	
19. Security Classif. (of this report) Unclassified	20. Security Classif. (of this page) Unclassified	21. No. of pages 247	22. Price A11